ABSTRACT

Title of dissertation: FLUID DYNAMICS OF BOUNDARY LAYER COMBUSTION

Colin H. Miller, Dissertation, 2017

Dissertation directed by: Assistant Professor Michael J. Gollner
Department of Fire Protection Engineering

Reactive flows within a boundary layer, representing a marriage of thermal, fluid, and combustion sciences, have been studied for decades by the scientific community. However, the role of coherent structures within the three-dimensional flow field is largely untouched. In particular, little knowledge exists regarding streamwise streaks, which are consistently observed in wildland fires, at the base of pool fires, and in other heated flows within a boundary layer. The following study examines both the origin of these structures and their role in influencing some of the macroscopic properties of the flow. Streaks were reproduced and characterized via experiments on stationary heat sources in laminar boundary layer flows, providing a framework to develop theory based on both observed and measured physical phenomena.

This first experiment, performed at the University of Maryland, examined a stationary gas burner located in a laminar boundary layer with stationary streaks which could be probed with point measurements. The gas temperature within streaks increased downstream; however, the gas temperature of the regions between

streaks decreased. Additionally, the heat flux to the surface increased between the streaks while decreasing beneath the streaks. The troughs are located in a downwash region, where counter-rotating vortices force the flame sheet towards the surface, increasing the surface heat flux. This spanwise redistribution of surface heat flux confirmed that streaks can, at least instantaneously, modify important heat transfer properties of the flow. Additionally, the incoming boundary layer was established as the controlling mechanism in forming streaks, which are generated by pre-existing coherent structures. Finally, the amplification of streaks was determined to be compatible with quadratic growth of Rayleigh-Taylor Instabilities, providing credence to the idea that the downstream growth of streaks is strongly tied to buoyancy.

The next phase of the project was performed at the Missoula Fire Sciences Laboratory, where a hot plate in a laminar boundary layer was examined. In addition to manipulating the wind speed, the local buoyant force was controlled via the surface temperature of the hot copper plate. Infrared thermography was employed to detect streaks by means of local surface temperature fluctuations, and a novel and consistent method for tracking streaks and quantifying important properties was developed. Streak spacing was seen to be lognormally distributed, and the initial spacing, which was consistently between 60-70 dimensionless wall units, was shown to be governed by the incoming boundary layer. Streak spacing increased downstream of the plate, with higher plate temperatures resulting in larger magnitudes of spanwise fluctuations in surface temperature. Finally, streak behavior became more chaotic downstream, as streaks would meander rapidly and persist for shorter durations.

The final phase of the study, performed at the Missoula Fire Sciences Laboratory, examined a saturated fuel wick in the same experimental configuration as the hot plate. Streaks were detected in the flame via high speed video, and tracked using the previous developed algorithm. Streak spacing was lognormally distributed, with the initial spacing (60-75 wall units) again being controlled by the incoming boundary layer. Spacing between coherent structures increased downstream, likely due to buoyant amplification. The width of streaks grew to an apparent assymptote, indicating a settling of length scale controlled by the time and rate of growth. Further downstream, coherent structures no longer resembled well-ordered streaks but more complex structures resulting from streak aggregation.

Overall, trends for streaks are consistent in both the hot plate and the flame, indicating that the behavior of streaks is governed by similar mechanisms in both scenarios. Although the initial instabilities are governed by the incoming wind, buoyant forces cause the growth and aggregation of these structures. These local instabilities are capable of affecting macroscopic properties of the flow, including heat transfer to the surface, indicating that a two-dimensional assumption may fail to adequately describe heat and mass transfer during flame spread and other reacting boundary layer flows.

FLUID DYNAMICS OF BOUNDARY LAYER COMBUSTION

by

Colin H. Miller

Dissertation submitted to the Faculty of the Graduate School of the
University of Maryland, College Park in partial fulfillment
of the requirements for the degree of
Doctor of Philosophy
2017

Advisory Committee:
Professor Michael J. Gollner, Chair/Advisor
Professor Elaine Oran, Dean's Representative
Professor Arnaud C. Trouvé
Professor Peter B. Sunderland
Professor Andre W. Marshall

© Copyright by
Colin H. Miller
2017

Acknowledgments

When I began this research project, I could never have anticipated where it would take me. I suppose this is a natural consequence of its exploratory nature. Looking back, I consider myself quite lucky to have studied such an open-ended question because it has enabled significant collaboration with incredible researchers from a wide variety of disciplines. I could never have completed this thesis without immense help - so many people have contributed to this project, and I would like to at least try to express my gratitude to a few of them.

First of all, I have to thank my advisor, Dr. Michael Gollner. Michael has such a personal approach to his interactions with everyone, and this ability simply transforms the nature of the work that is being done. People really want to work with him, not simply because he does good research, but because he is a great person to be around. I really have been blessed because I somehow fell under his mentorship as a Master's student when he was a relatively new professor. I had no idea he would be such a great advisor with exciting projects and valuable connections. He is a true mentor, and he has encouraged me in ways that have given me so much more confidence as a researcher. Michael has continually pushed me to take advantage of opportunities that I would never have even considered or felt qualified to pursue, and this has allowed me to interact with some phenomenal researchers. He has also given me the freedom to take the project in my own direction at times, and I think this style has suited my growth quite well. Michael works hard for all his students, so we try to work hard for him. Don't work too hard, Michael!

I would also like to thank my thesis committee. They have all provided me with valuable feedback on this project, and I have taken interesting classes with all of them. They are all exceptional teachers, and their insight into the fields of fire science have proven invaluable in shaping my understanding. I would particularly like to thank three teachers who have taught me in graduate school: Dr. Elaine Oran, Dr. Randy McDermott, and Dr. Johan Larsson, all of whom bring enthusiasm and a depth of knowledge to a subject, take time to personally address student concerns, and encourage students to think critically.

The fire protection department and support staff at the University of Maryland has been particularly instrumental in shaping my development. Again, I am blessed to be a part of this community. It is a close-knit group, and I routinely interact with individuals here who are truly willing to sit down and help you through whatever problem you may have. This is a unique trait that has proven invaluable to so many students who are floundering their way through the messy process of graduate school. In particular, I want to thank Mary Lou Holt and Sharon Hodgson, who routinely go above and beyond the call of duty to assist the many who come to them every day.

I would also like to thank all the students from the department who have assisted and encouraged me. Dr. Gollner's lab group has always been pretty dope, and I have many good friends in this department with whom I have had conversations and interactions that I truly value. I would especially like to thank: Ajay Singh and Dan Gorham, for showing me how much it means to personally and intentionally devote time to assisting and guiding others looking for help; Evan Sluder, for all

the assistance at Missoula and giving me an outlet for my inner wild man; and Wei Tang, who supported me in the lab on countless occasions and who is slowly teaching me how to ball hard(er).

I would like to thank Dr. Arnaud Trouve and Salman Verma for their indispensable contributions to this project, including many fruitful discussions and assistance with theoretical development.

I am incredibly grateful to the Missoula Fire Sciences Lab, which provided funding, facilities, and the impetus for this project. Everyone from this lab was so helpful and provided incredible insights on some of the phenomena we were seeing in the lab and in field-scale fires. Mark Finney, Sara McAllister, Torben Grumstrup, and Jason Forthofer, all contributed significantly to the work that is presented here; while I was at their facility, they were extremely generous with their time in addition to guiding me through the experiments. Additionally, Josh, Randy, John, Andrew, and Kyle provided an incredible amount of help in the lab, and their expertise assisted greatly in building and running experimental setups.

I would like to give a huge shout out to my family and my friends. My friends and family provided incredible support for me on so many different levels as I made my way through graduate school. I would never have made it through if they weren't encouraging me every step of the way and providing me with relationships that really built me up. I have been blessed to be a part of some really incredible communities in addition to having awesome friends. I cannot overstate how much of a role this has played in my life and in enabling this degree.

Finally, I want to voice my gratitude to God for blessing me with such an

incredible opportunity and for creating a universe replete with beautiful phenomena for humans to study and describe. It is a great gift to work in the field of science, where I can study a world which declares the glory of God and his love for humanity. Nothing is possible without the Lord, "for in him we live and move and have our being" (Acts 17:28).

The authors would like to acknowledge financial support for this work from the USDA Forest Service Missoula Fire Sciences Laboratory and National Fire Decision Support Center under collaborative agreement 13-CS-11221637-124. Additional support for CM and MG came from the National Science Foundation under Grant No. CBET-1554026. Any opinions, findings, and conclusions or recommendations expressed in this material are those of the author(s) and do not necessarily reflect the views of the National Science Foundation or USDA Forest Service.

Table of Contents

List of Figures

Chapter 1: Introduction

Reactive flows within a boundary layer, representing a marriage of thermal, fluid, and combustion sciences, have been studied for decades by the scientific community. Although boundary layer combustion represents an important phenomenon in combustion, the aerodynamic structure of these boundary layers is rarely examined [9], especially for low-Re flows typifying problems in fire safety. The majority of experimental and theoretical studies on boundary layer combustion examine the problem from a two-dimensional perspective. However, a boundary layer flow field is fully three-dimensional, possessing coherent structures and vortices of various spatial orientation; this behavior is even observed in non-reacting boundary layer flows [10]. It is well-known that disturbances and instabilities in non-reacting boundary layers can produce important effects, such as transition to turbulence or variation in wall heat transfer. Yet, we still lack a fundamental understanding of how coherent structures in a boundary layer affect global and local properties of combustion, and, conversely, how combustion modifies the structure of the boundary layer.

The original motivation for this problem comes from observations in wildland fires, which are illustrative of low-Re uncontrolled boundary layer combustion. Coherent structures have been observed across length scales in these fires, and saw-

toothed flame geometry has been observed in both the laboratory and in field experiments [1]. Notably, streamwise streaks have been observed in both flames and in smoke trailing the flame (see Fig. 1.1), a manifestation of counter-rotating vortices, which promote upwash and downwash regions [1]. Given recent findings that have supported convection as a dominant mechanism of preheating in wildland fire spread, there is reason to believe that the coherent structures observed in the flow field, including streaks, are important to the flame spread process [1]. These streaks have also been observed in other canonical fire problems, including pool [2, 11] fires and buoyant plumes [3], where these "finger-like" instabilities lead to the breakdown of periodic toroidal vortices. In such scenarios, the energy cascade flows from smaller scales to larger scales, indicating that an understanding of streaky instabilities may be essential to describing the macroscopic structure.

1.1 Similar flow structures observed in literature

Streamwise streaks are not simply a combustion phenomenon, as these aerodynamic structures are known to exist in non-reacting boundary layer flows [10]. It is understood that, in the near-wall region, streamwise counter-rotating vortices exist, and these vortices produce upwash and downwash regions. Streaks consist of the upwash regions, in which low-speed fluid from the wall is swept up into higher regions of the flow. Streaks are hypothesized to play an important role in both stability considerations and in transition to turbulence. These coherent structures consistently populate the near-wall region while spanwise vortices are observed at

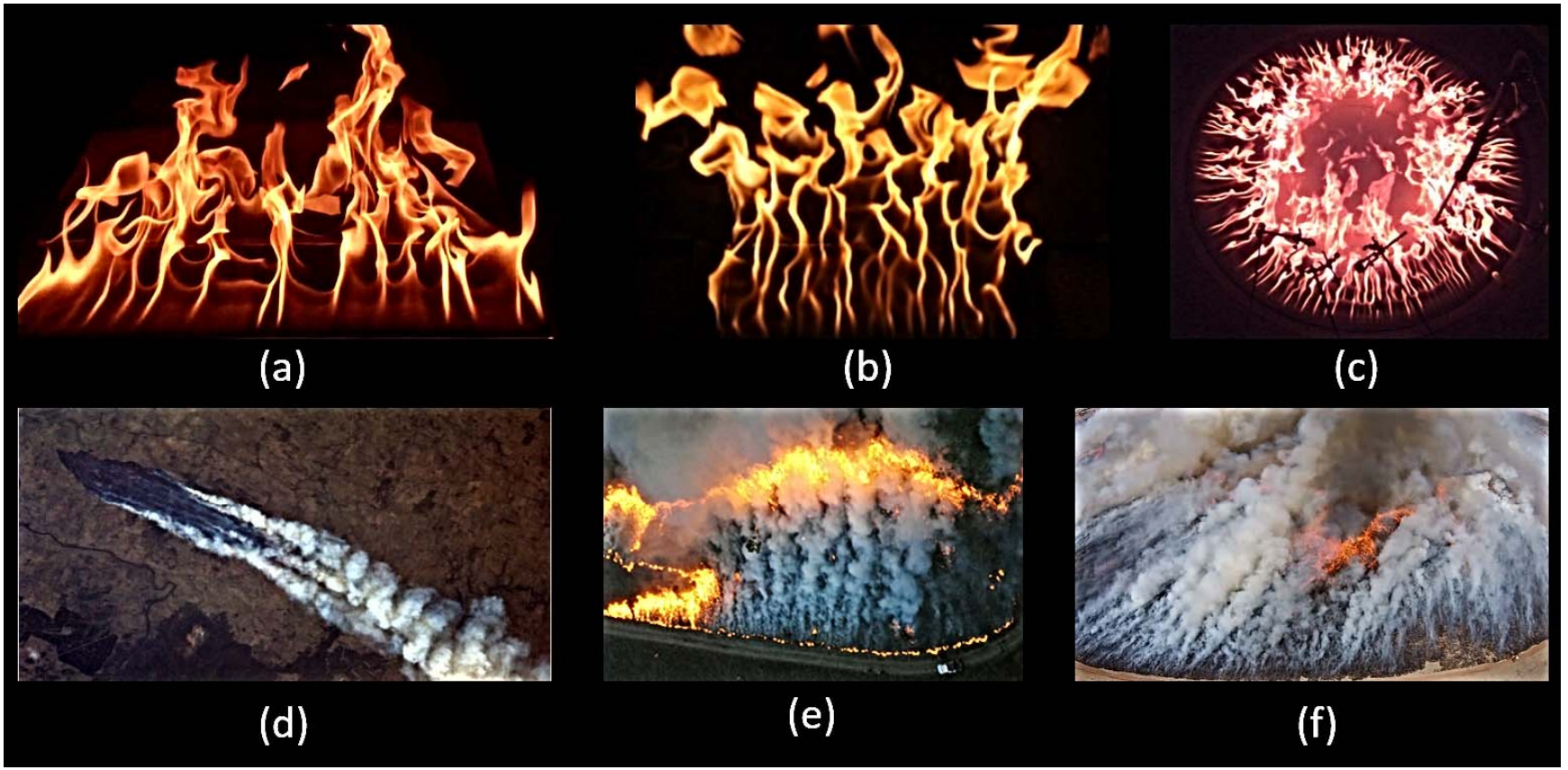

Figure 1.1: Coherent structures in the form of streaks observed in wind-blown flames. Clearly visible streaky structures can be seen emanating from the leading edge of all these wind-blown flames. (a) Top view of flames from an inclined ethylene burner (b) Top view of propane burner in crossflow (c) Ring pool fire at Missoula Fire Sciences Laboratory (d) View of Australian brush fire from International Space Station (Credit: NASA/ Chris Hadfield) (e) Aerial view of flames and smoke from prescribed burn (NPS/ John Nobles) (f) Closing the circle on a prescribed burn, Deerhead, KS (https://youtu.be/lcLnhs4FXvI).

the outer edge of the boundary layer [4].

Although streaks are typically discussed in relation to high-Re, turbulent boundary layers, they are also observed in laminar boundary layers. Such coherent structures have been observed by experimentalists; in particular, streaklike instabilities are observed in the near-wall region of the boundary layer. These structures are denoted Klebanoff modes, which are often induced by low levels of freestream turbulence [12], and their breakdown promotes transition to a turbulent boundary layer [13]. These streaks produce a local thinning/thickening of the Blasius boundary layer.

Streaky structures known as Görtler instabilities appear within a boundary layer forming over a concave wall and are created by counter-rotating streamwise vortices. Flow stability in these flows is known to be affected by wall temperature [14]. Görtler vortices are known to modify wall heat fluxes [15], grow in time, decay, and cause transition to turbulence [16], effects that have also been seen or hypothesized for flame streaks.

Finally, streaks have been observed in heated boundary layers, a scenario which is roughly analogous to a boundary layer diffusion flame. Experimental studies of flow over heated plates have examined thermal instability and flow regimes in the presence of longitudinal streaks [17–21]. Sparrow and Husar [22] studied inclined heated plates, finding that the number of streaks increases with the temperature difference between the plate and the ambient flow. Coherent structures including thermal plumes and streaks are commonly observed in Rayleigh-Benard convection [23].

Streaks in both laminar and turbulent boundary layers have been observed to grow, often due to the non-orthogonality of Navier-Stokes operators [24, 25, 25, 26]. In the presence of a flame, temperature and density gradients will surely contribute to the development of these three-dimensional disturbances. An instability in the boundary layer could be significantly modified once it encounters a flame. A combination of buoyant forces and vorticity could lead to a dramatic acceleration in the growth of this instability.

1.2 Coherent structures in diffusion flames

Diffusion flames have been studied for nearly a century, largely beginning with the pioneering work of Burke and Schumann [27], who developed a fundamental theory of combustion of diffusive gases. Later, Shvab [28] and Zel'dovich [29] attained further theoretical progress, managing to rewrite the energy equation in total enthalpies to eliminate source terms. Shortly thereafter, Spalding [30] addressed the process by which heat transfer from the flame would establish fuel pyrolysis. In 1956, Emmons [31] examined a diffusion flame within a boundary layer, developing a solution for the burning rate of a liquid fuel subjected to horizontal crossflow. This study represents one of the first and most well cited solutions of boundary layer combustion. Since Emmons, many researchers have delved into this phenomena, and several studies have closely examined the two-dimensional temperature field [32–35]. Unfortunately, a lack of detail on experimental configurations often inhibits the generalization of results; notably, the aerodynamic structure of these

boundary layers is rarely delineated [9].

In wildland fires and laboratory-scale tests, streamwise streaks (Fig. 1.1) represent the first observed instabilities, at least when the boundary layer is sufficiently developed upstream of the flame. Secondary instabilities, transition to turbulence, or conglomerations of the flame sheet into macroscopic saw-toothed structures are also observed in these flames. However, flame streaks, generally being the first observable instability, may control the development of downstream coherent structures. Length scales for these downstream structures could be governed by the growth and aggregations of streaks. It has been hypothesized that streaks could be related to the development of the flame towers (Fig. 1.2), which are the fingerlike projections along the further extent of a turbulent flame. The spacing of flame streaks and flame towers has been briefly investigated [36], but no connection between these parameters has been confirmed. Finney et al. [1] displayed a linear, positive relationship between the wavelength of flame towers and the flame length. Gorham [37] correlated the flame length with the streak spacing, obtaining a slightly negative correlation. Streaks can also be seen in pool fires and buoyant plumes, such as the experiments of Weckman et al. [2], the simulations of DesJardin et al. [11], or the simulated turbulent helium plume from Sandia [3]. In Figs. 1.3 and 1.4, these "fingering" instabilities can be observed at the base of the flame. In these cases, the streaks also appear to be oriented in the streamwise direction because the incoming flow due to entrainment is oriented towards the center of the pool.

The consistent observation of streaks in flames, even with vastly different scales and configurations, seems to indicate that a common controlling mechanism exists.

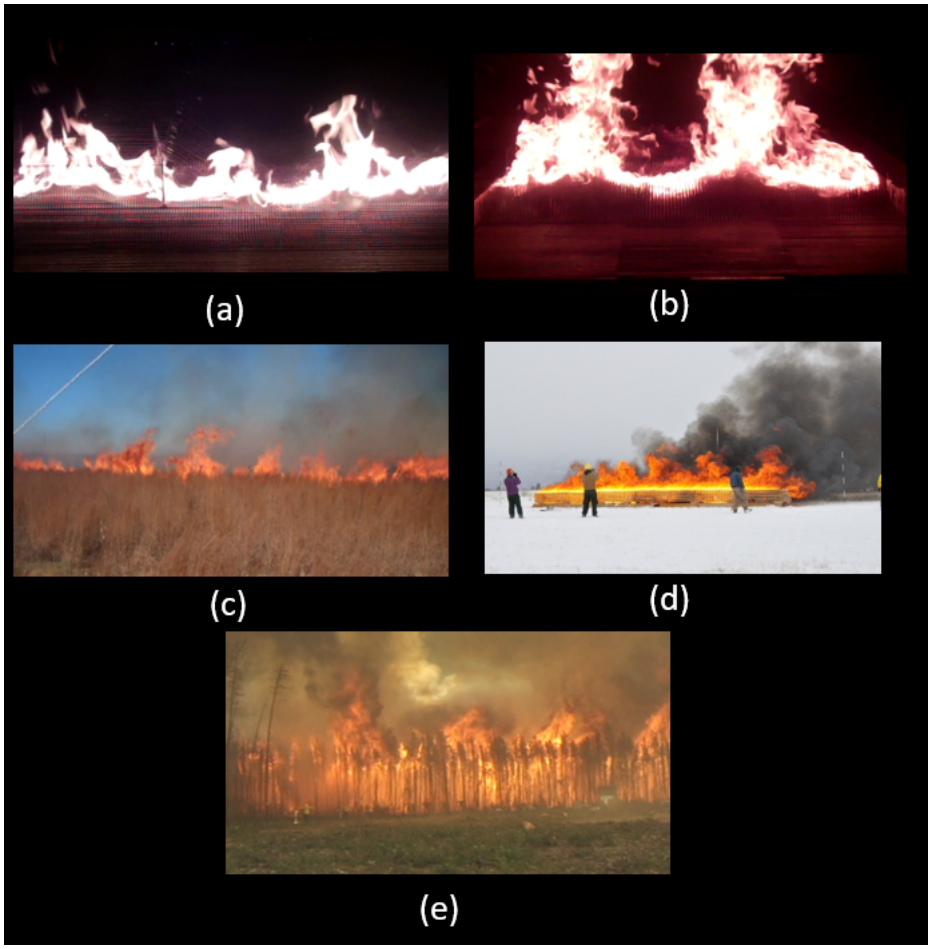

Figure 1.2: Coherent structures observed in wind-blown flames in the form of flame towers. In all pictures, a periodic sawtooth structure can be seen dominating the large-scale motion of the flame. (a) and (b) are taken from laboratory experiments, (c) is taken from a grassland fire, (d) is from a large experiment, (e) is from a crown fire. Figures have been reproduced from Finney et al. [1].

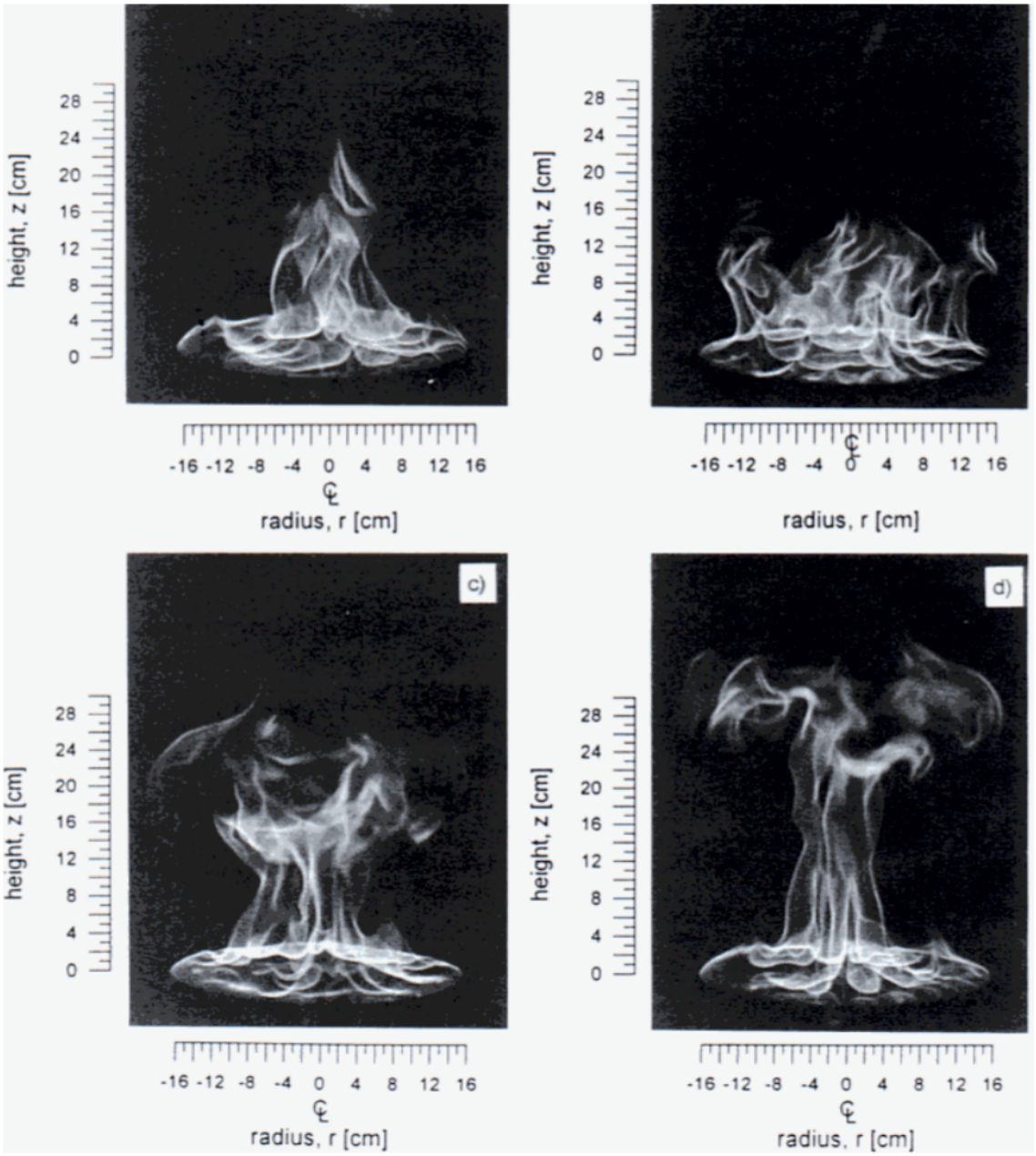

Figure 1.3: Photos of 31-cm-diameter methanol pool fire reproduced from Weckman et al. [2].

Figure 1.4: Isocontour of streamwise vorticity from LES simulations of buoyant turbulent helium plumes, reproduced from DesJardin et al. [3].

Nevertheless, the physical mechanisms establishing streaks and describing their behavior have not been satisfactorily identified, and the role of local instabilities in affecting the global properties of the flame is still unclear. The answer to this question will be relevant to types of boundary layer combustion other than wildland fires, such as that of hybrid rocket engines, process flows, building fire spread, or other wall-flame interactions. The consistent observation of streamwise streaks, in both small and large-scale fires with naturally-induced or externally-imposed winds, indicates that an account for these phenomena may be necessary for a faithful description of boundary layer combustion.

Given the novelty of discussion on this phenomenon, an exploratory investigation has been undertaken to address unresolved questions, including the following:

- What mechanisms are responsible for the onset of these instabilities?
- What mechanisms govern streak growth and development?
- Do streaks influence heat and mass transfer properties of the flow?
- What effects do these streaks have on the macroscopic properties of the flame?
- Does streak behavior govern the development of larger-scale downstream structures?

In order to breach these gaps in our understanding, a multi-faceted approach was needed. Experiments with field-scale wildland fires were unfeasible due to the scarcity of meaningful measurements that could be obtained. Wildland fires are inherently destructive and have a wide range of relevant length scales (e.g., flame

thickness, vegetation scale, atmospheric boundary layer) and variables which are difficult to control (e.g., wind, slope, fuel properties). Even spreading laboratory-scale fires are difficult to instrument with the resolution and accuracy needed to resolve such a complex problem. Consequently, stationary fires and heat sources were employed because they have known inputs, structures can be visualized clearly, measurements of high density and accuracy can be taken, and fixing the burning region to the origin gives us a statistical viewpoint of the problem. Stationary sources of buoyancy ensure that the relevant length scales associated with mixed convection, such as the development length of the upstream boundary layer, remain fixed. This important simplification allows for a detailed study of physical phenomena by providing a framework to develop wildland fire spread theory based on both observed and measured physical phenomena.

Chapter 2: Flame streaks

2.1 Introduction

It is currently unknown how a boundary layer flame modifies upstream coherent structures, and, conversely, how the introduction of instabilities modifies important characteristics of the flame, including heat and mass transfer. Approximating boundary layer combustion as a two-dimensional problem does not account for these phenomena. Given current boundary layer combustion literature, which "contain[s] a large number of assumptions [which] need careful experimental support" [9], it is necessary that the impact of the three-dimensionality observed in real flows be examined more closely. In particular, it would be useful to understand the role instabilities have in the development of a flame. This initial study represents a fundamental investigation into the importance of flow three-dimensionality in boundary layer combustion.

Characterizing flame streaks observed in boundary layer combustion represented a logical first step in the current study. Due to the chaotic nature of turbulent flow, it is more desirable to begin by characterizing these instabilities in a laminar, well-characterized flow. In the following study, these structures were actually stabilized in a laminar boundary flame, which represents a novel and powerful approach

to fundamentally characterize a streaklike instability in boundary layer combustion. A sustained streak can be carefully probed and reproduced to examine both how it responds to specific parameters and how it affects heat and mass transfer. The achievement of steady-state flow even makes it possible to use time-averaged point measurements to obtain significant spatial resolution on important flow properties. This stabilization process enabled significant analysis of a streaklike instability in a reactive boundary layer that would not have been possible otherwise.

2.2 Experimental setup and procedure

A laminar wind tunnel was employed in all experimental tests, and Figs. 2.1 and 2.2 depict relevant schematics. This wind tunnel was previously built by two former graduate students, and more detail on the construction can by found in their theses [37, 38]. The 100 x 75 x 100-cm plenum region of the wind tunnel is pressurized by an Ebm papst variable speed blower, which is controlled via a pulse-width-modulator controller. This pressurized plenum system minimizes the effects of the blower on the airflow, which passes through a 30.48-cm converging section and turbulence reduction screens. After passing through these screens, the conditioned flow moves through a 122-cm straight section with a 30.48 x 30.48-cm cross-section, open to the ambient. Through the combination of the pulse-width-modulator and an adjustable exhaust duct in the plenum region, exit wind velocities can reach anywhere between 0.5 to 6 m/s.

In boundary layer transition studies, the turbulence level can affect the be-

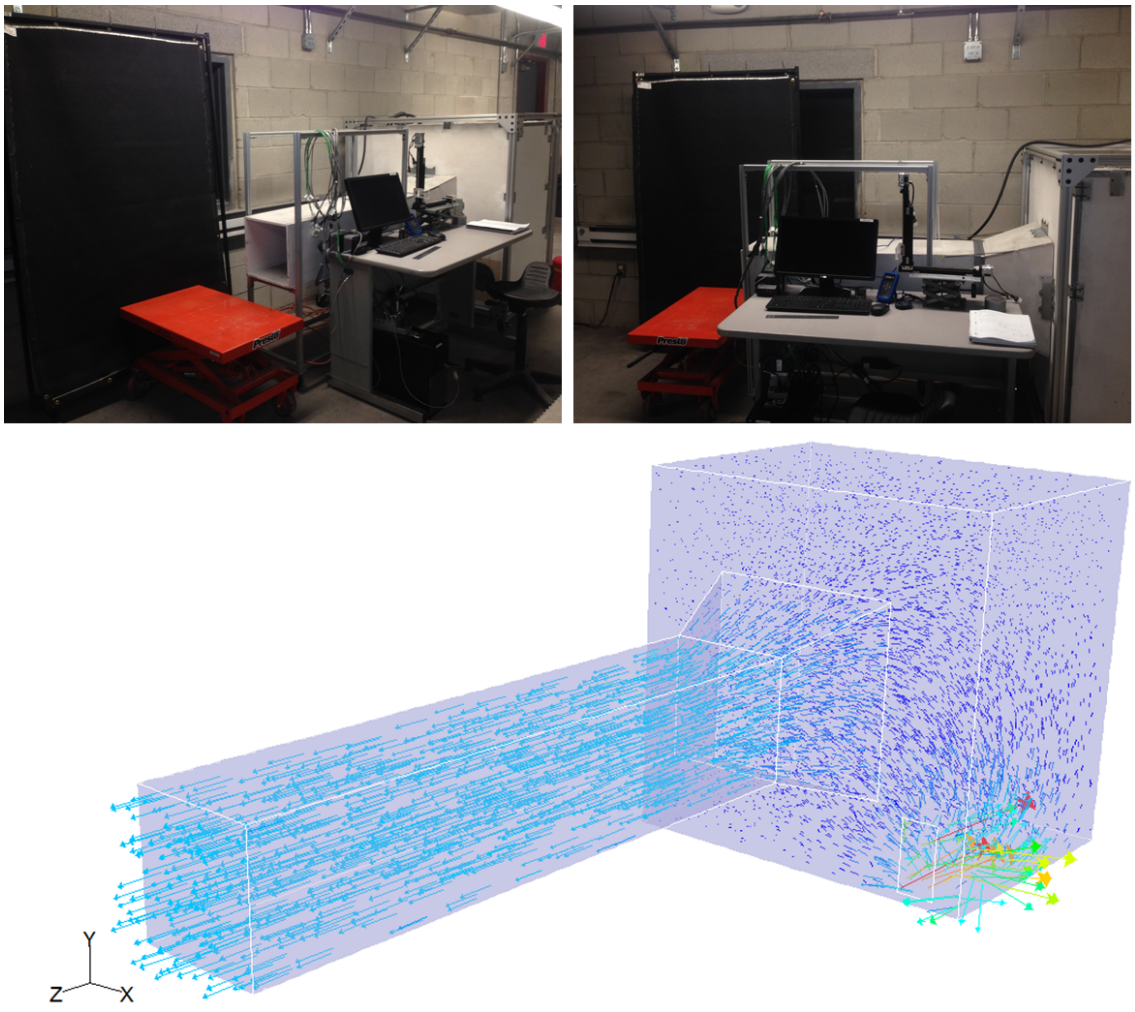

Figure 2.1: Photographs of laboratory-scale laminar wind tunnel (top) along with Fluent simulations depicting flow field taken from original wind tunnel design (bottom).

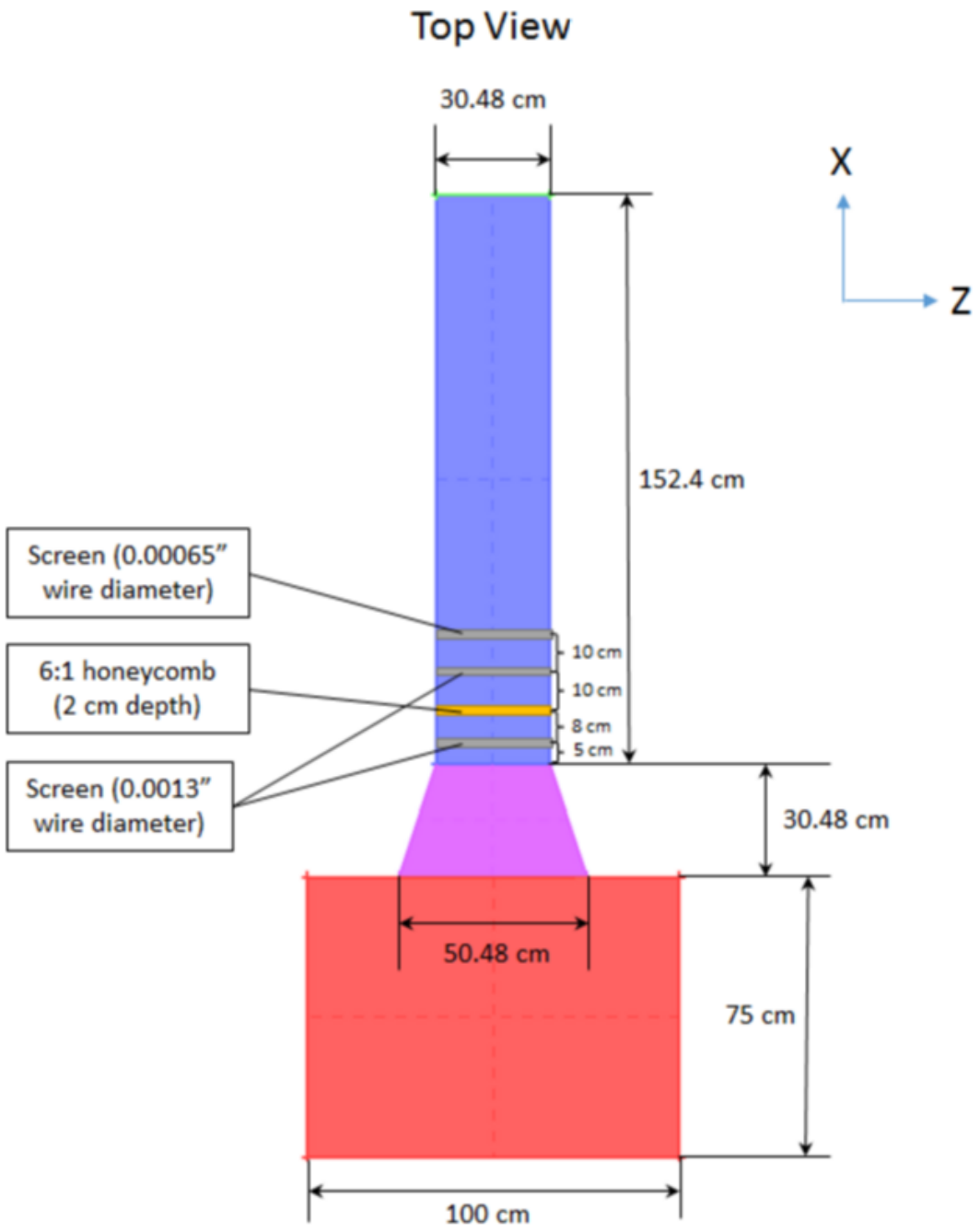

Figure 2.2: Overhead schematic of wind tunnel, depicting the chambers and flow settling screens and honeycombs.

havior of instabilities and the transition to turbulence [39]. Beyond freestream turbulence intensities of 5%, it is impossible to identify turbulent spots or flow structures [40]. For this reason, it is vital that the turbulence level be reduced to a low intensity to ensure laminarization of the flow and experimental repeatability. Therefore, a honeycomb was employed to dampen swirl and lateral velocity variations within the flow, and wire mesh screens were used to reduce turbulence by breaking up large-scale turbulent eddies [39]. Moving downstream through the wind tunnel, these screens consisted of a 0.033-mm wire mesh, a 6:1 honeycomb, another 0.033-mm wire mesh, and a 0.017-mm mesh. The maximum Reynolds number associated with the mesh screens was 105, calculated using a wire diameter and the maximum wind velocity. In order to test flow uniformity, the wind tunnel exit was fully characterized. At all blower speeds, the turbulence intensities in the bulk portions of the wind tunnel exit were on the order of 0.3-0.6%. For a wind tunnel setting of 1 m/s, maps of the velocity field and turbulence intensities are displayed in Figs. 2.3 and 2.4. Low levels of turbulence were observed across the vast majority of the cross-section, so the wind tunnel was determined to be adequate for the repeatable development of a laminar boundary layer.

The rest of the experimental configuration, displayed in Fig. 2.5, was placed at the exit of the wind tunnel. A 0.25-inch-thick aluminum plate of length 30 cm and width of 45 cm with a super elliptical 8:1 aspect ratio leading edge was positioned nearly adjacent to the wind tunnel exit. This design was employed to minimize boundary layer separation and bluff body effects [41, 42], which could disturb the development of a laminar boundary layer, create a recirculization zone, or introduce

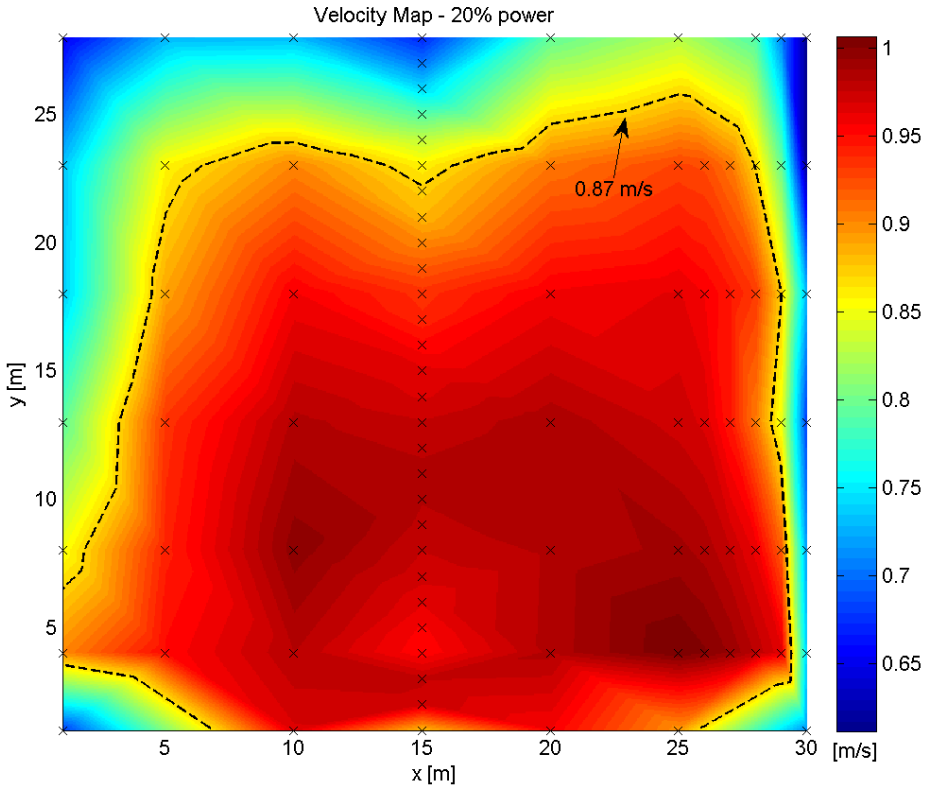

Figure 2.3: Velocity map at the wind tunnel exit for a velocity of 1 m/s. Measurement locations are indicated by X's, and the data is interpolated between these locations. The dashed line represents the outer edge of the region within 13% of the prescribed velocity.

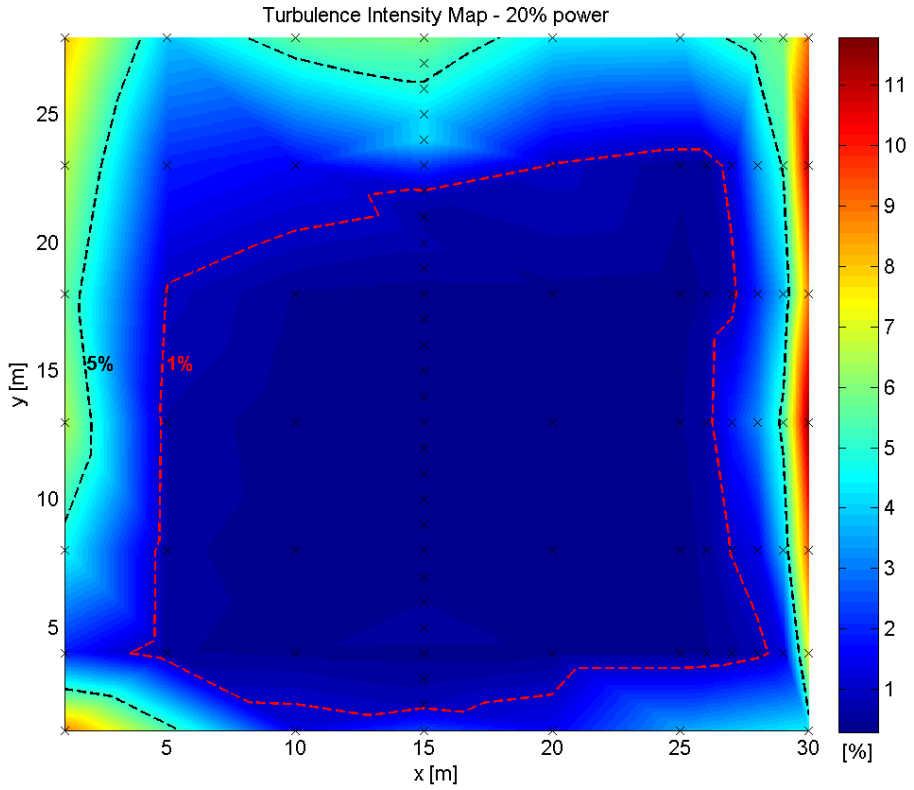

Figure 2.4: Turbulence intensity map at the wind tunnel exit for a velocity of 1 m/s. Measurement locations are indicated by X's, and the data is interpolated between these locations. The dashed line represents the outer edge of the region within a turbulence intensity of 1%.

strong disturbances into the boundary layer. For several of the flame visualization tests, this aluminum plate was replaced with 0.032-inch-thick aluminum sheets of various lengths; the thin metal lip of these sheets would minimize bluff body effects, albeit not as effectively as the machined aluminum plate. The boundary layer development length was dictated by the length of the metal sheet or plate. Immediately following this length, a propane sand burner was placed, with its surface held flush to the lip of the aluminum. The 8-cm-deep burner was made with 3-mm-thick stainless steel with a 25 x 5-cm cross-sectional opening to the ambient. 100 % propane fuel (50.3 MJ/kg heat of combustion) entered an NPT bulkhead fitting towards the bottom, distributed within a 2-cm-tall plenum, passed through a metal honeycomb and mesh screen, and finally diffused evenly through 6 cm of multi-purpose sand (diameter of 0.1-0.5 mm). The flow rate through the sand burner was monitored by a mass flow meter connected to a propane cylinder, and care was taken to ensure gases were distributed evenly. Unless indicated, the flow rate of propane was maintained at 2.5 slpm (7.8×10^{-5} g/s). Beyond the burner, a horizontal sheet of insulation (1.27-cm-thick alkaline earth silicate wool) was used to maintain a horizontal surface over which the flame would develop. A laminar boundary layer formed over the upper surface of the apparatus, and a diffusion flame was stabilized within this boundary layer. Two 30-cm-tall sidewalls served to extend the vertical walls of the wind tunnel for 85 cm downstream; this lessened the effects of ambient mixing and eliminated disturbances due to crossflow.

Temperature measurements were made using R-type (Pt/13%Rh vs. Pt) thermocouples of 75 μm (0.003 in.) wire diameter with a bead of approximately 150 μm

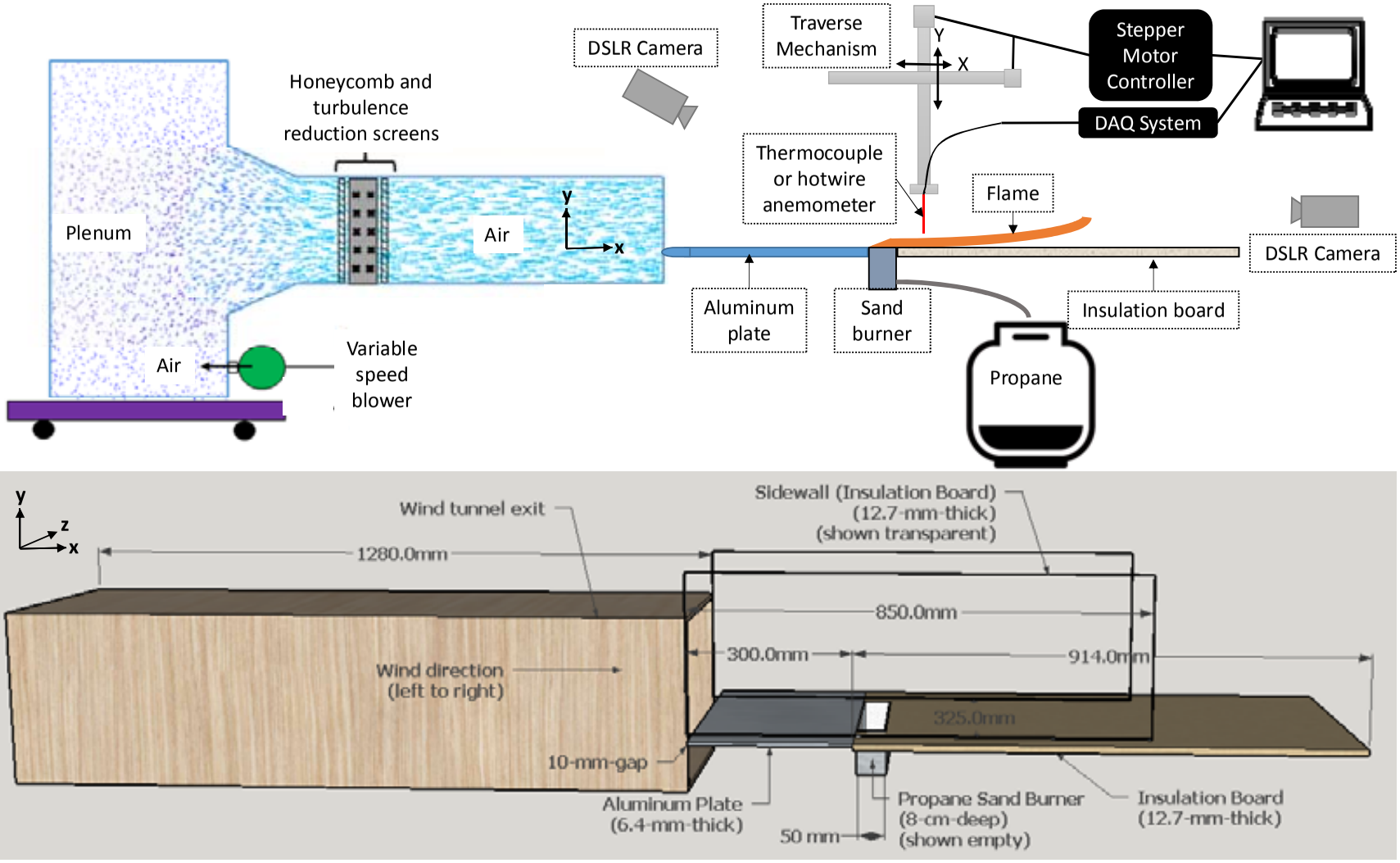

Figure 2.5: Schematic of experimental setup (top) and a three-dimensional rendering of the outlet of the tunnel and experimental setup (bottom). Note that sidewalls on the bottom frame are displayed as transparent.

in diameter. The measurement range for these thermocouples extends to approximately 1900 K. The thermocouples were sheathed with a twin bore ceramic cylinder which left the bead exposed. Voltage signals from the thermocouples were acquired, conditioned, and digitized though a National Instruments 24-bit high-density 16 channel thermocouple module (NI 9214). The measurement sensitivity of this device was up to 0.2°C. LabVIEW software was employed for all data acquisition. In order to measure temperatures at precise locations in the flow, the thermocouple was mounted to a Velmex X-Y unislide, which could traverse the flame with a spatial resolution of up to 1.5 μm. This traverse mechanism enabled temperature mapping across 2-D cross-sections of the diffusion flame. All temperature data was acquired at the rate of 100 samples/second.

Velocity measurements were made using a Dantec Dynamics MiniCTA anemometer system. This system employed a cable equipped miniature wire probe (55P16), which housed a hot wire sensor of 5 μm in diameter and 1.25 mm in length. Voltage date from the CTA was acquired using LabVIEW infrastructure at a sampling rate of 50,000 samples/second. For all velocity measurements recorded at a given spatial position, data was collected for a duration of at least 30 seconds.

Two cameras, a Nikon digital SLR camera (D7100) and a Sony digital camera (DSC-RX10M II), operating from two different vantage points were employed in order to visualize coherent structures in boundary layer flames. The Nikon was placed above the wind tunnel exit in order to photograph the flame from an overhead view. The Sony was placed downstream of the experimental apparatus, oriented into the flow and at the same level as the burner. Camera settings were adjusted

in order to obtain crisp, instantaneous images of the luminous flame at intervals of approximately one second over a 30-second period. Most images clearly revealed the nature of coherent structures within the flame.

Surface heat fluxes were measured by a Vatell water-cooled total heat flux gauge (model HFM1000-0, serial number 3128) at 100 Hz. Before taking the measurement, the heat flux gauge was calibrated against a known standard incident heat flux sensor in a cone calorimeter. An amplifier was employed to make the data output readable by the data acquisition system.

2.3 Mechanisms driving onset of flame streaks

Streamwise streaks have been observed in both flames and in smoke from flames [1]. The observed saw-toothed structure is a manifestation of streamwise counter-rotating vortices, which promote upwash and downwash regions of the reaction zone. Dominant modes appear to govern the spanwise spacing, or the wavelenth λ, of streaks. In fact, this length scale has been shown to be lognormally distributed [36,37] even when flame streaks are meandering. This consistent behavior points to some sort of physical mechanism that is controlling the spacing. The two most viable mechanisms for the onset of streaks are momentum, in the form of the incoming boundary layer, and buoyancy, in the form of a buoyant instability. The following sections describe analysis each of these possibilities in turn, one of which is eventually shown to be the clear controlling mechanism.

2.3.1 Buoyancy-driven onset (Rayleigh-Taylor Instability)

It is arguable that the buoyant force of the flame governs the spanwise spacing through the onset of streaks in the form of a Rayleigh-Taylor instability (RTI). This phenomenon occurs at the interface of fluids with different densities, such that a high-density fluid lies below a low-density fluid where gravity can accelerate mixing. Small perturbations at the interface eventually lead to the displacement of the lighter fluid by the denser fluid. In our experimental study of a wind-blown flame, the hot gases surrounding the reaction zone would comprise the lower, lighter fluid, while the ambient air in the crossflow would be the upper, dense fluid. In this scenario, it is conceivable that observations of flame streaks would represent the initial perturbations of a Rayleigh-Taylor instability. In fact, it has been argued that Rayleigh-Taylor instabilities develop at the small-scale in buoyancy-dominated diffusion flames and eventually encompass the entire flow [43]. Mushroom-cap structures have been observed emanating from streaks in several inclined laboratory experiments [36], as shown in Fig. 2.6. Mushroom-caps are characteristic manifestations of Rayleigh-taylor instabilities, giving credence to the idea that buoyancy controls the onset of streaks.

If Rayleigh-Taylor instabilities govern the onset and spacing of the flame streaks, linear stability theory may govern the early-time dynamics. The following analysis is based on methods used by Verma [44], who detailed linear stability theory (LST) more thoroughly and provided significant insight for this analysis. LST is valid while the perturbation size is small in order that higher order terms can be

Figure 2.6: Characteristic mushroom-cap manifestations of an RTI in several images from previous inclined experiments. The left and middle images are taken from the top- view of a 20° inclined test. The rightmost image is taken from the downslope-facing view for a 20° inclined test.

eliminated in a Taylor expansion to linearize the governing equations. Consequently, the perturbation height is described as:

$$H(t) = a_0 \cosh nt - \frac{u_0}{n} \sinh nt \tag{2.1}$$

where a_0 is the initial perturbation height, u_0 is the initial velocity at the interface, n is the exponential growth factor, and t is time. There are several ways to account for n, the exponential growth factor. Perhaps the simplest definition would be to ignore viscosity and diffusion such that

$$n_1 = \sqrt{Agk} \tag{2.2}$$

where g is gravitational acceleration, k is the wavenumber, and A is the Atwood number. A is a measure of the density difference, and it is defined as

$$A = \frac{\rho_1 - \rho_2}{\rho_1 + \rho_2} \tag{2.3}$$

where ρ_1 is the density of the heavier fluid and ρ_2 is the density of the lighter fluid.

If we include viscosity in our analysis, the exponential growth factor becomes

$$n_2 = \sqrt{Agk + v^2k^4} - vk^4 \tag{2.4}$$

where v represents viscosity. We can also incorporate diffusivity. In our scenario, we expect thermal diffusivity, α, to have roughly the same effect as the mass diffusivity; consequently, we can write the exponential growth factor as

$$n_3 = \sqrt{\frac{Agk}{\psi} + v^2k^4} - (v + \alpha)k^2. \tag{2.5}$$

These three growth factors represent increasingly complex descriptions of instability amplification. For n_2, which incorporates viscosity, and n_3, which incorporates viscosity and diffusion, a most dangerous mode appears. In other words, there is a specific wavenumber that corresponds to maximum amplification. This mode will outpace all other modes, causing the most exagerrated spatial growth of an instability such as a flame streak. The most dangerous mode (MDM) predicted by these formulations can then be compared to experimental and numerical observations. Using the aforementioned equations, plots of the growth rates were obtained vs. the wavenumber k in Fig. 2.7. A simple conversion enabled a spanwise length scale λ to be extracted from the wavenumber, and plots vs. this distance are displayed in Fig. 2.8. These results were obtained using dry air properties of 300 K for the heavier fluid and 1000 K, a reasonable assumption for a flame temperature, for the lighter fluid. As you can see from these plots, two most dangerous modes are predicted. Looking at Fig. 2.8, n_2 predicts the MDM at a spanwise wavelength

of approximately 1 cm, while n_3 predicts a wavelength of 2.5 cm. These results are on the same order of experimentally measured wavelengths (2.6 cm for a 30-cm boundary layer and 1.9 cm for a 10-cm boundary layer). However, these results still do not explain why there appears to be a dependence of wavelength on the boundary layer height. Additionally, experiments, even well-controlled investigations of Rayleigh-Taylor Instabilities, typically exhibit uncharacterized initial perturbations and undesirable flow disturbances [45]. Without characterizing potential disturbances, one cannot definitively conclude that buoyant instabilities are governing the spacing onset.

Different results for linear stability theory can be obtained if the temperature of the hot gas is altered, thereby changing the density. Although a flame temperature is not easily manipulated, it is possible to alter the strength of a different source of buoyancy, such as a hot plate. By changing the temperature of an isothermal hot plate, the source of buoyancy can be easily modified. Numerical simulations of heated plates in crossflow have already revealed remarkable similarity to our wind-blown flames, both in the large-scale geometry and in the appearance of streaky coherent structures [44]. The amplification and liftoff of coherent streaks in both reactive and non-reactive flows is likely controlled by the relative buoyancy of hot gases. Regardless, it is unclear whether these buoyant forces also control the onset of streaks. If the arguments applied in linear stability theory hold, we should be able to extend this analysis to a hot plate with lower gas temperatures than a flame. Fig. 2.9 displays the results if we lower the hot gas temperature to 500 K. In this scenario, the most dangerous modes for n_2 (viscosity) and n_3 (viscosity and diffusion)

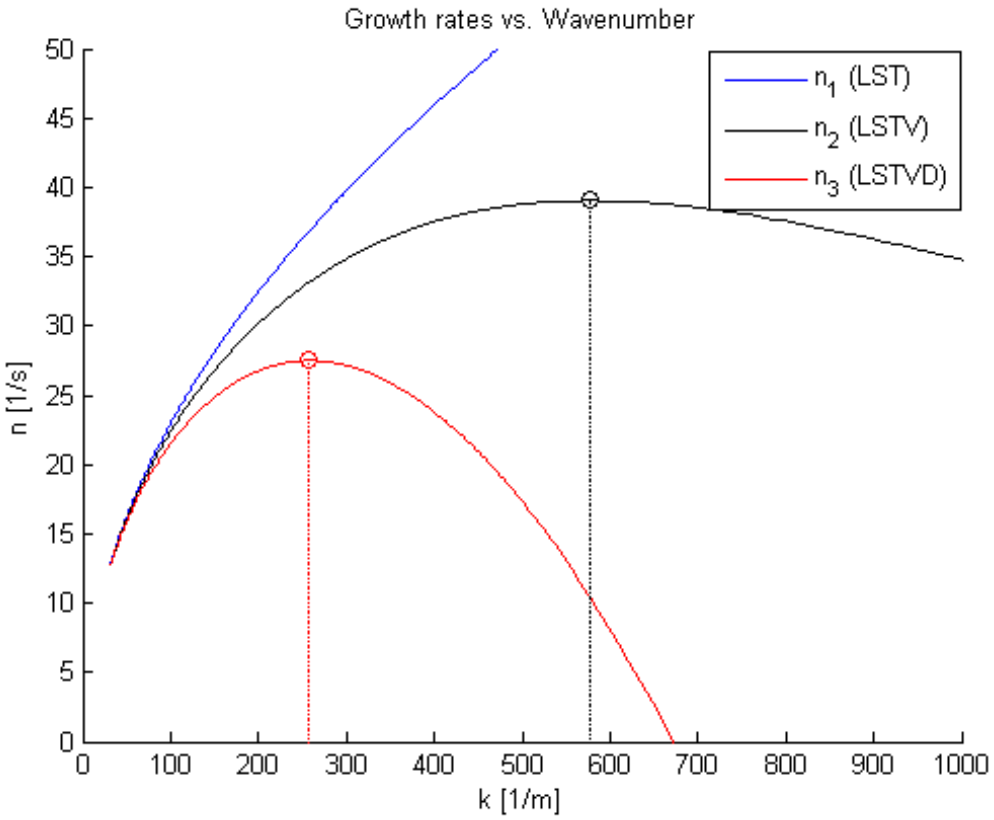

Figure 2.7: Growth rates of Rayleigh-Taylor instability vs. wavenumber, for three different variants of linear stability theory. n_2 accounts for viscosity and n_3 accounts for both viscosity and thermal diffusion. The most dangerous mode is depicted by the line descending from the peak growth rate. The temperature of the hot fluid is $1000K$, representative of a flame, while the cold fluid is 300 K.

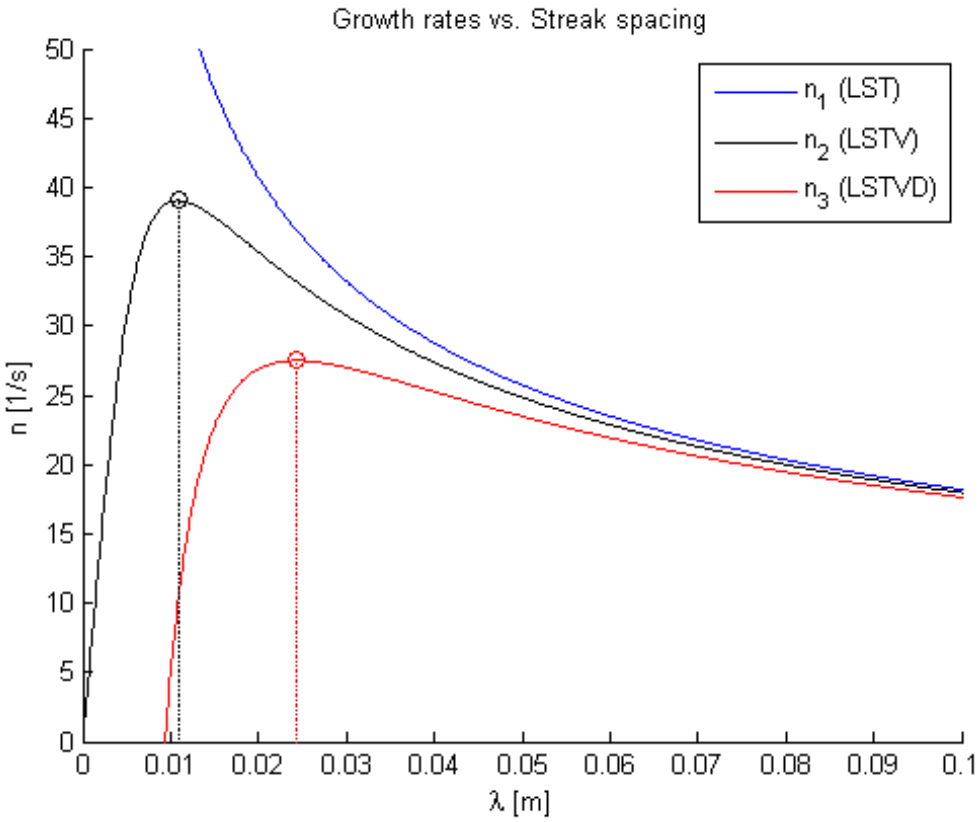

Figure 2.8: Growth rates of Rayleigh-Taylor instability vs. wavelength, for three different variants of linear stability theory. n_2 accounts for viscosity and n_3 accounts for both viscosity and thermal diffusion. The most dangerous mode is depicted by the line descending from the peak growth rate. The temperature of the hot fluid is $1000K$, representative of a flame, while the cold fluid is 300 K.

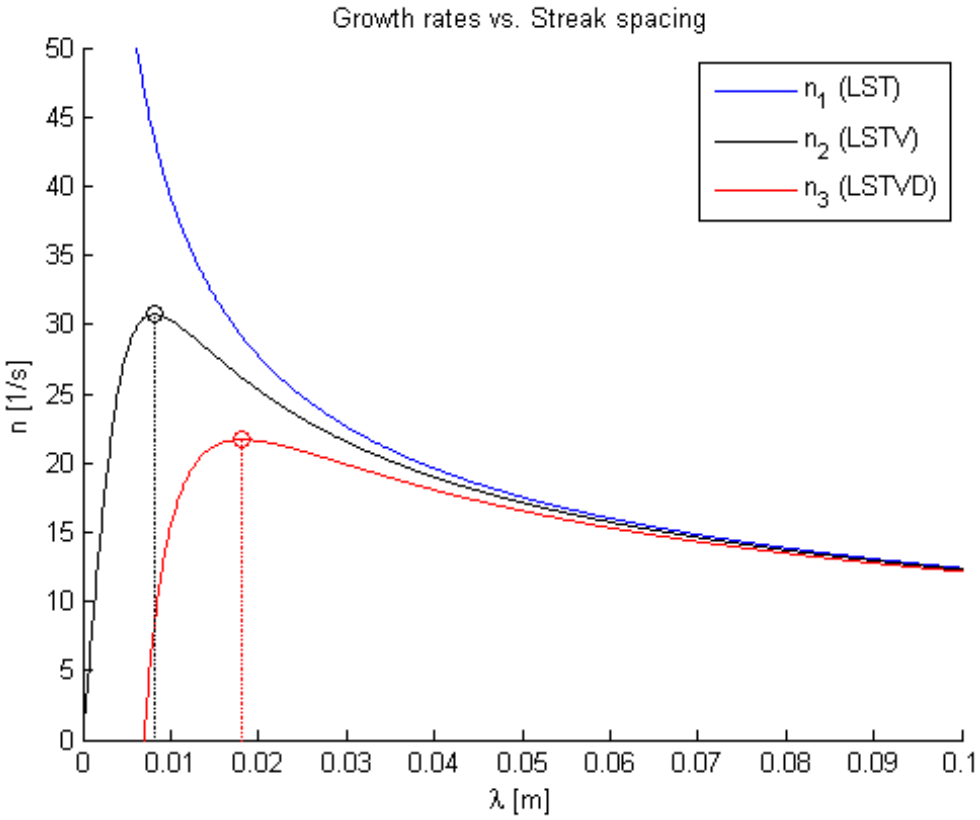

Figure 2.9: Growth rates of Rayleigh-Taylor instability vs. wavenumber, for three different variants of linear stability theory. n_2 accounts for viscosity and n_3 accounts for both viscosity and thermal diffusion. The most dangerous mode is depicted by the line descending from the peak growth rate. The temperature of the hot fluid is $500K$, representative of a hot plate, while the cold fluid is 300 K.

are observed at 0.9 and 1.8 cm respectively. Linear stability theory clearly predicts a significant dependence of streak spacing on temperature difference. Future tests with isothermal hot plates can re-examine this predicted trend.

2.3.2 Onset due to shear: pre-existing disturbances in upstream boundary layer

Although buoyancy undoubtedly plays a strong role in the late-time fluid dynamics of a wind-blown flame, it is likely that a different mechanism could govern

the onset of flame streaks (at least for this particular experiment). Streaklike instabilities may actually develop due to disturbances that already exist in the incoming flow. In such a scenario, inhomogeneities associated with the incoming boundary layer would preset the spacing and onset of observed flame streaks.

Assessment of our experimental setup in light of existing literature indicates that streamwise streaks are commonly observed in laminar boundary layers with low levels of free stream turbulence. In laminar boundary layers, streaks caused by Klebanoff modes are generated by certain receptivity mechanisms, some of which include propagation of a freestream vortex into the boundary layer [46, 47], interaction of oblique waves [48, 49], or stretching of vortex lines around the blunt leading edge [40, 50, 51]. Evidence from experiments indicates that freestream disturbances from small nonuniformities in wind tunnel screens can also instantiate Klebanoff modes [52]. Streaks remain the dominant flow structure as turbulence intensity increases [53]. The theory proposed by Goldstein et al. [40] describes how distortions in flow upstream of the leading edge can promote Klebanoff modes. Mechanisms in this paper apply for turbulence intensities of less than 5%, implying that the relevant theory is quite applicable to our experimental setup. The boundary layer on the surface of our plate likely acts as a filter for free-stream turbulence, amplifying low frequency structures to initiate Klebanoff modes. Stretching of the vortex lines around the leading edge introduces the necessary streamwise vorticity and amplifies the low frequency component of vorticity. Perturbations originating from the free stream turbulence are passed into the boundary layer by vortex stretching at the leading edge.

Behavior of flame streaks could certainly be analogous to Klebanoff modes. As described previously, we see a transition in flame streaks as the boundary layer is extended. We see streaks transition from meandering structures with a smaller wavelength to stable, ordered structures with increased spacing as the boundary layer development length is increased. The transition to flame streaks with fixed spanwise locations seems to occur after a distance of about 15-20 cm. This is not unlike the experiments of Deng et al. [13]. Here, the earliest-born streaks are shorter in length and are not sustained, but, beyond a certain distance, a set number of streaks persists over time at fixed locations. The observed transition to a constant spanwise length scale was also explained by Goldstein et al. [54]. Free stream turbulence and/or flow distortion at the leading edge drive Klebanoff modes. These modes eventually run out of energy when the spanwise length scale becomes too small. In essence, this forms a selection mechanism for the spanwise length scale. This explanation appears to reasonably explain the behavior of streaks in our experiment. Klebanoff modes are known to have a spanwise length scale on the order of the boundary layer thickness. Linear analyses performed by Luchini [47] and Andersson et al. [46] indicate that streamwise vortices with a spanwise separation of 1.4 times the boundary layer thickness experience the most amplified growth. According to Blasius scaling at 1.2 m/s, our boundary layer thickness should be approximately 1 cm in height 30 cm downstream of the leading edge. This results in an estimated streak spacing of 1.4 cm, which is of the same magnitude as our observations (2.6 cm).

We experimentally investigated whether disturbances analogous to Klebanoff

modes existed in our velocity boundary layer. Hotwire anemometer measurements were taken while the burner was inactive because the maximum operating temperature of the hotwire was only 150°C. Furthermore, cold flow measurements were necessary to confirm that velocity perturbations were not induced by the flame. The spanwise distribution of streamwise velocity within the boundary layer was measured 27 cm downstream of the leading edge (3 cm ahead of the burner). Klebanoff modes have been reported to have a peak value at a Blasius η value ($\eta = y\sqrt{\frac{U}{2\nu x}}$) of about 2.3 [40]. This results in a value of $y \approx 2$ mm for $U = 2.2$ m/s, so we decided to traverse our probe 3 mm above the surface. The wind tunnel free stream velocity was 2.2 m/s and the boundary layer development length was 30-cm. Measurements were taken in the spanwise direction every 5 mm, with a sampling period of at least 30 seconds. Results are displayed as the black line in Fig. 2.10, and it is immediately clear that inhomogeneities exist within the boundary layer flow. Regular velocity fluctuations of +/- 0.15 m/s exist at intervals of approximately 2.6 cm.

Subsequently, the propane burner was turned on and top-view pictures of flame streaks were taken. Images were processed in MATLAB. Examining a spanwise subset of the flame streaks, the luminous intensity was obtained as a function of spanwise distance. Because the bright flame streaks are expected to appear in regions of low velocity, the luminous intensity was inverted and plotted on top of the previous velocity measurements. In this way, the peaks in velocity should correlate with the high levels of darkness between the streaks, and results are plotted in Fig. 2.10. Looking at this plot, we see a clear correlation between the location of the flame streaks and the velocity perturbations in the cold flow. Not only do

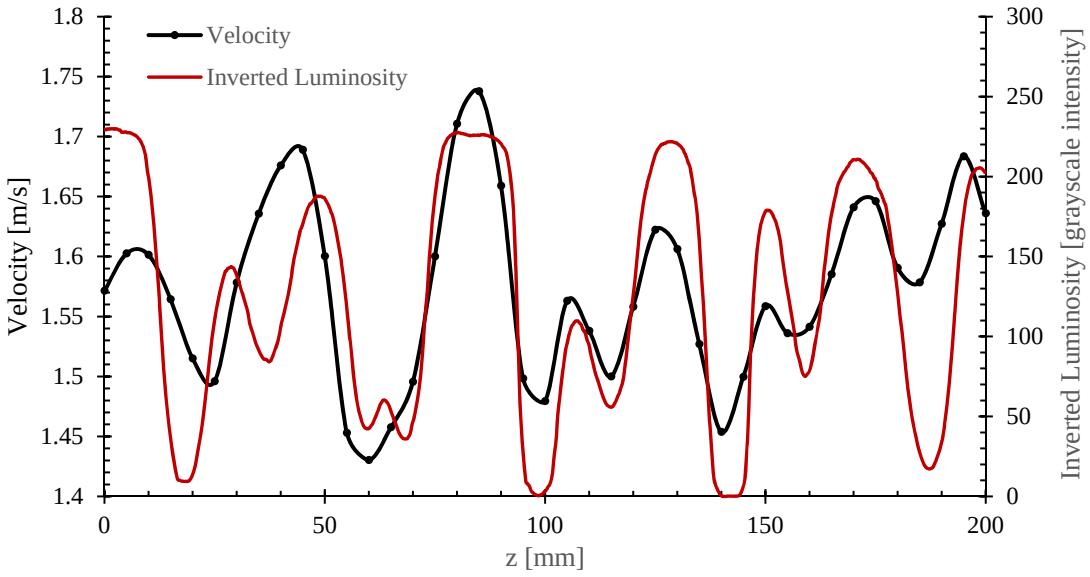

Figure 2.10: Spanwise variation of streamwise velocity overlaid with the spanwise variation of the inverted luminous intensity of a picture of flame streaks. The velocity was measured 3 mm above the surface and 27 cm downstream of the leading edge in a test where no flame was present. The inverted luminosity was obtained from an overhead picture of luminous streaks in the flame. Results are plotted over the spanwise direction, and the free stream velocity was 2.2 m/s in both tests.

the locations of the perturbations align well, but the amplitude of the perturbations correlates as well. When the velocity perturbation is large, the associated perturbation in luminosity is also large. This result effectively confirms the hypothesis that the flame streaks in our specific experiment are controlled by pre-existing structures in the flow.

2.4 Coherent structures in flame visualizations

It is common practice to employ tracers in wind tunnels to obtain greater insight into the nature of the flow field around obstructions. In boundary layer diffusion flames, the flame itself can function as a tracer, revealing coherent structures

within the flame sheet. Examining these coherent structures in detail can give valuable insight into the mechanisms controlling both heat and mass transfer. In our experiments, the upwash regions of counter-rotating vortices serve to create streaks, which are visible as luminous regions. This luminosity is a direct consequence of the presence of soot, which is produced in the upwash regions more than the downwash regions where oxygen is more readily supplied. In other words, soot acts as a unique flow tracer that can be used to track coherent structures such as streaks.

Digital SLR cameras were employed to photograph coherent structures, which were observed to change with the parameter space of the experiment (i.e., as the wind speed and the boundary layer development was varied). Perhaps the most notable observation was due to the change in the boundary layer development length, which is depicted in Fig. 2.11. When the boundary layer development length was only 10-cm in length, the flame resembled a lattice, within which spanwise waves and streamwise streaks would appear, meander, and disintegrate. This behavior was reproducible at all wind velocities above 1 m/s. As the wind speed was lowered, spanwise waves propagating through the flame would become wider and more pronounced.

Markedly different behavior was observed when the boundary layer development length was extended to 30-cm in length. This experimental observation is shown in the bottom row of pictures in Fig. 2.11. For all wind speeds above 1 m/s, steady, streamwise streaks were observed. These streaks would not meander across the width of the burner, but would remain locked in place with only slight sinuous movements. Visible streaks would remain distinct and avoid merging with

neighbors. We witnessed the transformation from a meandering, unsteady lattice to ordered, stationary streaks as the boundary layer was extended. The streak spacing is approximately 2.6 cm, which matches the wavelength of velocity perturbations from Fig. 2.10.

Fig. 2.12 displays the aforementioned observations from a surface-level viewpoint, obtained downstream of the burner. In this way, the vertical growth and development of the coherent structures is visualized. For the 10-cm boundary layer development length, structures are seen to rapidly meander across the spanwise width, exhibiting short, volatile lifespans. For the 30-cm development length, steady flame streaks exhibiting minimal fluctuations are observed across the entire width of the burner.

Examination of multiple images for different configurations enabled quantification of the spanwise spacing between streaks. In tests where the boundary layer development length is 30 cm, image analysis reveals spacing that is on the order of 2.6 cm. As this development length is *decreased* to 10 cm, the spacing also decreases, falling to roughly 1.9 cm at the onset of the burner. Due to the meandering nature of streaks in the 10-cm boundary layer, this number fluctuates significantly. Additionally, the choice of the measurement location can alter the reported spacing. Further downstream, streaks begin to merge, leading to an increase in the reported spacing between streaks. Consequently, reported measurements are taken from the earliest (most upstream) visual indications of flame streaks; in this way, the reported result represents a reasonable estimate when averaged over multiple images.

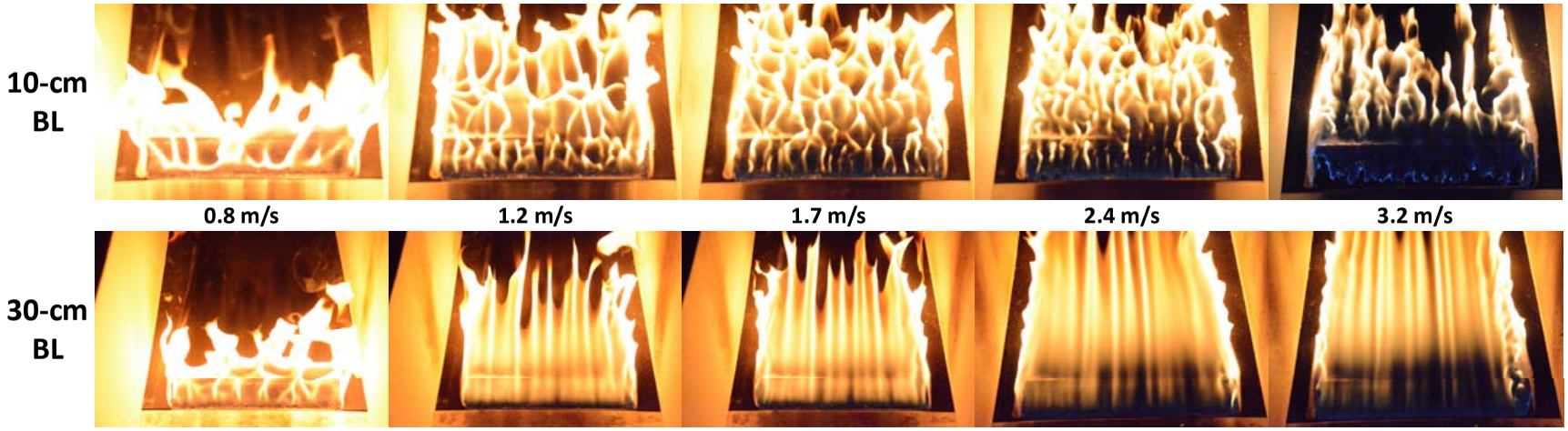

Figure 2.11: Overhead view of flames under different wind velocities and boundary layer development lengths. The top pictures were taken from experiments with a short boundary layer development length, resulting in a meandering lattice of spanwise waves and streamwise streaks. The lower pictures were taken from experiments with a longer boundary layer development length, which exhibited stable streamwise streaks. In order to highlight coherent structures, the flow rate of fuel in these pictures was 5.5 slpm (1.7×10^{-4} g/s), slightly elevated above typical experimental conditions used in later analyses of the study. The width of the burner and the resultant flame is 25 cm, and the total distance between the white sidewalls is 32.5 cm.

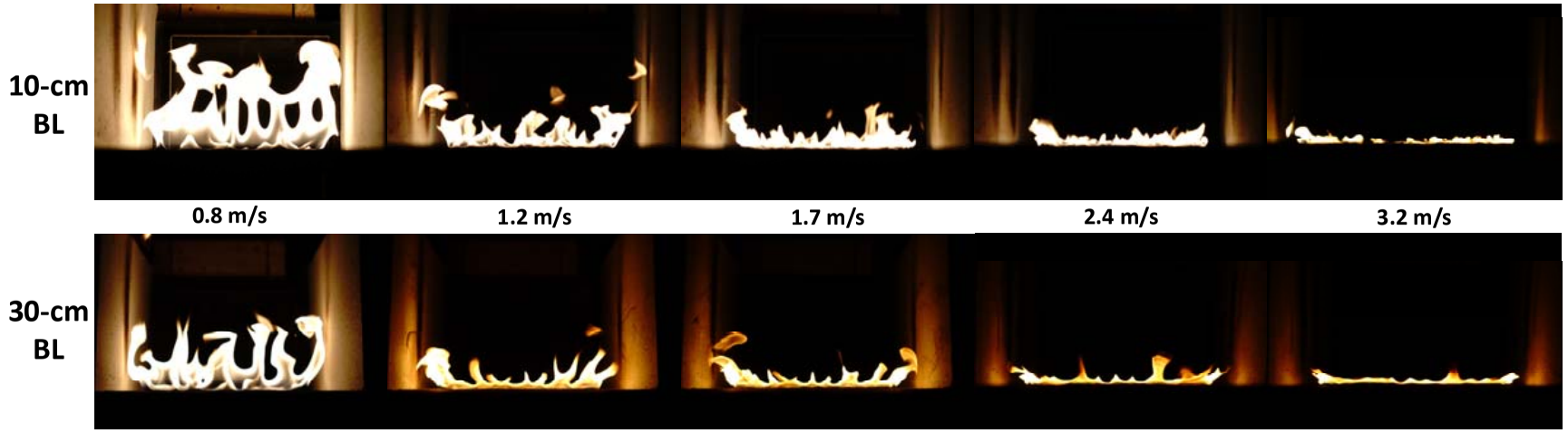

Figure 2.12: Downstream view of flames under different wind velocities and boundary layer development lengths. The top pictures were taken from experiments with a short boundary layer development length, resulting in meandering structures. The lower pictures were taken from experiments with a longer boundary layer development length, which exhibited stable streamwise streaks. In order to highlight coherent structures, the flow rate of fuel in these pictures was 5.5 slpm (1.7×10^{-4} g/s), slightly elevated above typical experimental conditions used in later analyses of the study.

2.4.1 Discussion

The recognition that pre-existing structures control flame streak spacing in our configuration provides several insights into the nature of these instabilities. As a first point, this finding helps to explain the divergent behavior observed in different boundary layers: a short boundary layer development length (10 cm) produces varied, meandering structures, including spanwise waves, while consistent flame streaks will not form unless the development length is longer (30 cm). The flame appears to be taking on the coherent structures already present in the velocity boundary layer. Observed structures appear analogous to coherent structures in nonreactive boundary layers (see Fig. 2.13), in which streamwise vortices inhabit the near-wall region, spanwise vortices are observed in the outer region, and a mix of spanwise and streamwise vortices populate the intermediate region [4]. This behavior also mirrors observations from Rayleigh-Benard convection (natural convection phenomenon between a hot lower surface and a cold upper surface). Haramina [55] describes coherent structures, visualized with dye, moving along the hot lower surface of his water-filled apparatus. Spanwise waves are seen when the layer of dye is thicker than the velocity boundary layer; streamwise streaks are seen when the layer of dye is thinner than the velocity boundary layer. These findings are in agreement with an earlier study [23], where waves were described atop the velocity boundary layer in Rayleigh-Benard convection. Our experiments coincide with these observations. The height of the incoming boundary layer determines whether streamwise streaks, spanwise waves, or a combination of the two will inhabit the flame sheet. For this

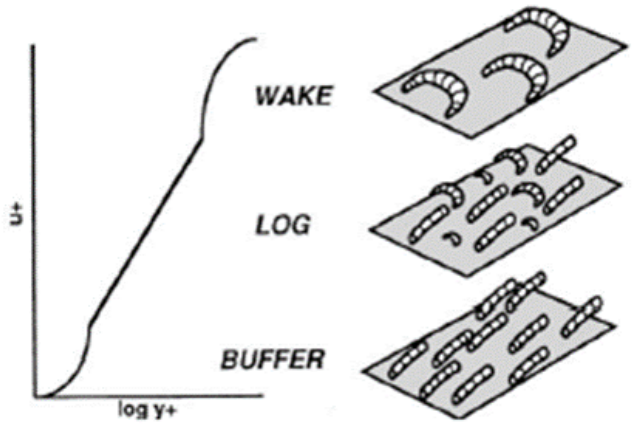

Figure 2.13: Coherent structures observed in shear flow. Reproduced from Robinson [4].

experimental configuration, the incoming velocity field, and not just the buoyant force of the flame, clearly plays a role in governing coherent structures.

Fig. 2.14 provides a schematic to describe the processes believed to be responsible for the onset and development of streaks in our experiment. The leftmost diagram depicts a flame sheet that is initially unperturbed. However, pre-existing disturbances, likely in the form of counter-rotating streamwise vortices, lie directly above the diffusion flame. These vortices create the inital perturbations associated with the flame streaks, lifting the flame in upwash regions and suppressing the flame in downwash regions. It should be noted that the upwash regions in non-reactive flow consist of fluid that has been lifted up from the near wall region; consequently, it has a low streamwise velocity [10].

If the upwash region has a lower velocity, we expect the buoyant force to be relatively higher than the downwash regions, leading to noticeable growth. This amplification process is due to a buoyancy difference, so the observed growth is likely described by Rayleigh-Taylor scaling. Further downstream, the Rayleigh-Taylor

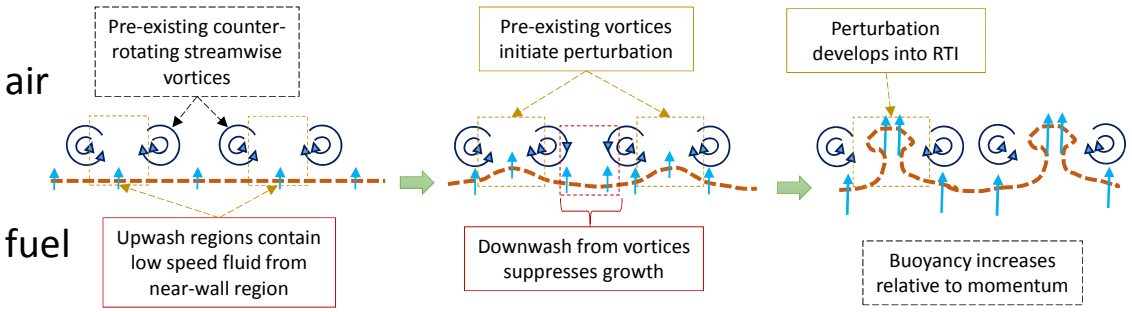

Figure 2.14: Schematic displaying the process by which flame streaks originate and develop in this experimental setup.

growth will progress beyond the linear regime. This process is likely responsible for the observed mushroom-caps in preliminary experiments (see Fig. 2.6). Finally, it should be noted that the spacing of streaks in the ambient flow happens to match up well with the predicted streak spacing of linear stability theory. Because there is no discrepancy between the natural disturbances of the flow and the most dangerous mode of buoyant instabilities, streaks do not merge and new streaks are rarely born. Buoyant instabilities readily adopt the preset spanwise frequency since it closely mimics their own natural wavelength.

It should be noted that stationary streaks, which we have established in this experiment, will not be producible within a turbulent boundary layer. In a turbulent boundary layer, large velocity fluctuations will increase the volatility of streaks. Flame streaks will meander rapidly in spanwise directions, occasionally merging and aggregating. This behavior was accidentally witnessed in our own experimental configuration, when blockage of the screens promoted high values of turbulence. At larger scales such as a wildland fire, where turbulence is more likely, this behavior is expected. Additionally, the source of these instabilities will differ. In the laminar

boundary layer of our experiment, Klebanoff modes dictate the instabilities passed into the flame; in a wildland environment, upstream vegetation or atmospheric instabilities could govern the vortices which are passed into the flow. In such scenarios, it may be necessary to describe the strength and nature of these pre-existing instabilities. Klebanoff modes represent relatively weak sources of vorticity, so it is quite likely that disturbances existing in scenarios of larger scale are even more influential in manipulating the flame sheet. Boundary layer streaks, which are observed at the atmospheric scale [56], may also drive some macroscopic behavior of a spreading flame front.

2.5 Streak characterization

A study of stationary flame streaks represents a novel and powerful approach to fundamentally characterize a streaklike instability in a flame. A sustained streak can be carefully probed and reproduced to examine both how it responds to specific parameters and how it affects heat and mass transfer. Extensive refinement of the experimental apparatus, including employment of a leading edge with minimal separation and laminarization of the flow through turbulence reduction screens, was necessary to stabilize a flame streak. This stabilization process enabled significant analysis of a streaklike instability in a reactive boundary layer that would not have been possible otherwise.

An investigation of the thermal and spatial properties of stabilized flame structures was undertaken in order to examine how local instabilities affect the macro-

scopic properties of the flow. The following sections detail experimental measurements undertaken in the previously described laminar wind tunnel. In all experiments characterizing the streaks, the boundary layer developed ahead of the burner over an inert distance of 30 cm. Two wind speeds (1.1 m/s and 2.2 m/s) were employed during experiments. The Froude number ($Fr = U/\sqrt{gL}$), is commonly employed to describe the ratio of inertia to buoyancy in wind-blown flames. In wildland fires, a flame length is often employed as the buoyant length scale L while U is taken as the free stream velocity. Using measured flame lengths for wind speeds of 1.1 and 2.2 m/s, our experimental flames possess Froude numbers of 0.7 and 1.3, respectively. Comparing these numbers with the results plotted in Finney et al. [1], our results lie in the realm of inertia-dominated boundary layer flames including wildland fires.

2.5.1 Flow characterization

The velocity profiles and turbulence intensities of the incoming flow were measured for both velocities, and results are displayed in Figs. 2.15-2.18. Measurements were obtained at three streamwise positions: the wind tunnel exit ($x = -1$ cm), near the middle of the plate ($x = 10$ cm), and just before the burner ($x = 27$ cm). The maximum Reynolds number Re measured at the burner onset is 44000, obtained using the boundary layer development length of 0.3 m and a wind speed of 2.2 m/s. This places the incoming flow well below the transitional regime for boundary layer flow over a flat plate. Stretching of the flow around the leading edge, which acts as

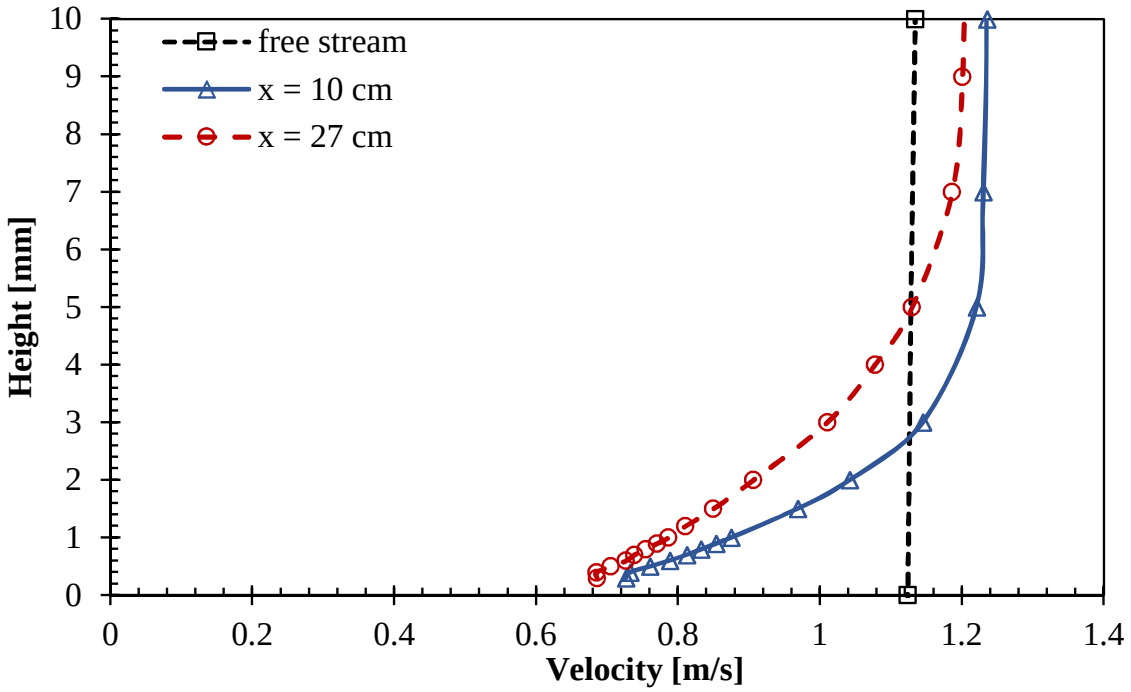

Figure 2.15: Vertical velocity profiles taken at a freestream wind velocity of 1.1 m/s.

an airfoil, was seen to slightly increase the bulk velocity. Nevertheless, the flow remained laminar. Fig. 2.19 shows that the boundary layer thickness deviated slightly from the Blasius profile, but this was not unexpected because we already knew that inhomogeneities in the form of streamwise streaks existed in the flow. These streaks, likely analagous to Klebanoff modes, produce a local thinning/thickening of the Blasius boundary layer.

In order to examine the extent that these streaks affect the boundary layer, a map of the velocity was taken over the y-z plane using the hot wire anemometer. Results are displayed in Figs. 2.20 and 2.21. The inhomogeneities in the flow are clearly visible in both of these images. The boundary layer height can be seen to fluctuate by as much as 1 mm in certain regions. This indicates that the deviation of the boundary layer heights from the Blasius solution in Fig. 2.19 are well within

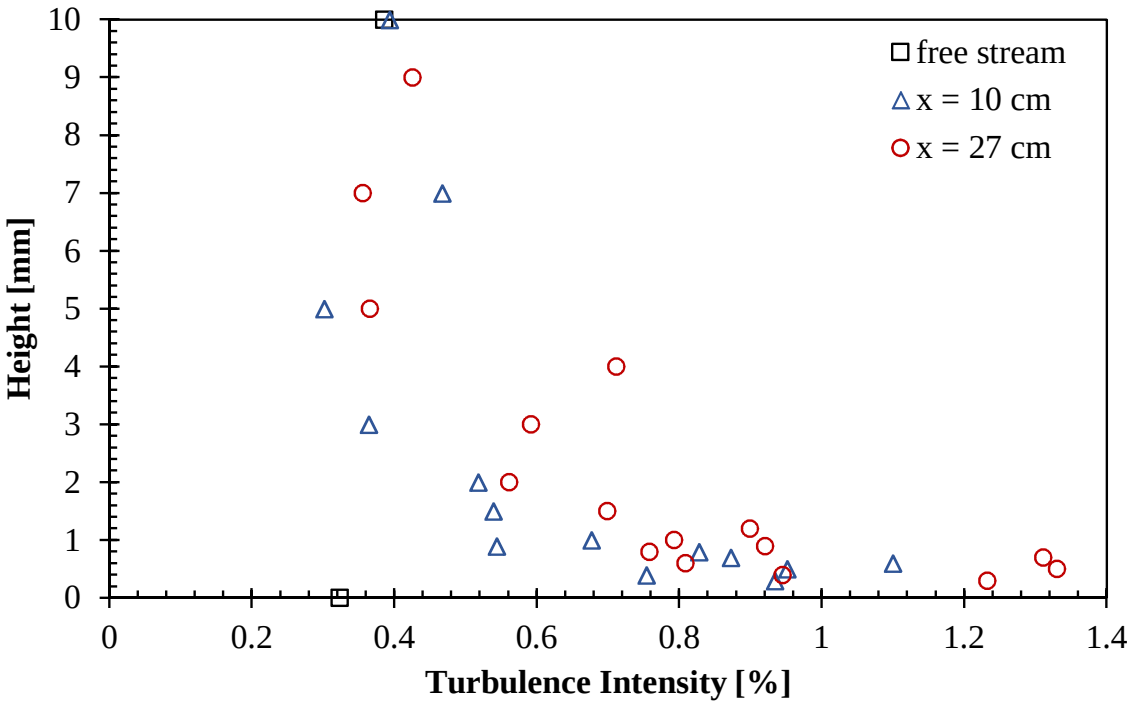

Figure 2.16: Vertical turbulence intensity profiles taken at a freestream wind velocity of 1.1 m/s.

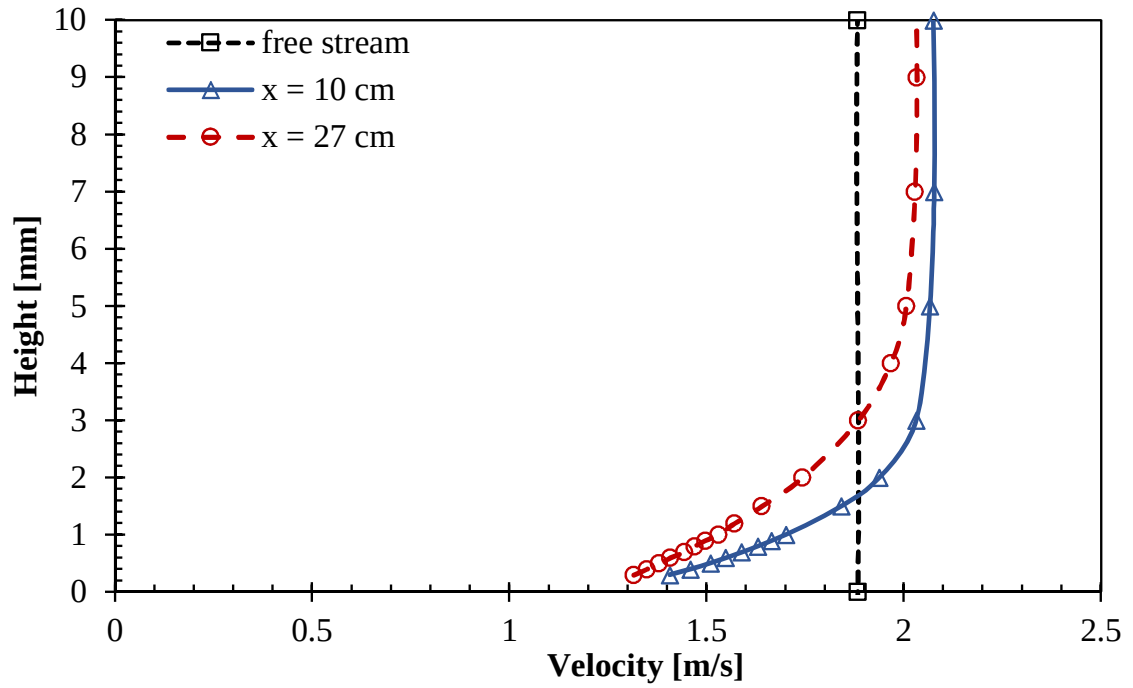

Figure 2.17: Vertical velocity profiles taken at a freestream wind velocity of 2.2 m/s.

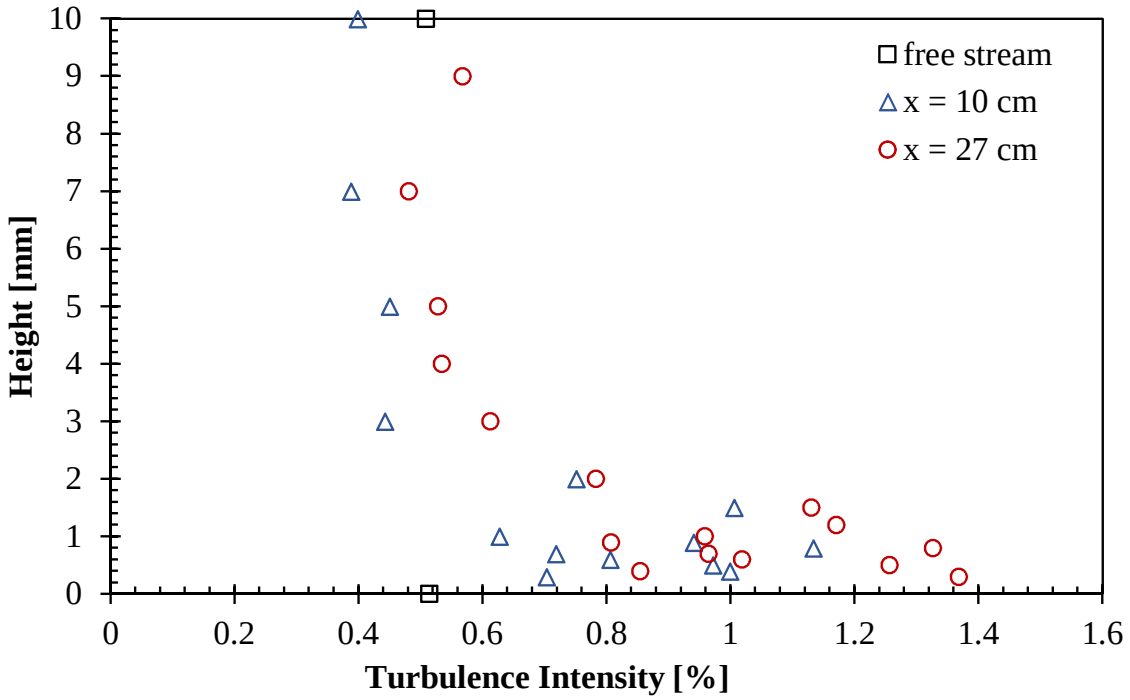

Figure 2.18: Vertical turbulence intensity profiles taken at a freestream wind velocity of 2.2 m/s.

error bounds. Furthermore, Figs. 2.20 and 2.21 reveal a laminar boundary layer that is clearly three-dimensional in nature. The streamwise streaks that exist within the boundary layer have modified the flow significantly. This modification is most pronounced in the case with higher wind speed. These results are in agreement with the finding that flame streaks are preset by inhomogeneities in the flow.

Klebanoff modes have been reported to have a peak value at a Blasius η value of about 2.3 [40]. This results in a value of $y \approx 3$ mm for $U = 1.1$ m/s and $y \approx 2$ mm for $U = 2.2$ m/s. The velocity mapping of our flow certainly indicates that inhomogeneities due to apparent streaks exist at these heights. Additionally, streaks are not observed above $y^+ \approx 40-50$, at least for turbulent boundary layers [10]. This limit, calculated at $x = 27$ cm, lies at heights of 9.5 and 5.1 mm for wind speeds of

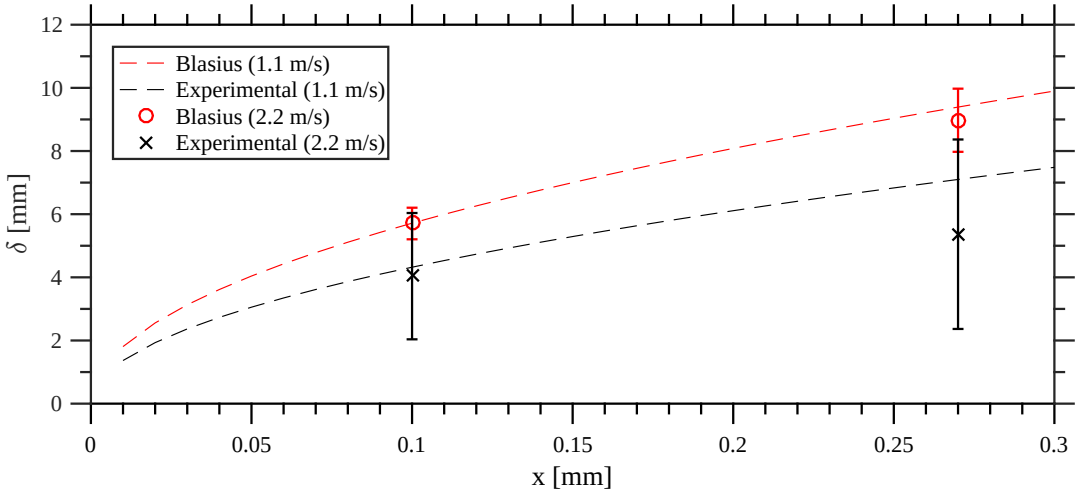

Figure 2.19: Comparison of experimental measurements of boundary layer height to Blasius boundary layer height. The data compares well with the exception of the estimation of the boundary layer height at 0.27 m for a wind speed of 2.1 m/s. This is likely due to the pronounced spanwise variation in boundary layer height, which is easily visualized in a more detailed velocity map. The velocity map (in Fig. 2.21) displays variation in boundary layer thickness, a phenomenon one would expect in the presence of Klebanoff modes [5]. The error bars, which are calculated based on a posteriori knowledge of the spanwise variation in boundary layer thickness, captures this effect.

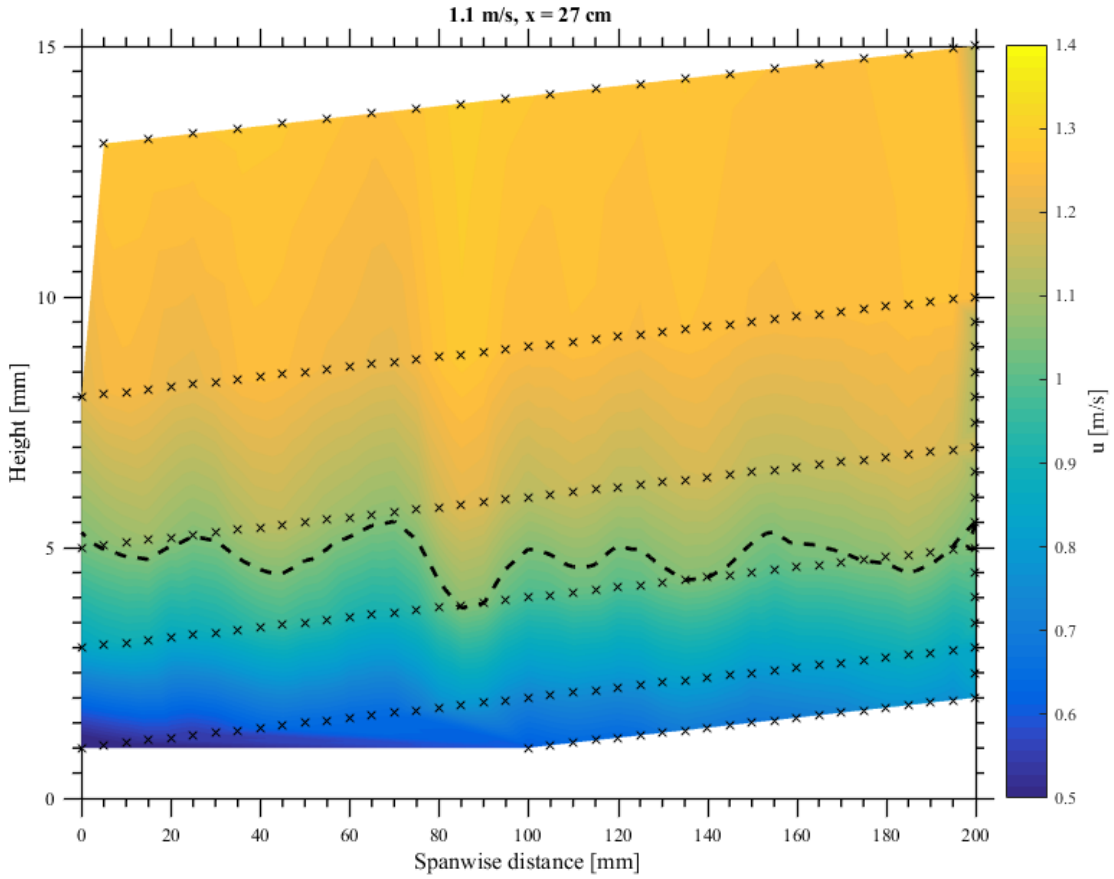

Figure 2.20: Interpolated velocity map at a streamwise distance of 27 cm for a wind speed of 1.1 m/s. Measurement locations are shown as x's, and a contour at 1 m/s is drawn to emphasize the variation along the spanwise distance.

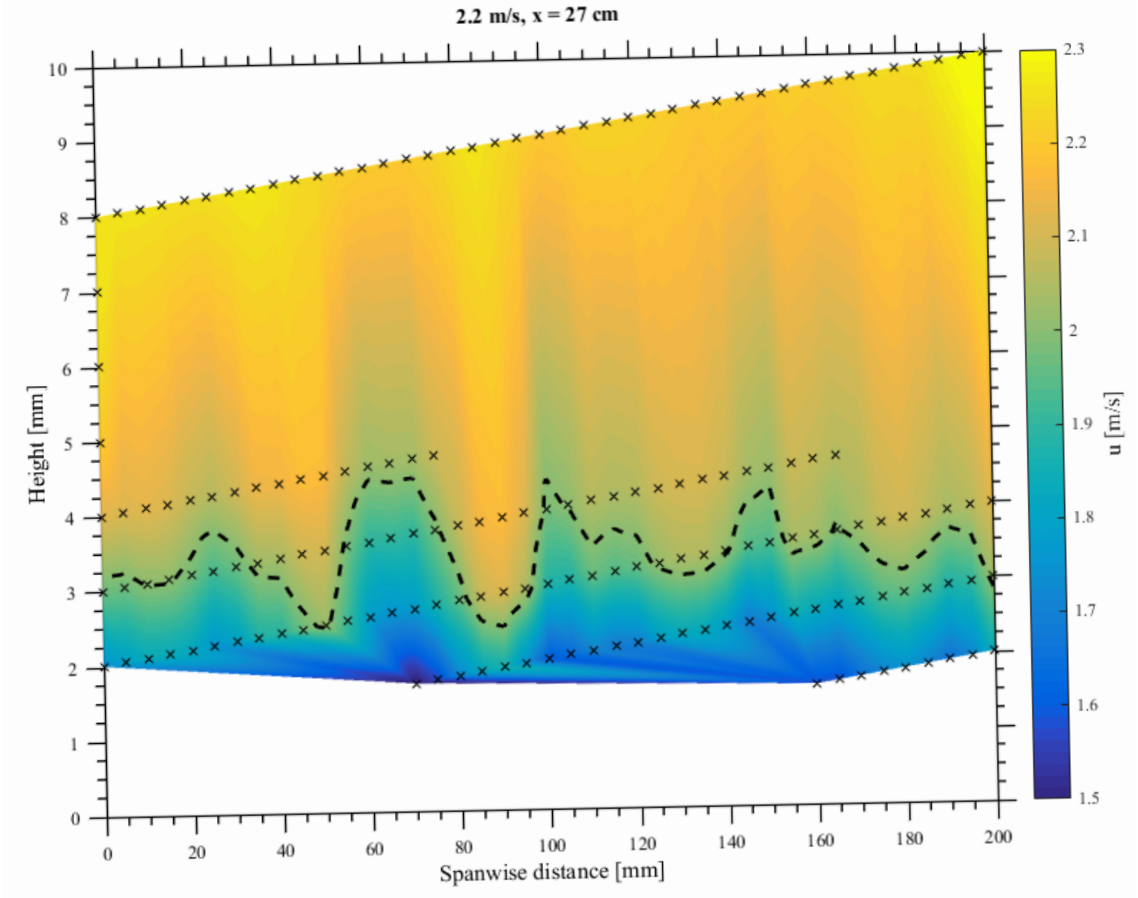

Figure 2.21: Interpolated velocity map at a streamwise distance of 27 cm for a wind speed of 2.2 m/s. Measurement locations are shown as x's, and a contour at 2 m/s is drawn to emphasize the variation along the spanwise distance.

1.1 and 2.2 m/s respectively. Examining the range of our data, it is unclear whether this limit applies.

The measured velocity profiles confirm that the flame lies well within the velocity boundary layer at the burner onset; however, buoyant forces can push a flame outside the boundary layer farther downstream. Although our flame detached from the wall at the lower wind speed (1.1 m/s), the flame remained within the boundary layer.

In turbulent boundary layers, streamwise streaks commonly occurring in the near-wall region are known to have a spanwise wavelength of approximately 100 viscous wall units [56–58], a unit of measurement given by $\lambda^+ = \frac{\lambda u_\tau}{\nu} = \frac{\lambda\sqrt{(du/dy)}}{\sqrt{\nu}}$ with λ being the wavelength, u_τ the shear velocity, and ν the kinematic viscosity. Utilizing the velocity gradient (du/dy) from Figs. 2.15 and 2.17, it can be shown that the reported streak wavelength (2.6 cm) is approximately 82 or 117 wall units for wind speeds of 1.1 and 2.2 m/s, respectively. The similarity in non-dimensional spacing between instabilities in our experiment and turbulent scenarios supports the possibility that boundary layer characteristics may provide a framework for future scaling arguments.

2.5.2 Temperature map

As described earlier, the flame streaks, which are preset by inhomogeneities in the upstream flow, remained stationary when the boundary layer development length was 30 cm. This behavior, attained after significant experimental refinement,

presents a unique opportunity to carefully characterize important properties associated with a flame streak. In fact, we were able to use a thermocouple to obtain detailed temperature maps of a pair of adjacent streaks under two wind velocities (1.1 and 2.2 m/s) and at two streamwise locations ($x = 5$ and $x = 10$ cm). These temperature maps can be seen in Figs. 2.22-2.25. It is important to note that the reported temperatures in this experiment have not been corrected for radiative losses. An upper bound on the radiation correction was obtained using the methodology of Singh [38], a cylindrical Nusselt number correlation from Collis and Williams [59], and a platinum emissivity correlation from Jakob [60]. The resultant equations are as follows:

$$T_g - T_{TC} = \frac{\epsilon d \sigma}{k(0.24 + 0.56(\frac{Ud}{\nu}^{0} .45)}(T_{TC}^4 - T_{surr}^4) \tag{2.6}$$

$$\epsilon = 1.507 * 10^{-4} T - 1.596 * 10^{-8} T^2 \tag{2.7}$$

Here, T_g is the true gas temperature, T_{TC} the measured temperature, ϵ the bead emissivity, d the bead diameter, k the thermal conductivity of the gas, U the local flow velocity, ν the gas kinematic viscosity, and T_{surr} the temperature of the surroundings (assumed ambient). The correction was found to be at most +127 K, obtained at the peak flame temperature ($\approx$ 1500 K) and the lowest assumed wind speed (1.1 m/s). This correction, proportional to T^4, declines rapidly for non-peak values, being no more than +19 K for a temperature of 1000 K. As applying this correction would only serve to increase the contrast between the flame and the

surrounding gases, the current thermocouple maps provide adequate detail on the spatial variation of gas temperatures.

The temperature maps display flame streaks that amplify significantly with streamwise distance. At the first streamwise measurement location, $x = 5$ cm, the flame streaks are visible only as small perturbations. Moving downstream to $x = 10$ cm, the flame streaks grow significantly, becoming larger and more distinct. This trend is observed at both wind speeds. The dramatic growth in the size of the flame streaks over such a short distance indicates that the buoyancy is playing an important role in the growth, which far outpaces the growth of a non-reactive boundary layer.

Additionally, the wind plays a significant role in suppressing the growth of the flame streaks. As the wind speed is increased from 1.1 to 2.2 m/s, the flame streaks at the same streamwise location are much less pronounced. The spatial growth of the flame streaks is strongly tied to the wind velocity.

This result is expected, as an increased velocity means that the flame has less *time* to develop before it reaches a designated location. The decreased *spatial* growth could simply be a consequence of a decreased amount of *time* to grow. However, it is possible that the shear from the velocity is also suppressing the growth of the streaks [61, 62]. Alternatively, the increased wind speed may even accelerate the temporal growth of the streaks by augmenting the strength of pre-existing vortices. Unfortunately, the temporal growth of the streaks cannot be known without accurate velocity measurements in the flaming region.

The overall temperature distribution at $x = 5$ cm, displayed in Figs. 2.22

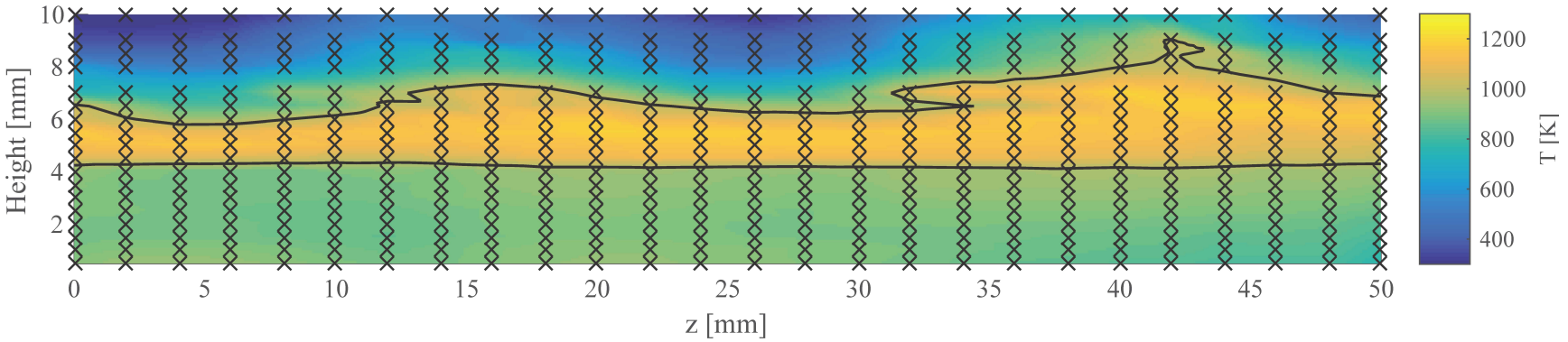

Figure 2.22: Temperature map taken at a wind speed of 1.1 m/s and a streamwise distance of $x = 5$ cm from the burner onset. Measurement locations are shown as x's, values are interpolated, and a contour of 1000 K is displayed to approximately demarcate the location of the flame sheet.

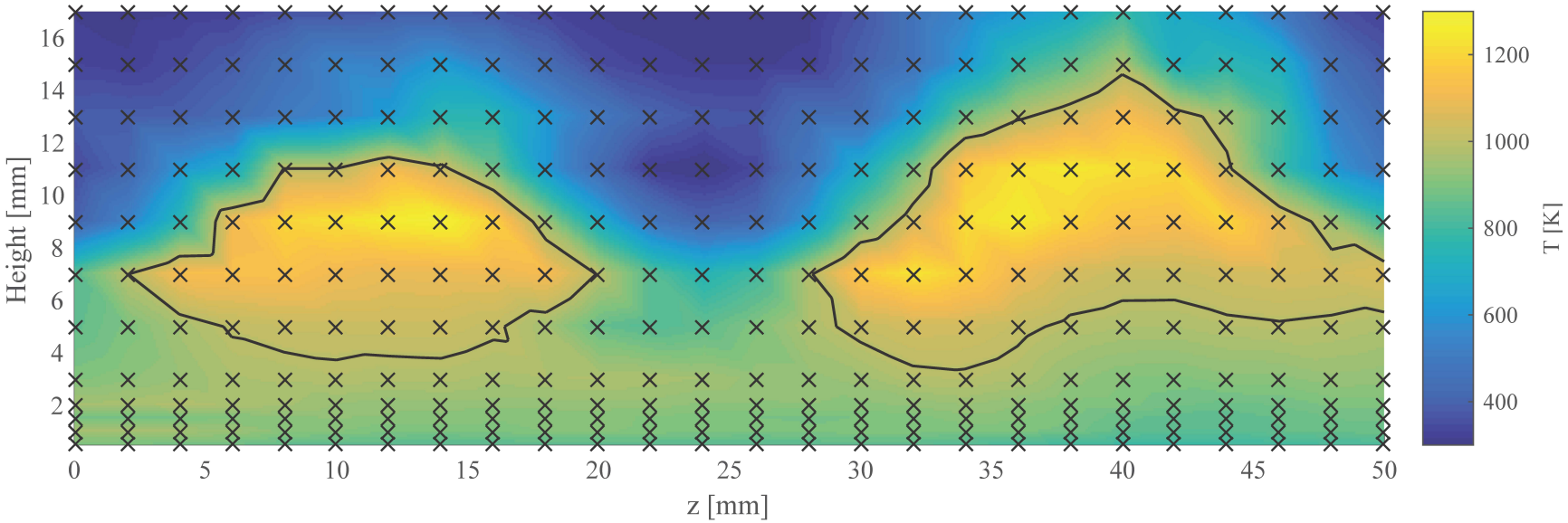

Figure 2.23: Temperature map taken at a wind speed of 1.1 m/s and a streamwise distance of $x = 10$ cm from the burner onset. Measurement locations are shown as x's, values are interpolated, and a contour of 1000 K is displayed to approximately demarcate the location of the flame sheet.

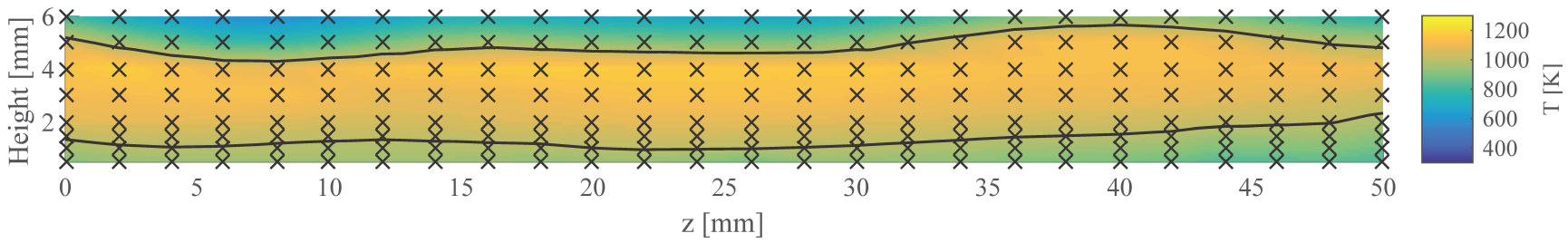

Figure 2.24: Temperature map taken at a wind speed of 2.2 m/s and a streamwise distance of $x = 5$ cm from the burner onset. Measurement locations are shown as x's, values are interpolated, and a contour of 1000 K is displayed to approximately demarcate the location of the flame sheet.

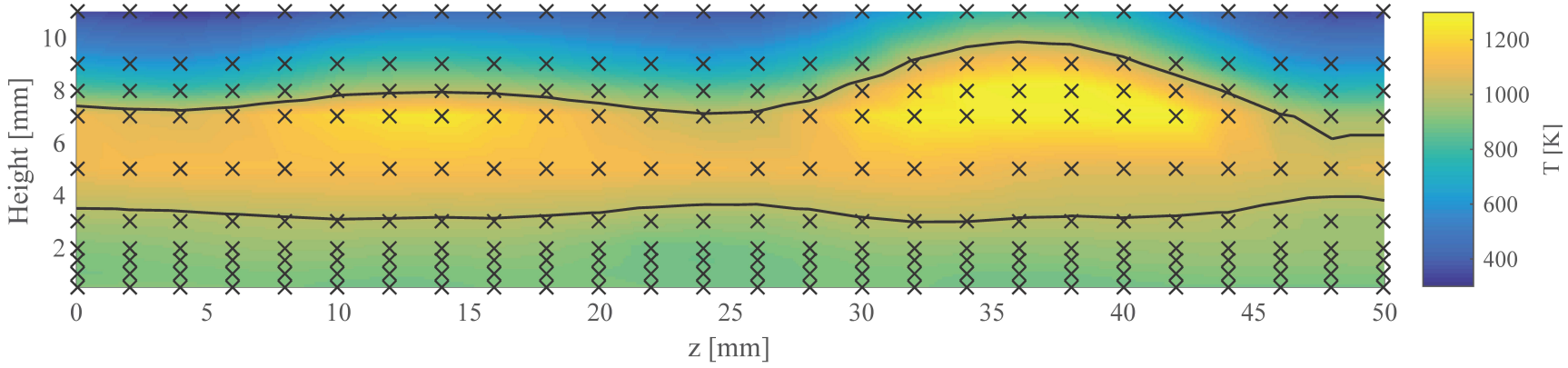

Figure 2.25: Temperature map taken at a wind speed of 2.2 m/s and a streamwise distance of $x = 10$ cm from the burner onset. Measurement locations are shown as x's, values are interpolated, and a contour of 1000 K is displayed to approximately demarcate the location of the flame sheet.

and 2.24 is relatively consistent. The temperature throughout the flame sheet is fairly uniform, with no perceivable difference between the flame streaks and the trough in between. However, this uniform distribution changes considerably at $x = 10$ cm (Figs. 2.23 and 2.25), where the temperature within the flame streaks is significantly higher than the temperature in the flame trough. For both wind speeds, the measured temperature within the flame streaks reaches more than 1300 K, but the temperature in the trough region changes significantly with wind. Under a wind of 2.2 m/s (Fig. 2.25), the temperature of the flame trough is only about 1050 K, while the temperature declines to value of 850 K for a wind speed of 1.1 m/s (Fig. 2.23). This represents a significant change in the spanwise distribution of gas-phase temperatures, revealing the three-dimensional effects of the flow.

There are several explanations for this redistribution of heat. It is possible that the lower temperature in the trough is due to a lean mixture fraction; this could occur because the counter-rotating vortices may be forcing unburnt out of the troughs and replacing it with ambient fluid. This variation in concentration may be the best explanation for the behavior observed. Alternatively, the counter-rotating vortices, which control the onset and assist the growth of the flame streaks, may have gained enough strength to stretch the flame sheet nearer to its extinction limit. The flame sheet in our experiment resembles a counterflow diffusion flame at early stages, until it is acted upon by a counter-rotating vortex pair on the oxidizer side to induce flame streaks. As the perturbations due to the interaction with the vortices amplify, the trough region can narrow, confining the vortex pairs and intensifying their vorticity [15]. Local extinction due to vortices injected from the

oxidized side in a counterflow burner has previously been observed numerically and experimentally [63–65]; Thevenin et al. [63] even witnessed intensified combustion adjacent to the area of quenching. This parallels the temperature map in Fig. 2.23, which portrays local extinction at the region of vortex penetration buttressed by heightened temperatures in the adjacent flame streaks. Liñan et al. [6] summarized some of the regimes of diffusion flame-vortex interactions, and their schematic is reproduced in Fig. 2.26. This schematic describes the expected behavior of flame-vortex interactions as a function of the vortex strength, the Peclet number, and the robustness of the flame. Examining the temperature distributions from our own data, we see that our behavior is best described by point 2, at which axial extinction is observed. This gives us possible insight into the nature of the vortices in our flame; unfortunately, verifying that our experimental observations occupy this region is impossible without velocity field data. It is likely that the eddies present in our laminar experiment simply do not have the vorticity to induce such significant extinction. Regardless, the significant spanwise variation in temperature distribution reveals the three-dimensional nature of the flow, which may need to be accounted for in certain applications.

The variation of temperature was also processed and plotted in Figs. 2.27-2.30. In all the figures, temperature fluctuations are relatively low in the region beneath the flame sheet, never exceeding a standard deviation of 10 K. The largest fluctuations are present at the interface between the flame sheet and the air. These fluctuations peak on either side of the flame streaks, particularly in the maps taken from $x = 10$ cm. This indicates a slight meandering of the streaks from side-to-side,

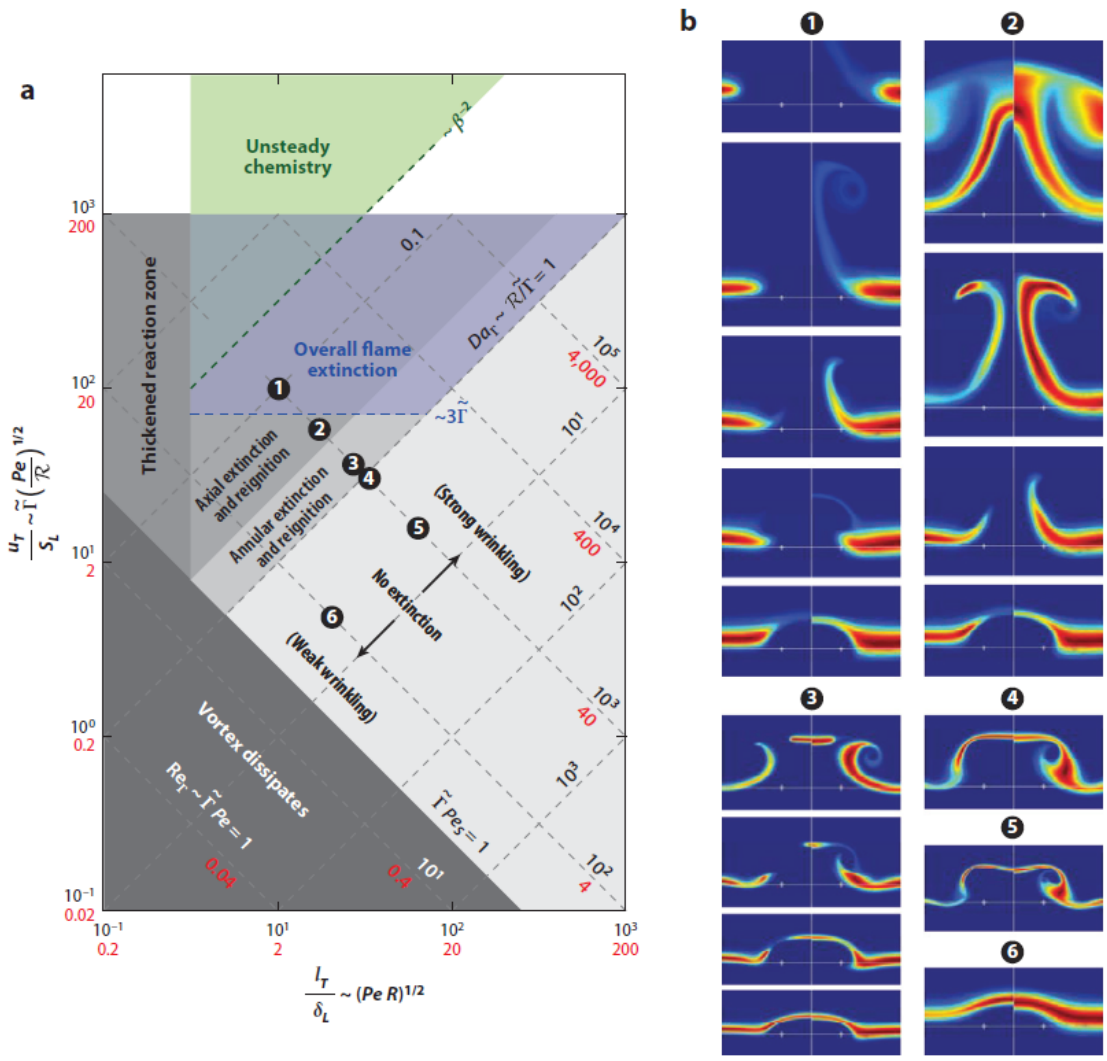

Figure 2.26: Regimes of vortex-flame interaction displayed on the left as a function of the non-dimensional vortex strength, Γ, the Peclet number of the unperturbed flow, Pe, and the flame robustness, R. The right image shows the observed behavior corresponding to each regime marked with a number. The trough in our flame seems to exhibit behavior similar to point 2, corresponding to axial extinction. Taken from Liñan et al. [6].

revealing a possible sinuous nature of these instabilities. Although regions beyond $x = 10$ cm were not mapped, the magnitude of these sinuous fluctuations could increase downstream. This movement mimics the behavior of Görtler vortices, a possible analog for flame streaks which has been previously discussed [1]. Similar to the flame streaks in this experiment, Görtler instabilities do not have a natural mechanism of wavelength selection, but they amplify the instabilities imposed by the experimental facilities on the incoming flow [66]. Görtler vortices are known to modify wall heat fluxes [15], grow in time, decay, and cause transition to turbulence [67], effects that have also been seen or hypothesized for flame streaks.

2.5.3 Streak amplification

Linear temperature profiles, measured at the centerline of either a prominent streak or trough, were obtained for both wind speeds. Measurements were made every 5 cm in the streamwise direction, and all profiles were obtained along a designated streak and a designated trough. These profiles, shown in Fig. 2.31, were used to create a spatial map of the flame streaks and flame troughs. Establishing 1000 K as the outer edge of the flame sheet enabled a spatial mapping that agreed with visual observations. Both the upper and lower extents of the flame streaks and troughs were established and plotted in Figs. 2.32 and 2.33. Fig. 2.32 displays the shape of the flame streaks at two wind speeds. At 1.1 m/s, the streak extends to twice the height of the streak exposed to a crosswind of 2.2 m/s. The growth of the flame streak appears to be accelerating at this low wind speed, indicated by the

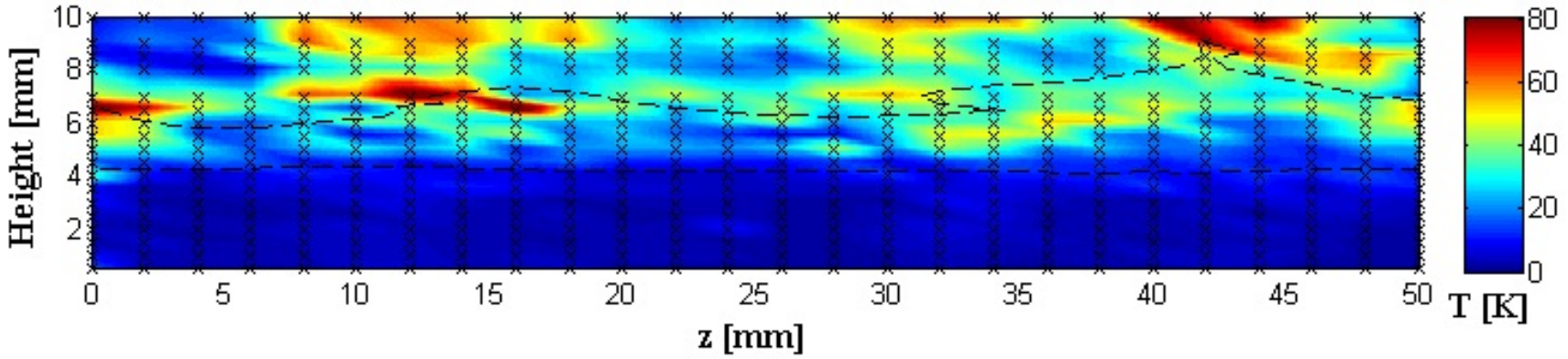

Figure 2.27: T′ map taken at a wind speed of 1.1 m/s and a streamwise distance of $x = 5$ cm from the burner onset. Measurement locations are shown as x's, values are interpolated, and a contour of 1000 K is displayed to approximately demarcate the location of the flame sheet.

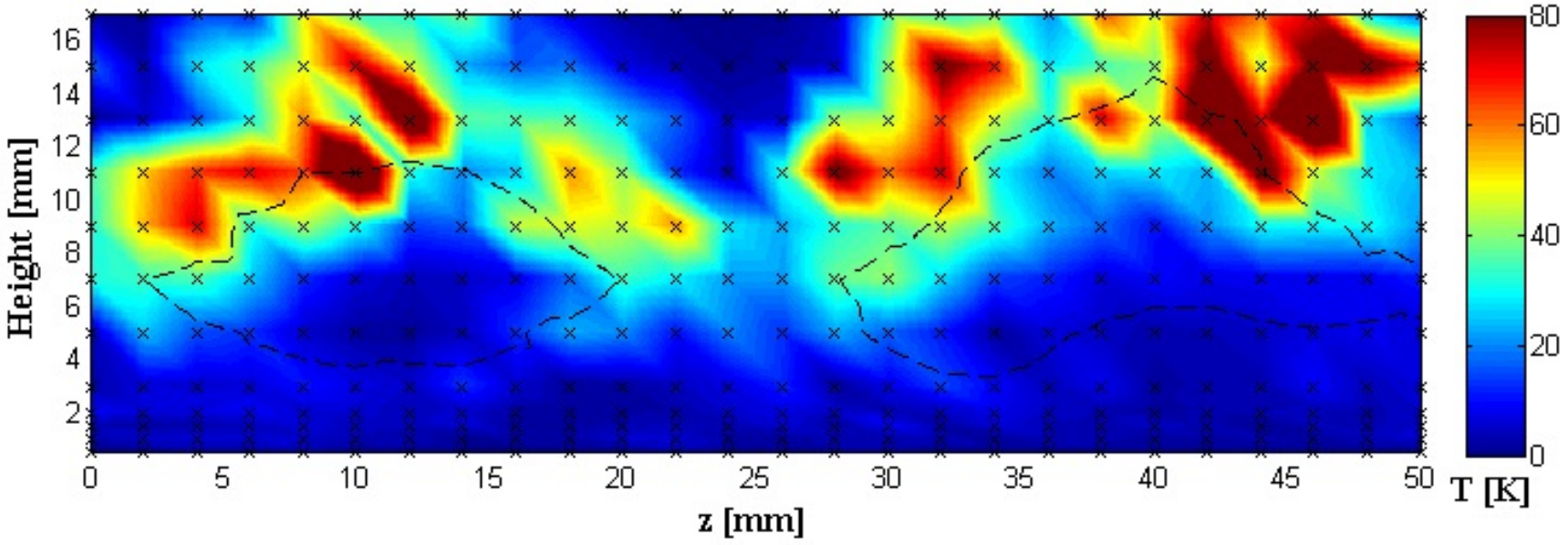

Figure 2.28: T′ map taken at a wind speed of 1.1 m/s and a streamwise distance of $x = 10$ cm from the burner onset. Measurement locations are shown as x's, values are interpolated, and a contour of 1000 K is displayed to approximately demarcate the location of the flame sheet.

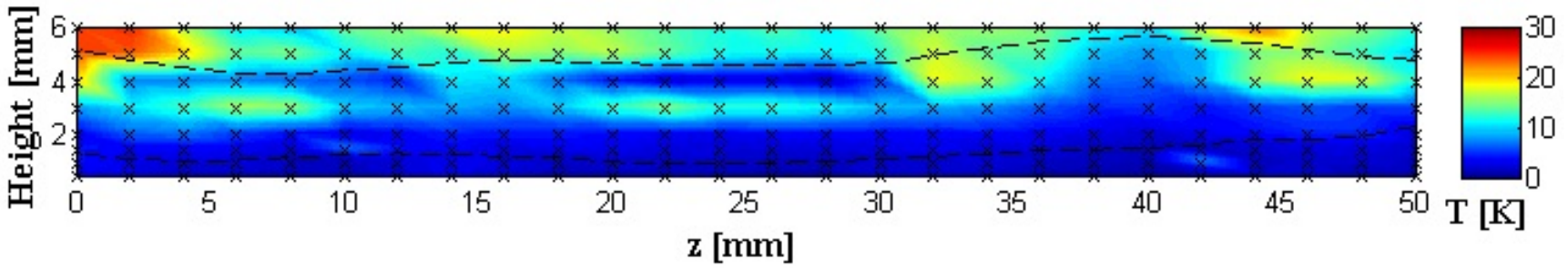

Figure 2.29: T′ map taken at a wind speed of 2.2 m/s and a streamwise distance of $x = 5$ cm from the burner onset. Measurement locations are shown as x's, values are interpolated, and a contour of 1000 K is displayed to approximately demarcate the location of the flame sheet.

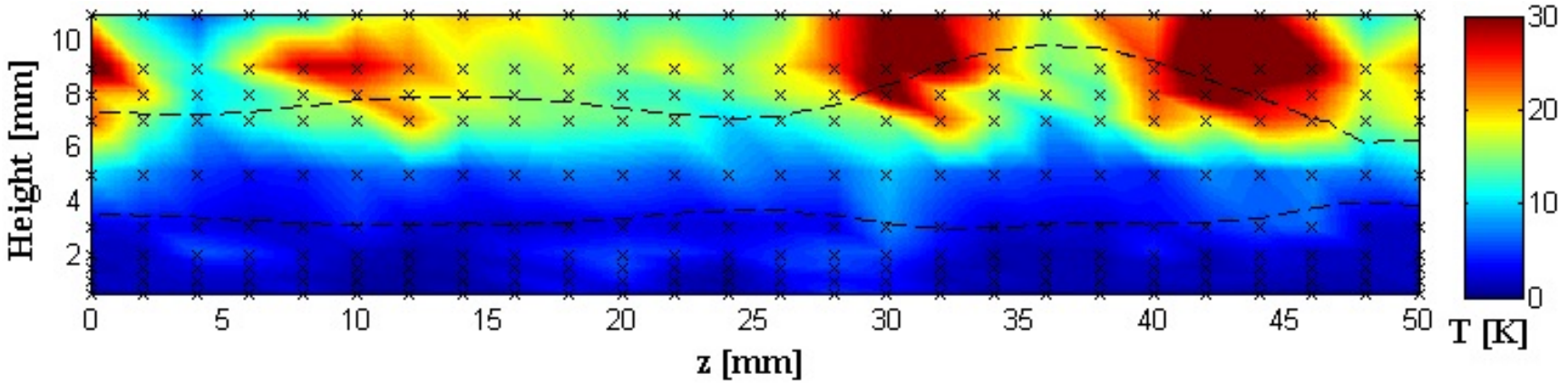

Figure 2.30: T′ map taken at a wind speed of 2.2 m/s and a streamwise distance of $x = 10$ cm from the burner onset. Measurement locations are shown as x's, values are interpolated, and a contour of 1000 K is displayed to approximately demarcate the location of the flame sheet.

concave upper surface. Additionally, this streak is seen to flare out downstream, extending upward and downward so as to occupy a significant depth before burning out. Meanwhile, the streak at 2.2 m/s remains narrower, and a deceleration of growth is indicated by the convex shape of the upper surface. The wind clearly plays a strong role in determining the shape of the flame streak; however, varying the wind speed minimally affects the shape of the troughs. At both wind speeds, the trough remains attached to the surface, exhibiting negligible growth at $x = 10$ cm. Both troughs also burn out quickly, exhibiting a streamwise length that is only half that observed by the adjacent flame streaks. It has been suggested that the behavior of the troughs, which remain close to the surface, is surprising given the significant blowing effect expected from the surface which will be heated significantly. Nevertheless, the troughs, which consist of regions with lower luminosity, exhibit lower amounts of soot and may also have lower radiative heat. This may explain why the downwash regions act to keep the trough suppressed even as we move downstream.

The growth of the flame streaks and the suppression of the flame troughs is a consequence of the counter-rotating streamwise vortices and the natural buoyancy of the flame (see schematic in Fig. 2.14). The accelerated growth of the streaks strongly points to the role of buoyancy, indicating that the amplification of these instabilities may be similar to the growth of a Rayleigh-Taylor Instability (RTI), which is controlled by the density difference between a suspended heavy fluid and a lower lighter fluid. Scaling laws to describe the growth and mixing of RTI's have been established; consequently, it was desirable to investigate whether this scaling could also describe the amplification of a flame streak. The growth of an RTI is typically

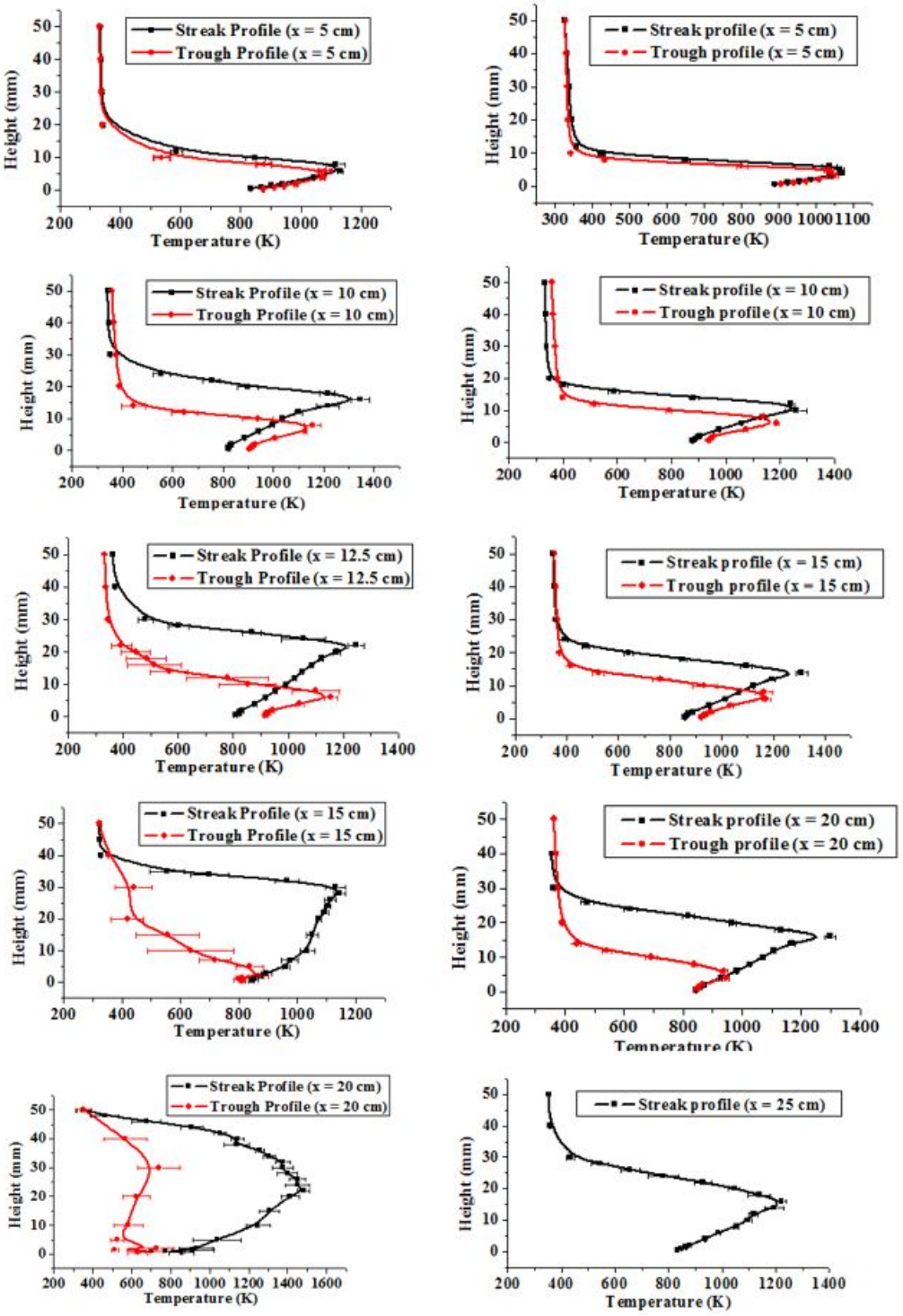

Figure 2.31: Linear temperature profiles taken from a series of measurements in the vertical direction. For each wind speed, displayed respectively on the left or right side, 5 streamwise positions were assessed. The red line indicates the temperature measured at the centerline of a streak, while the black line indicates the temperature measured at the centerline of a trough.

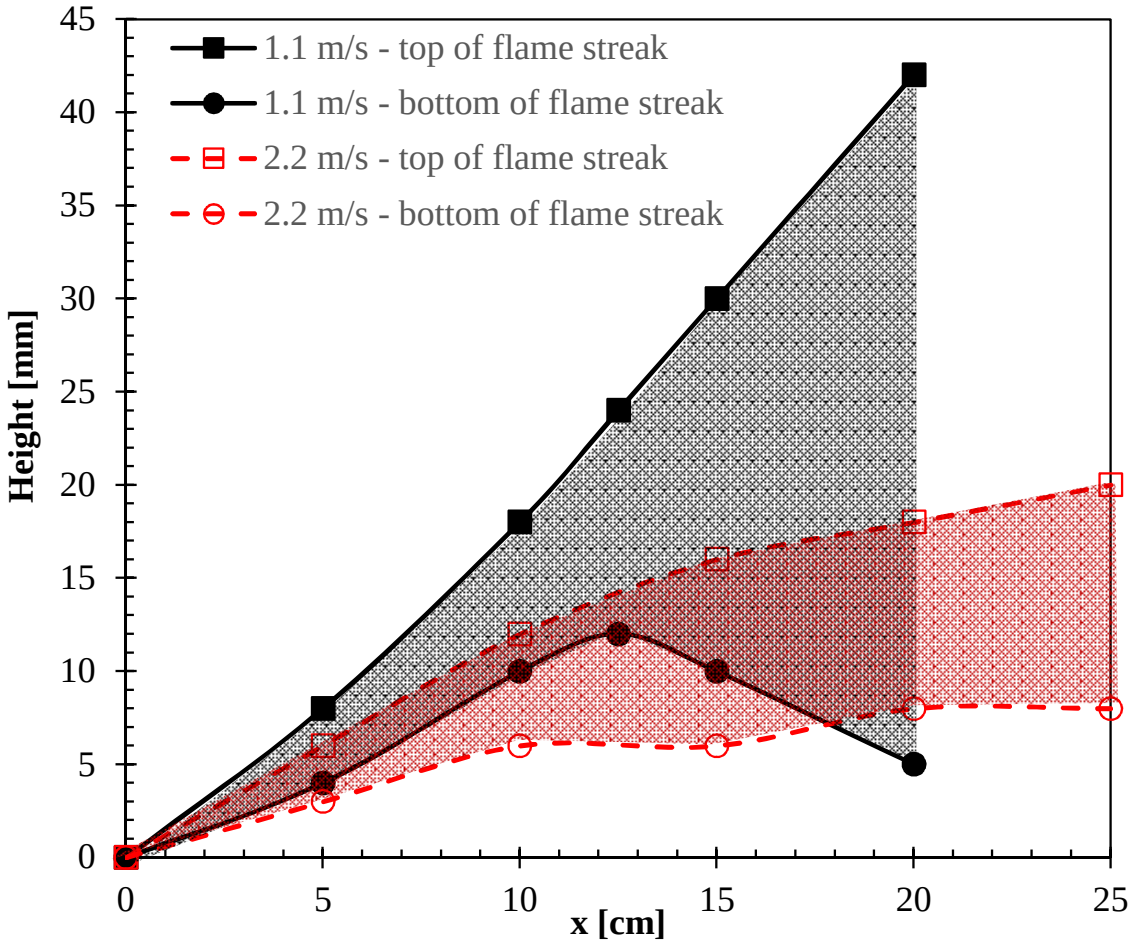

Figure 2.32: Growth of flame streak at two wind speeds. Edges of flame streak determined by the furthest upper and lower temperatures above 1000 K. The shape of the flame streak at a wind speed of 1.1 m/s is shown in black, while the flame streak at a wind speed of 2.2 m/s is shown in red.

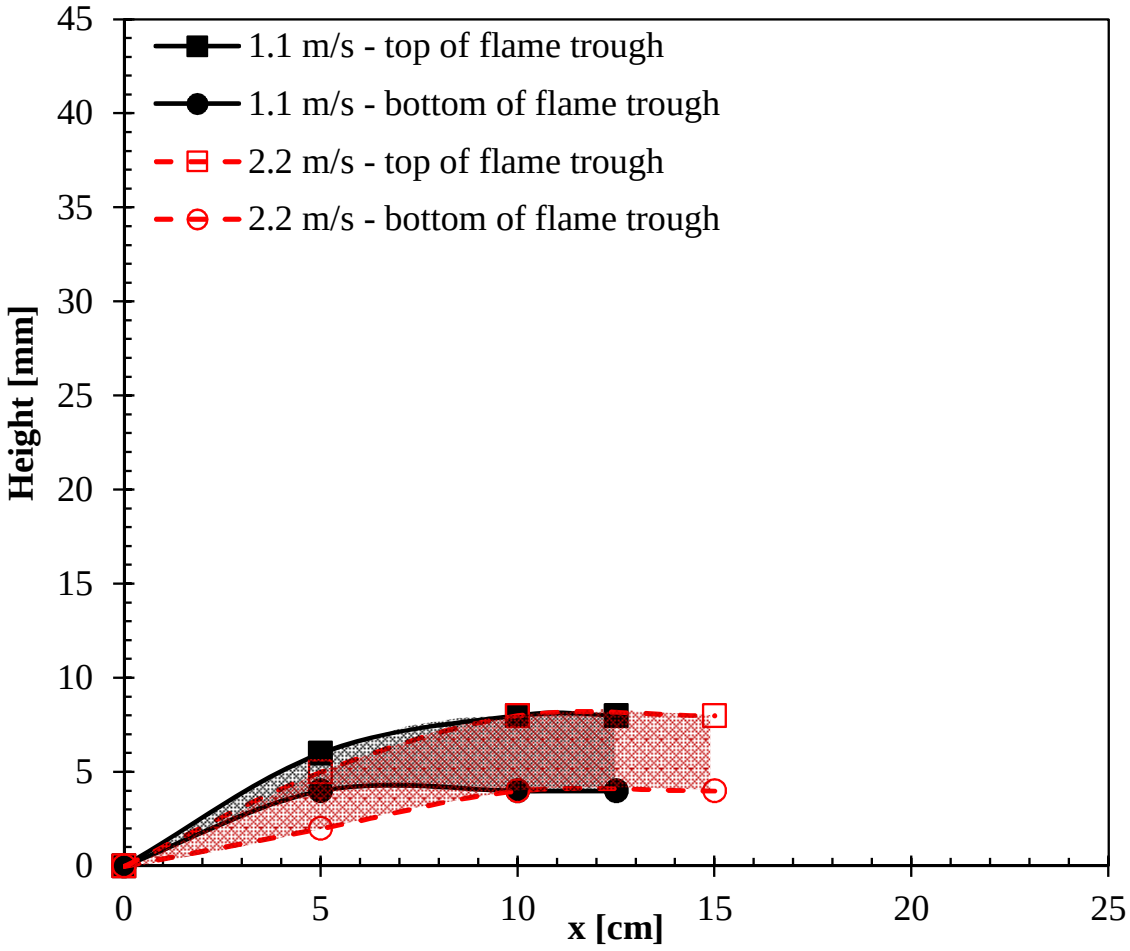

Figure 2.33: Growth of the flame sheet at the troughs (region between streaks) for two wind speeds. Edges of trough determined by the furthest upper and lower temperatures above 1000 K. The shape of the trough at a wind speed of 1.1 m/s is shown in black, while the trough at a wind speed of 2.2 m/s is shown in red.

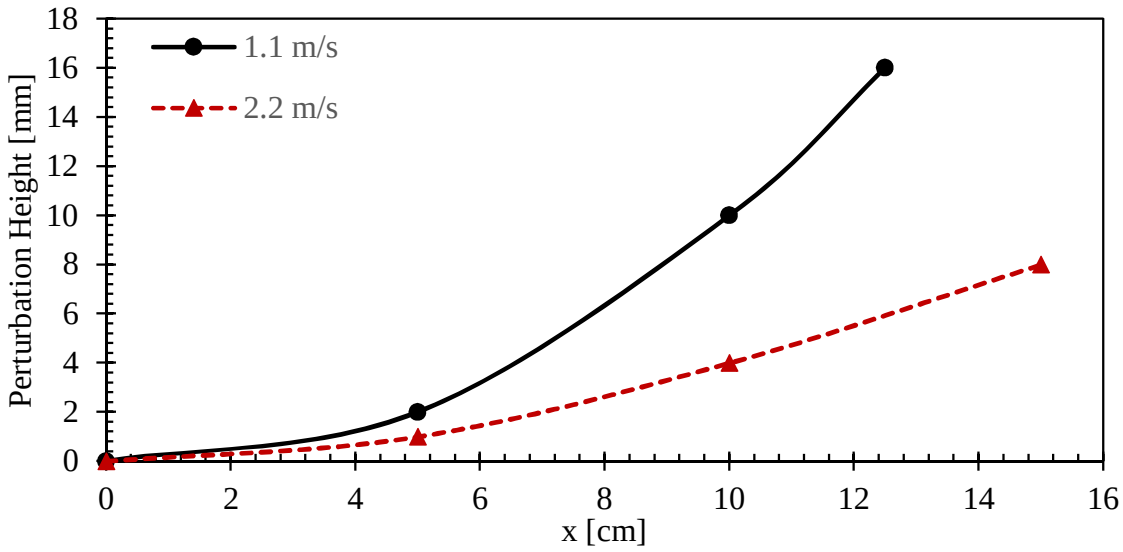

Figure 2.34: Perturbation amplitude vs. streamwise distance. The perturbation height is measured as the vertical displacement from the top of a streak to the top of an adjacent trough.

characterized by the height or amplitude of the perturbations, often measured by the peak-to-trough difference in height. In our measurements, this distance is the difference between the upper extent of the flame streak and the upper extent of an adjacent trough, as the top of the flame sheet represents the rational choice for a density interface. This perturbation amplitude has been plotted vs. the streamwise distance in Fig. 2.34. At both wind speeds, this perturbation height appears to grow exponentially. Additionally, the growth appears to be doubled when the wind speed is halved.

2.5.3.1 Early-time growth

This buoyant amplification could potentially be described by scaling laws for a Rayleigh-Taylor Instability (RTI). Early-time RTI growth is described by linear stability theory, but the early-time resolution of our measurements is inadequate for

comparison. Nevertheless, in this section we will briefly discuss a simple model for early-time RTI growth which was described in Eqs. 2.1-2.5. These equations were derived from linear stability theory (LST), which reasonably predicts RTI growth at times where the amplitude of the perturbation is significantly less than the wavelength, λ. The amplitude of the perturbation, H, is the vertical peak-to-trough distance measured from the interface between fluids of varying density. LST for similar Atwood numbers ($A = 0.5$) of our own experiment has been shown to approximate growth within 10% of detailed simulations for a amplitude-wavelength ratio (H/λ) of 0.1 [45], implying that LST should be reasonable until the perturbation height in our experiment reaches 2.6 mm. Looking at Fig.2.34, this theory should reasonably describe buoyant growth until at least $x = 5$ cm. Recalling Eq. 2.1, we see that the perturbation height in LST is described by

$$H(t) = a_0 \cosh nt - \frac{u_0}{n} \sinh nt \tag{2.1}$$

where a_0 is the initial perturbation height, u_0 is the initial velocity at the interface, n is the exponential growth factor, and t is time. The exponential growth factor, which was determined by one of three proposed theories, is described in Eqs. 2.2-2.5. In order to determine these growth factors, the Atwood number, A, was estimated assuming the hot gas temperature was 1000 K, and the wavenumber k was assessed using the mean streak spacing ($k = 2\pi/\lambda$ where $\lambda = 2.6$ cm). This resulted in $A = 0.54$. Next, reasonable estimates for the initial perturbation height, a_0, and the initial velocity, u_0, needed to be made. At the burner lip, where fuel first encounters

the crossflow, the flame sheet should be relatively unperturbed, meaning $a_0 = 0$. u_0 was unknown, so this variable was manipulated through an iterative process until LST was seen to barely overpredict our measurements. Finally, it was necessary to make some assumptions to convert the spatial scale shown in Fig. 2.34 into a time scale. Figs. 2.15 and 2.17 demonstrate that the flow velocity in the region of interest lies within the boundary layer, but a velocity overshoot, typically observed in laminar boundary layer flames, should push the velocity within the flame to about 1.5 times the ambient value [32]. Assuming a constant velocity over the development of the flame, a time scale was easily obtained by dividing the spatial scale by the estimated streamwise velocity within the flame.

Results for the linear stability theory plotted vs. early perturbation heights are shown in Fig. 2.35. In order to obtain these results, the initial perturbation velocity, u_0, was estimated to be 0.055 m/s for a wind speed of 1.1 m/s and 0.075 m/s for a wind speed of 2.2 m/s. These values appear reasonable, but a lack of measurement density hinders confirmation of early-time growth rates. Regardless, the early-stage of growth would only comprise a very small portion of the growth witnessed in our experiment.

2.5.3.2 Qudratic growth

After the earliest stage of growth, nonlinear terms begin to play a role in the amplification of RTI's. At sufficiently late times, the development of the mixing height has been assumed to scale with αAgt^2 [68, 69], where α is a dimensionless

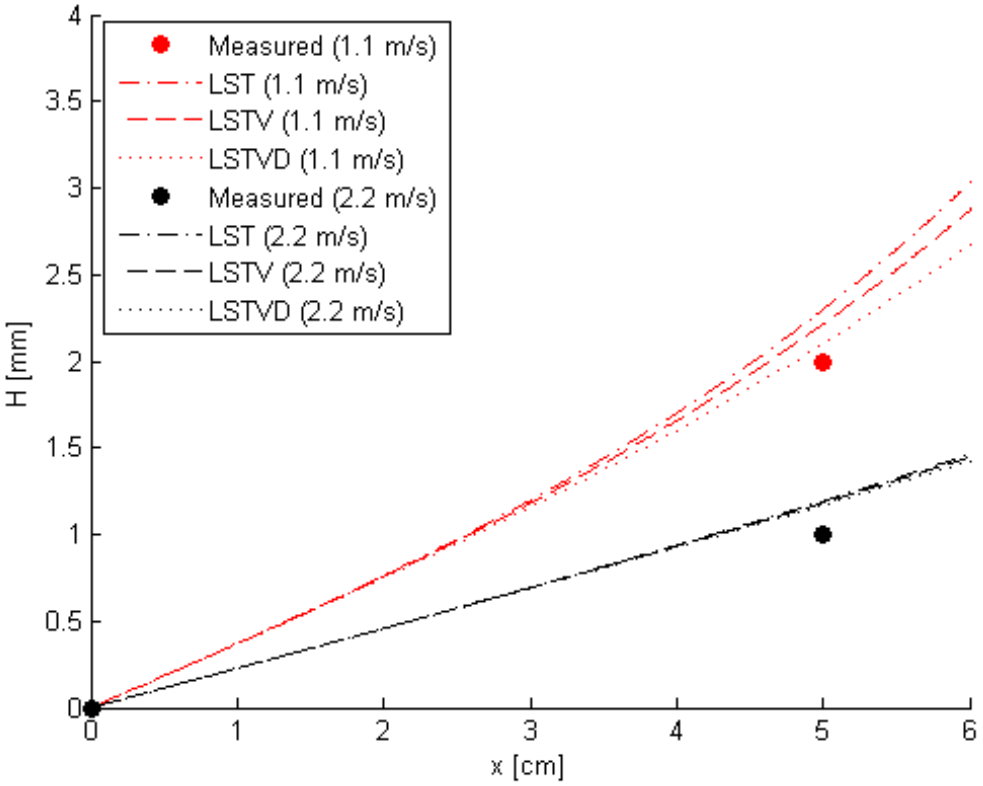

Figure 2.35: Measured and theoretical perturbation amplitudes plotted vs. streamwise distance. The predicted growth curves based on three theoretical fits to linear stability theory are shown as dashed lines. Measurements are shown as dots, and colors differentiate freestream wind speeds.

coefficient characterizing the growth, A is the Atwood number, g the gravitational constant, and t is time. The Atwood number, A, is determined from a density difference such that $A = (\rho_1 - \rho_2)/(\rho_1 + \rho_2)$ where ρ_1 is the density of the heavier fluid. The growth of our flame streaks does not quite reach the regime where α asymptotes to a constant value, instead residing somewhere between the extensively-studied linear and quadratic growth. Fortunately, two numerical studies in particular have tabulated growth covering this transition regime for flows with Atwood numbers similar to our experiment ($A = 0.5$). Both Burton [8] and Cook et al. [45] have performed numerical simulations and tabulated instantaneous values of α as a function of a dimensionless time parameter, t/τ, where τ, a dimensionless progress variable, is defined as $\tau = \sqrt{\lambda/(Ag)}$. In order to examine the scaling of α vs. these parameters, the following equation describing the late-time perturbation height [7] was fit to the downstream perturbation heights measured in our experiment:

$$H(t) = \alpha A g t^2 + 2(\alpha A g h_0)^{1/2} t + h_0 \tag{2.8}$$

Here, h_0 is a virtual starting thickness established by the perturbation height at the beginning of the curve fit and the time at this point is $t = 0$. It is standard practice to measure α by fitting Eq. 2.8 to data on the perturbation amplitude, but typical values, even in the asymptotic range, often vary between experiments [7, 8]. Applying Eq. 2.8 to our data, we obtain Fig. 2.36 using $\alpha = 0.14$ for the wind speed of 1.1 m/s and $\alpha = 0.17$ for the wind speed of 2.2 m/s. The quadratic fit aligns well with our downstream data points, and we can now compare our measurements for

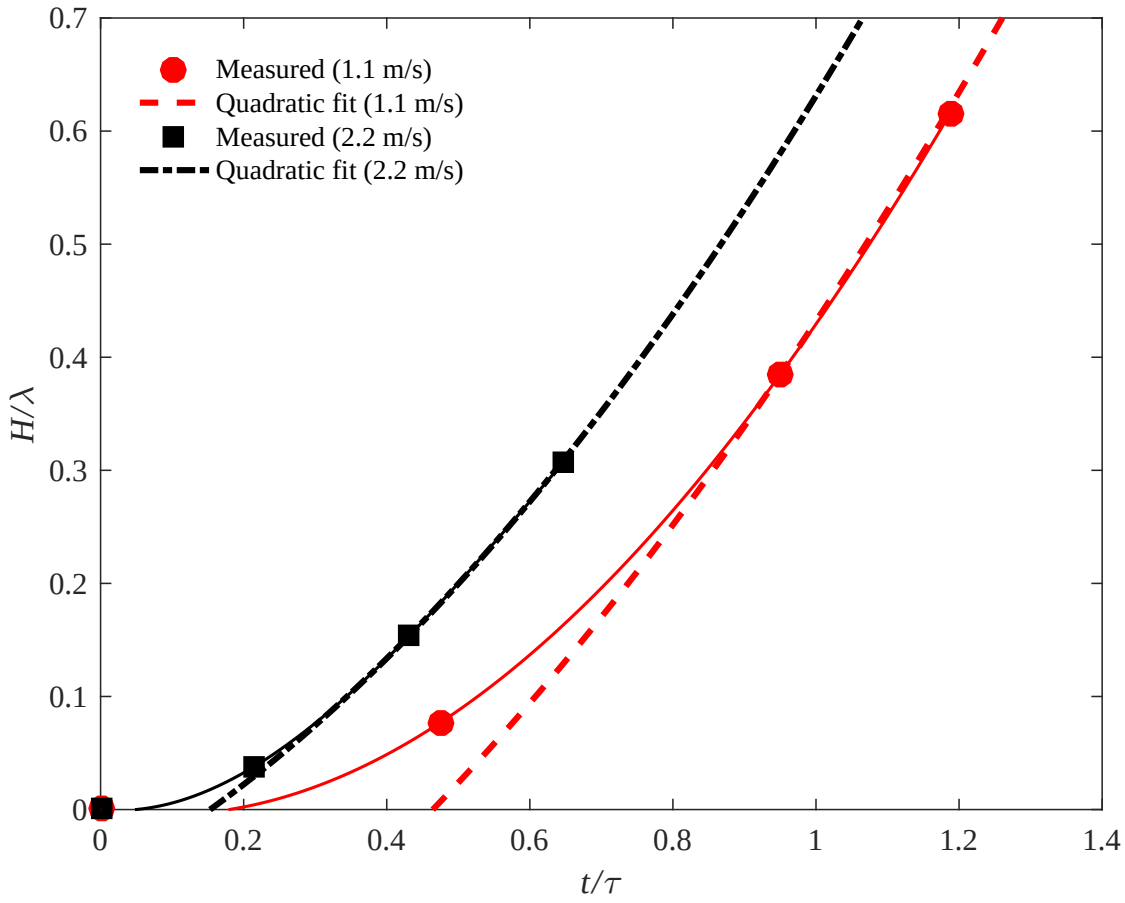

Figure 2.36: Dimensionless height (perturbation amplitude divided by wavelength) plotted vs. dimensionless time. For each wind speed, experimental data is plotted vs. a theoretical fit based on Eq. 2.8. A value for α was determined based on the best fit to our data.

α vs. values in the literature. This comparison can be seen in Fig. 2.37. The data from Cabot et al. [7] fails to fully extend to the regime of our data, but the α values obtained from Burton's simulations [8] match remarkably well with our data.

Overall, Rayleigh-Taylor scaling seems to present a viable option for describing the growth of a flame streak in a laminar boundary layer. Behavior during the transition to nonlinear growth appears to be within reasonable agreement with existing literature. However, the growth of the flame streaks may not be governed entirely by buoyancy. Pre-existing vorticity in the flow, while it may not be a dominant

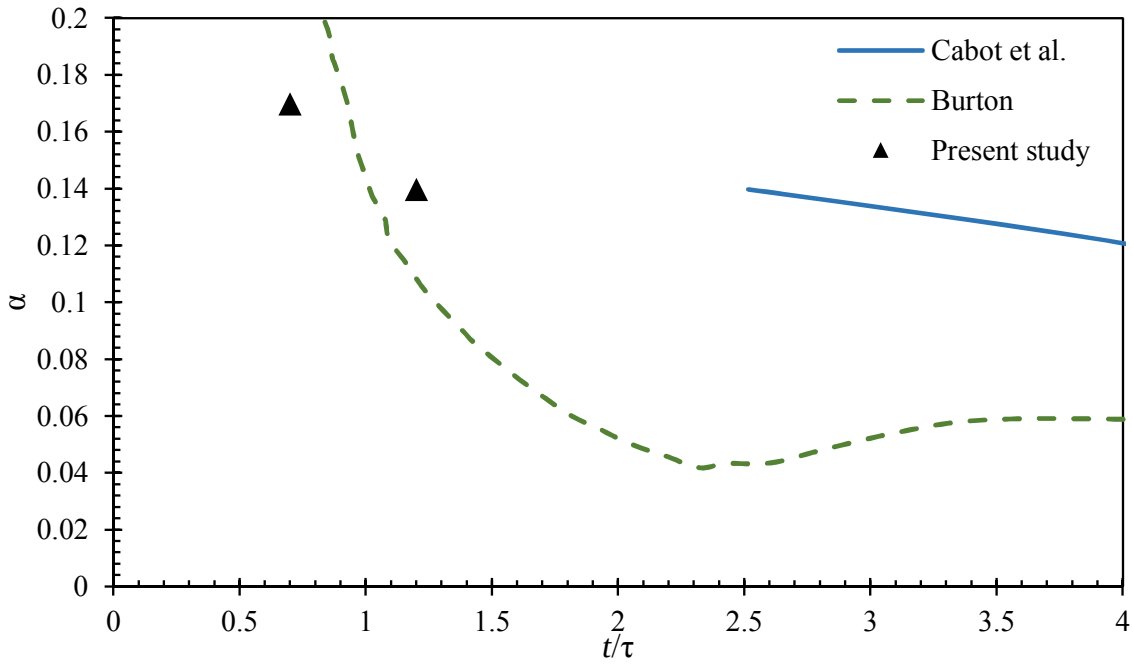

Figure 2.37: Examining the estimated value for α based on the best quadratic fits to our data. The two points display the calculated values while the lines represent values from existing literature [7, 8]. Plots are made vs. dimensionless time.

mechanism of instability amplification, likely contributes to the growth as well. The narrowing of the trough region may also play a role, as this will confine the vortices and intensify their strength [15]. A full decomposition of streak growth into its constituent mechanisms is beyond the scope of this study. Regardless, buoyancy, induced and proliferated by the combustion reaction, still asserts itself as the most likely driver of streak amplification. Additionally, the detailed experimental data we have provided may serve to validate future numerical simulations, which are likely needed to further probe these instabilities.

2.5.4 Surface heat fluxes

Although the streaks had been mapped with a thermocouple, it was still unclear what role they played in the overall heat transfer of the flame. In particular, it was unknown how the wavelike pattern of streaks and troughs affected the heat flux distribution to the surface, a controlling parameter in processes such as wildland fire spread. Consequently, a Vatell water-cooled heat flux gauge was employed to measure the total heat flux, and this device was mounted flush with the surface downstream of the burner. All measurements were taken under a flame streak or below a trough region in order to quantify the difference in heat flux between these structures. Four positions downstream of the burner were examined, x = 10, 15, 20, and 25 cm under two wind velocities, 1.1 and 2.2 m/s. Results are displayed in Figs. 2.38 and 2.39. The heat flux below the troughs, displayed as a dashed line, is greater than the heat flux below the streaks at all measurement locations. This indicates that the flame streaks are playing a significant role in modifying the spanwise distribution of the heat flux. This finding corresponds with the temperature profiles measured earlier, which indicated higher near-surface temperatures below the troughs.

The increased heat flux below the trough regions is likely a function of the flame standoff distance. Although we saw earlier that the flame streak can be significantly hotter than the trough, the flame sheet at the streaks is forced up and away from the surface by the upwash from counter-rotating streamwise vortices. Meanwhile, the trough is being pressed towards the ground by the downwash of the

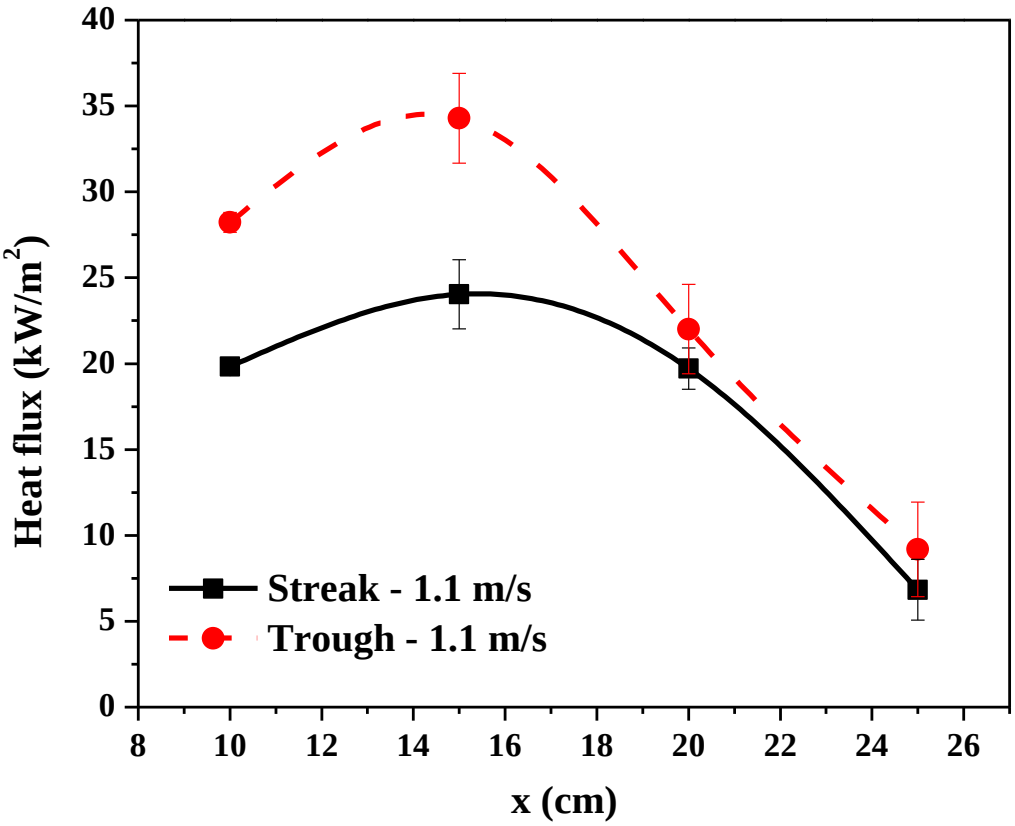

Figure 2.38: Measured heat fluxes vs. streamwise distance at a wind speed of 1.1 m/s. The solid black line indicates the heat flux measured below a streak while the dashed red line indicates the heat flux measured below a trough.

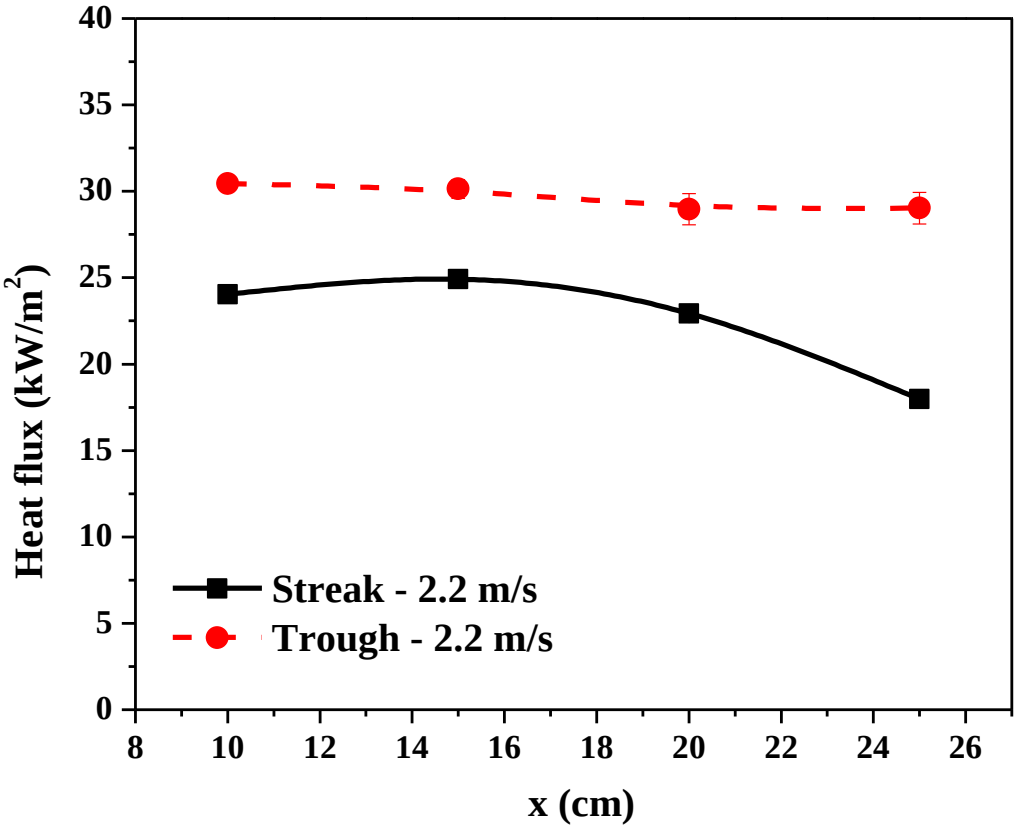

Figure 2.39: Measured heat fluxes vs. streamwise distance at a wind speed of 2.2 m/s. The solid black line indicates the heat flux measured below a streak while the dashed red line indicates the heat flux measured below a trough.

vortex pairs, decreasing the standoff distance from the surface and increasing the heat flux delivered.

2.5.5 Discussion

This study has identified two distinct regimes of the flame, streaks and troughs, which are differentiated not only by their visual appearance, but also by markedly different thermal properties. The flame streaks exhibit increased gas temperatures in a region that is lifted away from the surface. Meanwhile, troughs consist of a flame sheet which is forced downward, delivering a higher heat flux to the surface. Clearly, instabilities in boundary layer combustion can have an effect on the spanwise distribution of heat transfer. This finding has significant implications for boundary layer combustion, indicating that instantaneous properties can vary significantly in a three-dimensional flow field. While factors which increase the meandering of instabilities, such as turbulence, will serve to wash out *spatial* variation in the spanwise direction, there is still reason to expect that the mere presence of these instabilities could significantly alter time-averaged properties. In the first place, it is well-known that scalar dissipation affects flames, even influencing their stability and extinction [70]. The combined effect of powerful streamwise vortices, which would alter scalar dissipation, could serve to modify the large-scale behavior of a wind-blown flame. Secondly, the time-averaged properties of the flame can be considered to be the summation of intermittent fluctuations. As of yet, the role of intermittency in heating due to flames is still an area of active research. Finally, real-world situa-

tions exist where dominant instabilities will remain relatively stationary in boundary layer flames. For instance, upstream obstacles can introduce instabilities through vortex shedding. Downstream of this shedding process, dominant instabilities will be introduced to flames, potentially modifying important properties such as heat transfer. Results from this study have highlighted the ability for local instabilities to affect macroscopic properties of the flame. More research is necessary to investigate different regimes of instabilities in boundary layer combustion, but this study provides an experimental framework for future investigations.

2.6 Additional analysis on buoyancy and momentum

The location of the flame sheet in boundary layer flows is commonly described in terms of a competition between buoyancy and momentum. The buoyant force, which is derived from the high temperatures of the flame, serves to lift the flame sheet, while the momentum of the incoming wind threatens to push these hot gases back towards the surface. Flame attachment is commonly described using this analogy, but there is no scaling parameter for this parameter has been established in common practice. Much of the current analysis of flame attachment in wind-blown flames has been empirical in nature. Fundamentally, the problem of flame geometry can also be viewed as a mixed convection problem, in which the natural convection of the flame competes with the forced convection of the wind. Natural convection over a flat plate in flow is commonly described by the Grashof number, defined as

$$Gr_L = \frac{g\beta(T_s - T_\infty)L^3}{v^2} \tag{2.9}$$

where β is the coefficient of thermal expansion (equal to $1/T_{film}$ for ideal gases), T_s is the surface temperature, T_∞ is the ambient temperature, L is the relevant length scale, and v is the kinematic viscosity. The Grashof number quantifies the ratio of the buoyant force to the viscous force. Meanwhile, forced convection is typically characterized by the Reynolds number, or

$$Re_L = \frac{U_\infty L}{v}. \tag{2.10}$$

This parameter characterizes the inertial force relative to the viscous force. It would seem logical to characterize the buoyant force to the momentum force as a ratio of the Grashof and Reynolds numbers, and parameters of the form Gr/Re^n are commonly employed in the literature, where n is chosen differently based on the analysis. Among the earliest attempts to use such a parameter to quantify these flows was made by Lavid, who conducted a theoretical study of a chemically reacting laminar boundary over a horizontal plate in 1974. In dimensional analysis detailed in his PhD thesis [71, 72], Lavid determined that mixed convection was dominated by Gr_x/Re_x^2 for wedges and vertical walls and $Gr_x/Re_x^{5/2}$ for horizontal flat plates and small inclinations. These coordinate qualities were used to characterize the gravitational effects in the boundary layer flow. In mixed convection literature, Gr_x/Re_x^2 is commonly simplified to the Richardson number, defined as

$$Ri = \frac{g\beta(T_s - T_\infty)x}{U_\infty^2}. \tag{2.11}$$

This is a ratio of buoyancy to momentum, and it is commonly employed in mixed convection literature. In studies of wildland fires, this ratio has often been discussed in the form of the convective Froude number [73, 74], or

$$F_c = \sqrt{\frac{u - r}{g\frac{\Delta\theta}{\theta_\infty}L}}, \tag{2.12}$$

where r is the rate of spread of the fire and $\frac{\Delta\theta}{\theta_\infty}$ is analogous to the temperature difference in the Richardson and Grashof numbers. Upon rearrangement of terms, it can be seen that the convective Froude number is equivalent to $\sqrt{1/Ri}$ with a slight modifier on the wind speed to account for the spread of the fire. The inverse cube of this number is also occasionally discussed under the name of Byram's energy criterion. Sullivan [75] and Morandini and Silvani [76] have decried the role of this parameter in describing field-scale experiments, but a recent rebuttal to their conclusions has been made [77]. It is the opinion of this author that several studies which have decried the role of the convective Froude number or the Richardson number have suffered from improper or incomplete formulations. Neither Sullivan nor Moirandini and Silvani accounted for the boundary layer of the wind in their analyses, potentially mischaracterizing the wind velocity. In addition, the Richardson number in its simplest formulation, Eq. 2.11, neglects the likelihood that different length scales exist for both the Grashof and Reynolds number. When there is an

unheated starting length in horizontal mixed convection, the length scale for the Reynolds number includes the unheated length while the Grashof number does not. When the Richardson number is solved without account for this discrepancy, it no longer represents the relevant parameter Gr/Re^2.

These aforementioned parameters are not isolated to macroscopic scaling of boundary layer combustion. Researchers have also employed parameters of the form Gr/Re^n to describe instability onset in mixed convection over a horizontal heated plate. To determine the onset of thermal instability, several researchers [17, 18, 78] have employed the parameter $Gr_x/Re_x^{3/2}$ whereas several others [79, 80], have suggested $Gr_x/Re_x^{5/2}$. These studies have examined this onset by identifying the critical value at which longitudinal vortices appeared in the form of streaks. Imura et al. [17] even described three regions in the boundary layer: laminar forced convection ($Gr_x/Re_x^{5/2} < 100$), a transition regime where longitudinal vortices would appear and amplify ($100 < Gr_x/Re_x^{5/2} > 300$), and a transition to turbulence ($Gr_x/Re_x^{5/2} > 300$).

Whether the approach was focused on thermal instability of streamwise streaks or on dimensional analysis of boundary layer combustion, researchers have often employed a parameter of the form Gr_x/Re_x^n. For this reason, we chose to examine characteristics of our flow with respect to such controlling parameters. In particular, it was hypothesized that the shape of the flame and/or the shape of the streaks, both of which are governed by a competition between buoyancy and momentum, could be scaled with such a parameter. The flame shape was then defined similar to earlier analyses, demarcating the bottom and top of the flame sheet by 1000 K. Once this

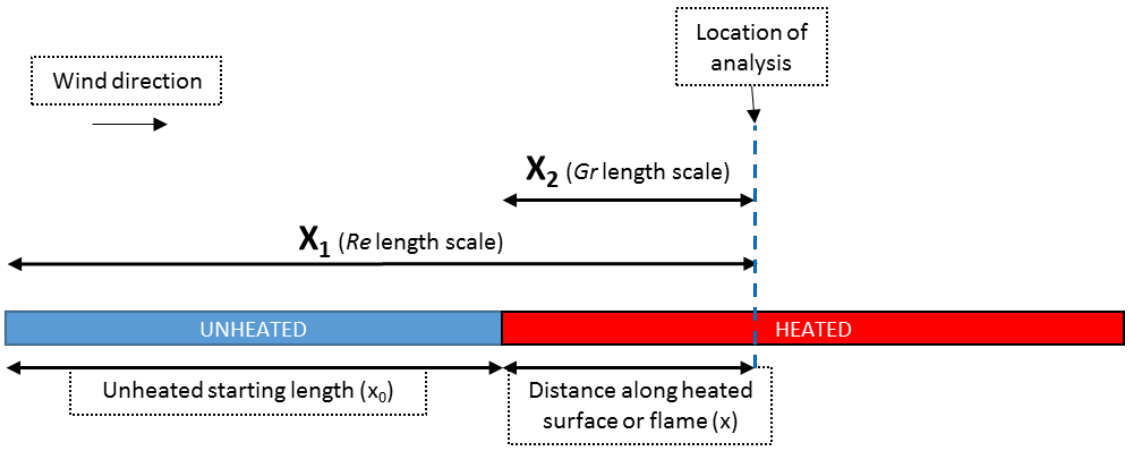

Figure 2.40: Schematic displaying proper length scales for use in the stability criterion.

was done, the location of the top of the flame sheet and the middle of the flame sheet were plotted vs. parameters of the form $Gr_{x_2}/Re_{x_1}^n$, testing historical values of n (3/2, 2, and 5/2). Re_{x_1} was established using the streamwise length scale from the leading edge (x_1), whereas Gr_{x_2} employed the streamwise length scale beginning from the burner's leading edge (x_2). Employment of appropriate length scales is necessary when an unheated starting length exists, and a schematic of these length scales is shown in Fig. 2.40. Neither of these parameters were static, as they varied with the streamwise location. Results plotted vs. $Gr_{x_2}/Re_{x_1}^{3/2}$ revealed no noticeable trend. However, the spatial development of the flame, taken as either the height or the middle of the flame sheet, was plotted vs. both $Gr_{x_2}/Re_{x_1}^2$ and $Gr_{x_2}/Re_{x_1}^{5/2}$ and revealed remarkable correlations. These results are shown in Figs. 2.41-2.44, on both normal and log-log plots. A power law fit was applied to the data, with all R^2 values exceeding 0.95.

These parameters show remarkable promise in terms of quantifying and predicting the flame geometry. In turn, an understanding of flame geometry can assist

a description of relevant heat transfer processes. It should also be noted that the fit of the power law to the data was independent of the flame temperature chosen in the Grashof number. For the plots shown, the approximate flame temperature (employed as T_s in Eq. 2.9) was estimated to be 1000 K. However, changing the temperature to another value had no effect on the accuracy of the fit, it simply changed the value of the coefficient a in the fit $y = ax^b$. As far as the author is aware, no other researchers have successfully scaled spatial growth of a flame or even of a thermal boundary layer with such parameters. This scaling shows remarkable promise for describing the growth of the flame, but more work remains be done to validate its applicability. Regardless, all parameters are known *a priori*, indicating the predictive power of the scaling. Additionally, this scaling has captured the effect of the unheated leading edge by using two different length scales for Gr_{x_2} and Re_{x_1}. In effect, this parameter may describe the interaction of the thermal boundary layer developing within a velocity boundary layer. In fact, the this parameter, which scales with downstream distance, is more properly understood as the scaling of the vertical length scales associated with the developing thermal and velocity boundary layers. The downstream length scales x_1 and x_2 were chosen because they can conveniently approximate the growth of these boundary layers. Further analysis of similar scaling parameters would benefit from detailed temperature and velocity measurements, which would concretely establish the boundary layer developments and could utilize these vertical length scales.

It should also be noted that this scaling is a local parameter. Further research would be useful to develop a global parameter describing the competition between

buoyancy and momentum. As mentioned earlier, several researchers have attempted to look at such a parameter, but the inherent assumptions and regimes of applicability seem to obfuscate extrapolation. One such common assumption is that a certain temperature difference must be assumed, which is not necessarily appropriate for a diffusion flame. It is more desirable to obtain a source-based parameter, such as that suggested by Yao [81]. Using dimensional analysis, Yao was able to show how a source based buoyant velocity could be described by the proportionality

$$U_0 \sim (Q^*)^{1/3}(gL_f)^{1/2}, \tag{2.13}$$

where L_f is the flame length and

$$Q^* = \frac{Q}{\rho_0 c_p T_0 g^{1/2} {L_f}^{5/2}}. \tag{2.14}$$

Further modifications would need to be made in order to apply such a parameter to a line fire, which would likely be described via a two-dimensional formulation with a heat release rate per unit depth. Further testing would also need to validate whether such a parameter could scale both bench-scale and field-scale fires or account for an unheated starting length. Scaling arguments could also be made to compare this reacting flow to the simpler mixed convection flows typically described in literature. Nevertheless, such a parameter would greatly assist researchers in quickly describing the regime of a wind-blown flame by means of a competition between a buoyant velocity and an inertial velocity.

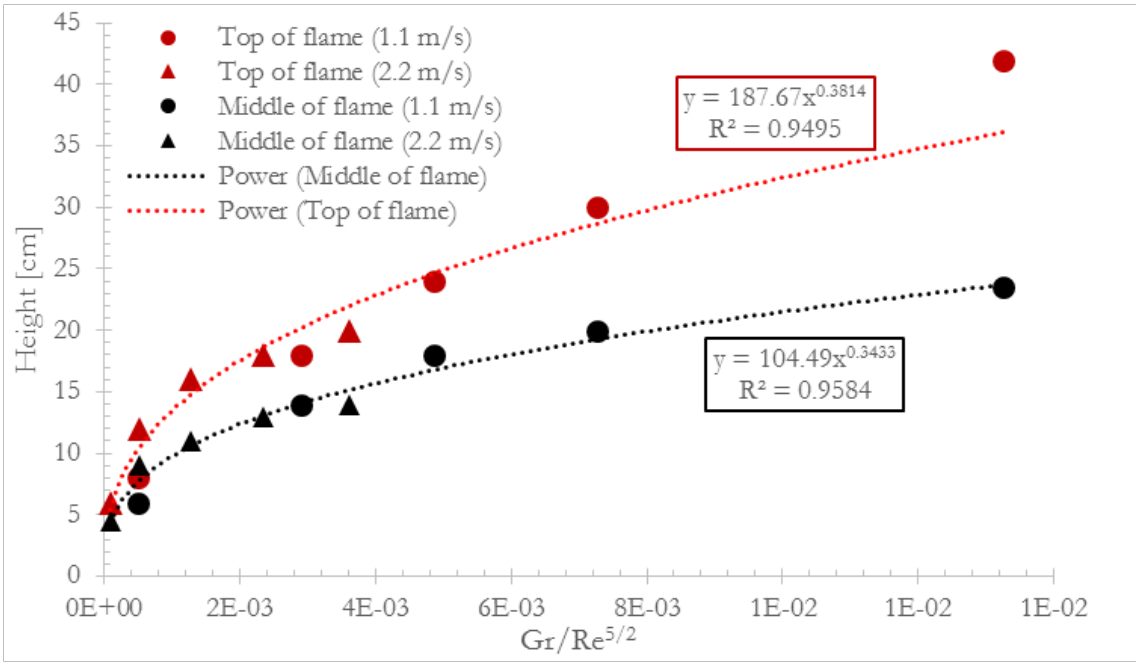

Figure 2.41: Flame heights, defined by either the top or middle of the flame , plotted vs. $Gr_{x_2}/Re_{x_1}^{5/2}$. A power law fit is applied to the data, and the equation and goodness of fit is displayed.

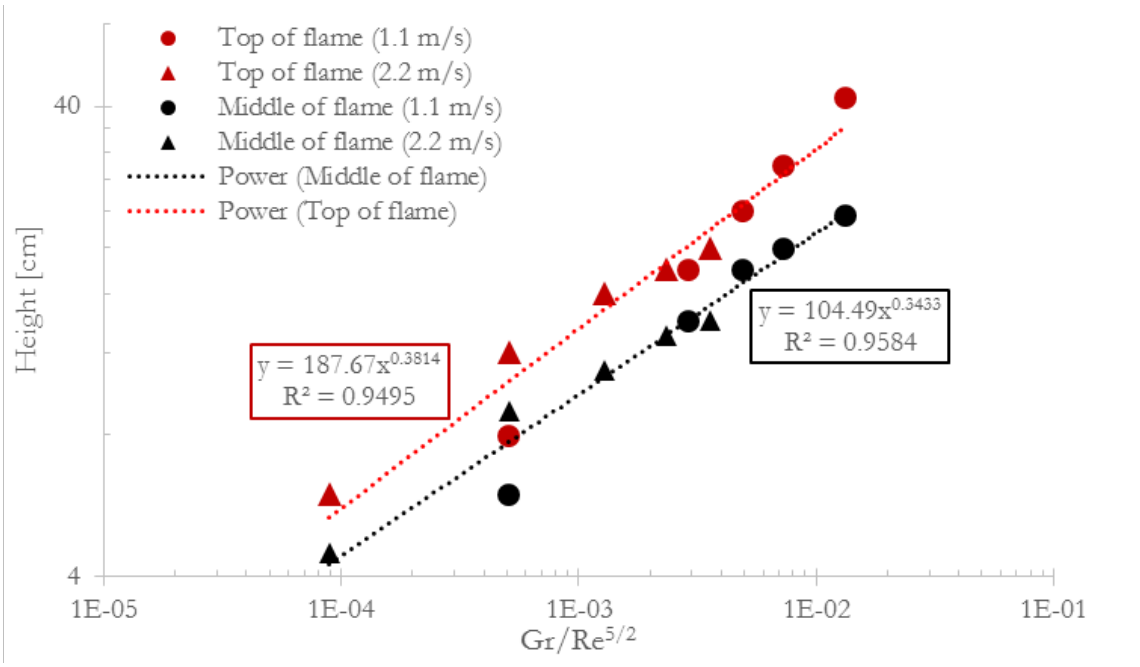

Figure 2.42: Flame heights, defined by either the top or middle of the flame , plotted vs. $Gr_{x_2}/Re_{x_1}^{5/2}$, on a log-log scale. A power law fit is applied to the data, and the equation and goodness of fit is displayed.

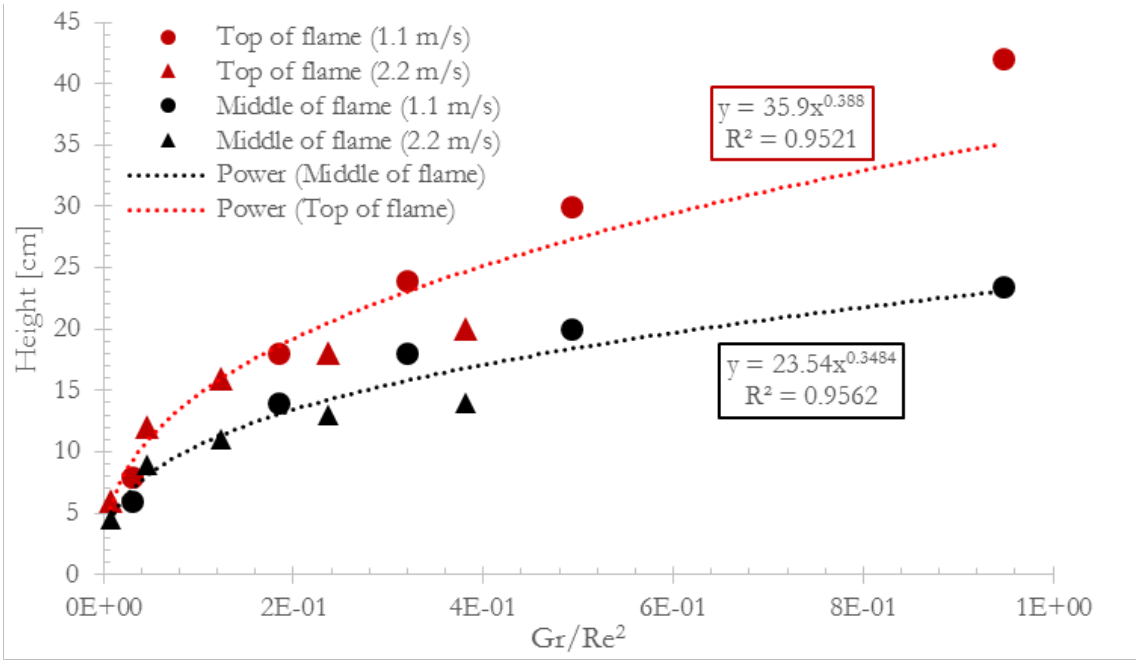

Figure 2.43: Flame heights, defined by either the top or middle of the flame , plotted vs. $Gr_{x_2}/Re^2_{x_1}$. A power law fit is applied to the data, and the equation and goodness of fit is displayed.

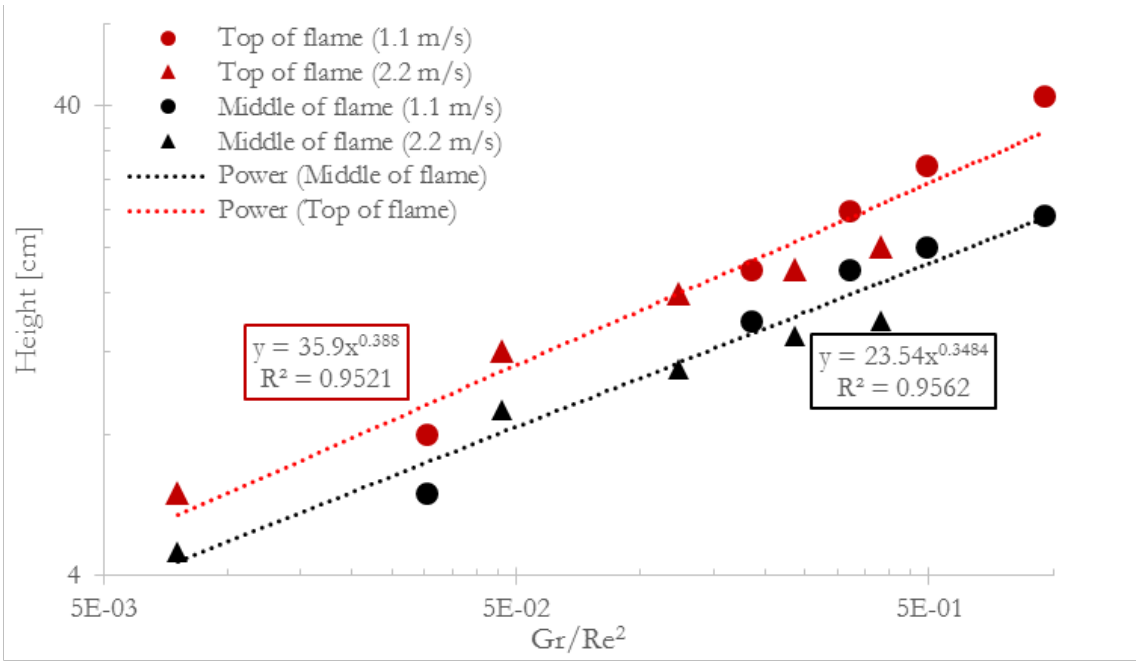

Figure 2.44: Flame heights, defined by either the top or middle of the flame , plotted vs. $Gr_{x_2}/Re^2_{x_1}$, plotted on a log-log scale. A power law fit is applied to the data, and the equation and goodness of fit is displayed.

2.7 Conclusion

This study examined the impact of streaks on a small-scale stationary flame in a laminar boundary layer. Initial observations revealed a strong dependence of the behavior of flame streaks on the development of the velocity boundary layer. Pre-existing velocity perturbations within the upstream boundary layer were employed to control the location of flame streaks. The temperature field was mapped by a thermocouple, and significant amplification of flame streaks was seen over the duration of the flame. The accelerated growth of streaks within the flame pointed to the influence of buoyancy, and results were determined to be compatible with Rayleigh-Taylor scaling. Gas-phase temperature redistribution, in the form of a higher temperature at flame streaks, highlights the variability of local properties due to the three-dimensional nature of the flow. Lower temperatures were observed in trough regions, but the decreased flame standoff distance enabled a higher heat flux below the troughs. Finally, the competition between buoyancy and momentum was examined by means of a stability parameter.

Two distinct regions of the flame, streaks and troughs, have been identified and shown to possess markedly different thermal properties. These instabilities clearly modify both the spanwise distribution of heat flux to the surface and the internal temperatures at the flame sheet. This finding has significant implications for boundary layer combustion, indicating that instantaneous properties can vary significantly due to a three-dimensional flow field. Scenarios may certainly exist where the typical two-dimensional assumption fails to capture controlling mecha-

nisms of heat and mass transfer. We have seen that an understanding of pre-existing sources of instability may be essential in describing coherent structures in a laminar boundary layer flame. Results from this study have highlighted the ability for local instabilities to affect macroscopic properties of the flame. More research at different scales is necessary to extrapolate these results to different regimes of instabilities in boundary layer combustion, but this study provides an experimental framework for future investigations.

Chapter 3: Streaks in mixed convection

3.1 Hot plate streaks

The previous experimental studies involved significant effort in characterizing flame streaks. However, there had been no effort to examine whether the behavior of such streaks could be scaled with respect to buoyancy. Consequently, the following experiment details measurements of streak behavior that were obtained over a heated plate in crossflow. Unlike the flame, which has a constant local source of buoyancy derived from the flame temperature, the heated plate can directly modify the local buoyant force through a modifiable surface temperature. The following experimental setup details results from streaks observed over a hot plate within a boundary layer, and it is followed by a subsequent study with a flame to determine whether streak behavior is analogous.

3.1.1 Experimental setup

All experiments took place in the low speed wind tunnel facility at the Missoula Fire Sciences Laboratory. The wind tunnel is 3.0 x 3.0 m in cross-sectional area, 26.21 meters in length, and is capable of reaching wind velocities of up to 3.12

m/s. The tunnel was operated under the recirculation operating mode, meaning that the air inlets and exhaust ports to the ambient were closed so that air is recirculated. This was done in order to avoid fluctuations due to ambient winds and pressure changes. An environmental conditioning section, which operates by means of heaters, chillers, steam generators, and spray nozzles, was employed to maintain a desired temperature and humidity. Before each test, conditions were checked to ensure that air properties were not deviating significantly. Overall, conditions were held nearly constant at 19 - 22°C and a relative humidity of 15 - 17%. Experimental wind speeds, as measured by a fixed centerline anemometer, were varied from 0.70 - 2.47 m/s.

A large horizontal platform, roughly resembling a table, was placed in the center of the wind tunnel, and its surface was 122 cm in width and 244 cm in streamwise length (see Fig. 3.1). A thin metal sheet (2-mm-thick) was fixed to the leading edge of this apparatus, and this sheet's horizontal surface, which was 26 cm in streamwise length, remained flush with the downstream platform. The metal sheet was employed in order to minimize bluff body effects which are often observed if the leading edge is obtuse. An aerodynamic boundary layer would develop over the horizontal surface, beginning at the front edge of this metal plate. 188 cm downstream of this edge, a large copper plate (2.5-cm-thick, 20.5-cm-long, 91.5-cm-wide) was embedded flush with the horizontal surface along the centerline of the platform. The bottom of the copper surface made direct contact with three electric strip heaters (1500 W, 240 V), which provided uniform heating throughout the conductive plate. A K-type thermocouple was wedged securely between the

copper plate and the surrounding insulation board to record the plate temperature via a temperature controller, which would regulate the plate temperature via on/off control. The downstream edge of the plate was normalized as $x = 0$, the origin for streamwise coordinates, and this distinction will be maintained in all discussions of the hot plate.

The macroscopic properties of both non-reacting thermal plumes and boundary layer flames is generally understood to be governed by a competition between momentum and buoyancy. Consequently, the parameter space of this experiment consists in varying the strength of momentum through the ambient wind velocity or in controlling the power of buoyancy through the surface temperature of the hot plate. For the following experiments, the bulk wind speed was held at either 0.70, 1.27, 1.86, or 2.47 m/s (+/- 0.04 m/s), while the surface temperature of the hot plate was either 150, 225, or 300°C. It should be noted that the local wind speed near the surface of the hot plate is less than the bulk flow velocity due to the development of a boundary layer.

A FLIR SC6811 infrared camera was placed above the hot plate in order to measure surface temperatures. The wavelength range detected by the camera was 3-5 μm, and five separate filters were employed to span temperatures from 0-350°C. An emissivity of 0.92 was assumed for both the copper plate and the surrounding insulation, which were painted black. The resolution of each image was 640 x 512 pixels covering a region roughly 42 cm x 35 cm over the center of the plate and the region just downstream. Temperatures recorded by the IR camera likely deviate from actual values by a small margin; nevertheless, this was not a great

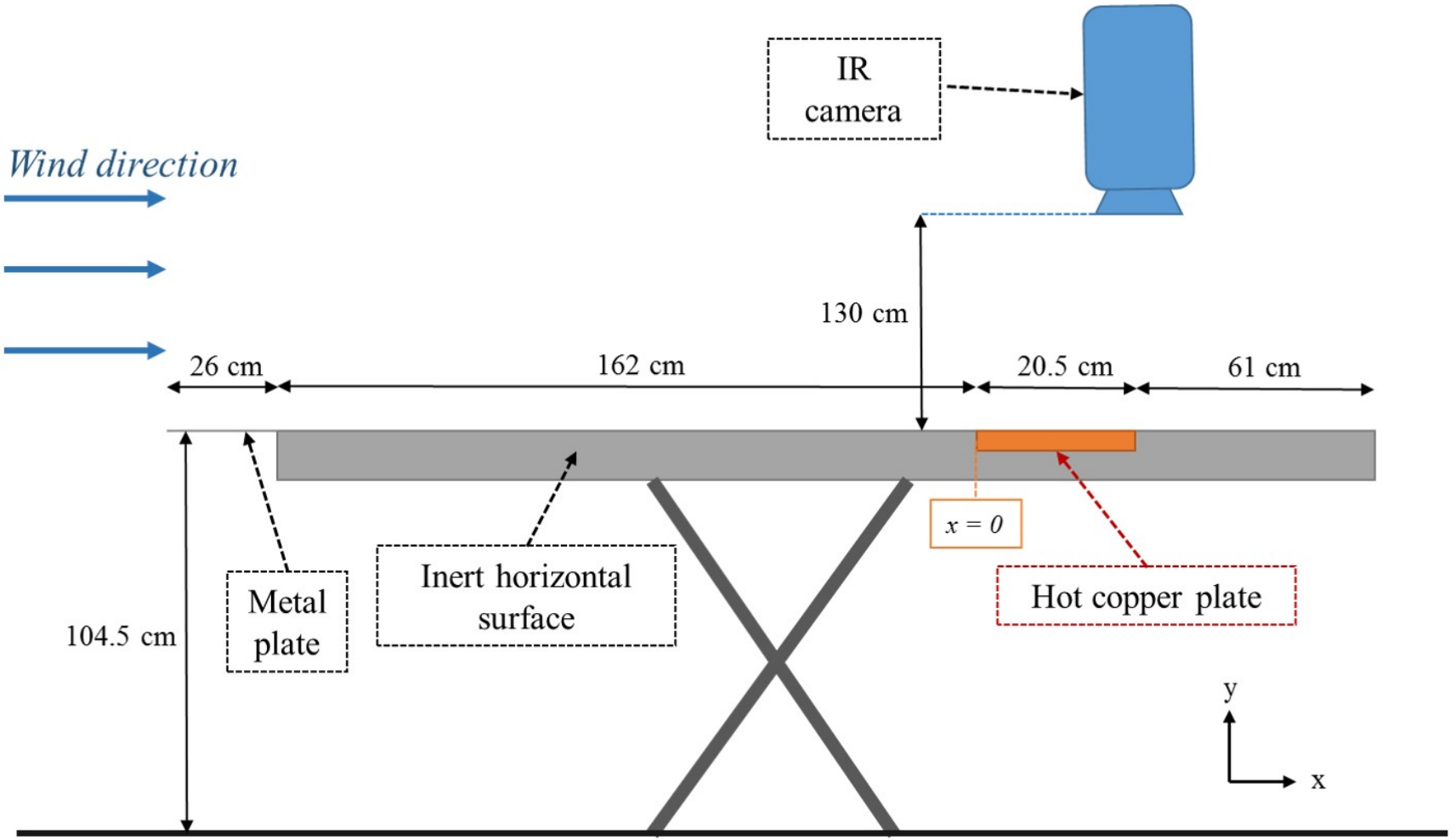

Figure 3.1: Experimental schematic of hot plate apparatus at the Missoula Wind Tunnel Facility. This apparatus was located in the center of a wind tunnel with a 3.0 x 3.0 m in cross-sectional area.

concern since our goal was detection of transient changes in surface temperature as opposed to precise measurements of absolute value. Errors due to refraction from hot gases appeared to be minimal, as images of surface temperatures remained well-resolved over the duration of the experiment. For each temperature filter and parameter space, the surface temperatures were recorded at 280 Hz for a duration of approximately 15 seconds. IR data was analyzed via MATLAB processing, in a methodology described later (see Section 3.1.2).

3.1.1.1 Velocity characterization

As a first step to characterizing the experiment, it is necessary to have some understanding of the incoming flow. For this reason, velocity measurements were taken in the region before the setup and just ahead of the hot plate. A TSI IFA 300 Constant Temperature Anemometer System was employed in the wind tunnel to obtain velocity profiles. This system is a fully integrated thermal anemometer-based system that measures mean and fluctuating velocity components in various fluids. The system consists of an anemometer, a thermocouple, data acquisition and analysis software, an A/D converter board, and an associated desktop computer (see Fig. 3.2). The T-type thermocouple was placed in the center of the wind tunnel to make sure temperature-based calibrations were accurate. Each measurements was made at a frequency of 1000 Hz for a period of 65 seconds.

All measurements were made in cold flow, meaning that neither the hot plate nor a burning fuel wick were active during velocity measurements. This was neces-

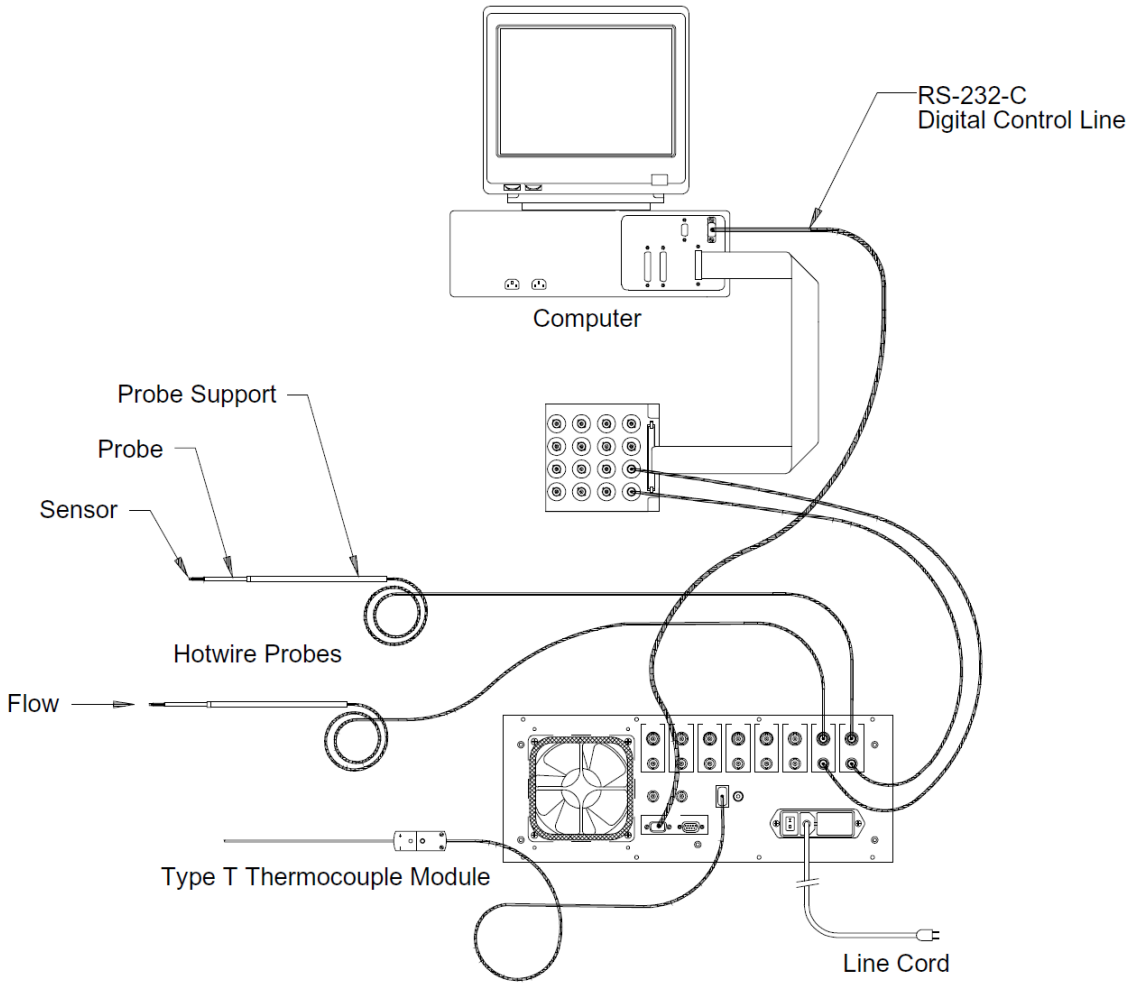

Figure 3.2: Overview of the TSI IFA 300 constant temperature anemometer system.

sary because the hotwire would be unable to account for the high frequency temperature fluctuations associated with these heat sources. For the profiles measured 1.5 cm upstream, it is possible that thermal effects could travel upstream to modify the measured velocity profiles in the presence of a heat source; regardless, the modification is expected to be marginal. The greatest deviations would occur for strongly buoyant flows with low incoming wind velocities, but all experiments exhibited inertial-dominated flow at upstream regions of the thermal plume. The measured profiles should provide a good indication of the incoming velocity.

The free stream velocity in the relevant portion of the wind tunnel was first characterized using the hotwire anemometer. Measurements were made at the centerline of the wind tunnel 1.5 meters upstream of the experimental apparatus. The surface of the apparatus sits 104.5 cm above the wind tunnel floor, so measurements were made at heights of 95, 105, 115, and 125 cm in order to capture the portion of the flow relevant to the experimental area. For each location, measurements were taken for a period of 65 seconds, and four wind speeds were tested. Results for each wind speed are shown in Fig. 3.3 below. The average of all four measurements from one wind speed were used to determine the free stream velocity, and these values are indicated in the legend of Fig. 3.3. The mean velocity varied minimally between heights, indicating a highly uniform flow across the height of the wind tunnel. Additionally, the flow was seen to be quite smooth, with turbulence intensity measurements were on the order of 0.01% (Fig. 3.4). These results indicate that the wind tunnel is well-conditioned and capable of providing repeatable incoming flow conditions for all experiments.

In addition to characterizing the bulk flow of the wind tunnel, the boundary layer forming over the experimental apparatus was also measured. Velocity profiles were assessed 1.5 cm upstream of the hot plate location, and measurement heights ranged from 3-200 mm. More spatial resolution was applied to the near-wall measurements in order to more properly characterize the shape of the boundary layer. Velocity measurements were taken over a period of 65 seconds for each data point, and results for all four wind speeds are displayed in Fig. 3.5. These results indicate that a boundary layer has clearly formed in the region upstream of the hot plate.

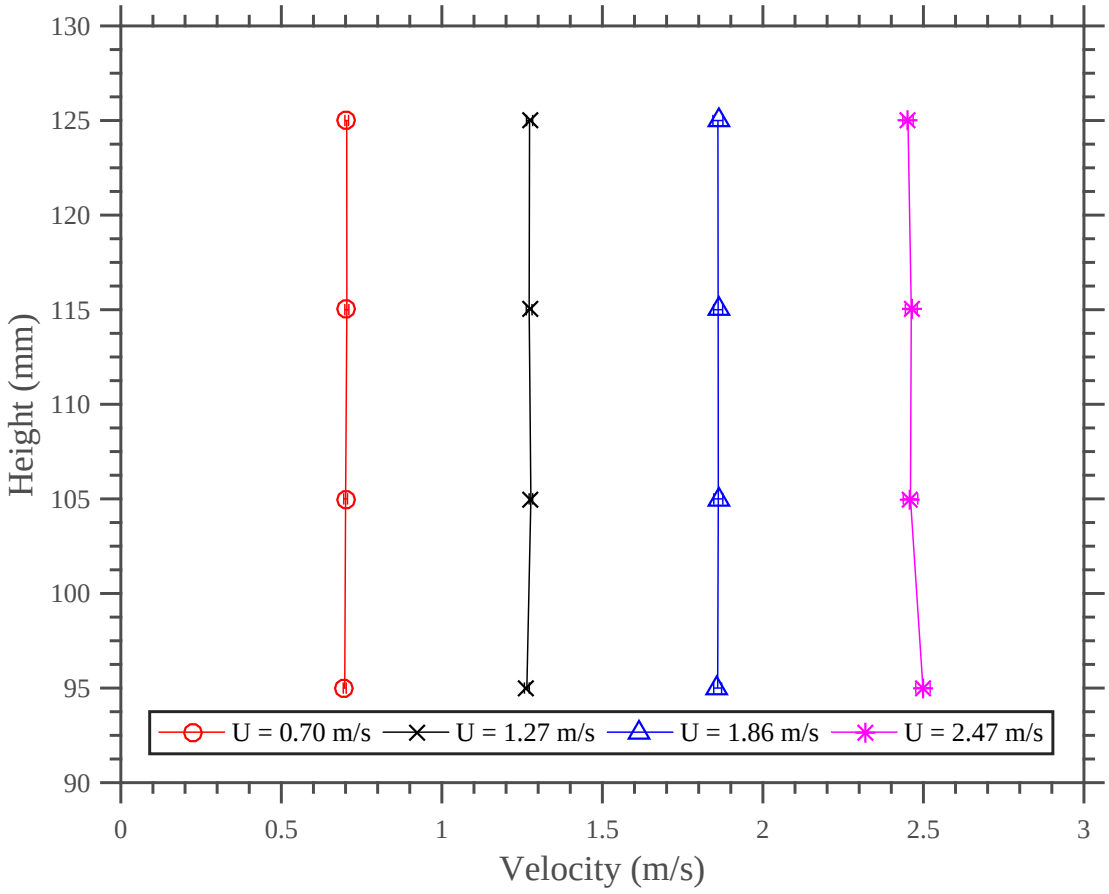

Figure 3.3: Plot of freestream velocity values at several heights in the center of the wind tunnel. Horizontal error bars indicate one standard deviation.

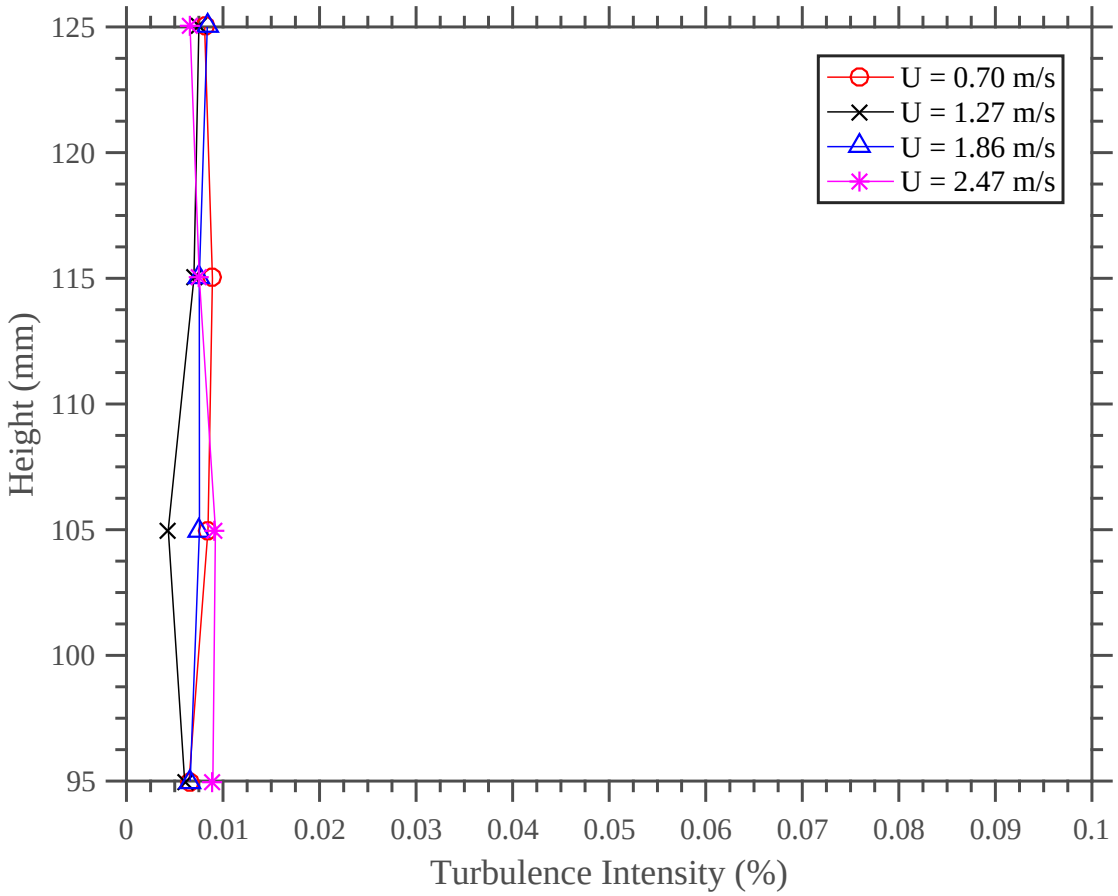

Figure 3.4: Plot of the turbulence intensity levels in the freestream flow at the center of the wind tunnel.

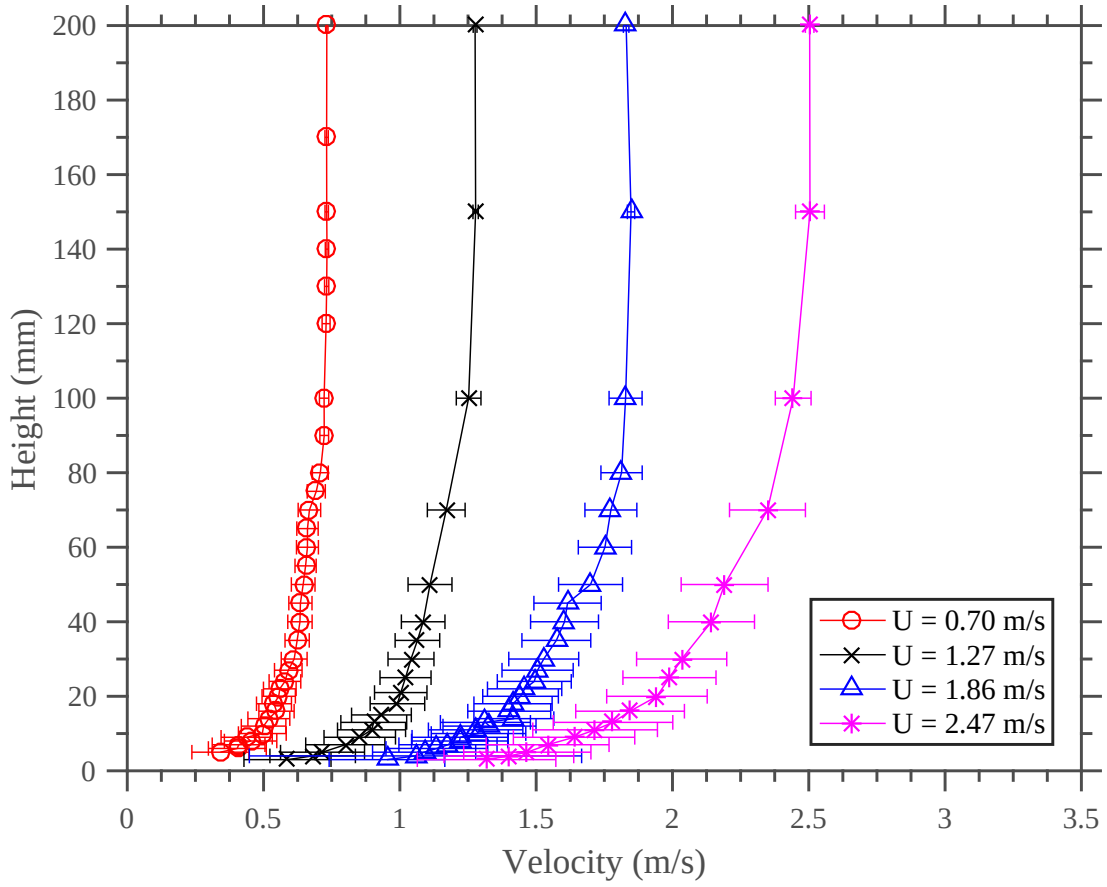

Figure 3.5: Height vs. velocity measured 1.5 cm upstream of the hot plate leading edge. Horizontal error bars indicate one standard deviation of the velocity data.

The turbulence intensities at these measurement locations were also determined by means of the following equation:

$$TI = \frac{u'}{U} \tag{3.1}$$

where U is the average of velocity at the same location over the measurement period and u' is the standard deviation of the associated fluctuations at this location. This measurement provides a good measure of the local flow perturbations, and results are shown in Fig. 3.6. For all wind speeds, the turbulence intensity profiles clearly collapse when plotted against height. This indicates that relative levels of velocity fluctuations are maintained throughout all tested boundary layers. Reported values for turbulence intensity do not exceed 1%, indicating minimal fluctuations.

The Reynolds number (Re) provides a measure of the relative strength of inertial forces to viscous forces, and it can be calculated as

$$Re = \frac{\rho U L}{\mu} = \frac{U L}{\nu} \tag{3.2}$$

where ρ is the fluid density, U the velocity of the bulk flow, μ the dynamic viscosity, ν the kinematic viscosity. L is a relevant length scale, and, in the case of a horizontal flat plate in crossflow, L is generally given as the distance downstream from the leading edge. At the velocity profile measurement location, which is immediately upstream of the hot plate ($x \approx 0$), the Reynolds number (Re) varies from 8.7×10^4 to 3.1×10^5, depending on the ambient wind speed. This places the relevant portion of the experiment at the upper end of the laminar regime for flat plate flow, in

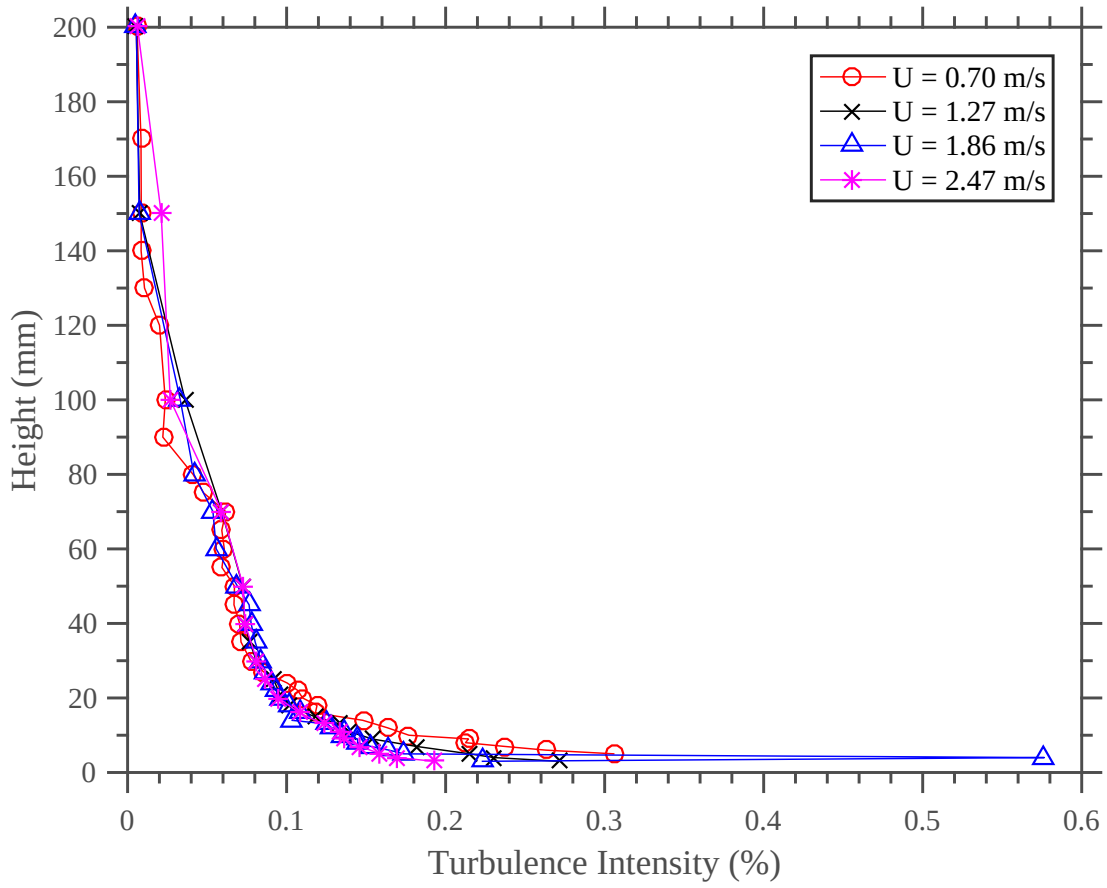

Figure 3.6: Height vs. turbulence intensities measured 1.5 cm upstream of the hot plate leading edge.

which transition is typically observed at $Re \approx 5 \times 10^5$. For this reason and due to unavoidable experimental non-idealities, we can expect slight deviations from the typical Blasius scaling for a laminar boundary layer.

It is often helpful to describe mixed convection in terms of competition between inertia and buoyancy. The Richardson number is generally employed in atmospheric flows and requires knowledge of temperature and velocity gradients, but a Froude number is frequently employed in wildland fire to describe the competition between inertia and buoyancy. This parameter is often formulated as $Fr = \dfrac{U}{gL}$, where U is the free-stream velocity and L is a relevant buoyant length scale. This length scale is often the flame length, flame height, or plume length. However, analogous buoyant length scales are not immediately apparent when comparing a heated surface to a fire. For this reason, it may be more appropriate to employ the definition of a convective Froude number given by Clark et al. [74],

$$Fr = \sqrt{\frac{U^2}{g\dfrac{\Delta\theta}{\theta}w}}, \tag{3.3}$$

where θ is the ambient temperature, $\Delta\theta$ is the temperature difference between the ambient conditions and the region of intense heating, and w is the length of the region of intense heating. For our parameter space, the convective Froude numbers range from 0.51-2.66. These values are nearly equal to values reported for simulated wildfires in Clark et al. [74], placing this experiment in a regime where both inertia and buoyancy are expected to govern the global flow structure.

In studies of boundary layers, scaling is often accomplished using a nondimen-

sional wall unit [82]. This wall unit is a non-dimensionalized quantity described by the following equation:

$$y^+ = \frac{yu_\tau}{\nu} \tag{3.4}$$

where y^+ is the distance in wall units, y is a relevant length, u_τ is the friction velocity and ν the kinematic viscosity. All properties were evaluated at a temperature of 20°C. Here, the friction velocity is defined as

$$u_\tau = \sqrt{\frac{\tau_w}{\rho}} \tag{3.5}$$

where τ_w is the wall shear stress and ρ is the density of air. Further, the wall shear stress is defined as

$$\tau_w = \mu \frac{\partial u}{\partial y}\Big|_{y=0} \tag{3.6}$$

where μ is the dynamic viscosity, and $\frac{\partial u}{\partial y}\Big|_{y=0}$ the velocity gradient at the surface. From these equations, we can see that the wall unit is directly related to the velocity gradient near the wall. In such a way, this measurement becomes a useful way to quantify the boundary layer profile, particularly for the near-wall portion which is relevant to near-wall streak formation.

We applied this procedure to the velocity profile from Fig. 3.5 in order to determine the length of a nondimensional wall unit at the leading edge of the hot plate. For each wind speed, the near-wall velocity gradient ($\frac{\partial u}{\partial y}\Big|_{y=0}$) was assessed via a linear fit; results are plotted in Fig. 3.7. These results are plotted against the hypothetical velocity gradient which would be obtained for a Blasius boundary

layer. This velocity gradient was calculated as

$$\frac{\partial u}{\partial y}\Big|_{y=0} = \frac{0.332\rho U^2}{\mu\sqrt{Re}}, \tag{3.7}$$

which can be derived from the well-established Blasius theory. For both theoretical and the experimental results, the trend for the velocity gradient to increase with the wind speed (in the form of the Reynolds number) remains remarkably similar. Once the near-wall velocity gradient was determined, the length of a non-dimensional wall unit was obtained via Eq. 3.4. Results are displayed in Fig. 3.8. Once again, the theory and the experiment exhibit a similar trend; here, the length of a single wall unit decreases with wind speed. This makes sense, as a wall unit is expected to scale with the boundary layer height, which decreases when the incoming wind speed is increased. These length scales can now be used to scale coherent structures observed in the flow; conversion of metric lengths to non-dimensional wall units will be applied in later section of analysis.

3.1.2 Detection algorithms

Significant post-processing was necessary in order to detect streaks from infrared images. The raw infrared image reveals a map of the instantaneous temperature based on an assumed emissivity for the object, and this data appears static if unprocessed. However, streaks that form over the hot plate and the surrounding inert material (which has been warmed by conduction) create regions of heating and cooling over the surface that can be visualized through post-processing. This

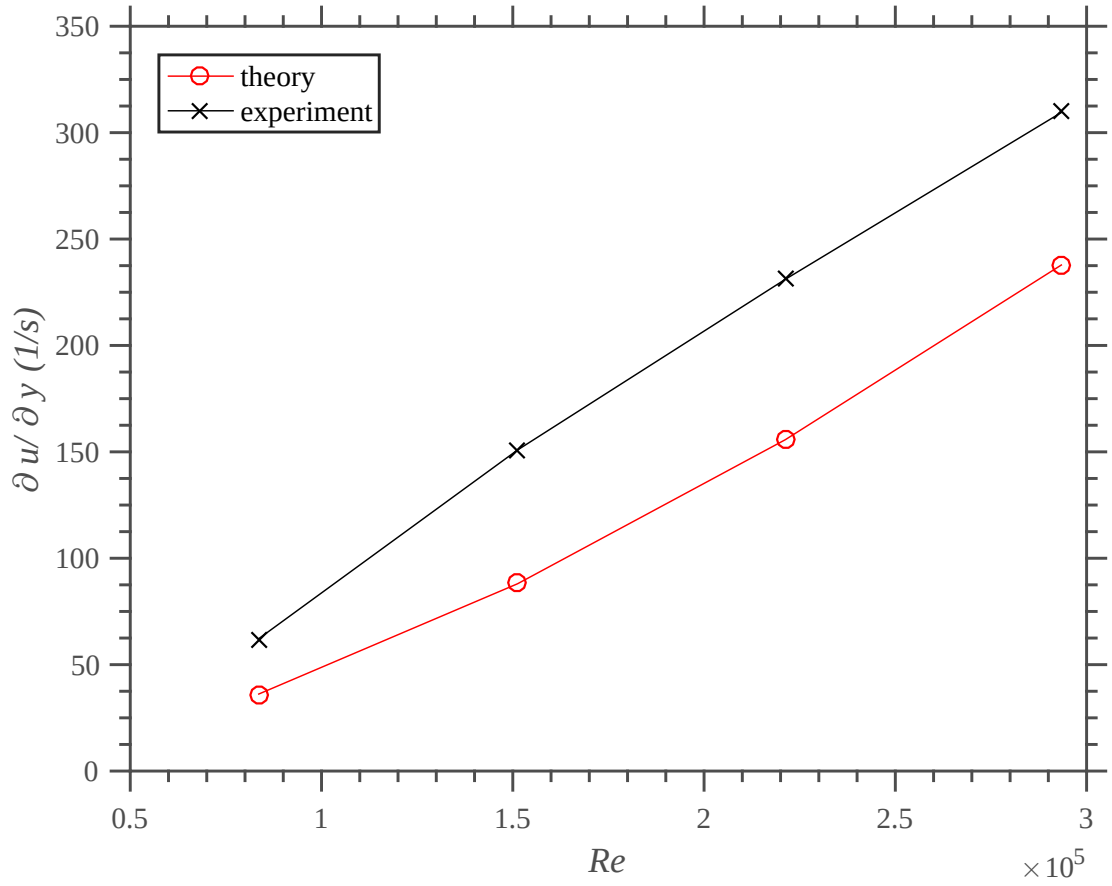

Figure 3.7: Near-wall velocity gradient vs. Reynolds number, as determined from experimental data and from Blasius theory.

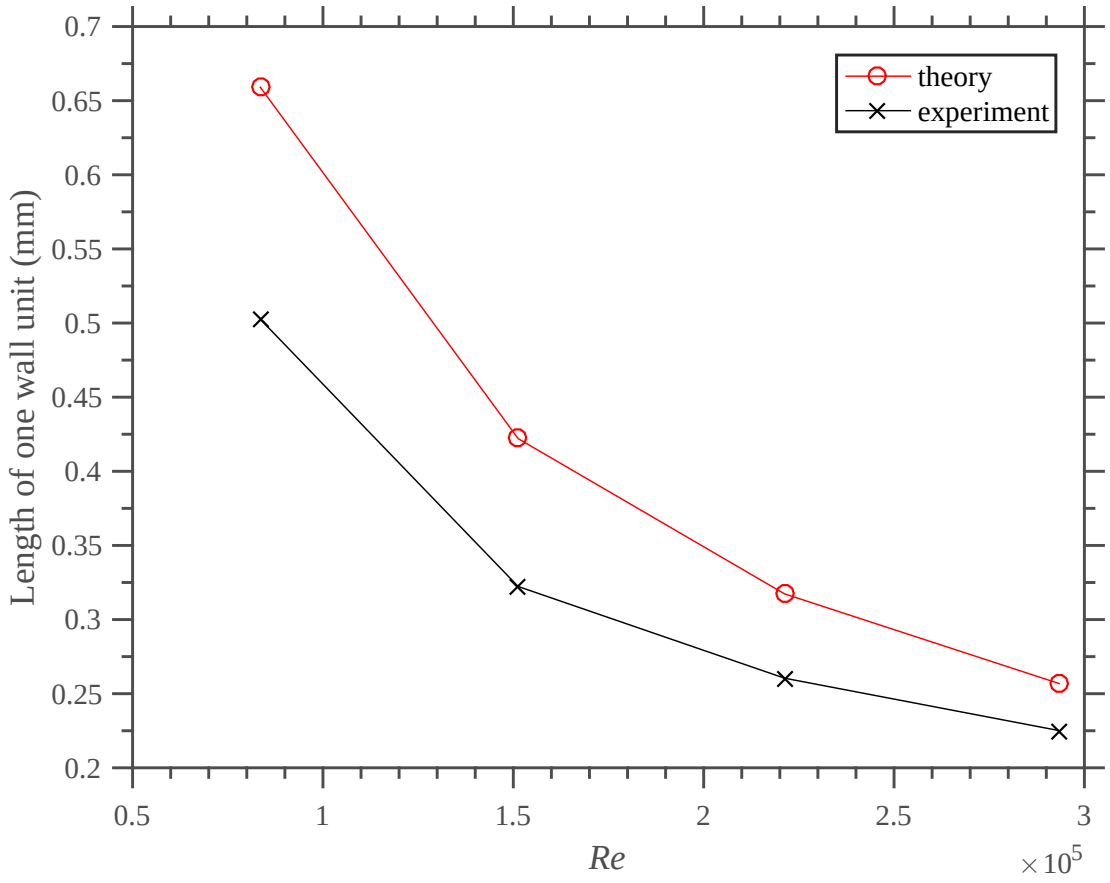

Figure 3.8: Length of a single wall unit vs. Reynolds number, as determined from experimental data and from Blasius theory.

phenomenon of surface heating and cooling is a consequence of the counter-rotating streamwise vortices which control the location of streaks (see Fig. 3.9). The downwash regions of these vortex pairs serves to pull cooler air from the ambient flow downward toward the heated surface. This fluid then cools the surface, creating a local region of decreased temperature in the downwash region, which is commonly termed a *trough*. In the upwash region, the hotter air from near the surface is pulled up and away from the ground. The resulting region of warmer, lifted air forms what we call a *streak*. Here, ambient fluid from the free stream is not readily entrained, so the surface is not cooled to the same extent as the trough region. It is this alternating pattern of heating and cooling on the surface that can be detected from infrared images. In this experiment, streak spacing is on the order of one centimeter, so significant spatial resolution is necessary in order to resolve this phenomenon. We found that a resolution of 640 x 512 pixels covering a region roughly 42 cm x 35 cm accurately resolved the streak spacings. Additionally, the streaks are seen to rapidly meander across the surface, which means that the sampling frequency of the associated infrared camera must be high enough to capture the instantaneous streak traces instead of washing out this motion. A frame rate of 280 Hz proved more than adequate for this purpose. Finally, the infrared camera must be sensitive enough to detect the magnitudes of these minute temperature changes.

In order to analyze this data, we elected to use a peak-finding algorithm because we found it to be the most intuitive. A variety of other methods have been employed by other researchers to look at streak properties, including visual inspection [58, 83–87], spectral methods [88, 89], and edge detection [90]. However, visual

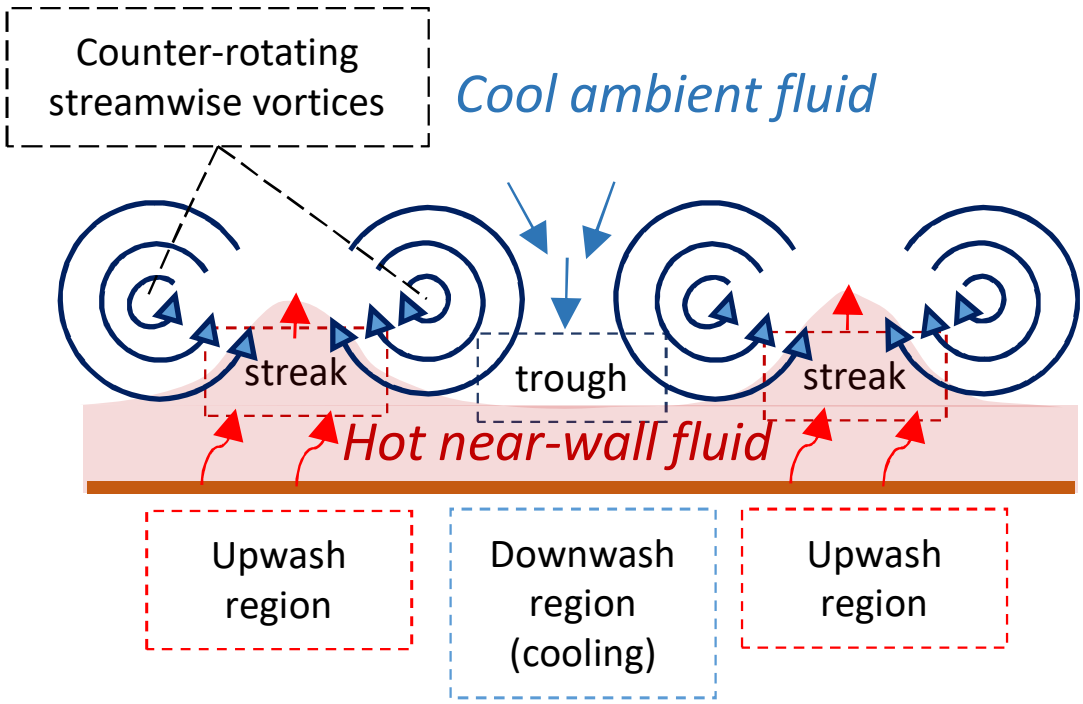

Figure 3.9: Schematic display the mechanisms by which counter-rotating streamwise vortices would create alternating surface patterns of heating and cooling.

inspection is simply too tedious and subject to human errors and biases to examine the large amount of infrared images available. Spectral methods, which tend to employ Fourier transforms and autocorrelations, have been reported to be unreliable [90–92]. Edge detection methods appear to hold promise [90], but we selected peak-detection because it is intuitive and repeatable when applied to a single spanwise profile of temperature fluctuations.

Streak traces become visible in spatial maps of temperature fluctuations. In order to extract this information, approximately 15 seconds of footage (4200 frames) were converted into MATLAB files (one file/frame). All images would then be imported into one large array, from which it was possible to determine a time-averaged image, which revealed a mean temperature map by looking at the average

temperature for each pixel. Next, it was necessary to look at the temperature fluctuations. Two methods were presented as viable options. The first was to simply look at the temperature change between a set number of frames. The second was to look at T', a measure of deviation from the mean. T' is calculated for each pixel by

$$T'|_{t=t_1} = \frac{T(t_1)}{\bar{T}}, \tag{3.8}$$

where $T'|_{t=t_1}$ is T' at a single time t_1, $T(t_1)$ is the instantaneous temperature, and $\bar{T}$ is the mean temperature over the sampling period.

The second method, which examines T', was selected as the more preferable option due to its repeatability and consistency. The only design choice to be made with this method is the total time period over which to determine the average temperature, which is generally insensitive when the range is large enough. Meanwhile, the first method necessitates the selection of a short time period which is highly sensitive to changes. This sensitivity is directly related to the meandering motion of streaks; as streaks move faster laterally, the optimal time period shortens, while the optimal time period increases when streaks meander more slowly. This sensitivity made the first method less desirable, so the second method was selected.

In order to validate the method for detecting T', the sensitivity of the mean surface temperature ($\bar{T}$) to the averaging period was assessed. Fig 3.10 displays a graph of a raw temperature signal overlaid with the average temperature determined by the length of the sampling period. From this figure, it is clear that the

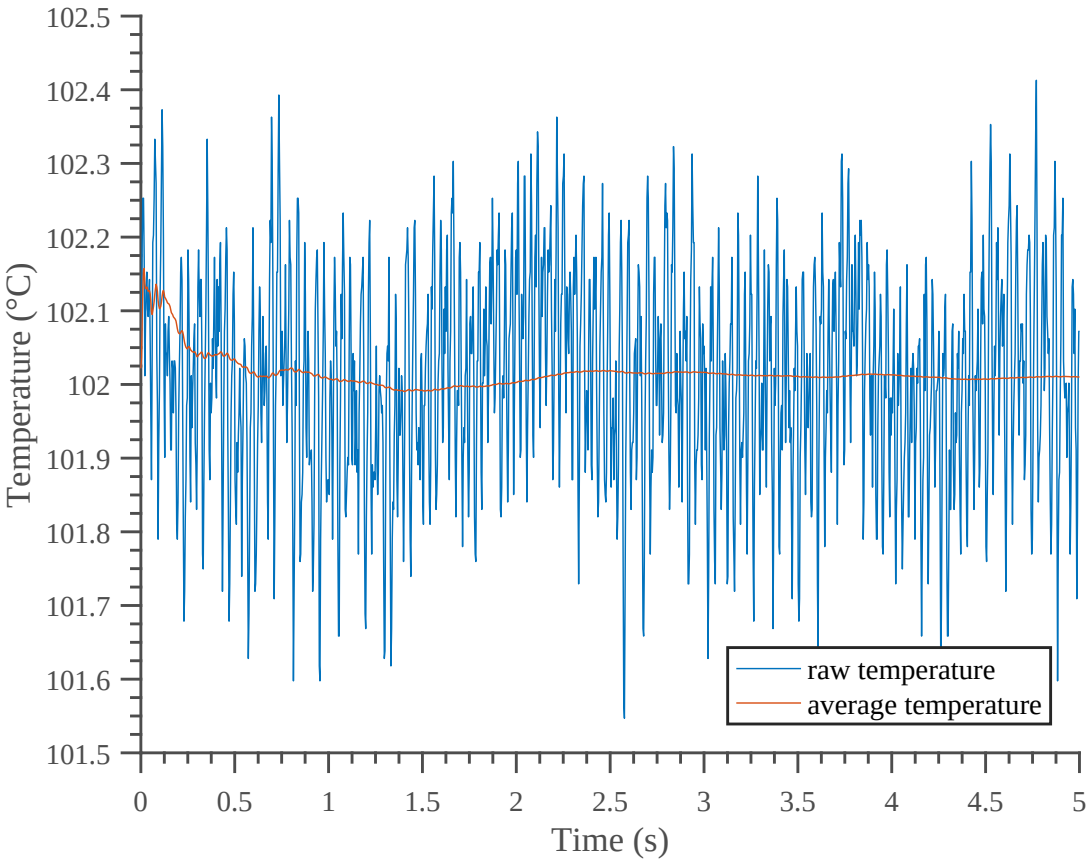

Figure 3.10: Graph of temperature vs. time for a representative location. Here, the average temperature at a single time is determined by an average of the raw temperature from 0 seconds to the specific time.

average period must be at least about one second in order to eliminate fluctuations. Beyond one second all the way up to five seconds, the average temperature changes minimally, indicating that a sampling period in this range is appropriate. It was determined that a sampling period of five seconds results in an average value that consistently assymptotes to an appropriate value. This enabled consistent determination of T' for detecting streaks.

A MATLAB program was then developed to post-process this data by scanning through each frame subsequently. For each tested parameter space, this program would tabulate T' over 1400 frames (5 seconds of data) by the aforementioned

method. Next, an example map of T' for one frame would be generated for the user to examine before proceeding to the next step. This map would display the traces of streaks made on the surface of the image in addition to displaying the region being analyzed, which was identified by the user at the setup of the program (see Fig. 3.11). This image would enable confirmation that the program was analyzing the correct region and at a position where streak traces could be seen. Fig. 3.11 is a good example, as clear traces of streaks can be seen in the map of temperature fluctuations around the selected region.

It should be noted that data taken by the IR camera would generally display either the heated plate or the area around it, depending on the temperature filter range selected for the camera during testing. This can be seen in Fig. 3.11, where the region over the heated plate is not captured by the camera. For this reason, temperature measurements over the hot plate at 150°C and 300°C were captured via temperature filters of 80-200°C and 150-350°C, respectively. Temperature measurements made over the surrounding insulated region at 150 and 300°C were possible with temperature filters of 35-150 and 80-200°C, respectively.

For all derived data, it was necessary to provide measurements of length scales in relevant units. Conversions from lengths in pixels to lengths in cm was made possible by measuring the depth of the hot plate in the derived images, and a conversion factor of 15.0 pixels/cm proved adequate. Since the camera angle was not modified between tests, the leading edge of the hot plate was consistently located approximately 19 pixels from the bottom edge of the image, meaning that this location could be normalized as $x = 0$ cm. All other streamwise distances were

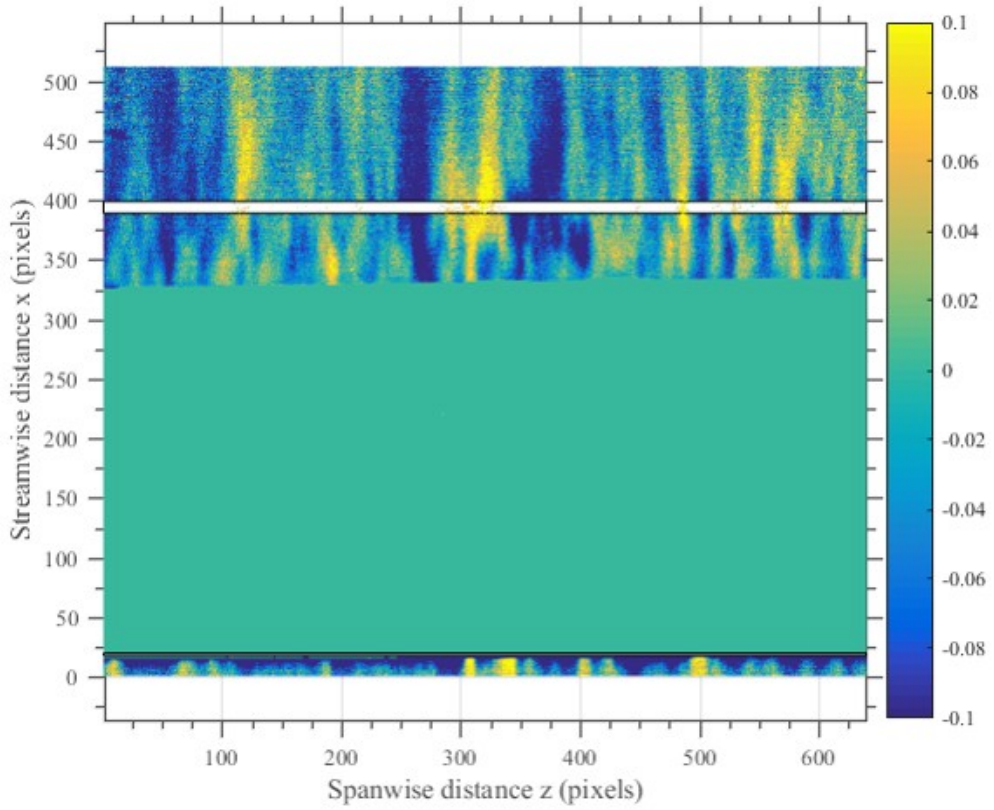

Figure 3.11: An example map of surface temperature fluctuations (T') generated for a test. Here, the instantaneous streak locations can be seen in yellow as positive fluctuations while troughs exist over the blue regions. All streak traces shown are found over the insulation surrounding the plate. The region over the heated plate does not display any streak traces because the temperature range of the infrared data for this example is not high enough.

then normalized using this reference point and the conversion factor. The user was instructed to input a specific streamwise location (in cm) to analyze, and this method enabled determination of the appropriate row of pixels to examine. Once this row was determined, a relevant region of the data above and below was selected in order to smooth out inconsistencies. The selection region was always 11 pixels (0.73 cm) in depth (i.e., 5 pixels (0.33 cm) above and 5 pixels below the user-indicated region).

Once the selection region was confirmed, a single spanwise temperature profile for T' was established by averaging the raw T' data in the streamwise direction. In other words, if the selection region was 640 pixels in width and 11 pixels in depth, all T' data would be averaged over the depth, resulting in an array with 640 data points. For a given selection region, this process would be repeated for all frames. Overall, this method proved to be very reliable, as it would smooth out some noise without smearing out the clear streaks and troughs in the resultant T' profile. Fig. 3.12 displays an example of this T' profile, in which clear traces of streaks and troughs are visible as peaks and minimums in the data.

Next, the MATLAB program would run through all frames in order to identify streaks in each T' profile. Significant work went into fine-tuning this analysis so that it could be consistently applied to all data regardless of profile characteristics. As a first step, the T' profile would be smoothed, with a smoothing span of 5 pixels (approximately 0.33 cm). This process made it easier for the peak-finding algorithm to avoid erroneous peaks. Once this signal was smoothed, it was ready to be thrown into the peak detection algorithm.

The peak detection algorithm was implemented by means of MATLAB's pre-

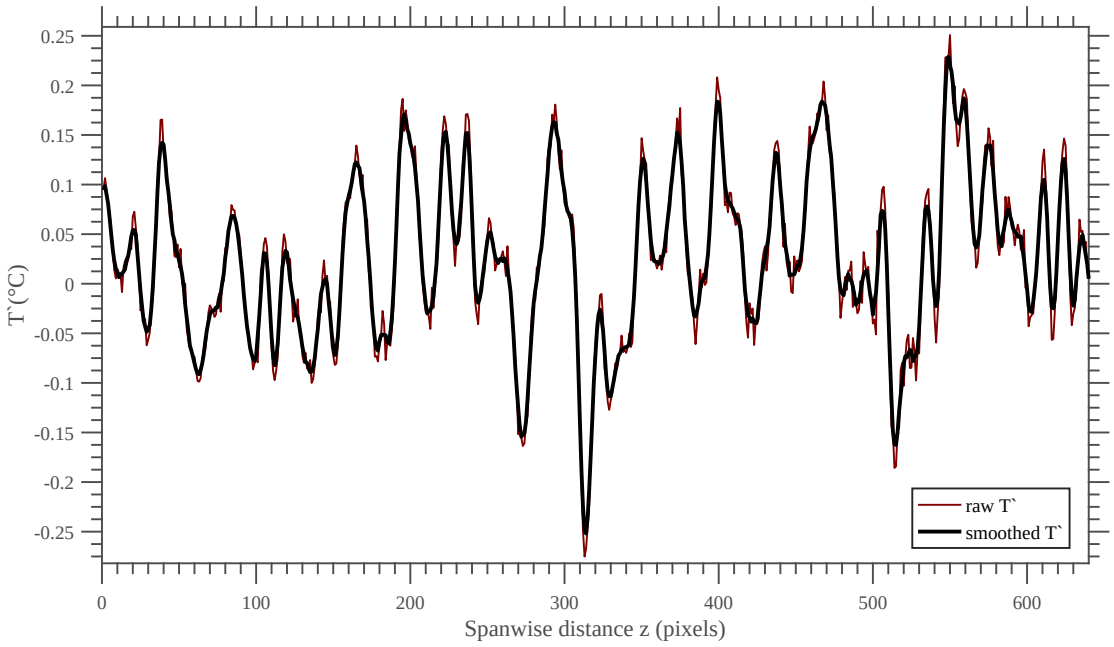

Figure 3.12: Example T' profile plotted vs. spanwise width along with the resulting smoothed T' profile.

existing command *findpeaks*, which returns local maxima from a given signal. The inputs to this command, nonetheless, had to be specified in order to reliably detect peaks. Several input parameters were considered for this algorithm, and these options included specifying minimum peak height, minimum peak prominence, minimum height difference, minimum peak separation, minimum peak width, or maximum peak width. After testing several options, it was decided that a minimum peak prominence would be most reliable. The peak prominence refers to the height of the peak in a signal, as determined by MATLAB's algorithm. It should be noted that the determination of prominence by MATLAB differs from the value for peak amplitude defined later. A minimum peak prominence proved reliable enough because it would eliminate peaks that were small while retaining peaks that clearly indicated streaks. In other words, large temperature fluctuations due to the presence

of upwash and downwash regions in the flow would be detected while erroneous detections of noise would be minimized. This process was repeated for all 1400 frames, providing a large dataset from which statistically sound deductions could be made. Nevertheless, a threshold minimum for the peak height had to be specified. Because the height of these peaks would change depending on the temperature of the plate or the streamwise location, choosing a single value was not desirable. Instead, the height was determined by looking at the T' profile, pulling out the standard deviation, and specifying the minimum prominence as 50% of the standard deviation. In this way, the minimum height was established as being proportional to the fluctuations observed in the signal. This process was able to be applied across all experimental conditions, and it seemed to be fairly robust. In analysis of results from various frames, a value of 50% for the percentage of the standard deviation could be seen to reliably detect most streaks and eliminate most noise. For each test, the user would be presented with results from 5 separate images to confirm that the detection algorithm was working as intended.

In addition to identifying the location of the streaks for each image, it was also desirable to look at streak width, streak amplitude, and streak spacing. The streak spacing was simply determined by tabulating the distance between peaks of adjacent streaks. The streak amplitude was determined by the following method: minimum values in the T' signal between the analyzed streak and its adjacent neighbors to the left and right would be indexed; from here, the amplitude was evaluated to be the difference between the T' value at the streak (necessarily a peak in the data) and the larger of the left or right minimum values. The streak width would then

be determined by the following method: the raw T' value between the larger of the left or right minimums and the peak value would be assessed and termed the *midval*; next, the algorithm would move left from the peak value at the streak to find where the signal was less than or equal to the midval - this would be the left extent of the streak; the algorithm would repeat this process to the right to identify the right extent of the streak; the width was then selected as the distance between the left and right extents. It should be noted that widths and amplitudes are determined separate from MATLAB's *findpeaks* command. The described algorithm was implemented in order to more properly model streak locations, which would not be expected to overlap in the way MATLAB's *findpeaks* command identifies peaks.

Fig. 3.13 shows the final results of this process for an example frame, where the streak locations, widths, and amplitudes are overlaid on top of the T' profile. It can be seen that there are a couple smaller fluctuations in the data that could be accepted as streaks if the sensitivity of the algorithm was increased. However, it could also be argued that these fluctuations are not representative of well-developed streaks. This is a fairly subjective decision, but examination of Fig. 3.13 clearly indicates that the detection algorithm is working at an adequate level, especially given that it can be consistently applied for all input conditions, including plate temperature, wind speed, and streamwise location. When averaged over 1400 images a consistent distribution of data can be derived, as subsequent results will show.

In addition to locating streaks at each frame, it was also desirable to track the movement of streaks between frames. The streaks observed in this flow do not maintain a fixed position, but meander rapidly in the spanwise direction, occasionally

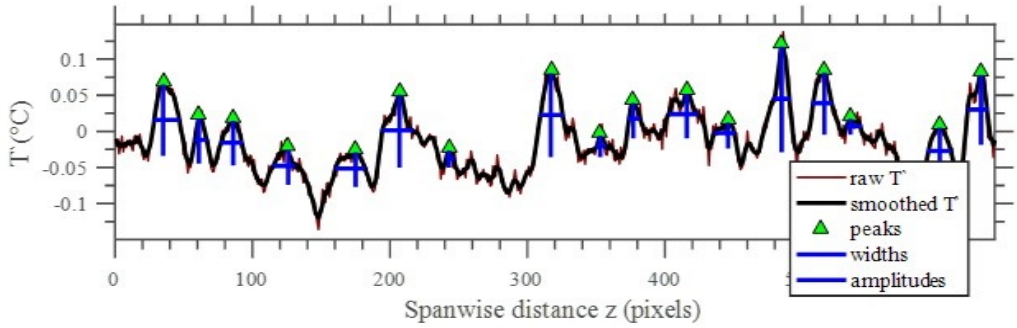

Figure 3.13: Example of the streak detection algorithm with displayed results for one image. Here, the raw T' profile is shown as a thin red line while the smoothed profile is shown as the thicker black line. This image also shows derived streak locations or peaks (green triangles), streak widths (horizontal blue lines), and streak amplitudes (vertical blue lines).

merging with other streaks, sometimes splitting, eventually dissipating and giving way to the birth of new streaks. If the streak detection algorithm is robust enough and the frequency of the camera is high enough, it should be possible to describe these processes. In fact, we developed an automated program that employs tools of image processing to attempt to quantify and visualize some of these complex streak behaviors.

In order to track the movement of streaks, it would be intuitive to posit that, between two consecutive frames, the most likely candidate as a match for a streak in the first frame is the one that is spatially nearest in the second frame. This intuition was applied to the compiled data, which now tabulated locations of streaks over time. By looking to see if a streak in a subsequent frame was near to a streak in a previous frame, the lateral movement of streaks was assessed. Of course, it is necessary to determine a distance threshold for this matching process, beyond which streaks are determined to be too far away to be a match. This distance could have

been specified as a static length scale, but it would be preferable to establish a scale that can adjust for varying streak behaviors. In particular, one would not expect a streak to shift laterally beyond a certain percentage of the streak spacing (given that the time between frames is small enough). For this reason, the maximum distance a streak could be observed to obtain a match was established as 85% of the mean streak width (later it will be shown that the width is more or less proportional to the streak spacing). Overall, this threshold appeared to work well.

Several other streak behaviors could be tracked via image processing. When two streaks from a previous frame both matched with a streak from the future frame, the closer streak was matched. This scenario, in which streaks would appear to combine forming an inverse 'V' shape, could be described as a streak merging event. This merging process could continue or fail to propagate along the upstream or downstream extents of the streak. Whenever a merging event was detected, the location and frame were recorded. In addition, if one streak from a previous frame obtained two possible matches in the next frame which were not closer to any other pre-existing streaks, a splitting event would occur. This behavior is visualized as a 'V' shape in the streak traces. The location and time of such events was recorded, similar to merging events. Finally, the birth and deaths of streaks was also tabulated. When a streak obtained no matches in the subsequent frame or if its only matches were closer to other pre-existing streaks, the lifetime of the streak would be terminated. Additionally, when a streak appeared in a subsequent frame that had no proper matches from the previous frame, it was determined to be a new streak. By assessing this birthing and dying process, it was possible to

attach lifetimes to streaks. These lifetimes are also described as streak durations in subsequent discussions. Other small programming conditions and checks were also embedded into the image processing program in order to ensure that streaks would not be double-counted or neglected in temporal analyses.

By examining the movement of a streak between frames, it was also possible to determine the lateral velocity attained by each streak. This lateral velocity was calculated as the distance traveled by the streak divided by the time between frames, and it was tabulated for every frame.

Overall, these image processing techniques resulted in a coherent framework to describe streak behavior. In fact, it was possible to obtain a descriptive picture of streak behavior over time at a particular streamwise location using the aforementioned process. Fig. 3.14 displays an example of the streak behavior obtained at a particular streamwise location over time. Realizing that the y-axis displays time, the resulting graph can be conceptualized as the traces streaks would make over time if viewed through a thin stationary slit. The resulting streak traces provide a beautiful and insightful description of streak behavior, which are described in more detail in the results section.

The aforementioned processes would be repeated at various streamwise locations in order to generate data immediately ahead of the hot plate (approx. $x = -0.6$ cm), over the hot plate ($x = 2.5$, 7.5, 12.5, 17.5 cm), and downstream ($x = 22.5$, 25, 27.5, 30, 32 cm). Data was available before the hot plate due to the fact that conduction would heat the inert material adjacent to the plate. Consequently, streak traces could be visualized even before the onset of the plate, a finding which later

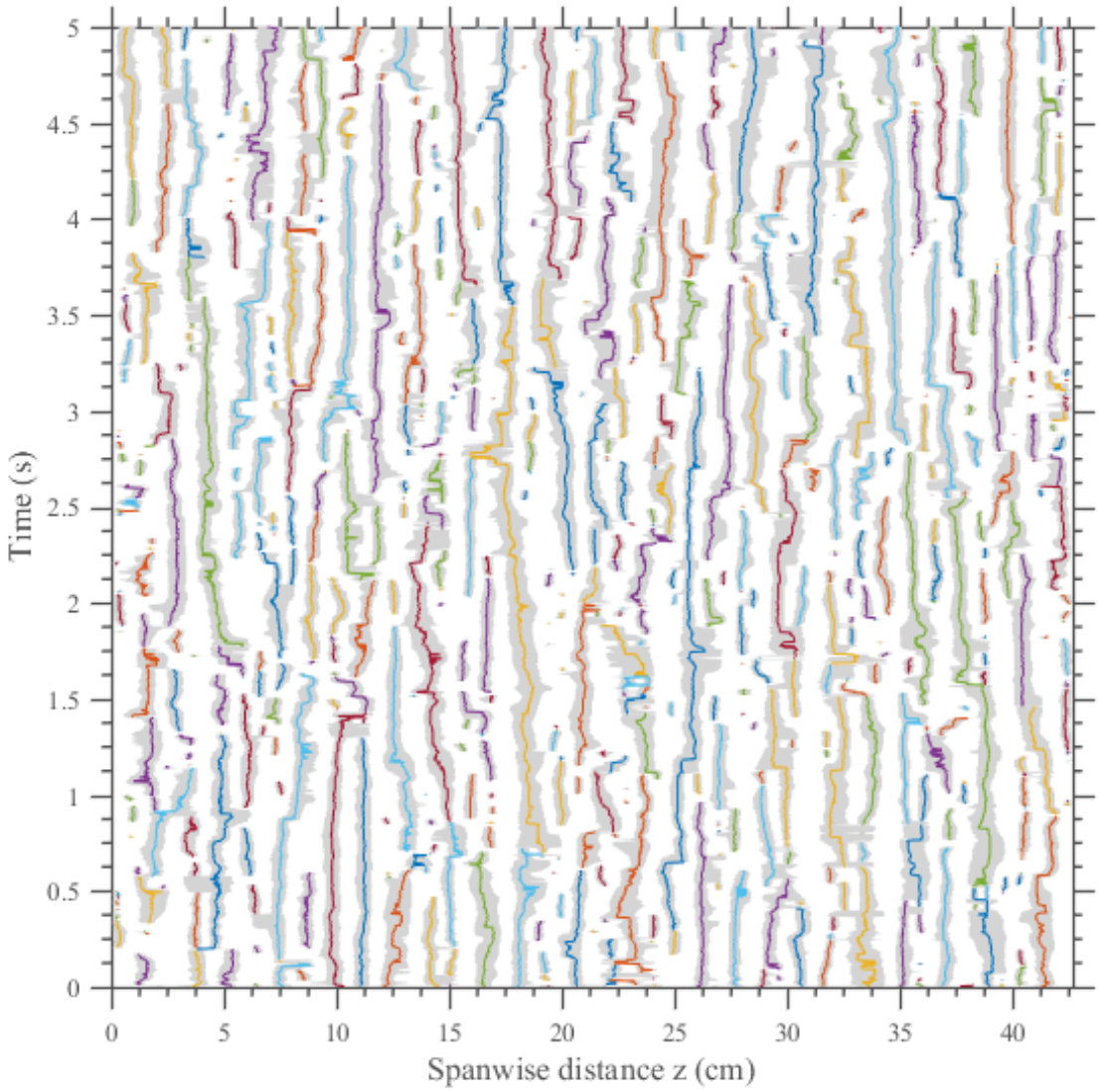

Figure 3.14: Graphical illustration of streak tracking, in which the spanwise locations of streaks are plotted against time. Thin colored lines represent streak centerlines whereas light gray areas represent streak width. Data for this figure was obtained 225 mm downstream of the plates leading edge at a wind speed of 1.27 m/s and a plate temperature of 300°C.

proved quite useful in assessing initial length scales.

Unfortunately, the data taken over the hot plate was generally obscured, and this appeared to be at least partially due to background noise at approximately 30 and 60 Hz. This was likely a result of background electrical noise related to the alternating current providing power to the heated plate. Taking an FFT of a single pixel's temperature signal over time reveals these noisy peaks. Fig. 3.15 displays a power spectral density where peaks at these noisy regions can be clearly seen. Consequently, bandpass filtering was employed for data taken from the heated region ($x = 0 - 20.5$ cm). The filter was designed as a bandstop infinite impluse response (IIR filter) directed towards the relevant frequencies (approximately 30 and 60 Hz). Fig. 3.16 displays the resulting T' data for the entire sampling period plotted over the frequency domain, where the noise at the problematic frequencies is adequately reduced.

Unfortunately, even after bandpass filtering, data over the hot plate was not as coherent as desired. For this reason, derived data from this region is less accurate than that of the inert regions. Filtering the signal also resulted in artificially reduced streak amplitudes. For this reason, discussion of final results often excludes data over the hot plate. This is performed because certain results are known to be inevitably modified by the filtering process.

For all parameter spaces, the user was provided with relevant graphs to assess whether different aspects of the aforementioned algorithms were working correctly. All important data was tabulated and saved, and eventually data from all parameter spaces was collectively compiled and used to generate graphs of important trends.

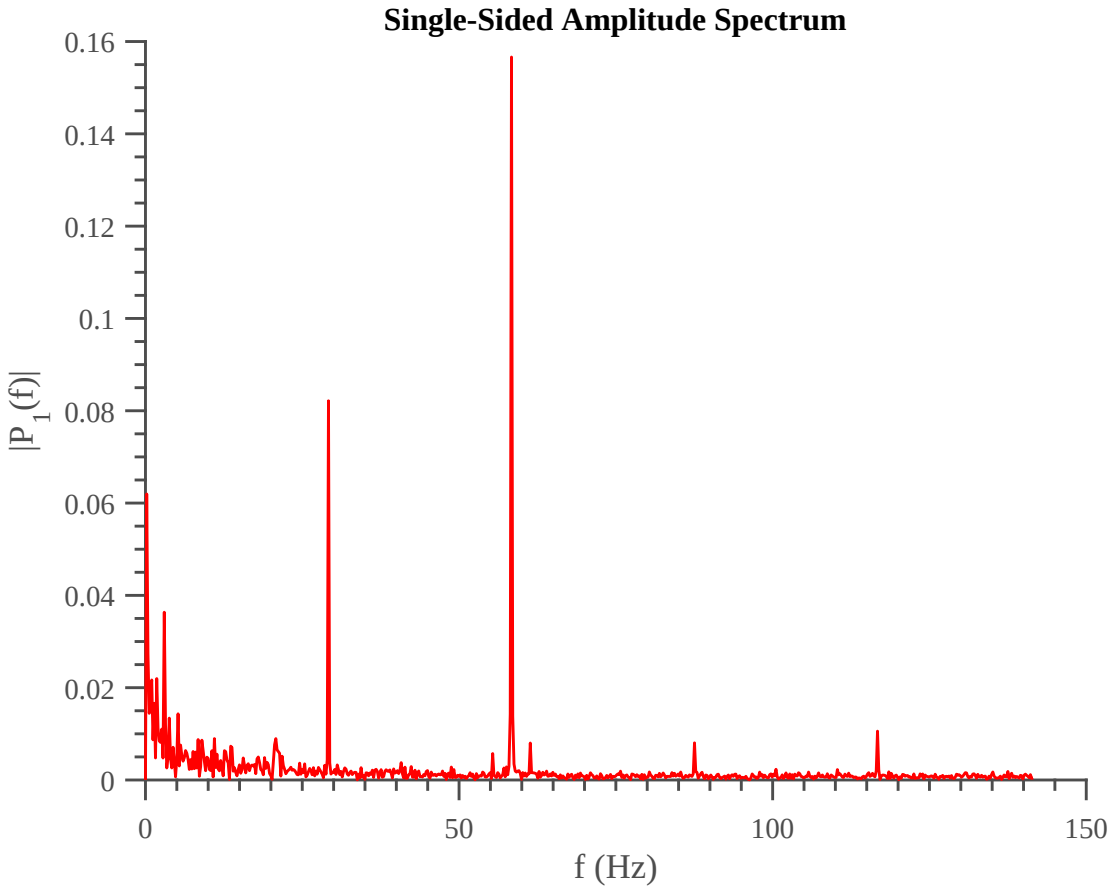

Figure 3.15: Sample FFT of the T' signal at a representative location. The graph displays the normalized power of the signal over the associated frequencies. Peaks can be clearly seen around 30 and 60 Hz.

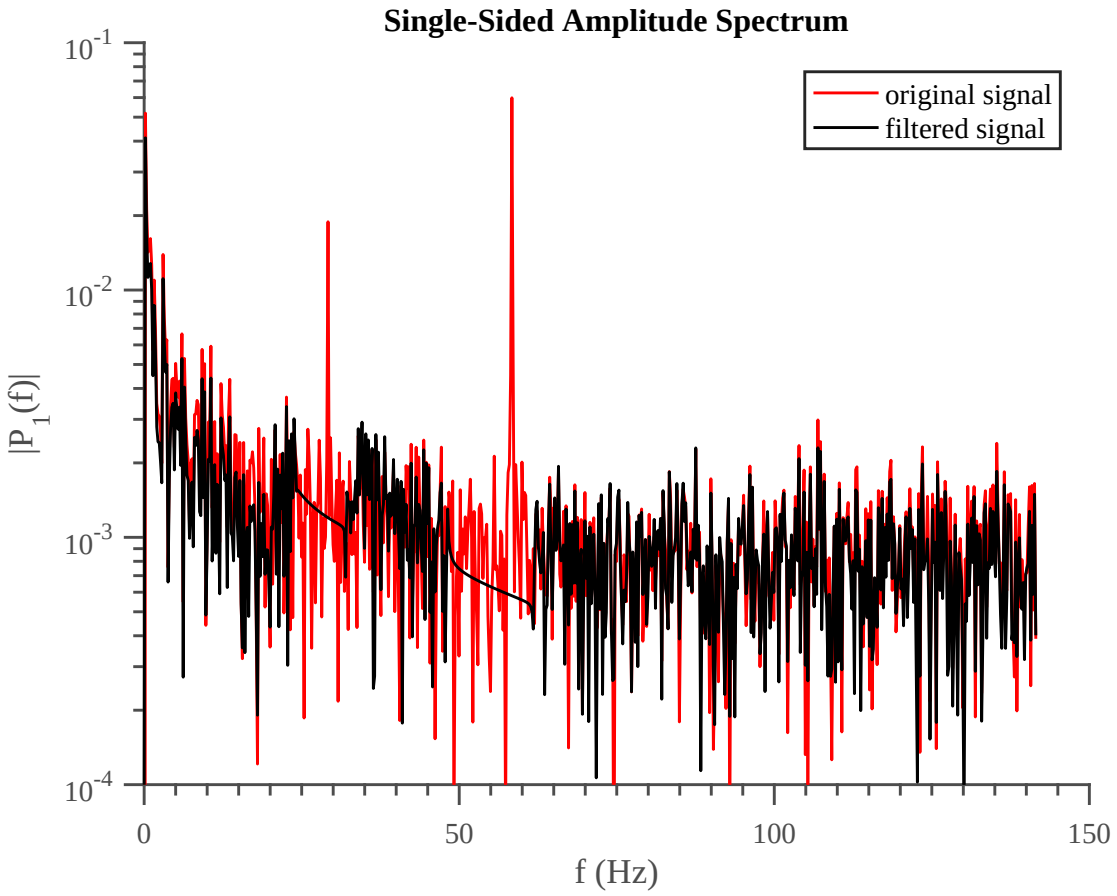

Figure 3.16: FFT of a raw T' signal plotted alongside a filtered signal. The graph displays the normalized power of the signals over the associated frequencies. The peaks located around 30 and 60 Hz are clearly reduced by the bandpass filter.

3.1.3 Results

The detection algorithm enabled the development of a significant amount of data for analysis. This data was then assessed in the interest of identifying pertinent trends. The following section details the results observed by analyzing data taken for the entire parameter space, which is obtained by varying the wind, plate temperature, and the streamwise analysis region.

3.1.3.1 Streak spacing

The spacing of the near-wall streaks detected by this algorithm comprised the first property we wanted to analyze. Before stating our own results, nonetheless, it will be useful to examine trends from other experiments in the existing literature. The spacing of near-wall streaks in boundary layer is a commonly-investigated phenomenon. As described earlier, streamwise streaks are known to exist in non-reacting boundary layer flows [10]. It is understood that, in the near-wall region, streamwise counter-rotating vortices exist, and these vortices produce upwash and downwash regions. Streaks consist of the upwash regions, in which low-speed fluid from the wall is swept up into higher regions of the flow. Sublayer streaks were originally discovered in turbulent flows by Kline et al. [58], but later work revealed that streaks also exist in laminar and transitional flows [5], similar to the current study. These laminar structures are generally termed "Klebanoff modes", and they have been described in an earlier section [13, 40, 46–54]. Near-wall streaks are a well-established phenomenon; however, they have never before been examined in

the light of mixed convection with an unheated starting length or combustion. This paper represents the first analysis of such phenomena.

The first step in examining streak spacing involved compiling a distribution of measurements from each parameter space. In every case, the data appeared to take on a lognormal distribution. This is unsurprising, as earlier research has long suggested that streak spacing should be distributed similarly to a lognormal probability density function [83, 93]. In order to confirm this hypothesis, a lognormal fit was applied using the built-in MATLAB functionality of the *lognpdf* command. Fig. 3.17 displays several examples which demonstrate that this lognormal fit was applied to all experimental conditions with remarkable success. The appendix contains a tabulation of the entire parameter space. Overall, the distribution can be seen to grow wider downstream, but it retains the lognormal shape.

Several important properties of the resulting lognormal fits were extracted from this data in order to confirm the acceptability of the lognormal probably density function (PDF). As a first step, we compared the means and standard deviation of the discrete experimental data to the mean obtained by the continuous lognormal PDF. A lognormally distributed random variable is generally described by two parameters, μ and σ, which are the mean and standard deviation of the variable's natural logarithm, respectively. Knowing these parameters, we were able to calculate the arithmetic mean via MATLAB's *lognstat* function, which is equal to $\exp(\mu + \sigma^2/2)$, and the arithmetic standard deviation, which is equal to $\exp(\mu + \frac{1}{2}\sigma^2)\sqrt{\exp(\sigma^2) - 1}$. In Fig. 3.18, you can see a comparison of experimental values vs. fitted values for all tested conditions. For all the derived mean and standard deviation values from

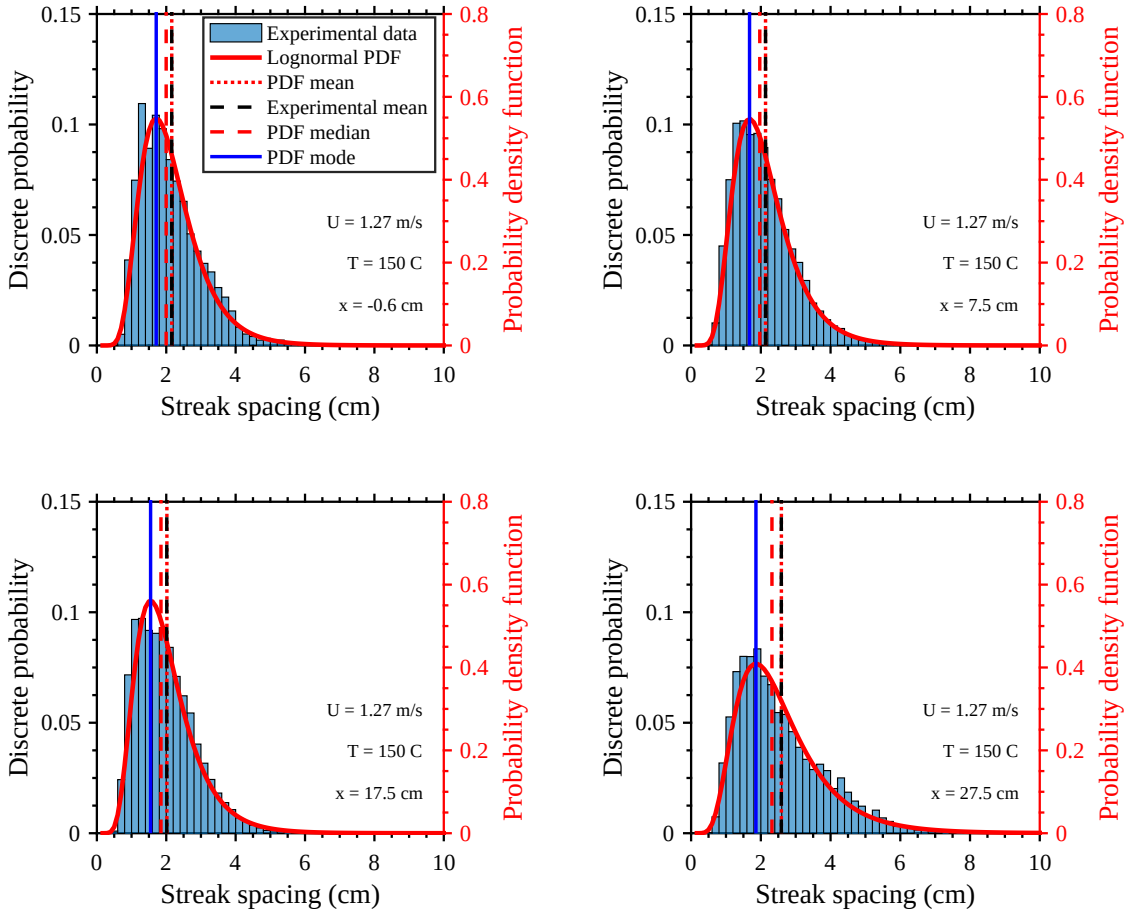

Figure 3.17: Plots of experimental distributions of streak spacing along with a lognormal fit of the data. All data is taken over either the heated plate or the insulated surface where the hot plate temperature is 150°C and the wind speed is 1.27 m/s. The indicated experimental means are derived from experimental data while other values are derived from arithmetic properties of the lognormal PDF. Experimental distributions for the remainder of parameter spaces can be seen in the appendix (Figs. A.1-A.6).

.

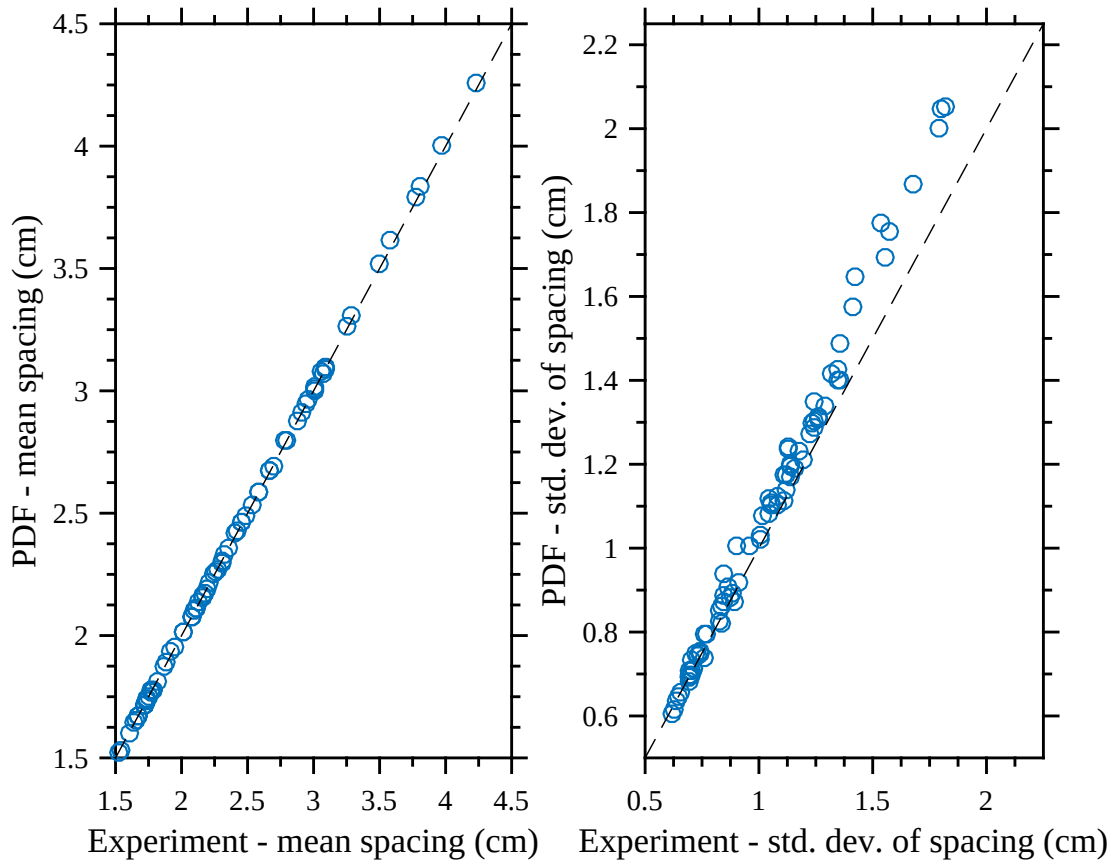

Figure 3.18: Displayed here are comparisons of statistics of the experimental data vs. the fitted lognormal distribution. To the left, the means of each distribution are compared; to the right, the standard deviations are compared. The dashed line indicates the line of unity.

experiments and the PDF's, all data points lie nearly adjacent to the line of unity. This is a strong indication that the lognormal PDF's are adequately capturing both the centrality and variability present in derived data.

Ideally, the trends associated with streak spacing can be described using the mean of experimental data. However, it could also be argued that the mode or the median could better describe the distribution. In order to demonstrate that the mean is an appropriate statistic, we compared the trends of the mean to the modes and the medians associated with the lognormal fit. The median of a lognormal

distribution can be calculated as $\exp(\mu)$ while the mode is equal to $\exp(\mu - \sigma^2)$. In Fig. 3.19, the experimental mean is compared to the median of the lognormal fit. While the data diverges from the line of unity, the median is consistently about 91% of the mean with an R^2 value of 0.99. This implies that utilizing the mean or the median will be adequate, as trends will remain unchanged. Additionally, Fig. 3.20 displays a graph of the experimental mean vs. the mode of the lognormal fit. Here, the mode is generally equal to 75% of the mean with an R^2 value of 0.93. Once again, this implies that, while absolute values of data reporting will shift, trends will be unchanged whether the mean or the mode is used. For the remainder of this thesis, the experimental mean will be the reported statistic as it is an adequate description of the data distribution.

A lognormal distribution is also commonly quantified using two quantities known as skewness and the coefficient of variation (CV). The skewness of a distribution is a measure of asymmetry about the mean, where a positive value indicates that the right tail is longer (skewed to the right) while a negative value indicates the left tail is longer (skewed to the left). For a lognormal distribution, the skewness is equal to $(e^{\sigma^2} + 2)\sqrt{e^{\sigma^2} - 1}$. Meanwhile, the arithmetic coefficient of variation measures the level of dispersion observed in a distribution. This value is equal to the ratio of the standard deviation to the mean, which can also be given as $\sqrt{e^{\sigma^2} - 1}$. These values were tabulated vs. all experimental conditions. No trend in these statistics was observed as the wind speed or the hot plate temperature was manipulated. However, there was a slight trend with the streamwise distance, and Fig. 3.21 displays a scatterplot of this relationship. Both of these values appear to

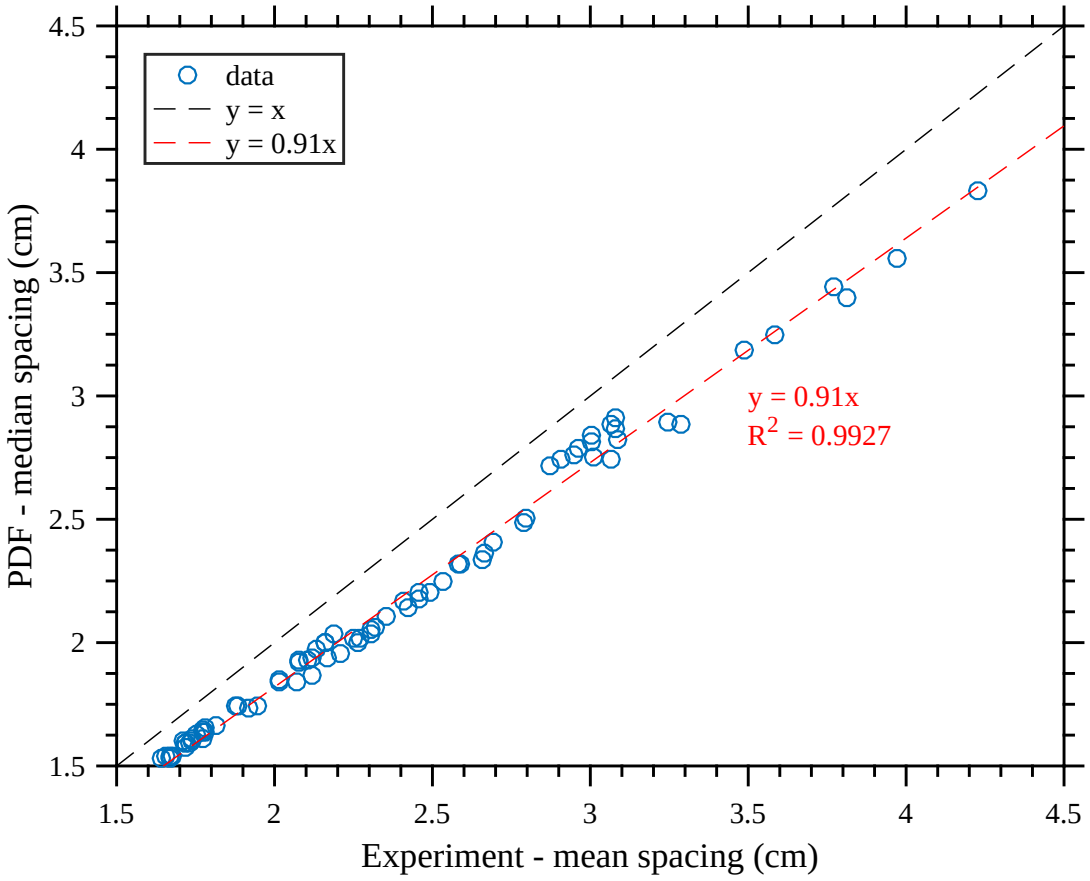

Figure 3.19: The median of the fitted lognormal distribution plotted vs. the mean of the experimental distribution. The black dashed line displays the line of unity while the red dashed line represents a best linear fit with a prescribed intercept of zero.

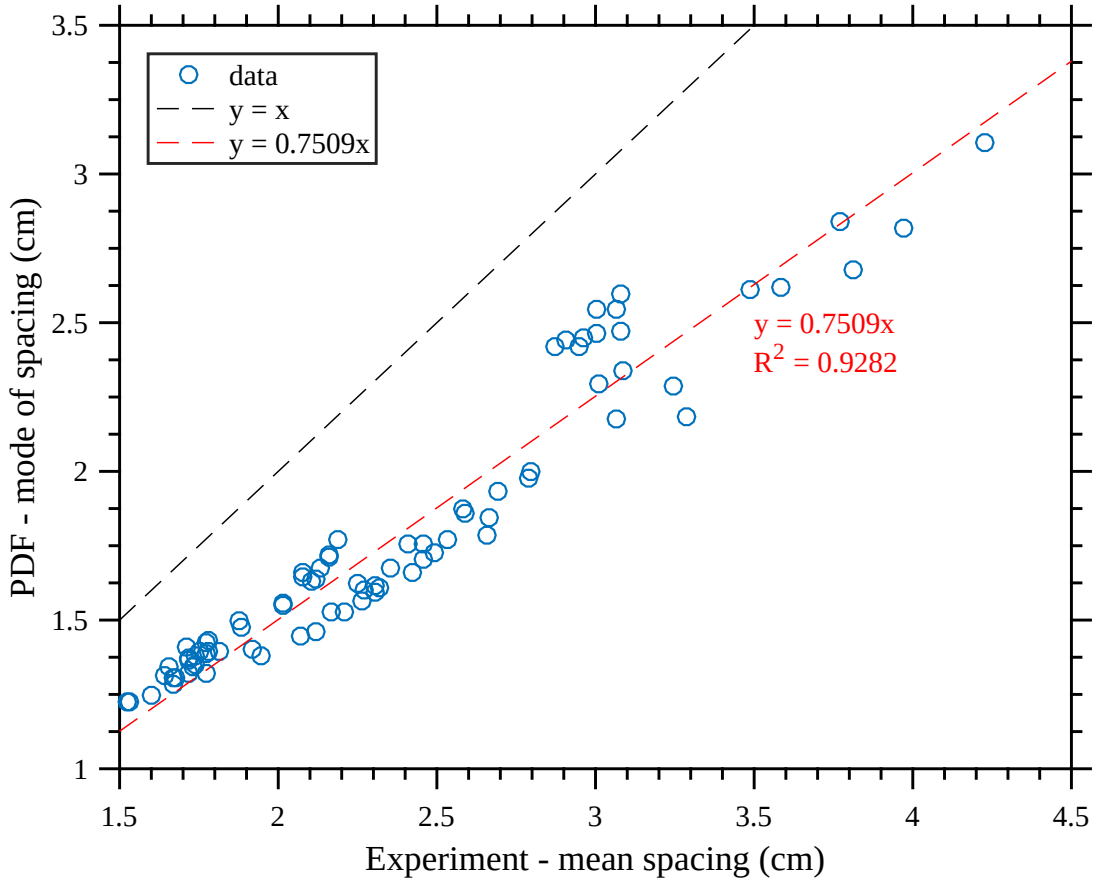

Figure 3.20: The mode of the fitted lognormal distribution plotted vs. the mean of the experimental distribution. The black dashed line displays the line of unity while the red dashed line represents a best linear fit with a prescribed intercept of zero.

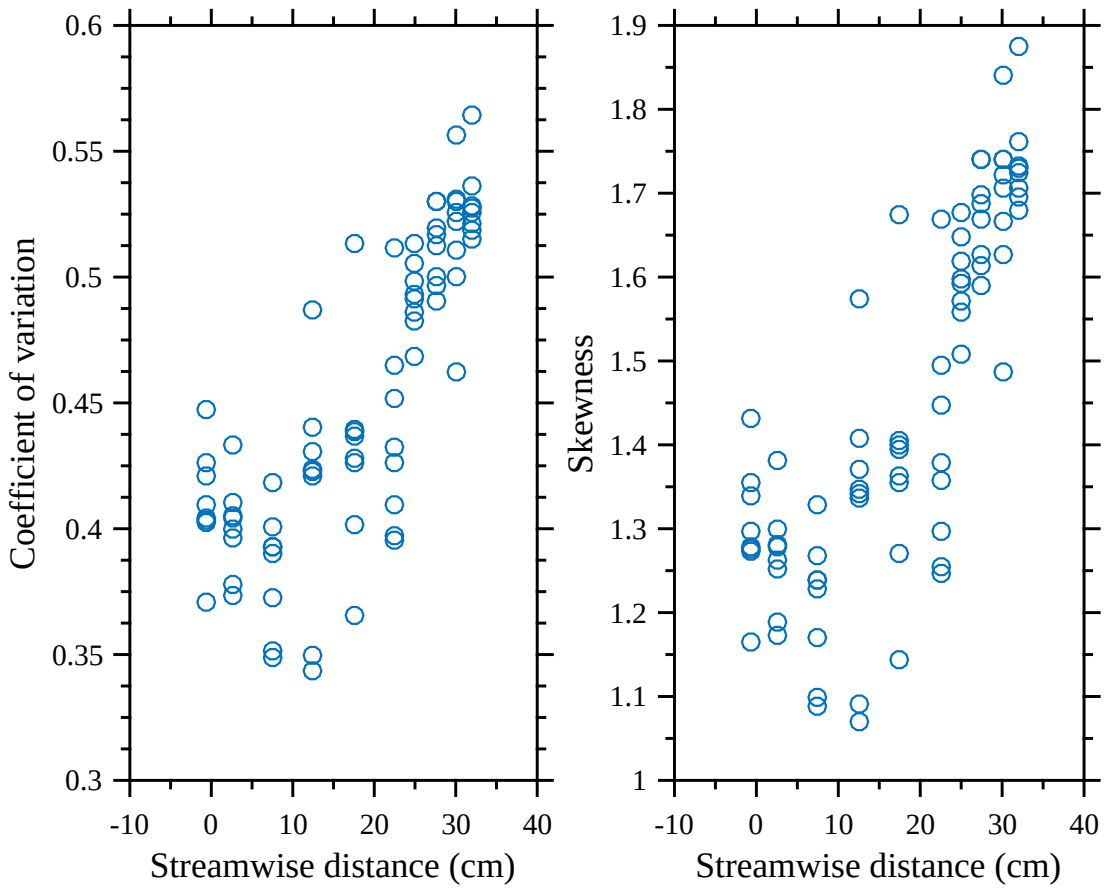

Figure 3.21: Plots of the coefficient of variation (left) and the skewness (right) vs. the streamwise distance. All statistics are derived from the fitted lognormal distributions.

increase slightly with downstream distance, indicating that there is a slightly wider dispersion of streak spacing downstream. This can be seen in the lognormal plots.

Zachsenhouse et al. [90] tabulated spatial characteristics of near-wall streaks from thermal images. Here, an automatic detection method based on edge detection was used to tabulate streak spacing. Their study included an investigation into properties of a lognormal distribution fitted to the spacing data, and they reported values of 0.44 for the coefficient of variation and 1.1 for the skewness. For nearly all our experimental conditions, the value of the coefficient of variation remained within

the range of 0.35-0.55 while the value of skewness remained generally between 1.1 and 1.8. Our values agree with Zachenhouse et al. reasonably well, indicating that both methods are identifying similar distributions for near-wall streaks.

In all subsequent figures with quantities derived from streak distributions, the standard deviation is not indicated. Instead, plots of the standard deviations of important properties have been added to the appendix. This has been done in order to avoid obscuring the more important trends of the graphs, as the standard deviations are generally quite large compared to the mean (i.e., the coefficient of variation is large). One might object to the large standard deviations obtained for the streak data, but this behavior is expected for the lognormal distributions of streaks in boundary layer flows, which observe similar values for the coefficient of variation [90].

Experimental means were extracted from all distributions, resulting in a significant amount of data for all three tested parameters: wind speed, hot plate temperature, and streamwise distance. Fig. 3.22 displays all of this data via a graph of the spacing vs. the streamwise distance (x). Several important trends can be identified by examining this figure in greater detail. First of all, it can be seen that the streak spacing differs significantly with the external wind. The lowest wind speed, 0.7 m/s, exhibits the largest spacing, while the smallest spacing values are observed for the highest wind speed. In other words, the frequency of streaks increases with wind speed. This trend is consistently observed across the entire tested region. This indicates that wind will be a significant player in the behavior of streaks.

Additionally, a consistent trend is observed in the streaks as one moves down-

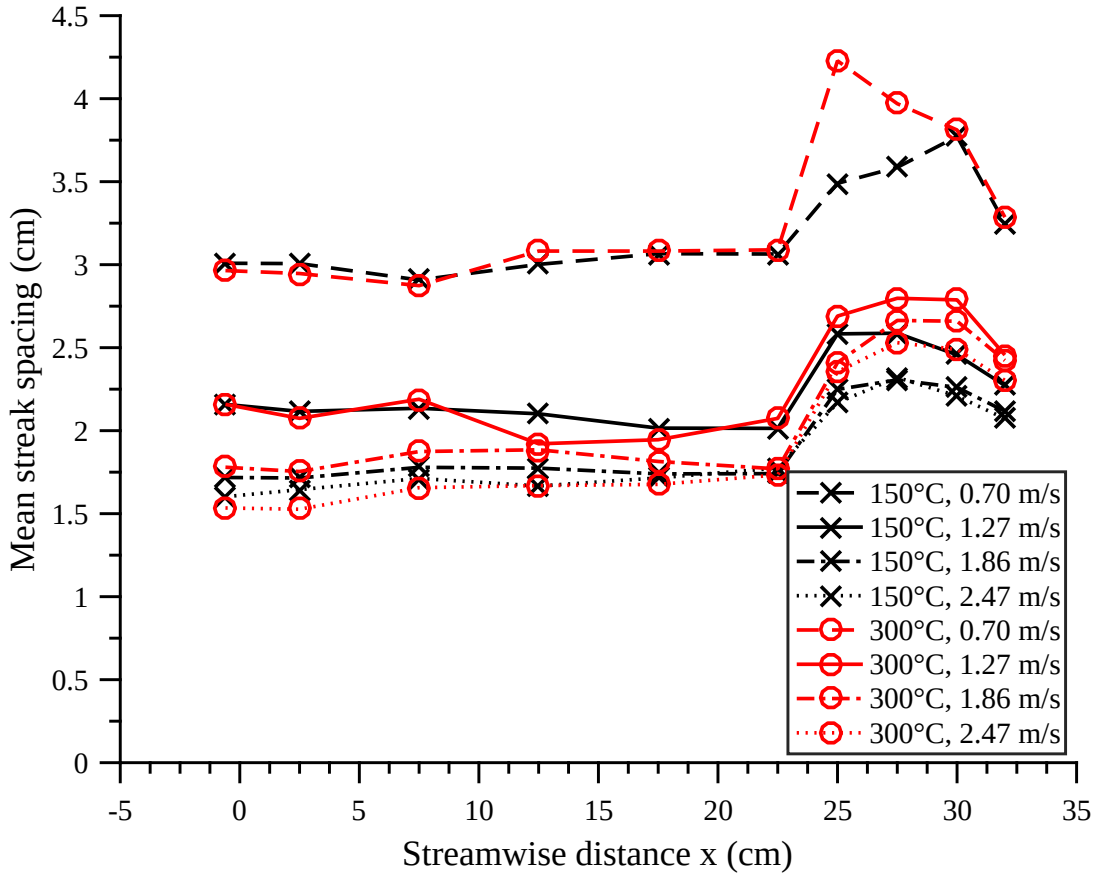

Figure 3.22: Plot of the mean streak spacing vs. streamwise distance for all experimental conditions. The hot plate is located between $x = 0$ and 20.5 cm while the surrounding area is inert.

stream. Streak spacing remains relatively constant before, above, and immediately downstream of the hot plate. However, 5 cm downstream of the hot plate ($x \approx 25$ cm) a steep rise in the spacing is observed, followed by a plateau at $x \approx 30$ cm. This trend could indicate several things about the observed coherent structures in the near-wall region. This behavior implies that the near-wall streaks remain relatively fixed over the heated plate, but new behavior is seen downstream. Downstream of the plate, structures appear to be growing in size. This amplification is more pronounced in all cases where the hot plate temperature is higher, and Fig. 3.23 demonstrates that the growth differs significantly based on the hot plate temperature. In other words, buoyancy seems to be controlling this amplification process, a finding which supports the idea that early growth of structures is similar to Rayleigh-Taylor growth.

Both inertia (wind speed) and buoyancy (hot plate temperature) appear to be playing a role in the streak spacing, albeit at different stages. The later growth seems to be more connected to buoyancy, but the early stage (i.e., the initial streak spacing) appears to be tied to the inertial force. In fact, the initial spacing is likely governed by structures that already exist in the upstream boundary layer. The fact that streaks can be detected ahead of the plate (i.e., $x = -0.6$ cm) supports this claim. Fig. 3.24 displays a plot of this initial streak spacing vs. the Reynolds number. Clearly, a negative correlation exists between the initial streak spacing and the incoming wind speed, which is described by the Reynolds number. From another perspective, the initial streak spacing is directly related to the boundary layer height. For a higher incoming wind speed, the boundary layer height at a given

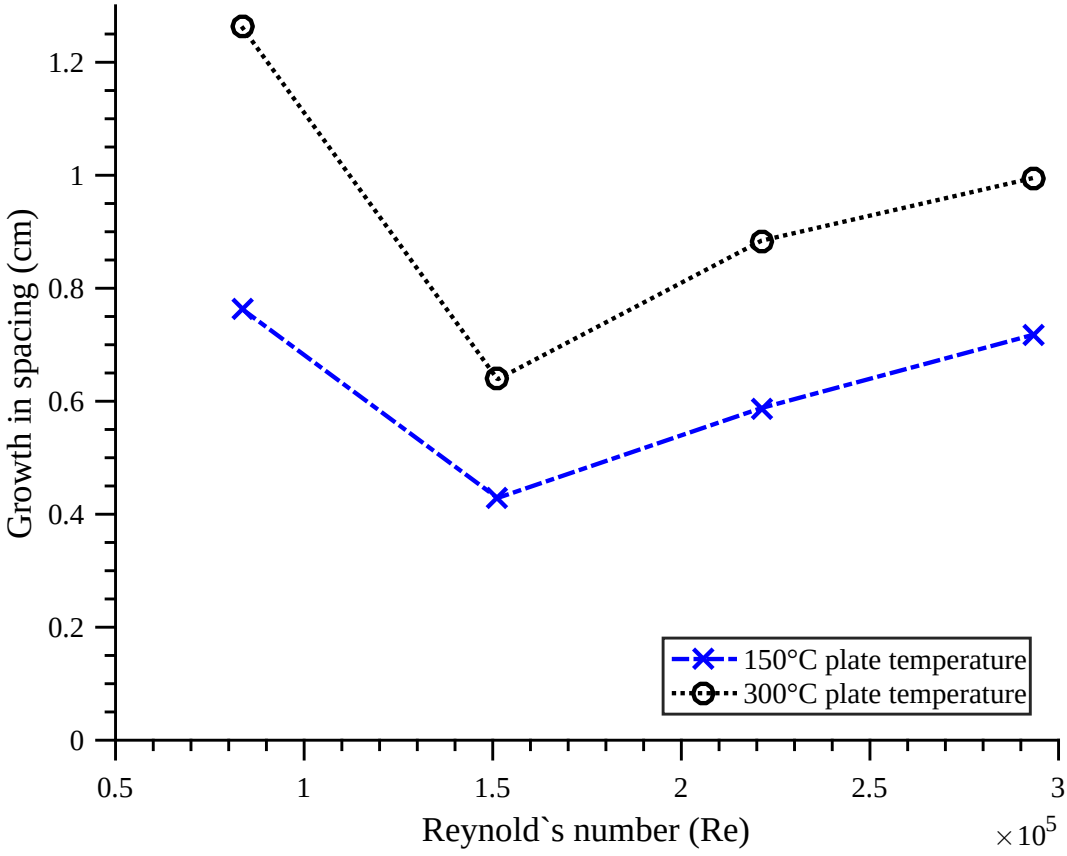

Figure 3.23: Plot of the growth in streak spacing vs. the Reynolds number at the leading edge of the plate. The growth is calculated as the difference between the maximum value and the initial spacing.

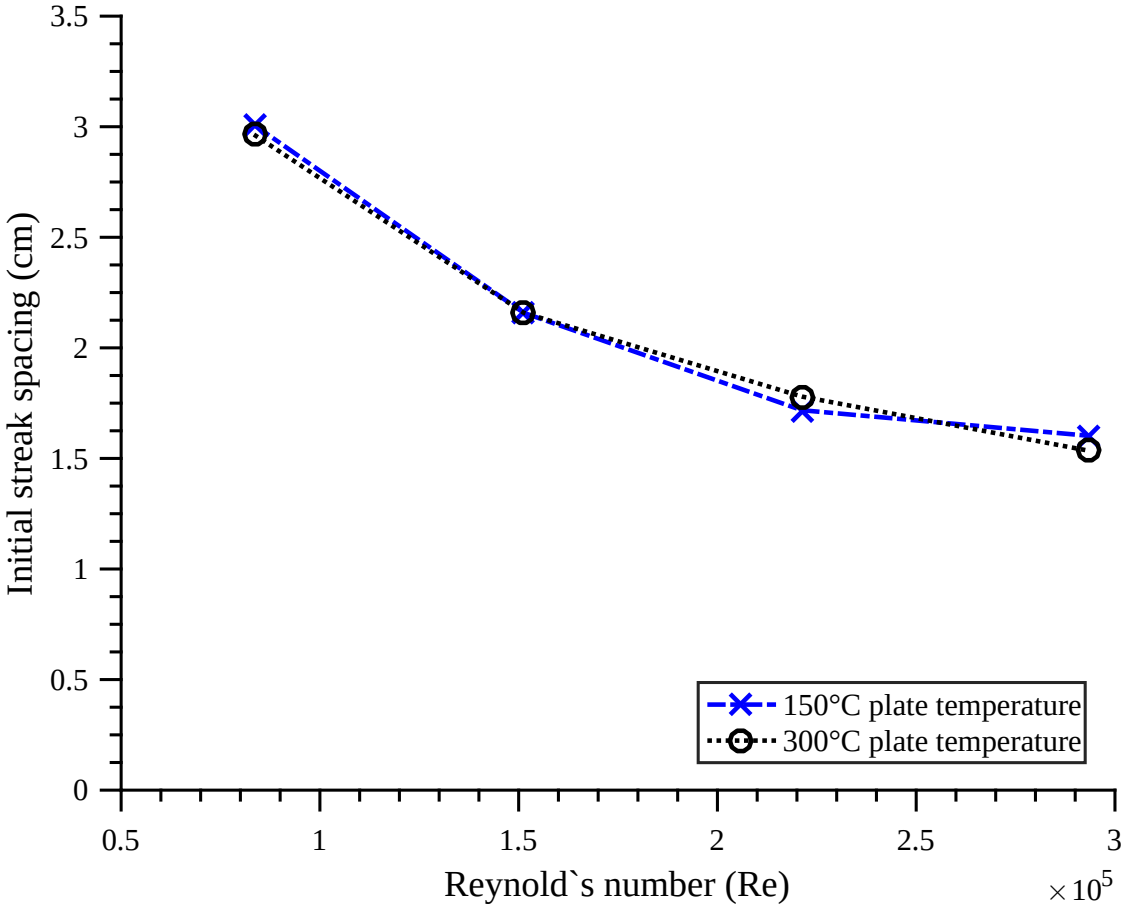

Figure 3.24: A plot of the initial streak spacing vs. the Reynolds number at the leading edge of the plate. The initial streak spacing was derived from data taken at $x = -0.6$ cm.

streamwise location becomes shorter; consequently, the coherent structures which populate this boundary layer will also be smaller. The reported trend supports this notion, and the initial streaks appear to be preset by the incoming flow.

If the incoming boundary layer is governing the initial spacing, this length scale should agree with that expected in the absence of a heat source. Fortunately, near-wall streaks observed in shear flows is a well-documented phenomenon. For turbulent boundary layers, near-wall streaks are typically organized into a spanwise pattern with a period of approximately 100 viscous wall units [56, 58, 83]. Nevertheless,

there is significant variation in reported experimental values for the mean streak spacing ($\bar{\lambda}^{+}$), as demonstrated by Table 3.1. Minimal experimental data seems to exist concerning the nondimensional spacing of streaks in laminar or transitional boundary layers. However, it has been theoretically demonstrated that transient growth of these early coherent structures can result in the standard spacing seen in turbulent boundary layers [94]. Algebraic growth has already been connected to longitudinal streaks in turbulent boundary layers [26, 95, 96], and Carpenter et al. [97] even goes on to say that this gives rise to "an implied equalence between the Klebanoff mode in the transitional boundary layer and the streamwise sublayer streaks in a fully turbulent boundary layer." Universal streak spacing in laminar flows has not been claimed; nevertheless, experiments have observed quasi-linear growth of streak spacing that could hypothetically asymptote to a stable value [13]. In other words, we should not be surprised to find that the streaks in this study scale similarly to turbulent boundary layer flows. The following analysis attempts to analyze whether streak spacing here behaves similar to that of those in a turbulent boundary layer, which exhibit predictable trends in non-dimensional spacing.

In Fig. 3.8 from Section 3.1.1.1, the length of a wall unit was derived for each tested wind speed by examining the near-wall velocity gradient. We used this knowledge to convert the initial streak spacing to non-dimensional wall units, and Fig. 3.25 displays the results of this conversion. Compared to Fig. 3.24, we see a significant collapse of the data. For all tested temperatures and wind speeds, the initial spacing lies between 60-70 wall units. This places our streak spacing at the lower end of reported values from Table 3.1. Given that our experiment exists

Reference	Year	$\bar{\lambda}^+$ (wall units)
Kline et al. [58]	1967	100
Achia and Thompson [88]	1977	79-93
Nakagawa and Nezu [93]	1981	100-103
Smith and Metzler [83]	1983	87-104
Lian [84]	1990	104-107; 68-69
Rashidi and Banerjee [85]	1990	100 ± 7
Hetsroni and Rozenbilt [86]	1994	79-98
Kaftori et al. [87]	1994	≈ 100
Sabatino [89]	1997	68-120
Zachsenhouse et al. [90]	2001	120

Table 3.1: Table reproduced from Zacksenhouse et al. [90] displaying experimental measurements of mean streak spacing in wall units.

at the upper end of the laminar regime, this is not surprising. If the upstream development length was increased to place us in the turbulent regime, it is likely that the reported non-dimensional spacing would move closer to the mid-range of reported values in the literature. This finding greatly supports the notion that the initial streak spacing is a function of the incoming boundary layer. In other words, the initial spacing can be predicted without any knowledge of the strength of the buoyant source. Further testing on streaks observed in flames will examine whether this remains true when the source of buoyancy is much stronger.

3.1.3.2 Streak width

In addition to the spacing between streaks, the width of streaks was also tabulated. This was done for the entire parameter space, and all distributions of width were seen to follow a lognormal trend, similar to the spacing. Additionally, the trends for width remained identical to the streaks when the mean values were

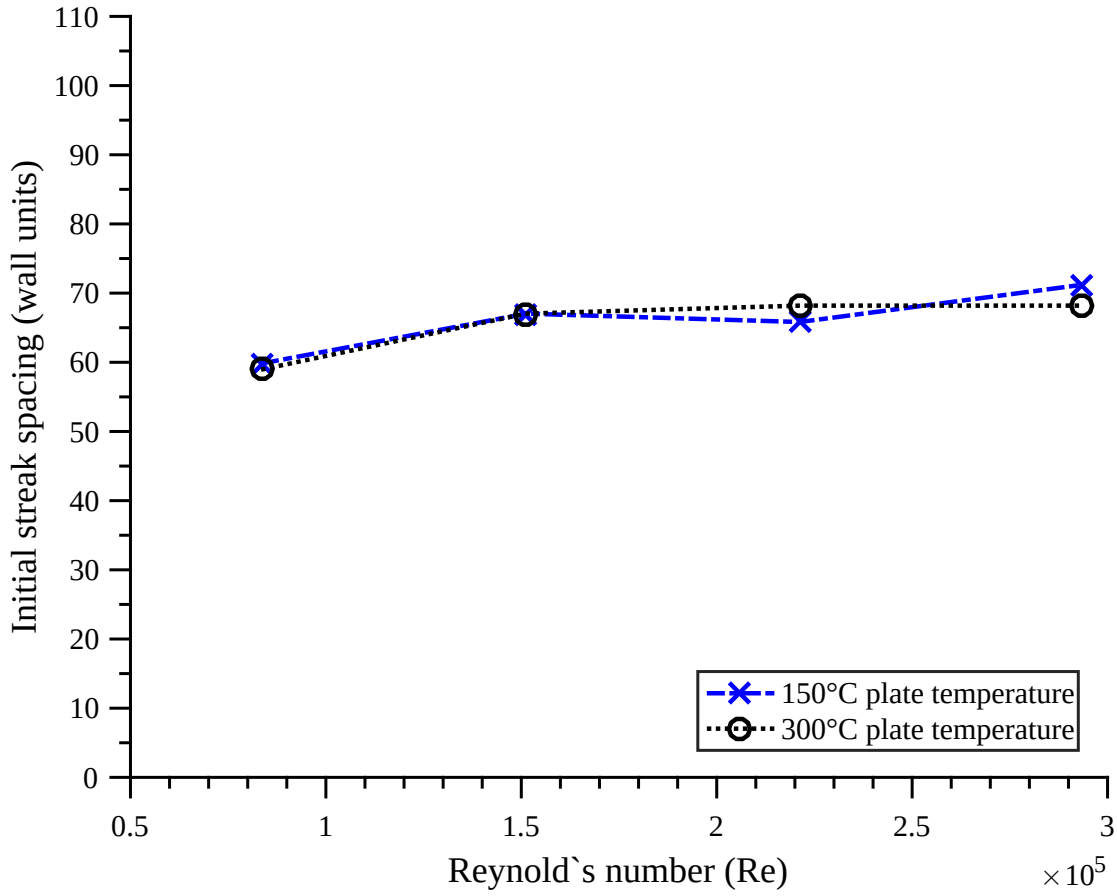

Figure 3.25: A plot of the initial streak spacing in dimensionless wall units vs. the Reynolds nunmber at the leading edge of the plate.

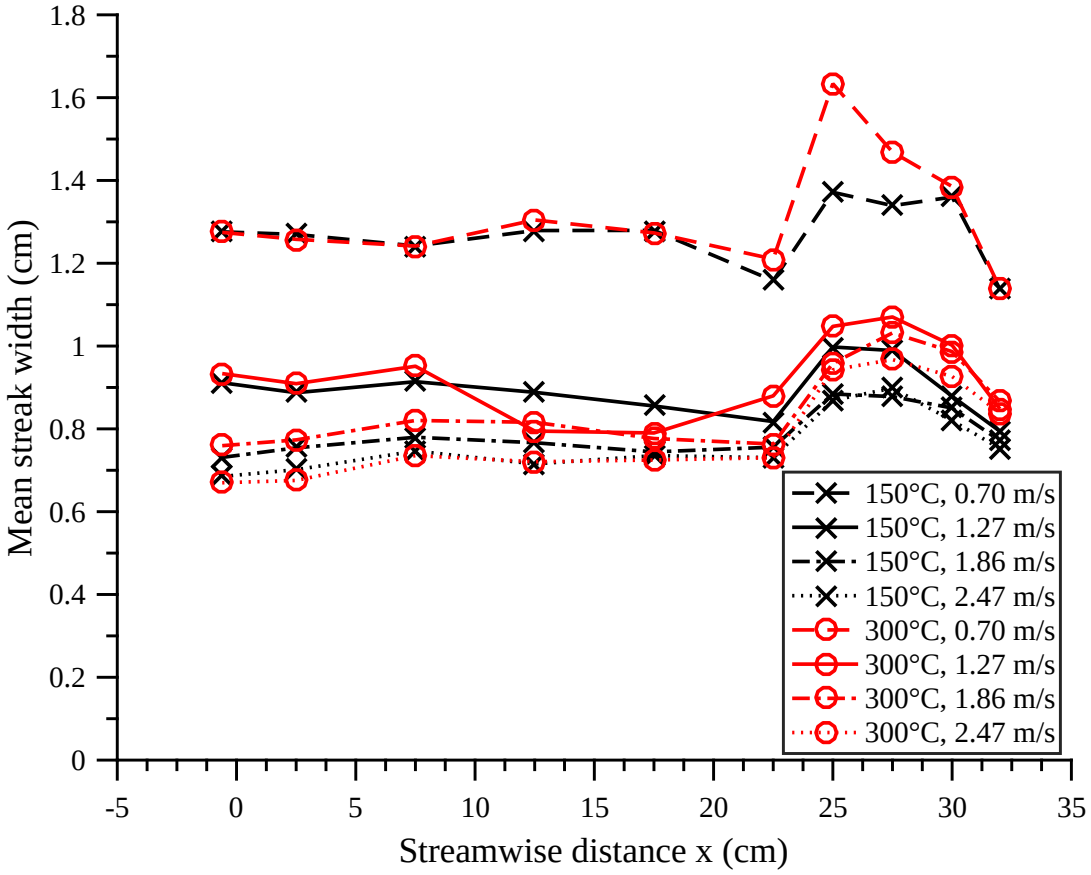

Figure 3.26: A plot of the mean width of streaks vs. streamwise distance for all experimental conditions. The hot plate is located between $x = 0$ and 20.5 cm while the surrounding area is inert.

plotted vs. the streamwise distance in Fig. 3.26. The widths identified by the detection algorithm consistently occupy about 40% of the spacing. Zachsenhouse et al. [90] identified widths that were about 50% of the spacing using an edge detection method.

3.1.3.3 Streak prominence

The mean streak prominence represents the amplitude of the perturbation in the T' profile (see Fig. 3.13). Because these perturbation amplitudes represent a

local change in temperature, they measure the magnitude of the local difference in heat flux between streaks and troughs. A larger streak prominence indicates that the presence of the streak has a more pronounced role in modifying the heat transfer to the surface. Because the heat transfer to the surface controls important real-world phenomena, including wildland fire spread, this value could have significant implications. Fig. 3.27 displays a plot of the mean streak prominence obtained vs. the streamwise distance. Ahead of the hot plate, the streak prominence appears to be fairly widely distributed, being positively correlated to the plate temperature and negatively correlated to the wind. However, downstream of the plate, the data is seen to collapse significantly. Here, there appears to be no significant correlation of prominence with wind speed; instead, the magnitude of the streak prominence is dependent on the hot plate temperature. A stronger source of buoyancy is leading to increased heat transfer effects from streaks, indicating the three-dimensionality of the flowfield. Lastly, as we move further downstream beyond the hot plate, we see the prominence decrease fairly rapidly, indicating that the contribution of streaks to the downstream heating remains largest towards the heat source.

3.1.3.4 Streak duration

Fig. 3.14 displays a graphical illustration of how the detection algorithm could track the streaks over time. This methodology made it possible to assess the lifetime of a streak at a particular streamwise location. Once a streak appeared, or was born, it would die if it was no longer detected in a subsequent frame or if it was absorbed

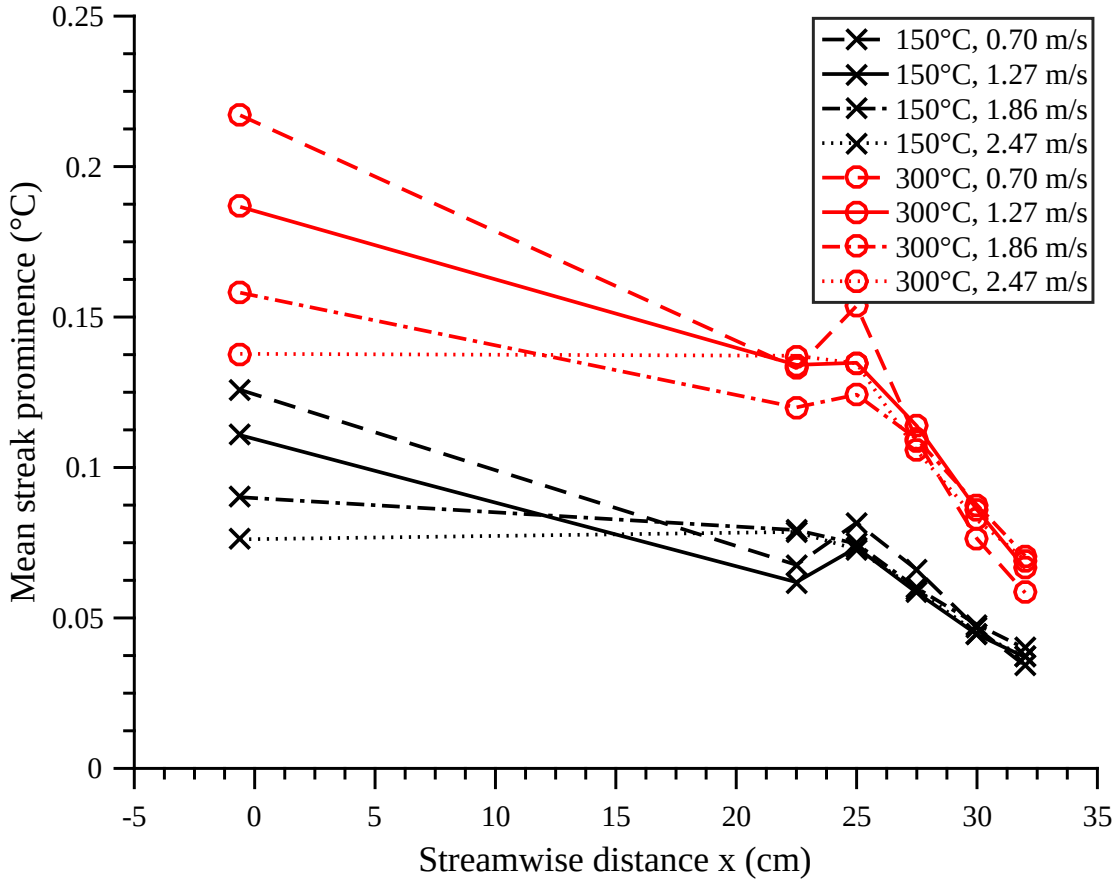

Figure 3.27: A plot of the mean streak prominence, or amplitude, vs. streamwise distance for all experimental conditions. The hot plate is located between $x = 0$ and 20.5 cm while the surrounding area is inert.

into a more powerful streak. The streak duration was tabulated for all wind speeds, plate temperatures, and streamwise locations, and the experimental mean for each scenario is plotted in Fig. 3.28. There is a clear decrease of the observed duration of streaks as one moves downstream. Ahead of the plate and just downstream, the streaks are generally quite coherent and can be seen to persist over a long range of frames. However, as one moves downstream, the duration of streaks decreases because the structures become less coherent and less streak-like. This is likely a natural consequence of the bulk flow beginning to lift off the plate. This disturbs the makeup of a typical boundary layer, and it likely also affects the coherence of streaky structures that would typically populate the near-wall region. Fig. 3.28 also demonstrates a significant collapse of the data as one moves downstream. There is a significant distribution in observed lifetimes ahead of the plate, in which the lifetime is most strongly associated with wind speed. A lower wind speed seems to promote streaks which persist longer in time. In the low wind scenario, the streaks exhibit the greatest spacing, making streak-streak interaction more difficult especially if the inertial forces are low. However, downstream of the hot plate, all the data collapses regardless of the wind speed or the hot plate temperature. This means that the injection of buoyancy into the flow serves to significantly alter the coherence of near-wall structures.

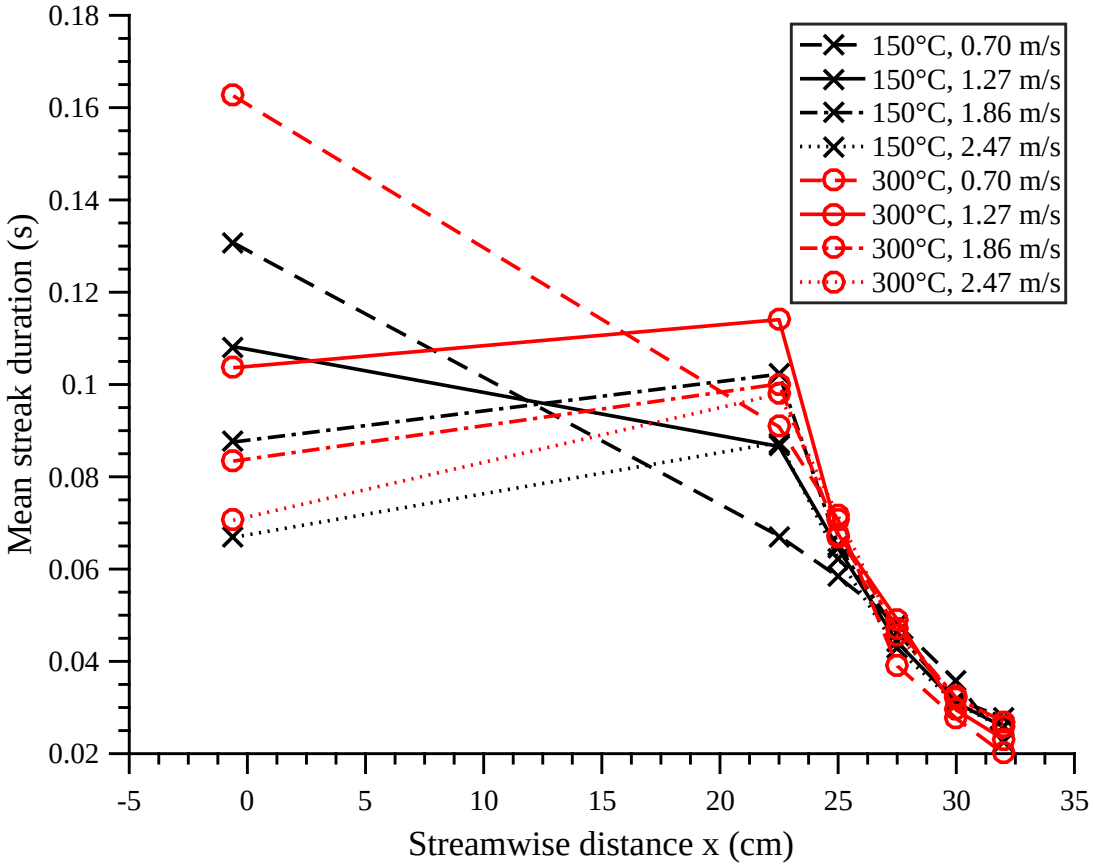

Figure 3.28: A plot of the mean duration of streaks vs. streamwise distance for all experimental conditions. The hot plate is located between $x = 0$ and 20.5 cm while the surrounding area is inert.

3.1.3.5 Streak meandering

Fig. 3.14 shows streak traces that regularly meander laterally across the surface. By examining how far a streak would meander between frames and dividing this value by the time between these frames, it was possible to determine the instantaneous lateral (spanwise) velocity of a streak. Once these velocities were tabulated, the instantaneous speed could then be determined by taking the absolute value of velocity. The instantaneous speed represents a measure of both how frequently and how rapidly streaks would meander laterally across the surface. Fig. 3.29 demonstrates how the mean lateral speed of streaks varied with the tested parameter space. Overall, we see that the meandering is minimal ahead of the plate; here, streaks are governed primarily by the incoming boundary layer with minimal buoyant disturbances. Moving downstream of the plate, we see a rapid acceleration of the streak speed. Combined with the earlier finding that the streak lifetimes decrease rapidly downstream, this presents us with a chaotic near-wall region, populated with rapidly meandering coherent structures with short lifetimes. When we compare this behavior to that observed just upstream of the plate, we can see that the injection of heat into the boundary layer serves as a significant disturbance to the near-wall coherent structures. The highly chaotic behavior of coherent structures downstream may serve to wash out some of the instantaneous effects streaks have on the heat transfer distribution, which could explain the decrease in streak prominence in Fig. 3.27. Nevertheless, it is still possible that this near-wall behavior has significant overall effects on the heat transfer, a possibility which was discussed in Section 2.5.5.

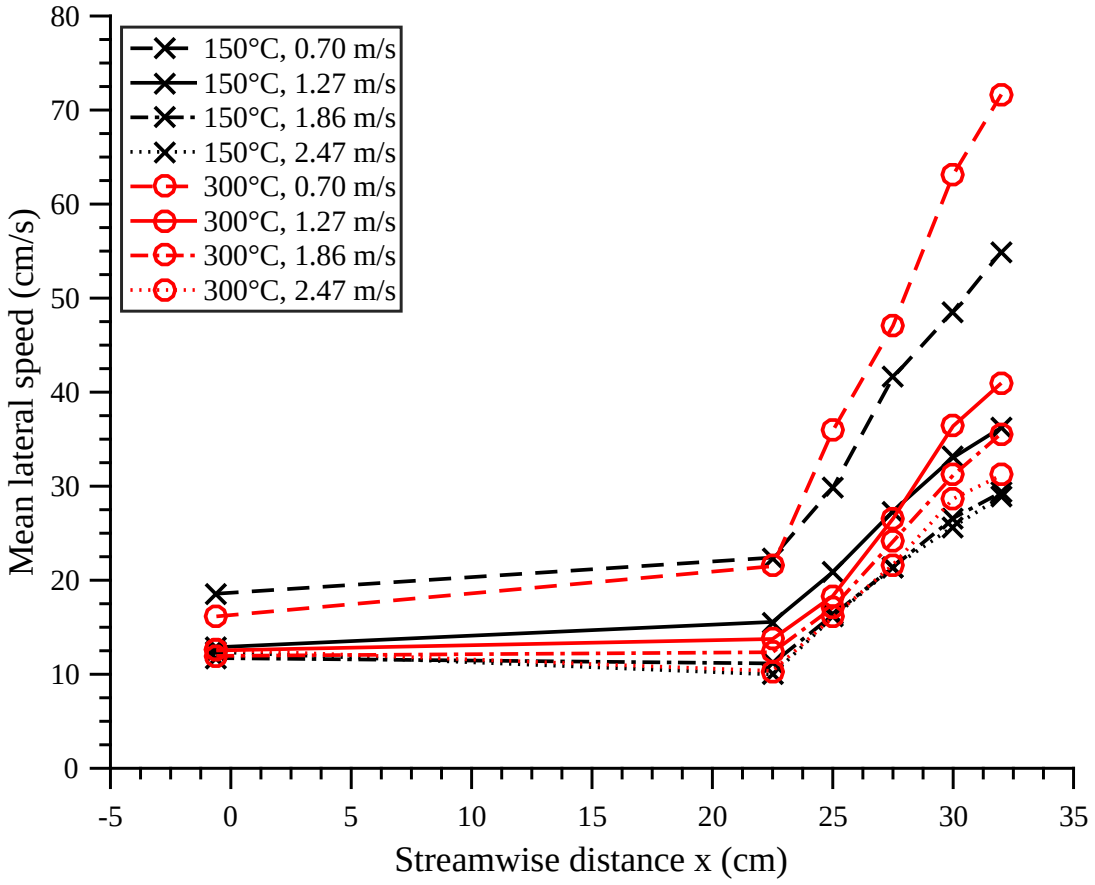

Figure 3.29: A plot of the mean lateral (spanwise) speed of streaks vs. streamwise distance for all experimental conditions. The hot plate is located between $x = 0$ and 20.5 cm while the surrounding area is inert.

3.1.4 Summary of hot plate data

Streaks have been observed over heated plates by means of infrared thermography, and important properties have been quantified via image processing. Several important findings have been made, including:

- An algorithm for detecting and qualitatively visualizing streak traces over time
- Lognormal distribution of streak spacing
- Streak spacing negatively correlated to wind
- Initial streak spacing governed by properties of the incoming boundary layer
- Initial streak spacing consistently between 60-70 wall units
- Increase in streak spacing downstream
- The ability to modify spanwise heat transfer, measured by the streak prominence, is positively correlated to the hot plate temperature and independent of wind
- Streaks meander more rapidly and persist for a shorter duration as the flow becomes more chaotic downstream

These findings provide new insights into the behavior of these instabilities. Although the initial instabilities are governed by the incoming wind, buoyant forces cause the growth of these structures and eventual liftoff from the surface. It does appear that regimes dominated by either inertia or buoyancy, which are generally agreed to cover

the macroscopic flow, also control the coherent structures populating the near-wall region. These coherent structures, which exhibit upwash and downwash regions of counter-rotating vortices, are intimately connected to the surface heat transfer and they may be involved in the downstream behavior of the flow. Buoyancy may amplify the streaks, and this growth and aggregation likely governs the nature of the larger-scale structures seen further downstream. However, further knowledge is needed to determine whether this same behavior can be identified in a boundary layer flame, which is a much more potent source of buoyancy. The next section analyzes this idea.

3.2 Flame streaks

The previous section detailed measurements of streak behavior obtained over a heated plate in crossflow. However, further work remained to determine whether these streaks were analogous to those observed in flames. This chapter examines streak behavior for a liquid fuel wick in the same experimental configuration.

3.2.1 Experimental setup

All experiments took place in the low speed wind tunnel facility at the Missoula Fire Sciences Laboratory. The experimental setup was actually identical to that from the previous experiment (Section 3.1.1) with a few notable exceptions. In these experiments, the copper hot plate from the previous setup was replaced by a porous ceramic fiber wick of identical dimensions (2.5-cm-thick, 20.5-cm-long, 91.5-

cm-wide) placed 188 cm downstream of the leading edge of the apparatus. The setup is shown in Fig. 3.30. The wick was saturated with 400 mL of isopropyl alcohol and ignited using a torch. Burning was conducted at four wind speeds (0.70, 1.27, 1.86, and 2.47 m/s), and a period of steady burning was seen to last for nearly 50 seconds. Overhead videos and photos of the experiment were taken; in particular, 12 seconds of high speed (120 fps), high resolution (1080 x 1920 pixels) video footage were made for each experiment. These images of flame streaks were subsequently processed via MATLAB.

3.2.1.1 Velocity characterization

The same data collected in Section 3.1.1.1 is applicable to this experiment.

3.2.2 Detection algorithm

Significant post-processing was necessary in order to detect and quantify properties of flame streaks from the high speed images. Streaks would be visible to the naked eye as thin elongated streamwise luminous traces in the flame. Between these streaks, i.e., at the troughs, the luminosity of the flame would decrease significantly. From previous experiments in the University of Maryland wind tunnel, we know that the luminous portion of a streak corresponds to the upwash region of counter-rotating streamwise vortices, which control the location of these streaks. Consequently, the luminous regions of streaks are relatively higher above the surface than the troughs.

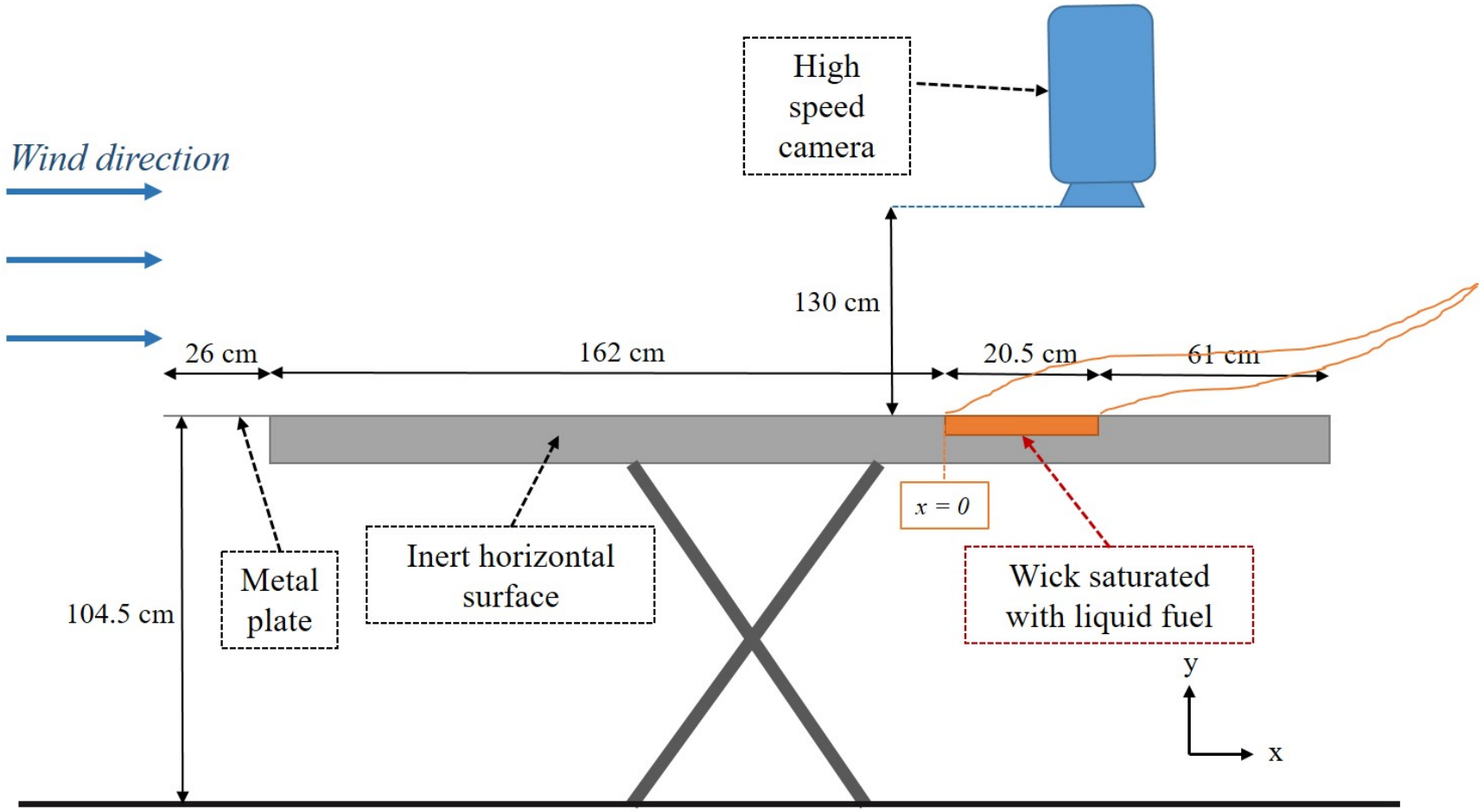

Figure 3.30: Experimental schematic of apparatus to hold flame in crossflow at the Missoula Wind Tunnel Facility. This apparatus was located in the center of a wind tunnel with a 3.0 x 3.0 m in cross-sectional area.

Detecting streaks in this experiment consists simply in identifying the luminous regions of the flame. In other words, the detection method of Section 3.1.2 is directly applicable if the spanwise T' profile observed in Fig. 3.13 is replaced with a spanwise profile of luminous intensity. Fig. 3.31 displays a plot of this detection algorithm used over the intensity profile taken from a high-speed video. The peak-finding algorithm works exactly the same with a couple of small tweaks to the input parameters: the number of pixels/cm was equal to 19.67; the duration of the analysis was 10 seconds (1363 frames); the streamwise depth of the analysis region was 7 pixels; the percentage of the standard deviation used as a minimum for peak prominence was 15%; the maximum movement of a continuous streak between frames was 85% of its width. Section 3.1.2 defines how all of these parameters are employed in much greater detail. Finally, a small portion on the left and right sides of the images were ignored in the analysis because the flame was only intermittently present in these areas.

3.2.3 Results

Overall, the detection algorithm performed quite well. Occasionally, certain luminous streaks in the image from the high speed camera would be saturated, meaning that the pixel would be maximally illuminated. This meant that the profile would appear to top out and remain flat in the saturated region, resulting in a plateau where there should be a peak (see Fig. A.22 in Appendix). Nevertheless, the detection algorithm still identified the location, spacing, and widths of these

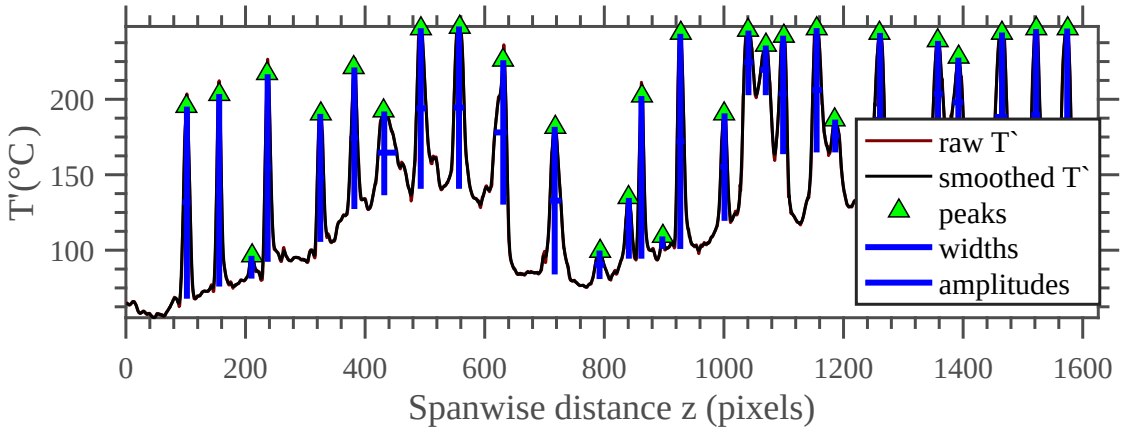

Figure 3.31: Example of the streak detection algorithm with displayed results for one image. Here, the raw luminosity profile is shown as a thin red line while the smoothed profile is shown as the thicker black line. This image also shows derived streak locations or peaks (green triangles), streak widths (horizontal blue lines), and streak amplitudes (vertical blue lines).

regions quite well; the prominence (or amplitude) of the peak was the only statistic that suffered. In addition, close to the leading edge of the wick, not enough light was visible to detect streaks. Fig. 3.32 shows an image taken from a flame exposed to a crosswind of 0.70 m/s. Here, it can be seen how the luminosity of streaks declines adjacent to the leading edge. Consequently, data could not be obtained consistently too close to the leading edge.

Fig. 3.33 displays an example of tracked streak movements over time along a single spanwise location. Here, we can see that streaks tend to persist for a certain amount of time before dissipating or being absorbed into another structure. During their lifetimes they meander laterally, occasionally coming into interaction with nearby structures. Qualitatively, these structures appear to move and interact laterally slightly more than those observed over the hot plate, which may be a result of the increased buoyant energy which is being supplied by the flame.

Figure 3.32: Image of the isopropyl flame taken from the high speed overhead camera. The flow direction is from the bottom to the top of the page. The thin white box represents an example of an analysis region used at $x = 75$ mm.

3.2.3.1 Streak spacing

Similar to the hot plate, data was seen to obtain a lognormal distribution, a finding which agrees with near-wall streak spacing in other boundary layer flows. Fig. 3.34, showing an example of histograms, confirms that distributions of streak spacing appear to be well described well by lognormal fits, particularly at upstream measurement locations. The lognormal distribution of spacing in both turbulent and laminar boundary layers observed in both buoyant and non-buoyant flows suggests that this behavior is a universal property of streak spacing distributions.

Additional statistical analysis was performed in order to see if the data from the lognormal statistics was appropriate. Overall, these checks confirmed that the lognormal fit worked well, similar to the previous results for the hot plate. As a first

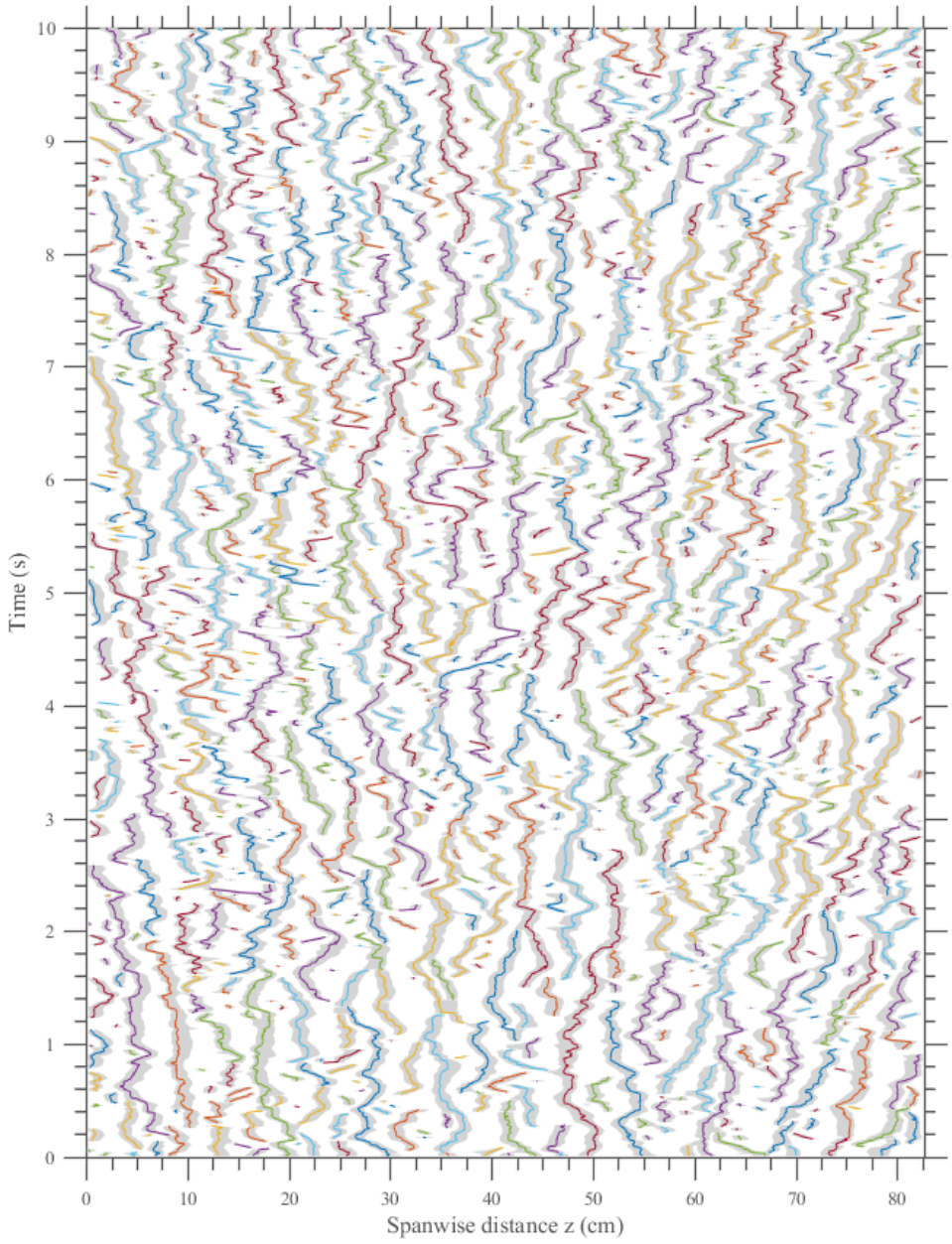

Figure 3.33: Graphical illustration of streak tracking, in which the spanwise locations of streaks are plotted against time. Thin colored lines represent streak centerlines whereas light gray areas represent streak width. Data for this figure was obtained 75 mm downstream of the isopropyl flames leading edge at a wind speed of 0.7 m/s.

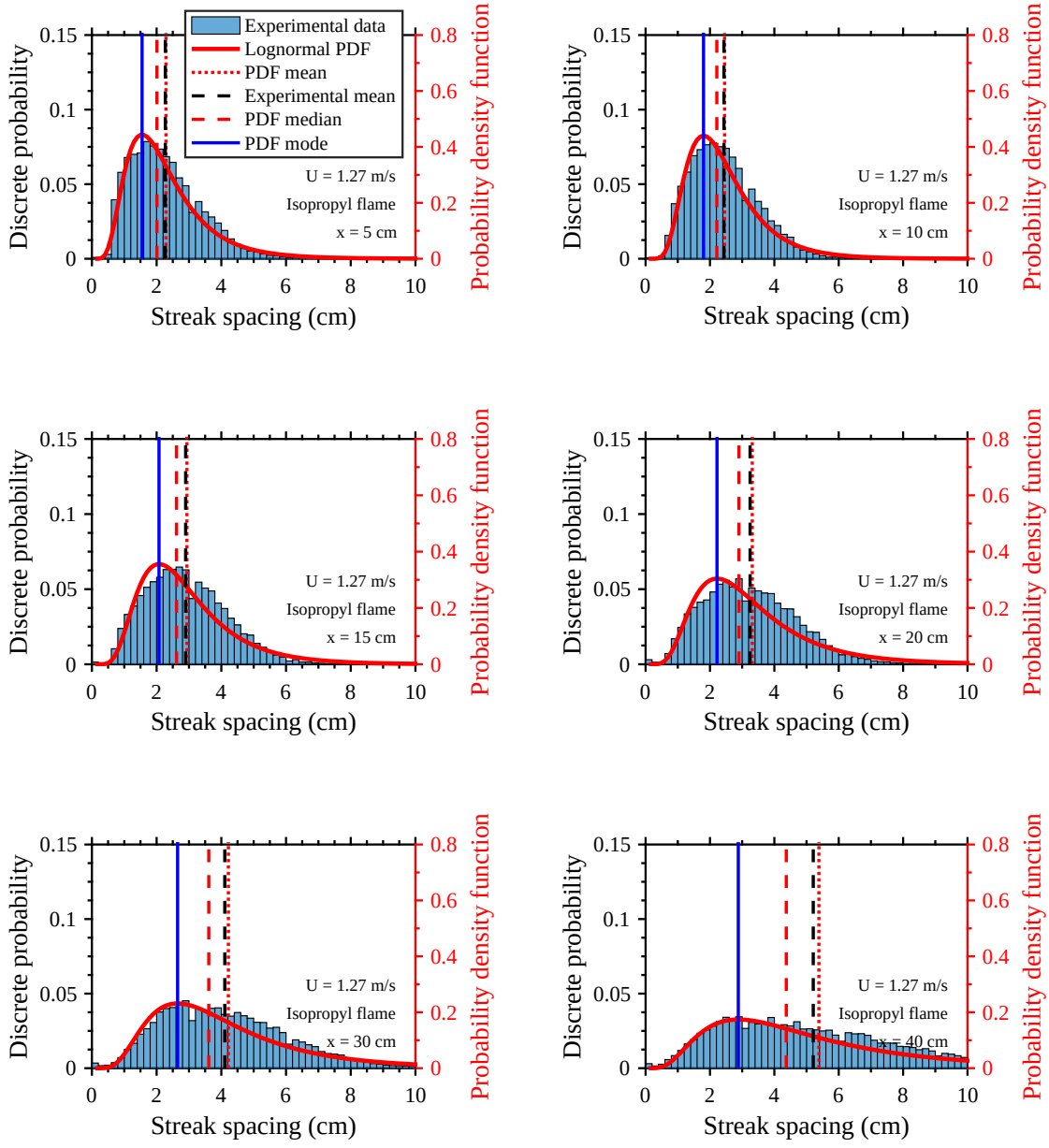

Figure 3.34: Plots of experimental distributions of streak spacing along with a log-normal fit of the data. All data is taken from high speed images of the isopropyl flame where the wind speed is 1.27 m/s. The indicated experimental means are derived from experimental data while other values are derived from arithmetic properties of the lognormal PDF. Experimental distributions for the remainder of parameter spaces can be seen in the appendix (Figs. A.12-A.15).

step, we compared the means and standard deviation of the discrete experimental data to the mean obtained by the continuous lognormal PDF. A lognormally distributed random variable is generally described by two parameters, μ and σ, which are the mean and standard deviation of the variable's natural logarithm, respectively. Knowing these parameters, we were able to calculate the arithmetic mean via MATLAB's *lognstat* function, which is equal to $\exp(\mu+\sigma^2/2)$, and the arithmetic standard deviation, which is equal to $\exp(\mu+\frac{1}{2}\sigma^2)\sqrt{\exp(\sigma^2)-1}$. In Fig. 3.35, you can see a comparison of experimental values vs. fitted values for all tested conditions. For the derived mean values from experiments and the PDF's, all data points lie fairly close to the line of unity. This is a strong indication that the lognormal PDF's are adequately capturing the centrality present in derived data. Meanwhile, the standard deviation values from the experiments look good compared to the PDF values, but the standard deviation of the PDF is seen to increase slightly for the largest values. This indicates a slight overprediction of variability by the lognormal fit for some cases, but it is well within an acceptable range.

In Fig. 3.36, the fitted median behaves similar to the experimental mean, consistently residing at about 87% of the experimental values. Consequently, we can say that either statistic will provide a similar description of the data and will reveal similar trends. Meanwhile, the mode, shown in Fig, 3.37, is consistently around 72% of all mean values below 4 cm, but this trend no longer holds at higher values. A fit to all data points reveals the mode being around 63% of the spacing, but this fit is a bit messier ($R^2 = 0.71$). This behavior of the mode at higher values of spacing, which occur furthest downstream, indicates slight differences in the distribution.

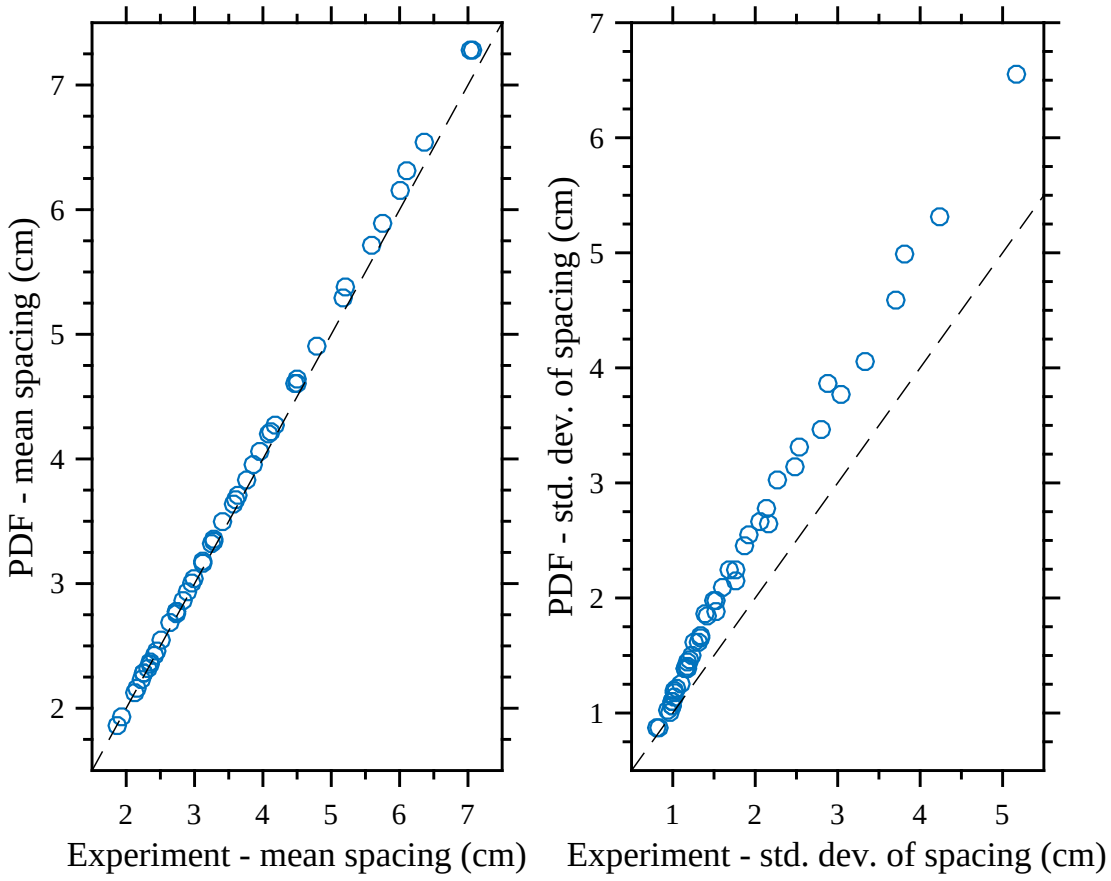

Figure 3.35: Displayed here are comparisons of statistics of the experimental data vs. the fitted lognormal distribution of flame streak spacing. To the left, the means of each distribution are compared; to the right, the standard deviations are compared. The dashed line indicates the line of unity.

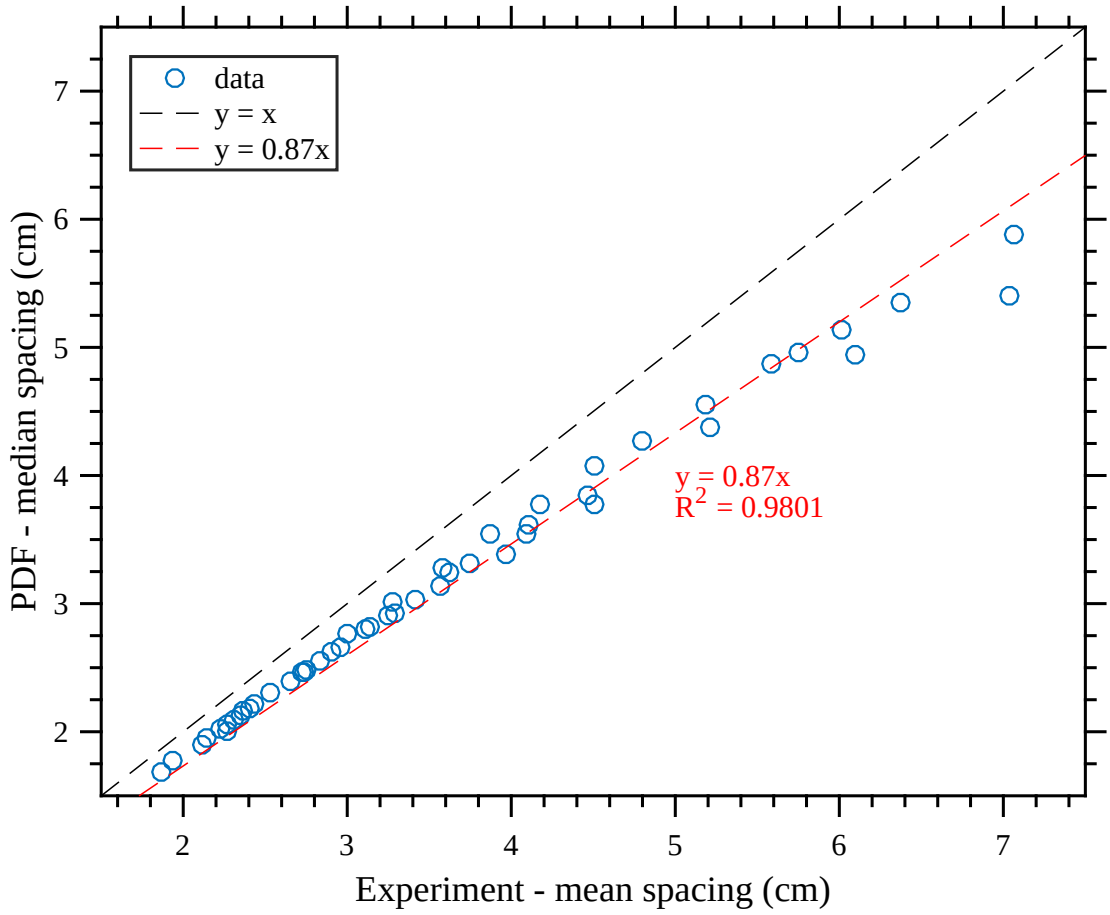

Figure 3.36: The median of the fitted lognormal distribution plotted vs. the mean of the experimental distribution for flame streak spacing. The black dashed line displays the line of unity while the red dashed line represents a best linear fit with a prescribed intercept of zero.

This is likely because the coherent structures measured downstream are no longer truly streak-like but more complex in shape resulting from an agglomeration of streak merging.

A lognormal distribution is also commonly quantified using the skewness, given by $(e^{\sigma^2}+2)\sqrt{e^{\sigma^2}-1}$, and the coefficient of variation (CV), calculated as $\sqrt{e^{\sigma^2}-1}$. These values were tabulated vs. all experimental conditions. No trend in these statistics was observed as the wind speed or the hot plate temperature was ma-

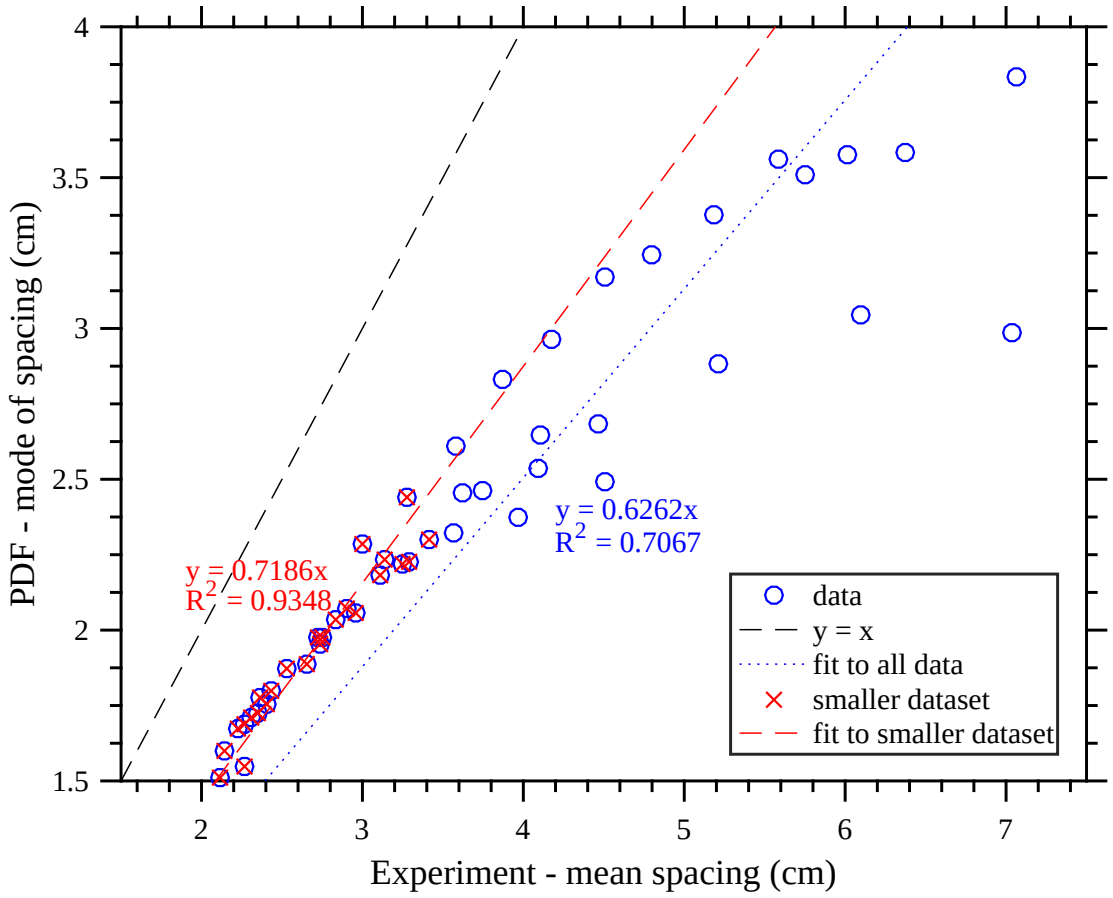

Figure 3.37: The mode of the fitted lognormal distribution plotted vs. the mean of the experimental distribution for flame streak spacing. The black dashed line displays the line of unity; the red dashed line represents a best linear fit to the data indicated by red x's with a prescribed intercept of zero; the blue dotted line represents a best linear fit to all data with a prescribed intercept of zero.

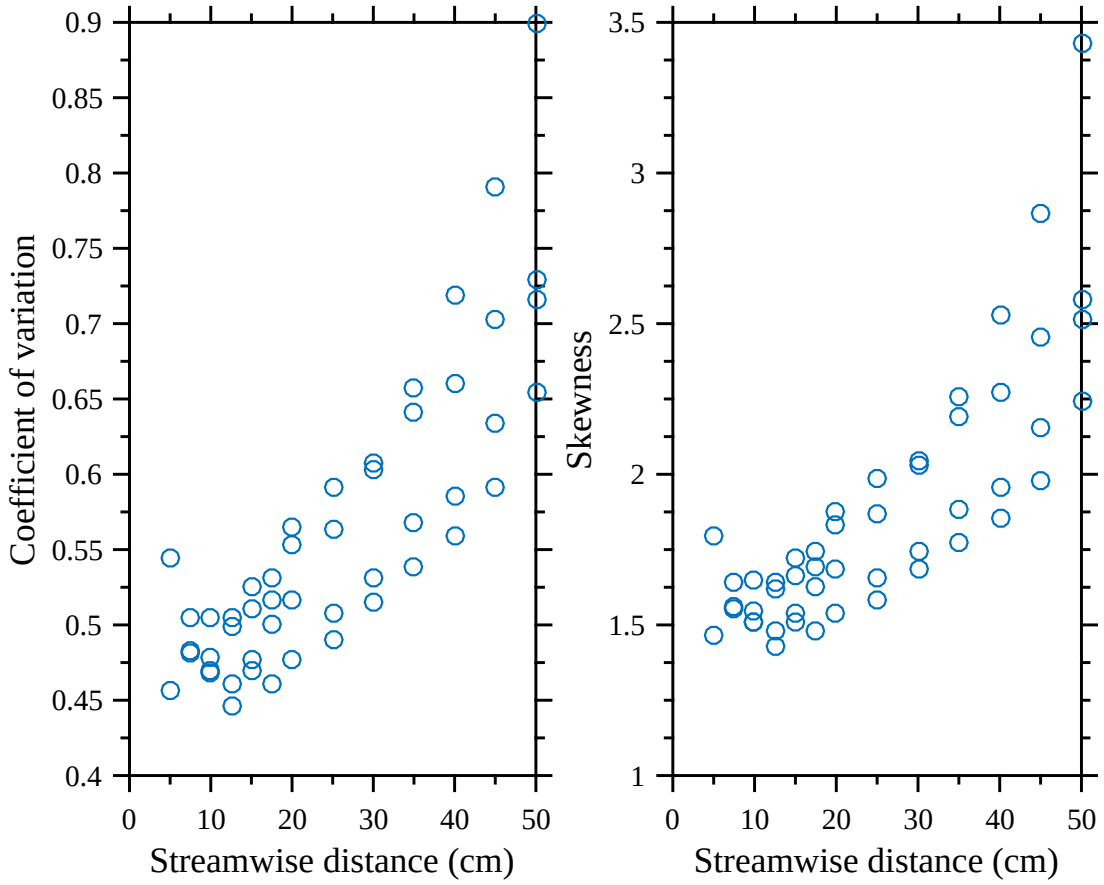

Figure 3.38: Plots of the coefficient of variation (left) and the skewness (right) vs. the streamwise distance. All statistics are derived from the fitted lognormal distributions for flame streak spacing.

nipulated. However, there was a slight trend with the streamwise distance, and Fig. 3.38 displays a scatterplot of this relationship. Both of these values appear to increase with downstream distance,indicating that there is a wider dispersion of streak spacing downstream. Respective values for the coefficient of variation and skewness (i.e., 0.45-0.7 and 1.5-2.5) are slightly higher reported values of 0.44 and 1.1 from Zachsenhouse et al. [90] and slightly higher than the hot plate streaks which had 0.35-0.55 and 1.1-1.8 for the coefficient of variation and skewness, respectively.

In addition to looking at the distribution of spacing data, the experimental

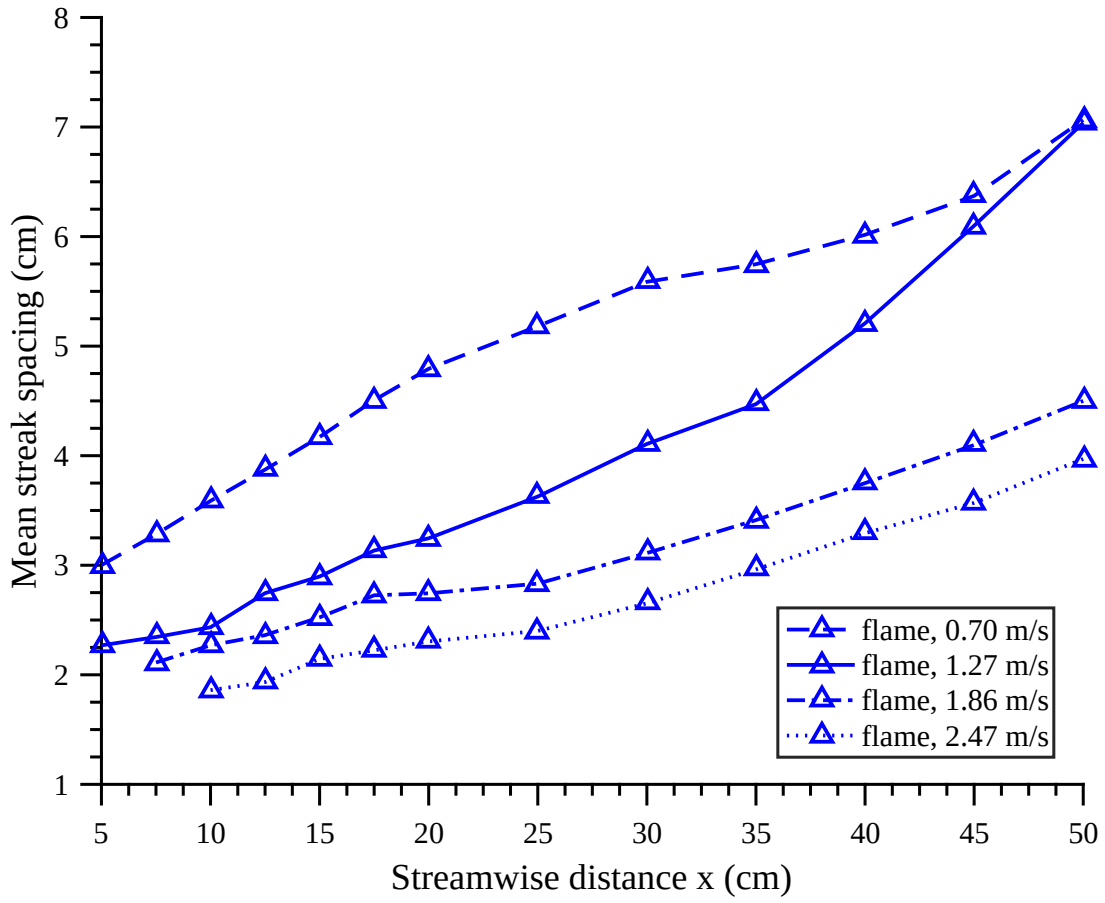

Figure 3.39: A plot of the mean spacing of flame streaks vs. streamwise distance for all experimental conditions.

means were tabulated for all tested winds and all streamwise distances visible in the high speed video. Unfortunately, at the exact leading edge of the fuel wick ($x = 0$), streaks are not immediately visible. Because of the lack of luminosity in this region, streaks could only be detected by a computer algorithm beyond $x = 5$ cm. Regardless, plotting all experimental data vs. the streamwise distance in Fig. 3.39 portrays an adequate picture of the development of streak spacing. Similar to the hot plate, there is clearly a negative correlation of streak spacing to wind speed at all regions.

The spacing is also seen to increase constantly as we move downstream. This is likely a function of the growth of coherent structures, which, as one can observe in the video, will grow in size and regularly merge with adjacent structures. This leads to a highly dynamic process with the rapid growth and changing of structures as they travel downstream. In fact, further downstream, it may be improper to describe the observed coherent structures as streaks; they no longer exhibit well-defined streak-like shapes, but they take on significant width and exhibit rather varied and jagged edges. It appears that the merging behavior of the streaks may actually dictate the growth or length-scales associated with the structures further downstream. This is important because this may describe the 'flame towers' seen at the furthest edges of a flame, which control patterns of intermittent heating and cooling to the surface [1]. If so, understanding the growth of these streaks can be useful in describing the instantaneous heating which drives wildland fire spread. This growth is almost certainly a function of buoyancy, which serves to amplify coherent structures. The amplification process may be analogous to that of a Rayleigh-Taylor Instability (RTI), which occurs at an interface between two fluids with varying density. It has been hypothesized that RTI begins at small-scale in buoyancy-dominated diffusion flames and eventually encompasses the entire flow [43]. If so, quantifying this growth would be valuable in assessing the behavior of the flow; in particular, it would be interesting to see how the growth of the mixing region compared to the quadratic growth predicted for RTI's. Further CFD modelling would likely be the best way to examine this claim, as the experimental data provided here cannot quantify the vertical growth of the flaming region.

Examining Fig. 3.39, we see that the negative correlation of spacing to the bulk wind speed is even seen towards the leading edge of the flame. This is quite interesting, because this behavior was also observed in hot plate experiments, where the streak spacing appeared to be preset by disturbances in the incoming flow. In order to investigate whether the same phenomenon is occurring in the presence of combustion, we can quantify the initial spacing by examining data near the leading edge ($x = 5$ cm). In the case where data was lacking in this region, a line of best fit was made from nearby data points to provide a reasonable estimate for the initial spacing. Fig. 3.40 plots the initial spacing vs. the Reynolds number, which quantifies the change in wind speed. The initial spacing is negatively correlated to the Reynolds number, which is similar to earlier results.

In addition, it is possible to convert the initial streak spacing from centimeters to non-dimensional wall units, which are derived from the earlier measurements of velocity gradients. This was done for all wind speeds, and Fig. 3.41 demonstrates that the initial spacing collapses when plotted vs. wall units. This furthers the argument that the incoming velocity boundary layer is controlling the initial streak spacing even in the presence of the strong buoyancy associated with a flame. In fact, if the incoming boundary layer governs this behavior, similar results for the initial spacing should be observed for both the hot plate and for the isopropyl fuel wick. Fig. 3.42 plots the results for the hot plate and the flame on one graph, and the agreement of results for spacing is remarkable. Fig. 3.43 repeats these results with spacing measurements converted to wall units, and it can be seen that the initial spacing remains between 60 and 75 wall units for all tested wind speeds and all

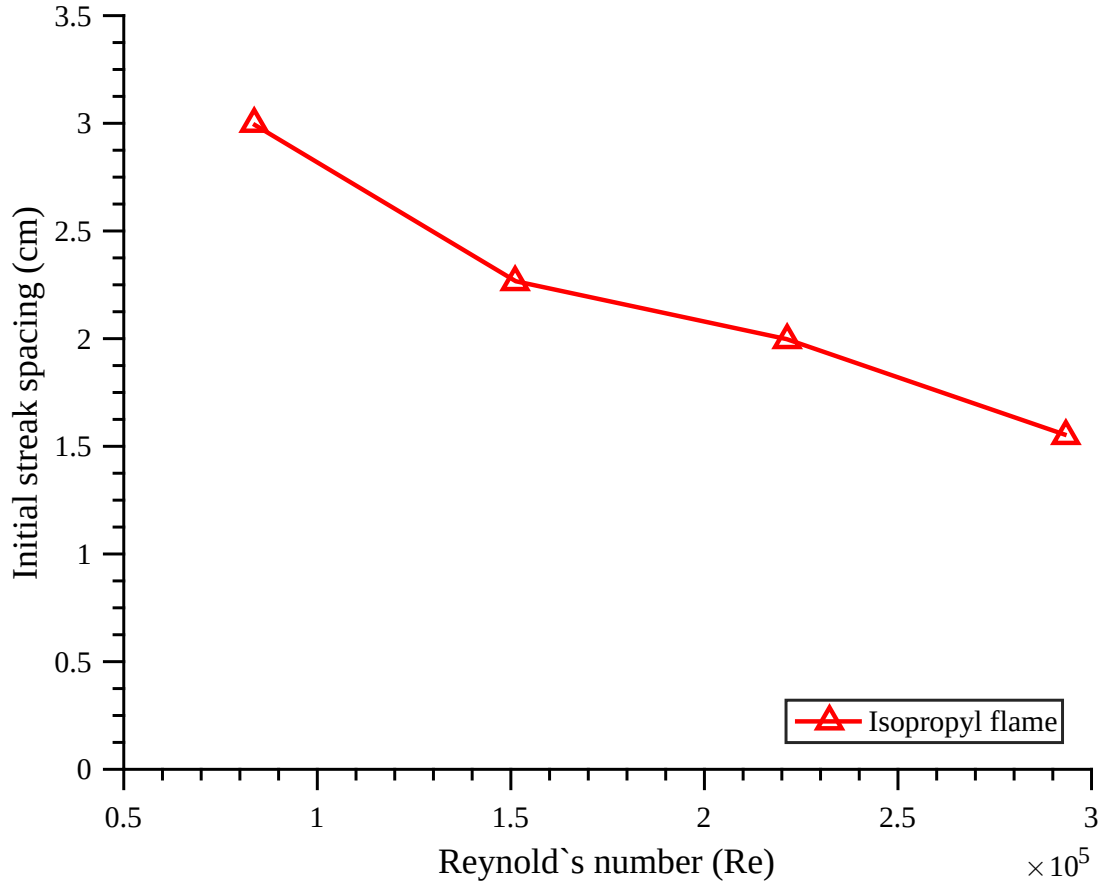

Figure 3.40: Initial flame streak spacing vs. the Reynolds number at the leading edge of the fuel wick. The initial streak spacing was calculated at $x \approx 5$ cm.

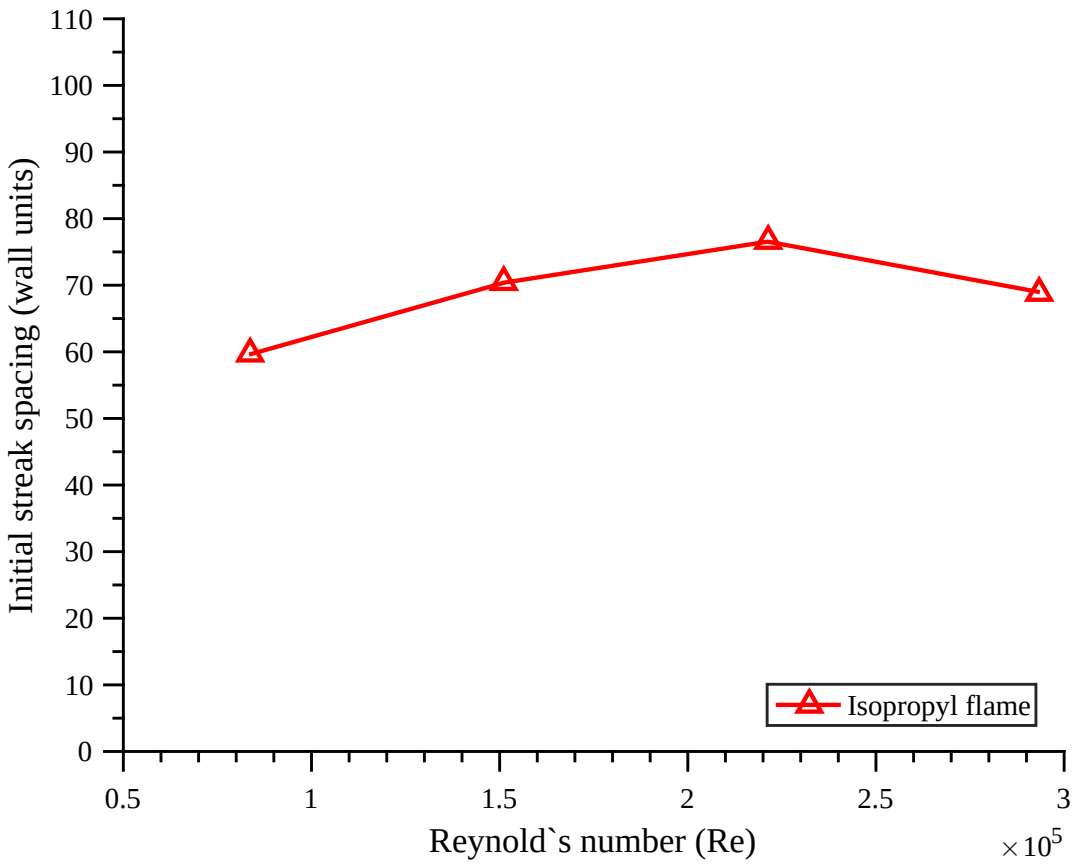

Figure 3.41: Initial flame streak spacing in dimensionless wall units vs. the Reynolds number at the leading edge of the fuel wick.

sources of buoyancy. Given the immense range in the strength of the source of buoyancy, which varies from a 150°C hot plate to an ≈ 1200°C flame, this result strongly indicates that the initial spacing is a consequence of the incoming boundary layer. The incoming coherent structures, including near-wall streaks, will be proportional to the height of the incoming velocity boundary layer. It is only downstream of the leading edge that the buoyancy will be able to modify these coherent structures.

This finding has several important takeaways. One of the first is understanding that the initial spacing might best be approached via theory for non-reactive boundary layers. For this reason, attempts at modeling these structures will need

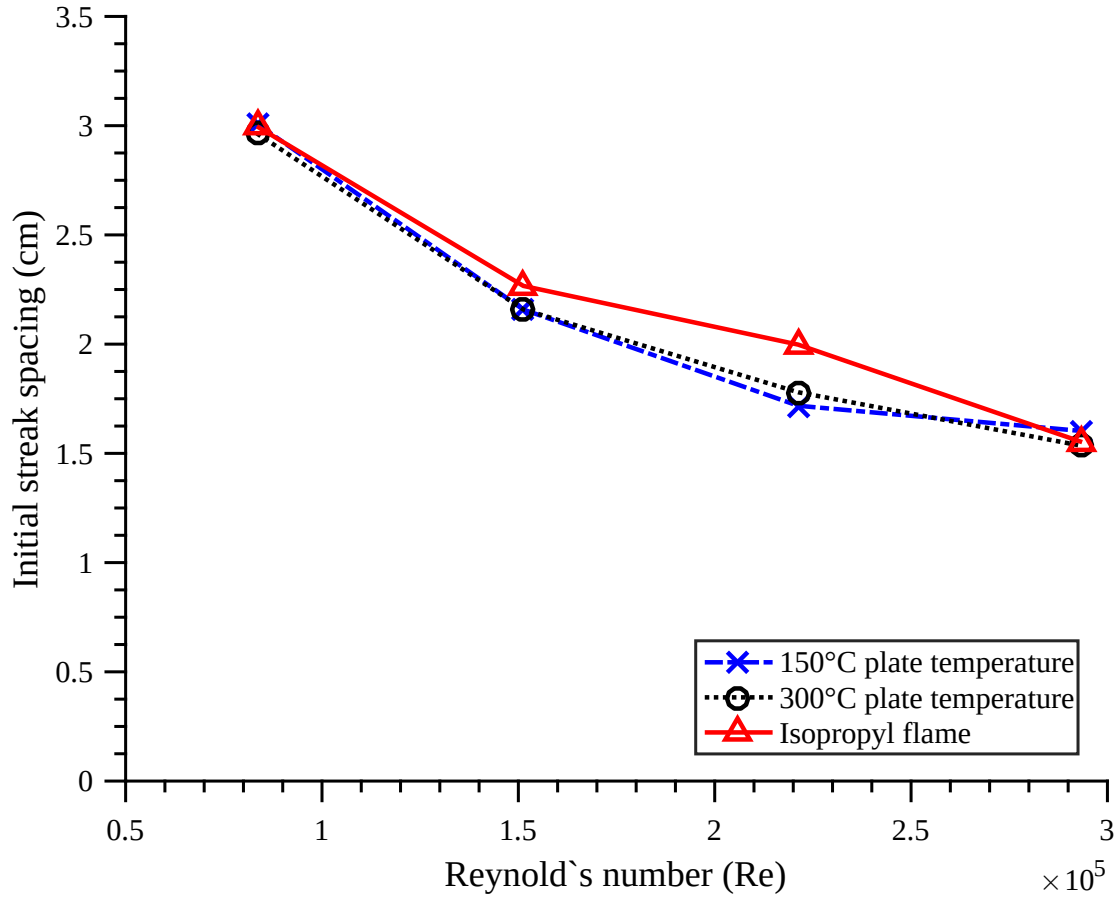

Figure 3.42: Initial streak spacing vs. the Reynolds number for all streaks, including data from the hot plate and isopropyl fuel wick experiments.

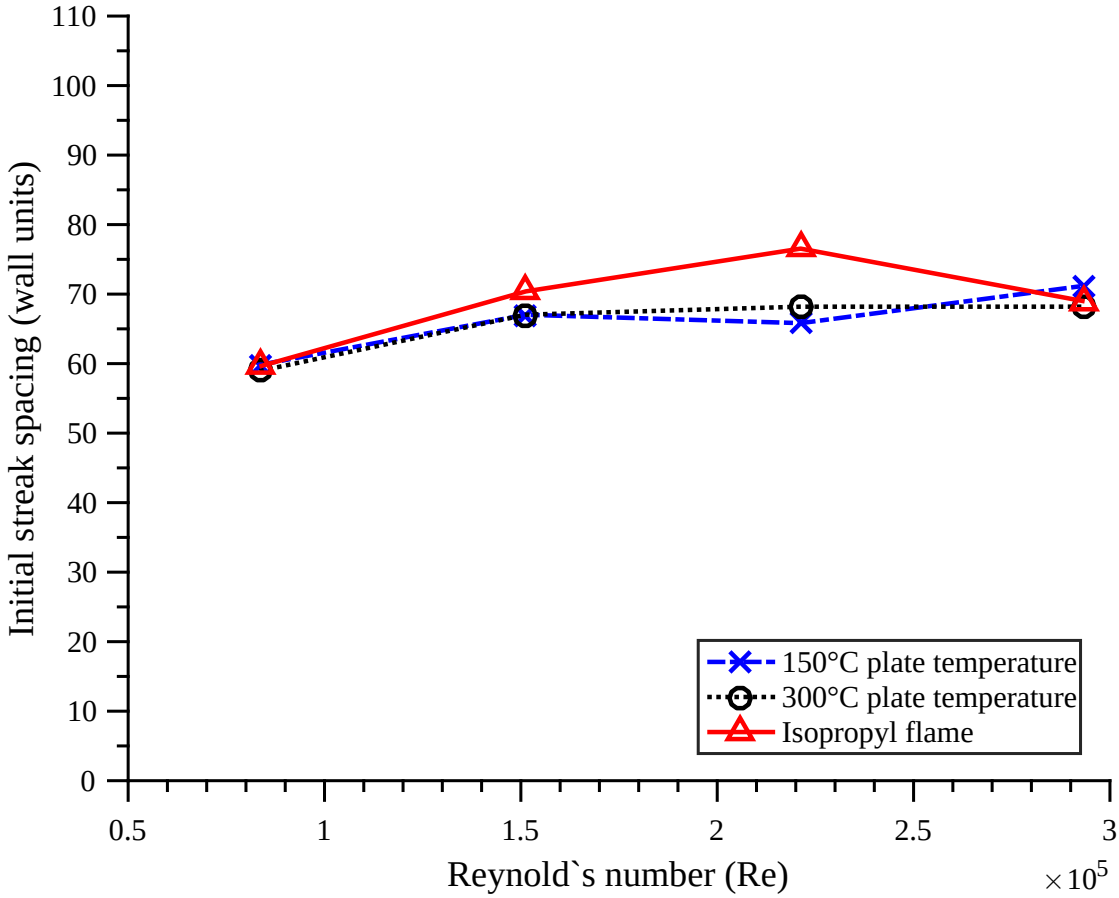

Figure 3.43: Initial streak spacing in dimensionless wall units vs. the Reynolds number for all streaks, including data from the hot plate and isopropyl fuel wick experiments.

to put significant effort into validating the incoming boundary layer. Theoretical considerations of the initial spacing, including linear stability theory, likely do not need to account for buoyancy. In addition, if the spacing of structures governs the downstream development of the flame or the local heat flux to the surface, properties of the incoming boundary layer will be essential to describing these behaviors. Finally, the universality of spacing in wall units implies that data on streak spacing can be applied to reveal properties of the incoming boundary layer. For instance, it may be possible to examine an aerial photograph of a spreading wildland fire exhibiting streaks, establish a length scale for the streak spacing, and use this data to approximate the height of the incoming boundary layer. This data could prove to be quite valuable in assessment of a wildland fire, where accurate measurements of incoming wind profiles or even instantaneous wind data are often unattainable. If nothing else, the presence of streaks may indicate that a boundary layer is governing the incoming flow and will modify the behavior of the flame.

As a final point, it should be noted that as we move further downstream, the coherent structures measured in the flame likely differ from the coherent structures measured over the hot plate. Over the hot plate, the data is always taken from the surface, meaning that we are observing coherent structures in the near-wall region. In the flame, the data observed is taken from the luminous flame sheet, which gradually lifts away from the surface as we move downstream. In a sense, the downstream data on flame streaks is taken at a particular height within the thermal boundary layer, which is directly related to the location of the flame sheet. This subtle distinction may serve to explain why some discrepancies are observed when

we move away from $x = 0$. Additionally, the flame sheet extends over a streamwise depth that is well beyond that of the hot plate depth. The process observed in these flames is governed by a continuous injection of heat along a reaction front; in contrast, hot plate experiment examines phenomena where the heat is supplied from the surface. This means that the experiments are not completely analogous - examining reactive flow is not simply equivalent to increasing the temperature of the hot plate. Nevertheless, the overall behavior is quite similar, and examining a non-reactive flow was an important step in looking at the simplest version of streaks in mixed convection.

3.2.3.2 Streak width

In addition to the spacing between flame streaks, the mean width of streaks was also quantified for all experimental conditions. Fig. 3.44 reveals a plot of the mean streak width vs. streamwise distance for all four tested wind speeds. Similar to the trend for spacing, the width of streaks is negatively correlated to the wind speed. The width is also seen to increase as we move downstream, a trend observed for spacing as well. However, there appears to be an assymptote reached for the width at a certain downstream distance. This can be observed around 30 cm for a wind speed of 0.70 m/s and around 40 cm for a wind speed of 1.27 m/s. In contrast, the growth in spacing (Fig. 3.39) does not appear to decelerate downstream. The asymptotic behavior of the flame streak width could be due to the fact that downstream measurements are taken towards the outer extents of a flame, where most

of the flammable gases have already reacted. However, it is possible that there are limitations on the width of these coherent structures which will restrict growth despite a constant increase in spacing between these structures. This behavior is likely related to the peak and trough structure of a flame, which has been shown to be correlated to the flame length [1]. It appears that there is a settling of length scale which is based on the time for growth of structures. This time scale is positively correlated to the flame length, which enables growth, and negatively correlated to the wind speed, which determines the time structures inhabit the flaming region. A time scale based on the flame length (or burning depth) and the wind speed may be related to the largest observed length scale of coherent structures; further research would help to show how this phenomena modifies the heat transfer to the surface at the furthest extents of a flame. It should be noted that for a semi-infinite hot plate or flame there will be no dominant length scale; growth and mixing will occur indefinitely. The behavior seen here is likely only reproducible when the heated source, such as a hot plate or a flame, is finite in length.

3.2.3.3 Streak prominence

The mean streak prominence represents the amplitude of the perturbation in the luminous intensity profile (see Fig. 3.31). A larger streak prominence indicates that the streak is quite bright compared to the regions on either side of it. Fig. 3.45 displays a plot of the streak prominence vs. the streamwise distance. In general, the prominence is seen to reach a minimum at an intermediate distance downstream.

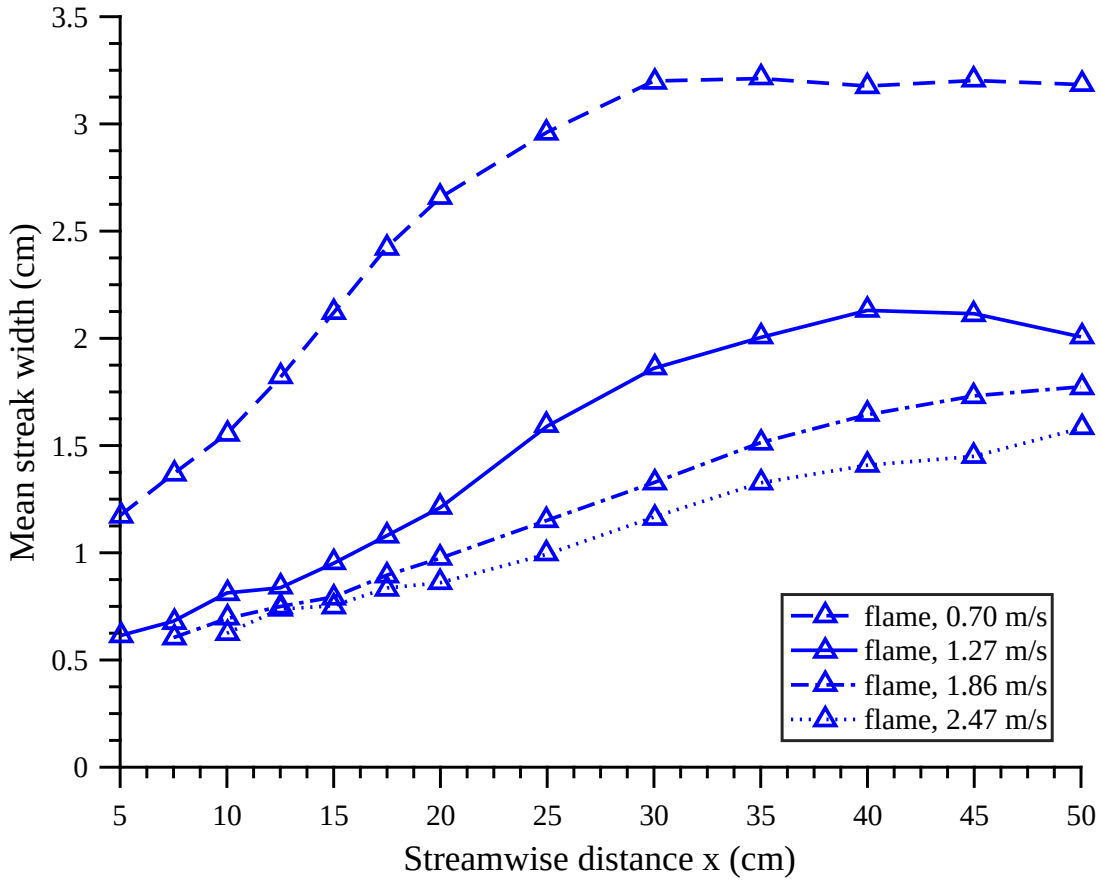

Figure 3.44: A plot of the mean width of flame streaks vs. streamwise distance for all wind speeds.

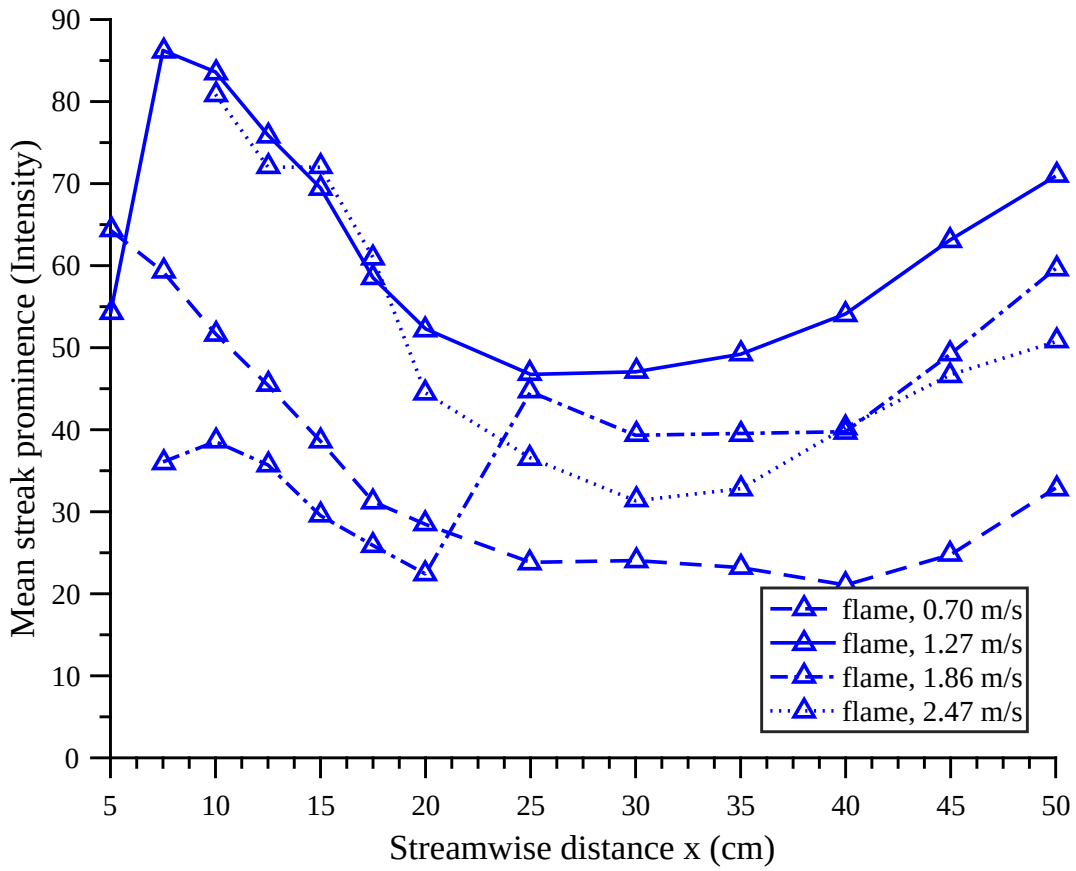

Figure 3.45: A plot of the mean prominence, or amplitude, of flame streaks vs. streamwise distance for all wind speeds.

However, this data is heavily skewed by the oversaturation observed in most of the high speed videos. For this reason, we are unable to draw any definite conclusions concerning the prominence of flame streaks.

3.2.3.4 Streak duration

The streak detection algorithm made it possible to assess the lifetime of a streak at a particular streamwise location. Once a streak appeared, or was born, it would die if it was no longer detected in a subsequent frame or if it was absorbed into a more powerful streak. Fig. 3.46 displays a graph of the mean duration of flame

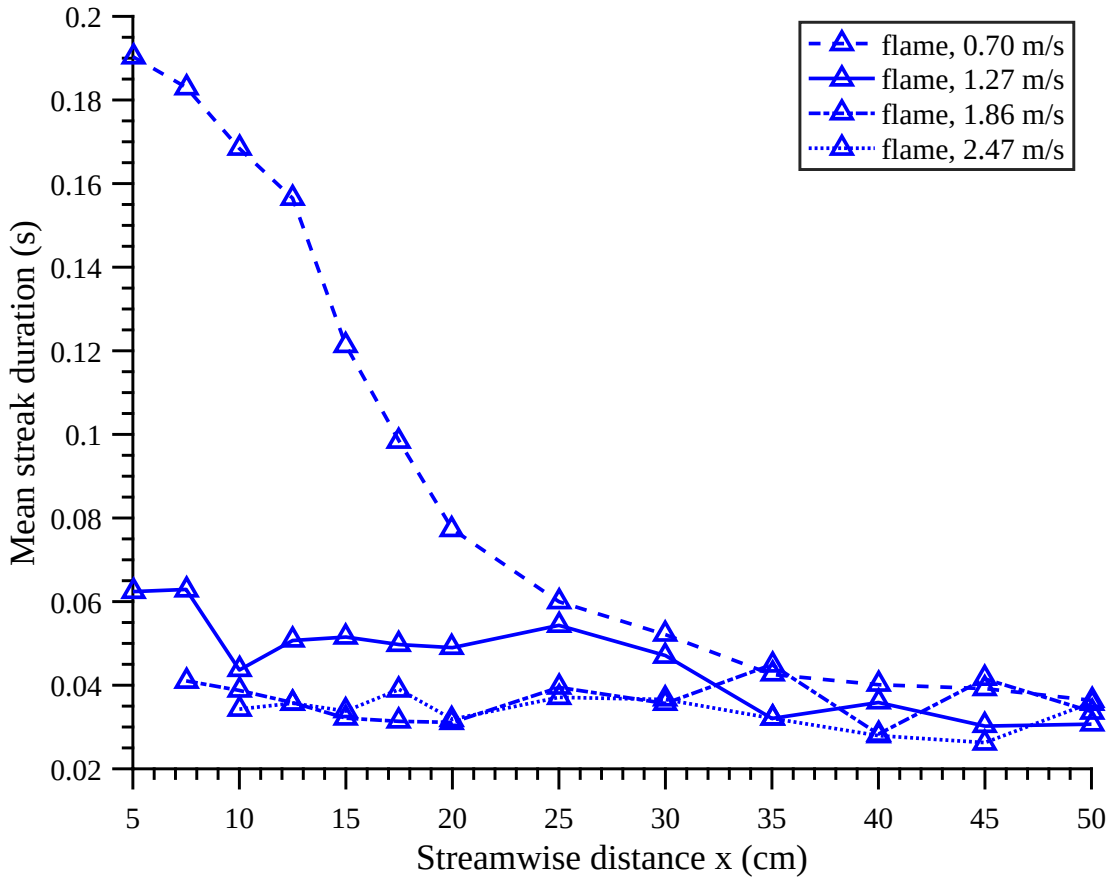

Figure 3.46: A plot of the mean duration, or lifetime, of flame streaks vs. streamwise distance for all wind speeds.

streaks vs. streamwise distance. Here, we see that the duration, or persistence of streaks in time, decreases as we move downstream. The most persistent flame streaks are observed in the case with the lowest wind speed. In this instance, the streaks are seen to meander less and avoid interacting with one another as often. This interaction increases dramatically as we move downstream, where coherent structures appear less streak-like and more chaotic. In other words, the presence of the flame serves to enhance the mixing and chaos associated with coherent structures.

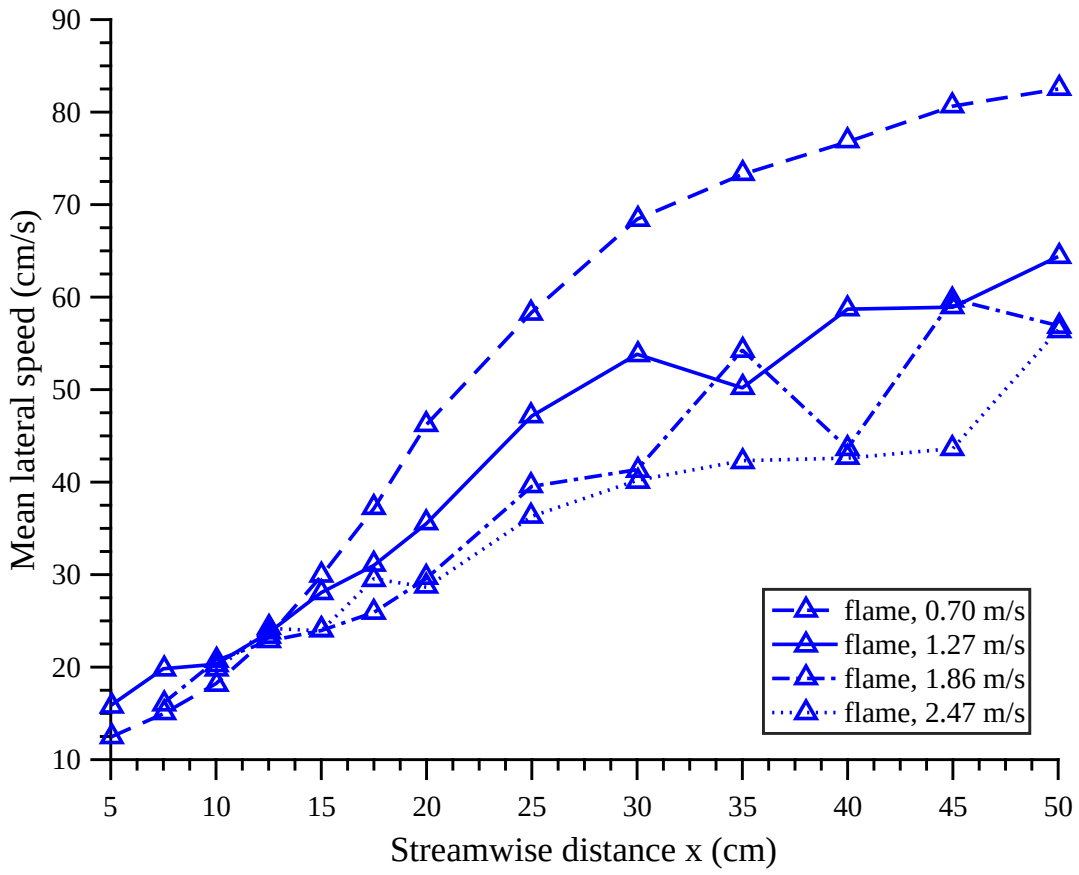

Figure 3.47: A plot of the mean lateral (spanwise) velocity of flame streaks vs. streamwise distance for all wind speeds.

3.2.3.5 Streak meandering

Fig. 3.47 demonstrates that the spanwise meandering velocity increases as we move downstream. Similar to streaks observed over the hot plate, we see a more chaotic region downstream in the flame. This region is characterized by rapid meandering of coherent structures and increased interaction with neighbors. Although the structures entering the flame appear quite regular and very streak-like in nature, buoyancy appears to significantly increase the volatility and variability of coherent structures.

As a further measure of coherent structure interaction, we attempted to quantifying merging instances utilizing a method described in Section 3.2.2. Fig. 3.48 displays a plot showing the number of merging instances over a 5 second period as a function of the streamwise distance. The data becomes slightly messier downstream, most likely due to greater variability in the shapes of coherent structures and slight inconsistencies associated with the detection algorithm. Nevertheless, there is a clear increase in the number of merging instances as we move downstream for all wind speeds. In addition, we were able to quantify the number of instances where coherent structures were seen to split, and these results are shown in Fig. 3.49. Once again, the number of splitting instances increases significantly as we move downstream. This indicates that coherent structures are less isolated, interacting regularly with their neighbors.

Fig. 3.50 displays the ratio of spltting to merging observed for all experimental conditions. It can be seen that the split-to-merge ratio decreases as we move downstream; consequently, we can conclude that more merging is occuring downstream and structures are aggregating more often. This finding agrees with the idea that the growth and aggregation of small-scale structures establishes the growing length scale of downstream structures. Although the initial length scale is governed by the incoming flow, the subsequent growth is clearly a consequence of buoyant forces acting on the flow. This may be related to an earlier hypothesis, which posited that RTI begins at small-scale in flames and eventually encompasses the entire flow [43].

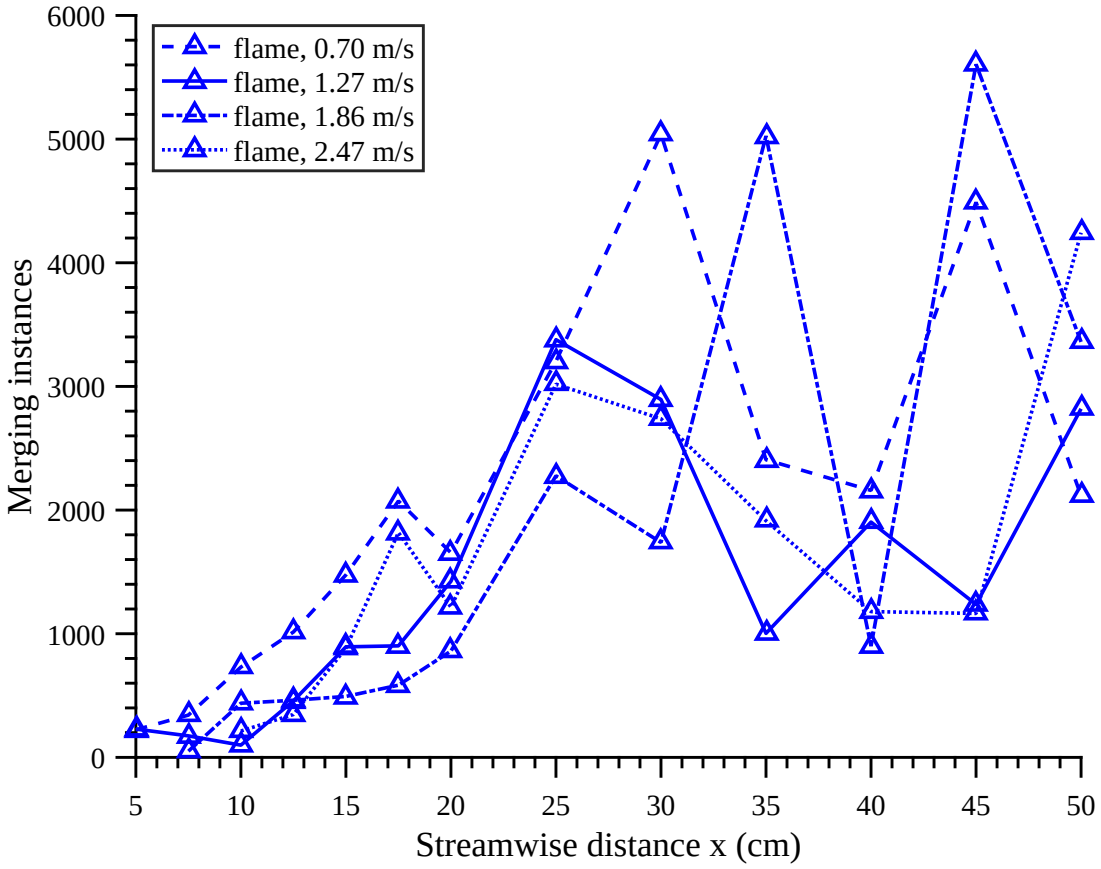

Figure 3.48: A plot of the number of detected merging instances of flame streaks vs. streamwise distance for all wind speeds.

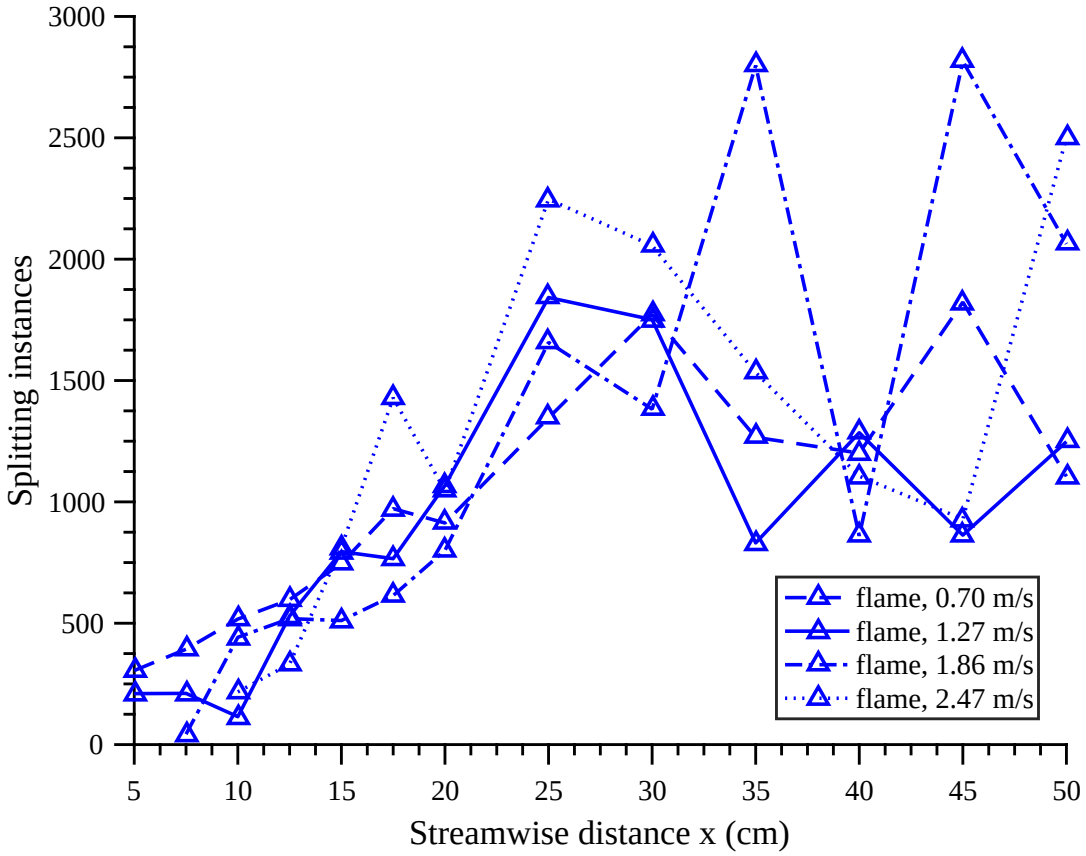

Figure 3.49: A plot of the number of detected splitting instances of flame streaks vs. streamwise distance for all wind speeds.

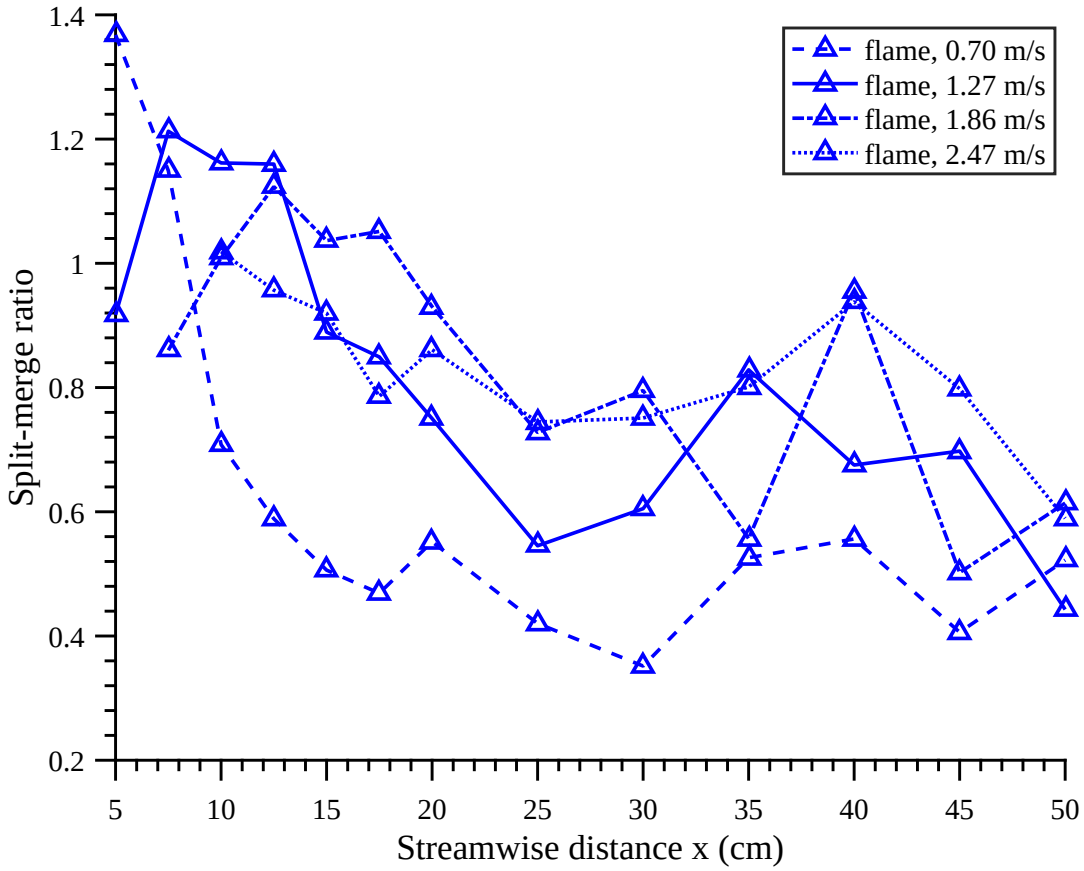

Figure 3.50: A plot of the ratio of splitting-to-merging instances of flame streaks vs. streamwise distance for all wind speeds.

3.2.4 Summary of flame data

Streaks were observed in a boundary layer flame by means of high speed video, and important properties have been quantified via image processing. Several important findings have been made, including:

- A means of visualizing flame streak traces over time
- Lognormal distribution of streak spacing
- Streak spacing negatively correlated to wind
- Initial streak spacing governed by properties of the incoming boundary layer
- Initial streak spacing consistently between 60-75 wall units
- Growth in streak spacing downstream
- Width of streaks grows before reaching apparent assymptote, likely controlled by time for growth
- Streaks meander more rapidly and persist for a shorter duration as the flow becomes more chaotic downstream
- Streaks interact more often downstream by merging and splitting
- Streak merging increases relative to splitting downstream, indicating structure aggregation

These findings are generally consistent with the data for the hot plate streaks, indicating that the behavior of streaks is governed by similar processes in both scenarios.

Although the initial instabilities are governed by the incoming wind, buoyant forces cause the growth of these structures and eventual liftoff from the surface. Coherent structures populating the flame and the hot plate flows appear to be governed by regimes dominated by either inertia or buoyancy; these regimes are also employed in discussions of the macroscopic flow. These coherent structures, which exhibit upwash and downwash regions of counter-rotating vortices, are likely connected to the surface heat transfer and they may be involved in the downstream behavior of the flow. Buoyancy may amplify the streaks, and this growth and aggregation likely governs the nature of the larger-scale structures seen further downstream.

3.3 Conclusion

Streamwise streaks have been seen to appear consistently in boundary layers which pass over heated surfaces and flames. This consistent observation prompted an examination into their role in the overall behavior of mixed convection, which is generally understood to be governed by a competition of momentum and buoyancy. This project examined the role of these two forces in the creation and development of streak-like structures. In order to assess the relative influence of momentum and buoyancy on these coherent structures, we experimentally manipulated the incoming wind speed (0.70 - 2.47 m/s) and the local source of buoyancy (150°C hot plate, 300°C hot plate, isopropyl flame). This wide parameter space enabled important findings and trends to be be derived from experimental data.

One of the first resolved questions concerned the mechanism controlling the

onset of the streaks. The initial spacing was found to be independent of the source of buoyancy, whether this source was a 150°C surface or an isopropyl flame. Instead, the initial length scale was clearly controlled by the wind speed. In fact, the streak spacing in this experiment was consistently between 60-75 wall units, a dimensionless length scale related to the near-wall velocity gradient. This finding mirrors the behavior of near-wall streaks in turbulent boundary layer flows, which are consistently on the order of approximately $100 + / - 30$ wall units. This implies that the disturbances already present in the incoming boundary layer represent the initial perturbations in these mixed convection flows. Coherent structures observed at the leading edge of the buoyant source are proportional to the size and structure of the incoming boundary layer. The incoming boundary layer is the mechanism responsible for the creation of streaks in heated boundary layer flows and boundary layer combustion.

This finding has several important takeaways. One of the first is understanding that the initial spacing might best be approached via theory for non-reactive boundary layers. For this reason, attempts at modeling these structures will need to put significant effort into validating the incoming boundary layer. Theoretical considerations of the initial spacing, including linear stability theory, likely do not need to account for buoyancy. In addition, if the spacing of structures governs the downstream development of the flame or the local heat flux to the surface, properties of the incoming boundary layer will be essential to describing these behaviors. Finally, the universality of spacing in wall units implies that data on streak spacing can be applied to reveal properties of the incoming boundary layer. For instance,

it may be possible to examine an aerial photograph of a spreading wildland fire exhibiting streaks, establish a length scale for the streak spacing, and use this data to approximate the height of the incoming boundary layer. This data could prove to be quite valuable in assessment of a wildland fire, where accurate measurements of incoming wind profiles or even instantaneous wind data are often unattainable. If nothing else, the presence of streaks may indicate that a boundary layer is governing the incoming flow and will modify the behavior of the flame.

Downstream of the initial appearance of these streaks, however, buoyancy quickly begins to be a dominant force. In both the flames and the hot plate, the spacing and width of the streaks is seen to grow downstream. In particular, the growth of the streak spacing in the flame is observed immediately and persists over the length of the flame. Meanwhile, the width of the streaks grows quickly until it reaches a maximum value, which is likely determined by the time for growth. The rate of growth, which is larger for the flame streaks, is most likely governed by buoyancy. This growth may even be analogous to that observed for Rayleigh-Taylor Instabilities. The larger coherent length scales encountered downstream are likely consequences of the amplification and merging of the flame streaks. This is most likely a function of the rate of growth, which is associated with the density difference between the heated flow and the ambient wind (i.e., the Atwood number in RTI scaling), and the time for growth, which is a function of the flame length and wind speed. This hypothesis is in agreement with the scaling of large-scale peak and trough structures to flame length [1] and the idea that RTI begins at the small-scale and eventually encompasses the entire flow [43].

Chapter 4: Conclusion

4.1 Summary of research findings

This research project began as an exploration into the phenomenon of flame streaks in wildland fires. These streaks were consistently observed in wildland fires and other wind-blown flames, at least when the boundary layer was sufficiently developed. However, the origin of these streaks, the mechanisms controlling their growth, and their influence on important heat and mass transfer properties was unclear. Therefore, this project was established to investigate these knowledge gaps; in particular, this project sought to answer the following questions:

- What mechanisms are responsible for the onset of these instabilities?
- What mechanisms govern streak growth and development?
- Do streaks influence heat and mass transfer properties of the flow?
- What effects do these streaks have on the macroscopic properties of the flame?
- Does streak behavior govern the development of larger-scale downstream structures?

In order to breach these gaps in our understanding, a multi-faceted approach was

needed. Experiments with field-scale wildland fires were unfeasible due to the scarcity of meaningful measurements that could be obtained. Wildland fires are inherently destructive and have a wide range of relevant length scales (e.g., flame thicknesses and atmospheric boundary layers) and confounding variables (e.g., wind, slope, fuel properties). Even spreading laboratory-scale fires are difficult to instrument with the resolution and accuracy needed to resolve such a complex problem. Consequently, stationary fires and heat sources were employed because they have known inputs, structures can be visualized clearly, measurements of high density and accuracy can be taken, and this really gives us a statistical viewpoint of the problem. Stationary sources of buoyancy ensure that the relevant length scales associated with mixed convection, such as the development length of the upstream boundary layer, remain fixed. This important simplification allows for a detailed study of physical phenomena by providing a framework to develop wildland fire spread theory based on both observed and measured physical phenomena.

This first study examined perhaps the simplest configuration of a boundary layer flame: that of a stationary gas burner located in a laminar boundary layer. As a further aid to characterization, this experimental setup actually produced flame streaks which remained locked in position - they did not meander back and forth or interact with adjacent streaks. This enabled detailed characterization of the peaks and the troughs of the streaks with point measurements, which would not be feasible if coherent structures would rapidly meander in and out of the measurement region. Point measurements, particularly thermocouples, proved to be highly advantageous in producing detailed results on the thermal properties of the streaks. The

gas temperature within streaks was actually observed to increase as the structure grew downstream; however, the gas temperature of the trough regions decreased relatively. This discovery highlighted the role streaks play in manipulating the distribution of heat within the flame. It was also desirable to examine the role of these streaks in manipulating the heat transfer to the surface, an important quantity in applications such as wildland fire spread. Here, the heat flux to the surface actually increased below the trough regions while decreasing beneath the streaks. At first glance this seemed contrary to the gas phase temperature distributions, but the controlling factor here is the flame standoff distance. The troughs are located in a downwash region, where the counter-rotating vortices are forcing the flame sheet towards the surface, increasing the surface heat flux. Meanwhile, the streaks are formed by upwash regions, which pull the flame sheet up and away from the surface, lowering the surface heat flux. This spanwise redistribution of surface heat flux confirmed that streaks can, at least instantaneously, modify important heat transfer properties of the flow. Additionally, it was shown that streak formation was strongly tied to the coherent structures already present in the velocity boundary layer. This established the incoming boundary layer as the controlling mechanism of streak formation, but additional experiments were necessary to examine whether this behavior held in other configurations. Finally, the amplification of streaks was determined to be compatible with quadratic growth of Rayleigh-Taylor Instabilities, providing credence to the idea that the downstream growth of streaks was strongly tied to the strong buoyancy of the flame.

Two distinct regions of the flame, streaks and troughs, were identified in this

first experimental phase and shown to possess markedly different thermal properties. These instabilities clearly modify both the spanwise distribution of heat flux to the surface and the internal temperatures at the flame sheet. This finding has significant implications for boundary layer combustion, indicating that instantaneous properties can vary significantly due to a three-dimensional flow field. Scenarios may certainly exist where the typical two-dimensional assumption fails to capture controlling mechanisms of heat and mass transfer. We have seen that an understanding of pre-existing sources of instability may be essential in describing coherent structures in a laminar boundary layer flame. Results from this study have highlighted the ability for local instabilities to affect macroscopic properties of the flame. More research at different scales is necessary to extrapolate these results to different regimes of instabilities in boundary layer combustion, but this study provides an experimental framework for future investigations.

The previous study was able to examine streaks in a parameter space where the inertial force could be manipulated by changing the incoming wind speed. However, the buoyancy force could not be directly manipulated, at least locally, because flame temperatures cannot be modified. Therefore, the next phase of the project was to examine a hot plate in crossflow. The thermal plume emanating from a hot surface approximates the buoyant behavior of a fire with the added advantage that the local source of buoyancy can be directly controlled through the surface temperature. Infrared thermography was employed to detect streaks by means of their temperature traces over a surface, and a novel and consistent method for tracking streaks and quantifying important properties was developed. Overall, streak spacing

was seen to be lognormally distributed as well as negatively correlated to the bulk wind speed. In fact, the initial spacing was consistently between 60-70 wall units, indicating that the initial length scale was likely governed by the wind speed and not the strength of the buoyancy source. Spacing was seen to increase downstream of the plate, and the magnitude of the spanwise fluctuations in surface temperature caused by the streaks was positively correlated to the hot plate temperature. Finally, streak behavior became more chaotic downstream, as streaks would meander rapidy and persist for shorter durations. These findings provided significant insight into streak behavior, but an additional experiment was necessary to examine whether such trends scaled to flames, which provide a much stronger source of buoyancy.

The final phase of the study examined a saturated fuel wick in the same experimental configuration as the hot plate. This was essential in order to examine whether the streaks from the hot plate would exhibit the same behavior as that of the flame streaks. Streaks were detected in the flame via high speed video, and the previous algorithm for tracking streaks over a hot plate was successfully applied. Post-processing of data revealed a lognormal distribution of streak spacing and a negative correlation to wind, agreeing with results from the hot plate. Moreover, the initial spacing nearly coincided with that from the hot plate streaks and remained between 60-75 wall units. This finding confirmed that the incoming boundary layer was the dominant mechanism in presetting the streak locations. Spacing between coherent structures increased downstream, likely due to buoyant amplification. The width of streaks grew to an apparent assymptote, likely controlled by the flame length, which limits the amount of time for these structures to grow. Similar to the

hot plate, coherent structures would meander more rapidly and persist for shorter durations downstream. In fact, the coherent structures would interact more readily further downstream, where they no longer resembled well-ordered streaks but often more complex structures resulting from streak aggregation. Overall, trends for streaks are consistent in both the hot plate and the flame, indicating that the behavior of streaks is governed by similar mechanisms in both scenarios. Although the initial instabilities are governed by the incoming wind, buoyant forces cause the growth and aggregation of these structures.

4.2 Broader Implications

At this point, it would prove useful to discuss how scaling these results to other regimes, such as the larger scales of wildland fire, could affect observed trends.

Perhaps one of the most important discussions centers around the role that a turbulent boundary layer would play. All three experimental configurations employed laminar boundary layers. The first experiment examined a laminar boundary layer with fixed perturbations, which is significantly different from the rapidly meandering near-wall streaks found in a turbulent boundary layer. This behavior was accidentally witnessed in our own experimental configuration, when blockage of the screens promoted high values of turbulence. One might argue that the meandering of instabilities will wash out spatial variation due to streaks, but an examination of stationary streaks was necessary to characterize local effects on heat and mass transfer. Additionally, there is still reason to expect that the mere presence of

these instabilities could significantly alter time-averaged properties; it is well-known that scalar dissipation affects flames, even influencing their stability and extinction [70]. The combined effect of powerful streamwise vortices, which would alter scalar dissipation, could serve to modify the large-scale behavior of a wind-blown flame. Secondly, the time-averaged properties of the flame can be considered to be the summation of intermittent fluctuations. As of yet, the role of intermittency in heating due to flames is still an area of active research. Third, there is reason to believe that the macroscopic behavior of the flow is derived from the development of streaks, which will be discussed shortly. For these reasons, one cannot conclude that turbulence will eliminate the effect of streaks.

In fact, the well-known spacing of near-wall streaks in turbulent boundary layers ($\approx$ 100 wall units) gives credence to the idea that scaling arguments can be made. Initial streak spacing remained between 60-75 wall units in the experiments with a hot plate and the fuel wick. In a turbulent boundary layer, we would expect this spacing to conform to $\approx$ 100 wall units, meaning that an initial length scale for streaks can be known. At the largest scale, in an atmospheric boundary layer (ABL), it may even be possible to predict the streamwise rolls which will affect a spreading fire.

In addition to the standard spacing of streaks in unobstructed boundary layers, real-world situations exist where dominant instabilities will remain fixed to an upstream obstacle. In boundary layer combustion, obstructions in the upstream flow, such as grasses, shrubs, trees, atmospheric instabilities, or mechanical obstacles in process flows, can introduce instabilities through vortex shedding. Downstream of

this shedding process, dominant instabilities will be introduced to flames, introducing fixed perturbations such as streaks. The subsequent instability will modify important properties such as heat transfer to the surface, similar to the behavior observed in the first experiment.

In wildland fires, it is often quite difficult to obtain reliable wind velocity data. Instantaneous wind velocities and directions can vary quite often locally, and the wind will assume a profile in the vertical direction based on a variety of factors. Often, it is necessary to make significant assumptions concerning the wind speed when modeling wildland fire, which often lies within some form of an incoming boundary layer. For this reason, any additional means of estimating the incoming velocity profile could be valuable in predicting spread or modeling a fire event. Because this study has shown that streaks in flames and heated flows are preset by the incoming boundary layer, we can actually use streak spacing to back out a more reliable estimate for the local velocity. Since turbulent boundary layers typically exhibit streaks of 100 wall units in spacing, obtaining an image of streak spacing in flames or smoke from a photo could be used to estimate the incoming boundary layer. This may even prove useful at atmospheric scales. Additional validation of this proposal would need to be undertaken. At the very least, the presence of streaks is highly indicative that the flame is subject to an incoming boundary layer, which should be accounted for in modeling/prediction.

Scaling arguments can also be made to describe the development from streaks to larger coherent structures in mixed convection. The initial length scale likely controls how readily streaks interact with one another. As streaks interact, they will

merge and aggregate, and the combined effect of merging and amplification may actually control the formation of larger-scale structures seen downstream. The consistent trends for growth seen for the width and spacing in the fuel wick experiment support this hypothesis. This growth is likely controlled by buoyancy, so the initial growth of the flame streaks is likely describable by scaling laws for Rayleigh-Taylor Instabilities. The growth of these instabilities, which quickly reaches quadratic growth, which is described by the acceleration time scale Agt^2. Here, A is the Atwood number $\left(A = \frac{\rho_{heavy} - \rho_{light}}{\rho_{heavy} + \rho_{light}}\right)$, which is likely the term controlling the growth of streaks. The higher the temperature of the hot flow, the greater the Atwood number will be; consequently, the growth and amplification of these streaks will be highest. This growth will continue as long as heat is continually supplied, meaning that a relevant time scale for the growth is likely the flame length or of a heated surface divided by the streamwise velocity of the flow at the density interface. Together, the rate of growth, proportional to the Atwood number, and the time of growth, proportional to the length of heating and inversely proportional to the wind speed, likely control the length scale of the larger coherent structures downstream, which result from the amplification and merging of streaks. This process is likely similar to streak growth observed due to the non-orthogonality of Navier–Stokes operators in both laminar and turbulent boundary layers [24–26]. Additionally, this behavior may explain the successful scaling of downstream coherent structures (i.e., flame towers) with the flame length [1]. Given the role larger-scale structures play in flame spread, this represents an important area for future research.

The scaling analysis, which related the flame shape to a stability parameter

(Gr/Re^n) characterizing buoyancy and momentum, shows promise in characterizing the flame behavior. This parameter, when properly formulated, can even capture the effect of an unheated starting length. This parameter has been utilized in mixed convection literature, and further theoretical and experimental work could show whether this scales to larger flames. It is also useful to note that the Froude number is a useful parameter to describe the overall ratio of inertial to buoyant forces of an experimental configuration or spreading fire. Values for Froude numbers have been reported for all experiments, and our experiments generally lie in the realm of inertia-dominated boundary layer flames, which includes most wildland fires.

4.3 Future research

Streaks clearly play a role in the instantaneous flame structure, and this has several important implications for modeling. In particular, CFD modeling of boundary layer combustion should be examined to see whether these structures are adequately captured, which requires proper modeling of the incoming boundary layer and its associated disturbances. This phenomenon appears in wildland fires, boundary layer combustion, pool fires, and mixed convection. Depending on the fidelity desired for the simulation, it may be essential to examine the role these structures play, particularly in modifying the instantaneous heat transfer to a burning surface. Given the highly-coupled nature of free-burning surfaces in crossflow, resolving flame streaks may prove useful. At the very least, these instabilities should appear when the simulation is well-resolved. Further research to this end is necessary.

Perhaps the most important data that is missing from this work consists of the relevant velocity fields. These fields would directly reveal the locations of the counter-rotating vortices in addition to revealing how the presence of buoyancy modifies the incoming boundary layer. This data would add significant depth to the amount of analysis that could be undertaken; unfortunately, obtaining such data requires significant technical work, and likely necessitates the use of laser diagnostics. As such resources were not available to us, we relied on creative uses of non-invasive measurements and natural flow tracers to track the locations of vortices. A more refined study would directly establish the behavior of the three-dimensional velocity field, which would also aid further numerical validations.

It would also be of great benefit to obtain numerical simulations which could describe the streamwise growth of streaks and the associated mixing layer. This data could be examined in greater depth; in particular, it would be interesting to compare the growth of the streaks and the mixing layer to that expected from Rayleigh-Taylor Instabilities. Numerical simulations could also aid in assessing the growth of coherent structures, which appear to begin on the small-scale of flame streaks and ends at the larger-scale of flame towers (i.e., peaks and troughs).

Finally, scaling arguments should be examined to see whether the findings here can be reproduced in other regimes. In particular, it would be useful to examine flame streaks in well-characterized turbulent boundary layers. Grid-generated turbulence applied to these well-instrumented, small-scale experiments may aid this endeavor. Existing images of streaks in wildland fires could also be examined to see if the mean spacing aligns with the expected turbulent length scale of 100 wall units.

Alternatively, one could assume that the spacing is on the order of 100 wall units and estimate the height of the incoming boundary layer. Further research on the nature of the atmospheric boundary layer and its effect on spreading wildfires would also be useful; it would be beneficial to obtain data on incoming velocity profiles and pre-existing instabilities to examine their role in near-flame fluid dynamics.

4.4 Epilogue

Overall, this research project has managed to provide adequate answers, or at least plausible explanations, for every question enumerated from the onset. Given the exploratory nature of this research, our knowledge of streak behavior in both boundary layer combustion and mixed convection has increased significantly. Implicit assumptions from previous descriptions of boundary layer combustion, such as the two-dimensional description of the flow, have been challenged. Future research will serve to elucidate remaining questions and confirm scaling hypotheses. Fire research has traditionally been studied starting at the small scale, where careful measurements have been used to develop theory, which is later translated to larger-scale processes. It is our hope that this project provides a strong framework for future investigations.

Chapter A: Additional figures on streak tracking data

A.1 Lognormal distributions for hot plate streaks

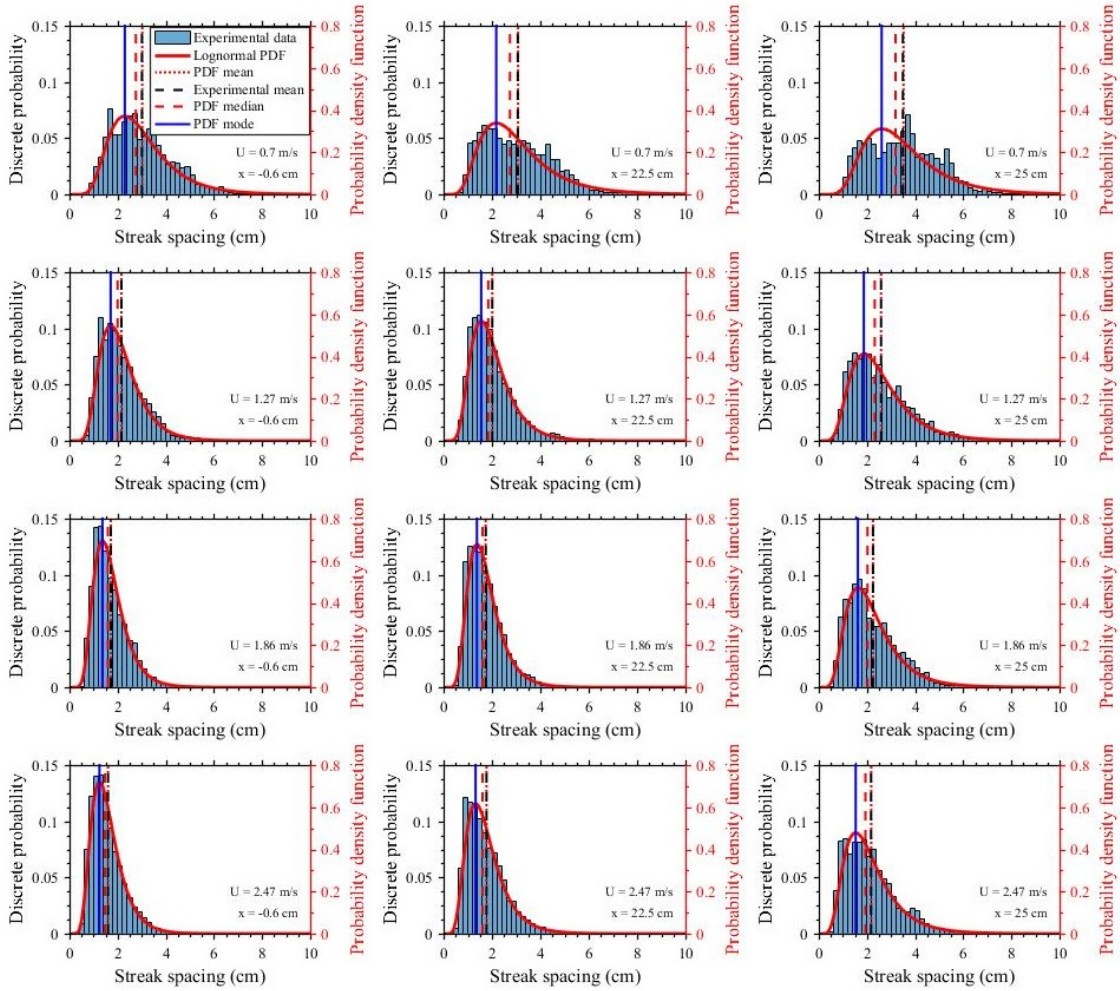

Figure A.1: Plots of experimental distributions of streak spacing along with a lognormal fit of the data. All data is taken over the insulated surface from experiments where the hot plate temperature is $150°C$. The indicated experimental means are derived from experimental data while other values are derived from arithmetic properties of the lognormal PDF.

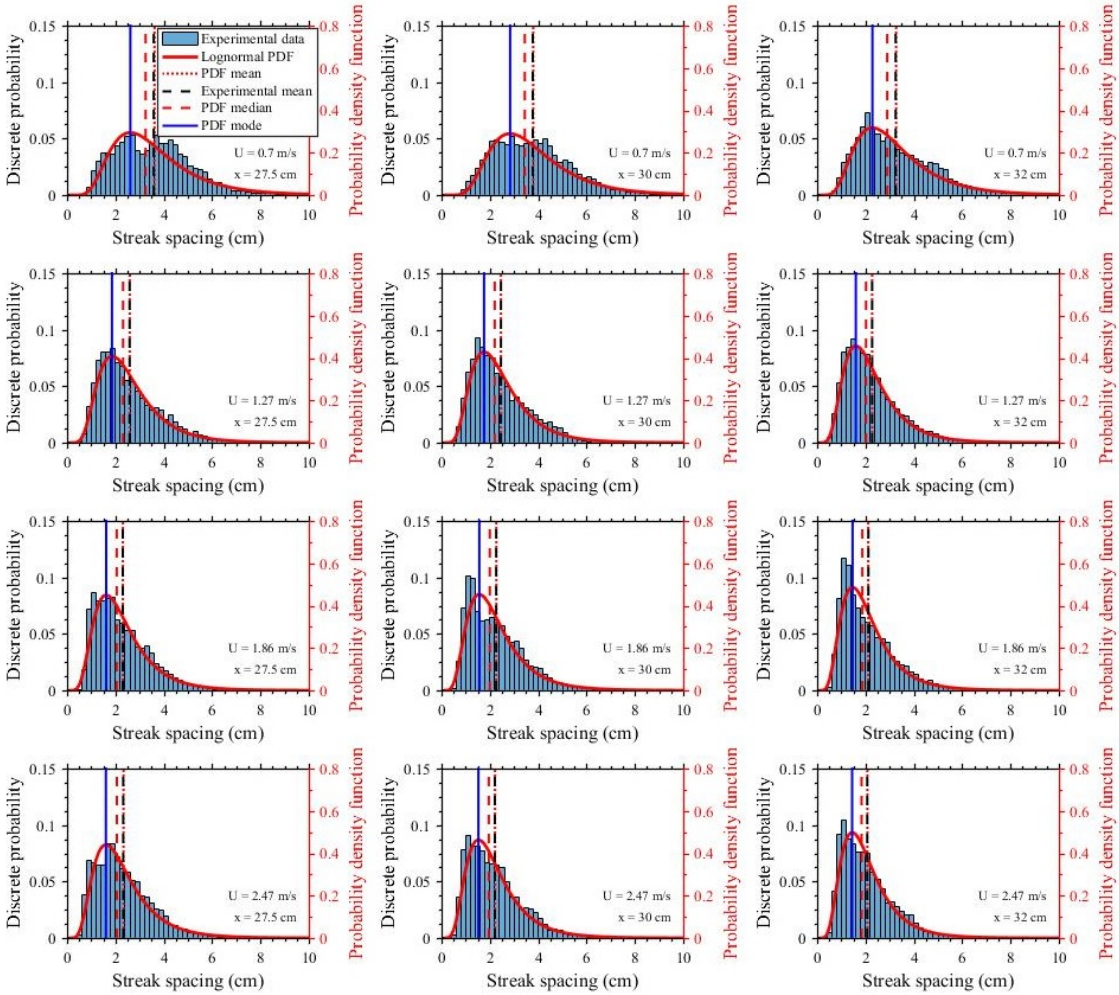

Figure A.2: Plots of experimental distributions of streak spacing along with a lognormal fit of the data. All data is taken over the insulated surface from experiments where the hot plate temperature is $150°C$. The indicated experimental means are derived from experimental data while other values are derived from arithmetic properties of the lognormal PDF.

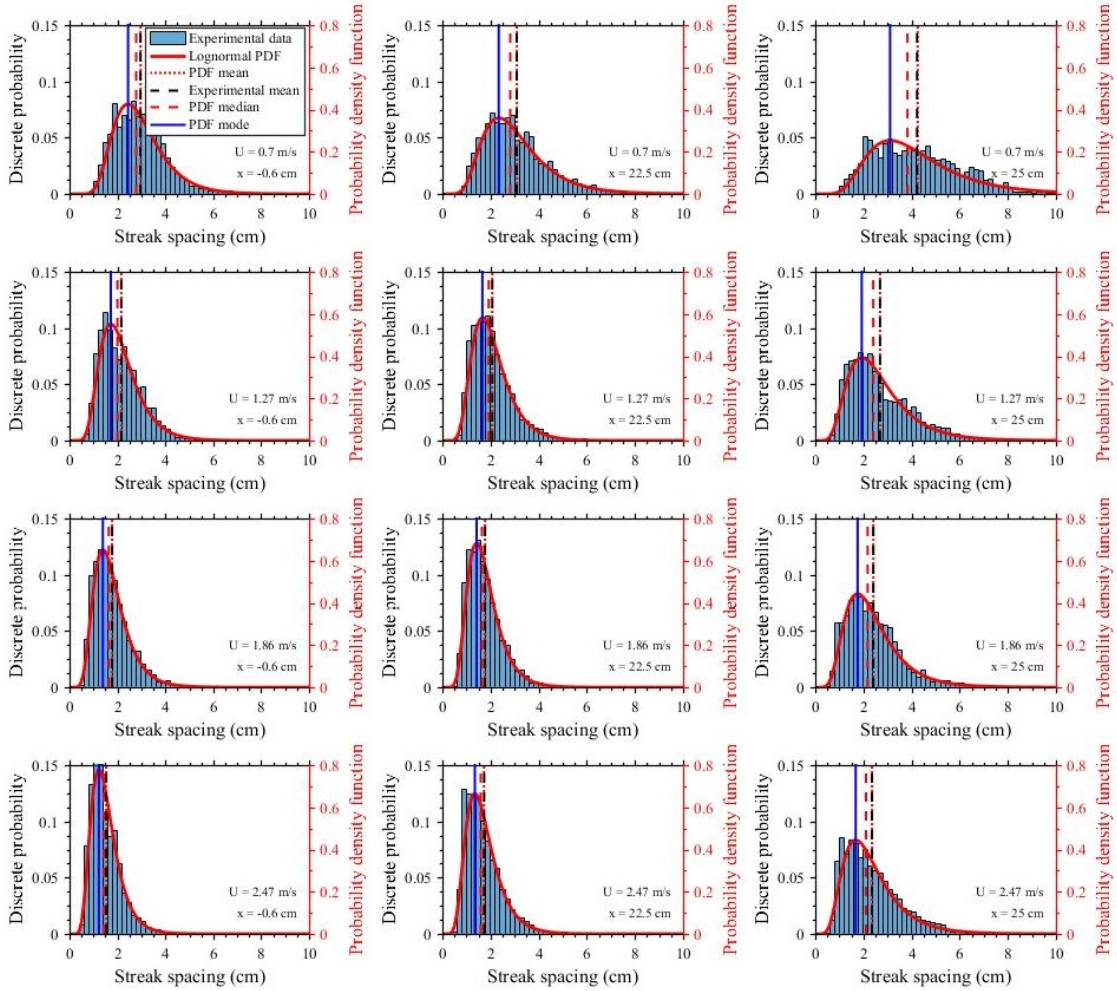

Figure A.3: Plots of experimental distributions of streak spacing along with a lognormal fit of the data. All data is taken over the insulated surface from experiments where the hot plate temperature is $300°C$. The indicated experimental means are derived from experimental data while other values are derived from arithmetic properties of the lognormal PDF.

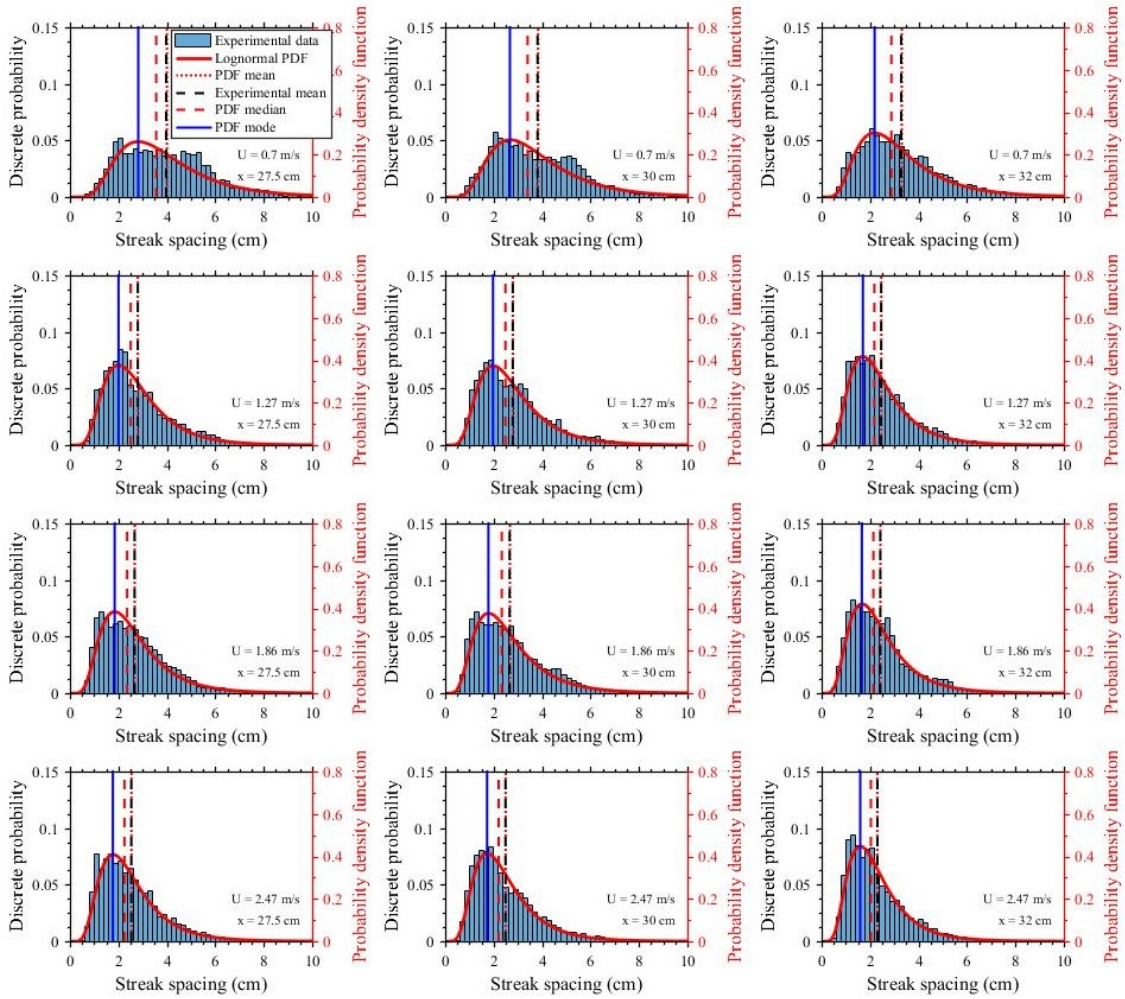

Figure A.4: Plots of experimental distributions of streak spacing along with a lognormal fit of the data. All data is taken over the insulated surface from experiments where the hot plate temperature is $300°C$. The indicated experimental means are derived from experimental data while other values are derived from arithmetic properties of the lognormal PDF.

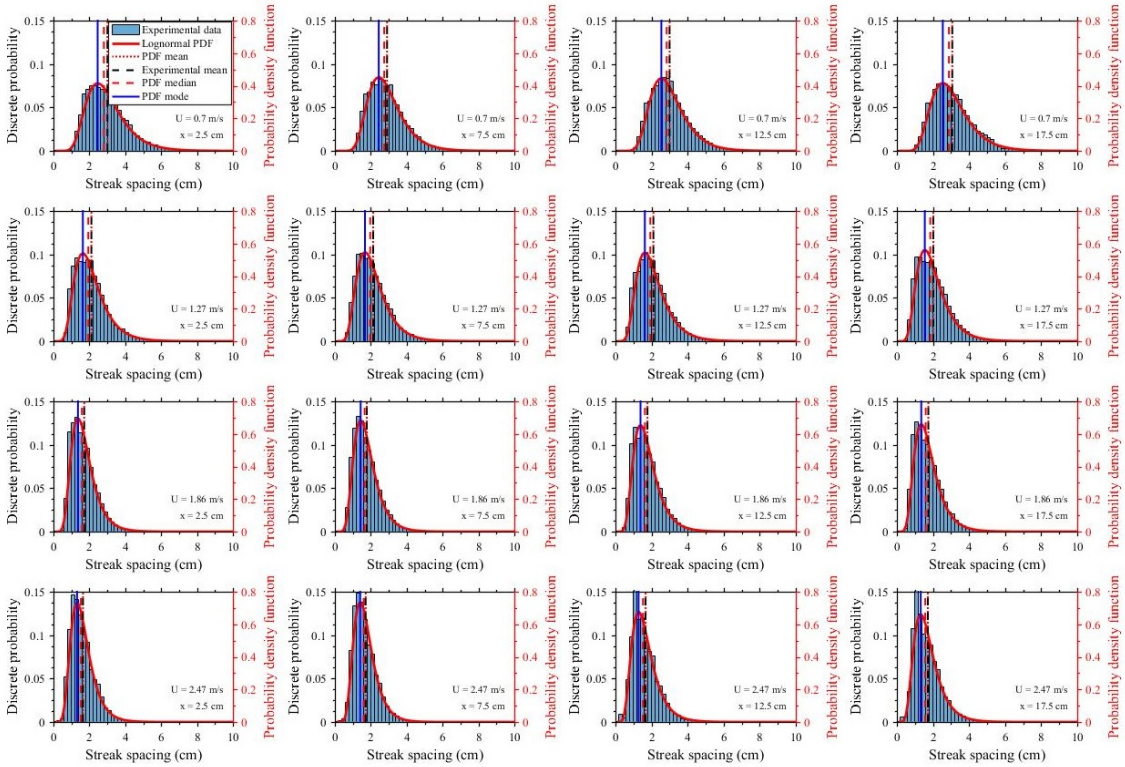

Figure A.5: Plots of experimental distributions of streak spacing along with a lognormal fit of the data. All data is taken over the heated surface from experiments where the hot plate temperature is $150°C$. The indicated experimental means are derived from experimental data while other values are derived from arithmetic properties of the lognormal PDF.

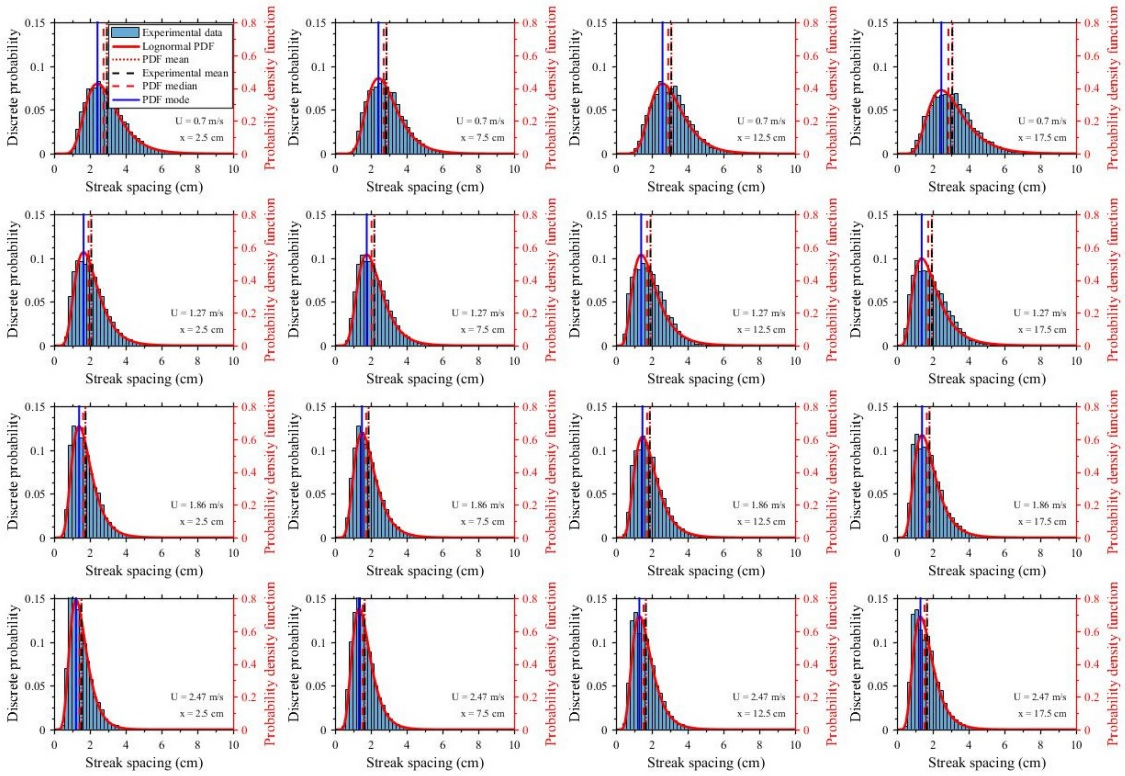

Figure A.6: Plots of experimental distributions of streak spacing along with a lognormal fit of the data. All data is taken over the heated surface from experiments where the hot plate temperature is $300°C$. The indicated experimental means are derived from experimental data while other values are derived from arithmetic properties of the lognormal PDF.

A.2 Standard deviation data for hot plate streaks

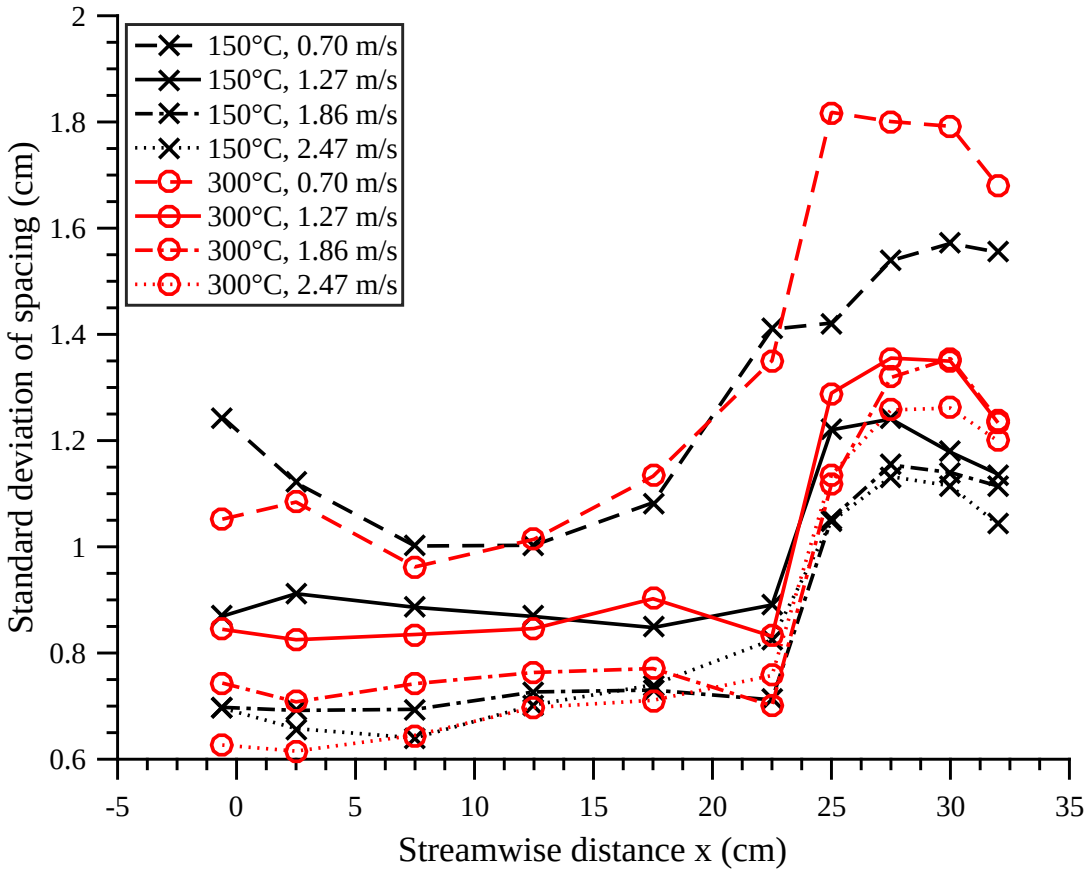

Figure A.7: Plot of the standard deviation of streak spacing vs. streamwise distance for all experimental conditions. The hot plate is located between $x = 0$ and 20.5 cm while the surrounding area is inert.

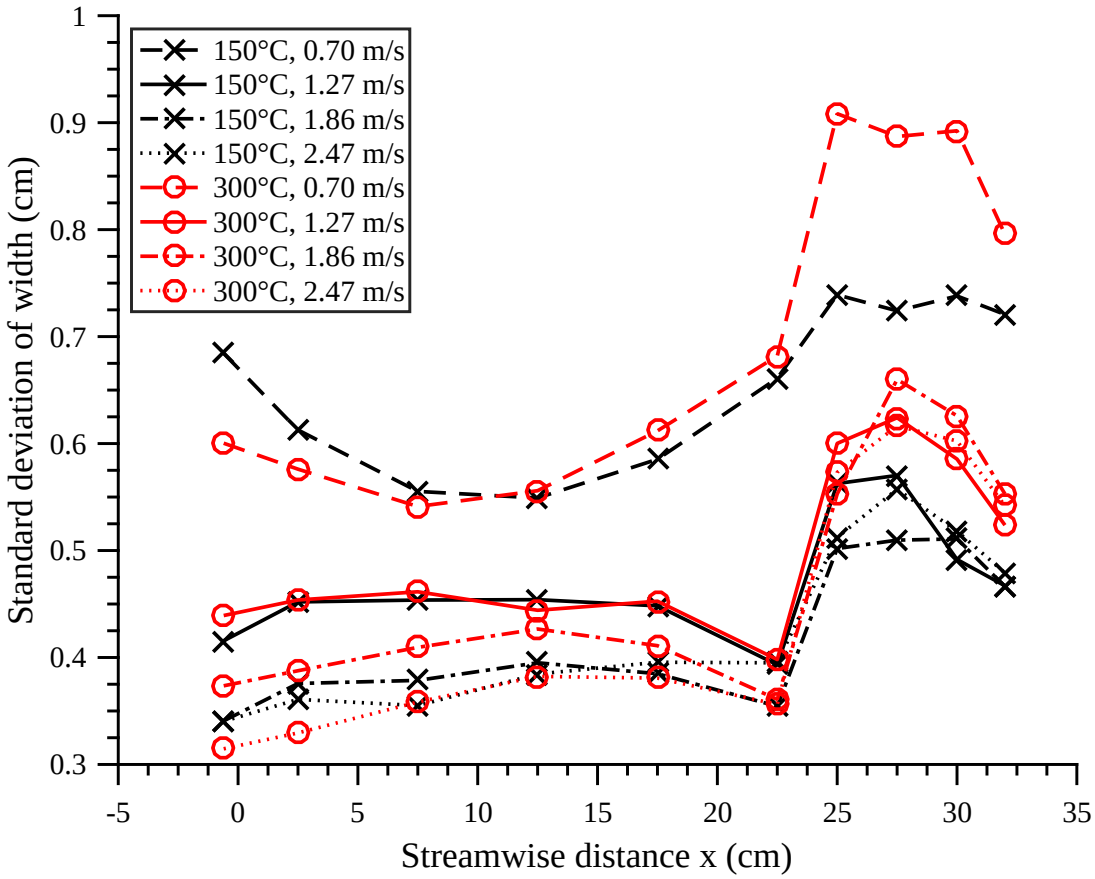

Figure A.8: Plot of the standard deviation of streak width vs. streamwise distance for all experimental conditions. The hot plate is located between $x = 0$ and 20.5 cm while the surrounding area is inert.

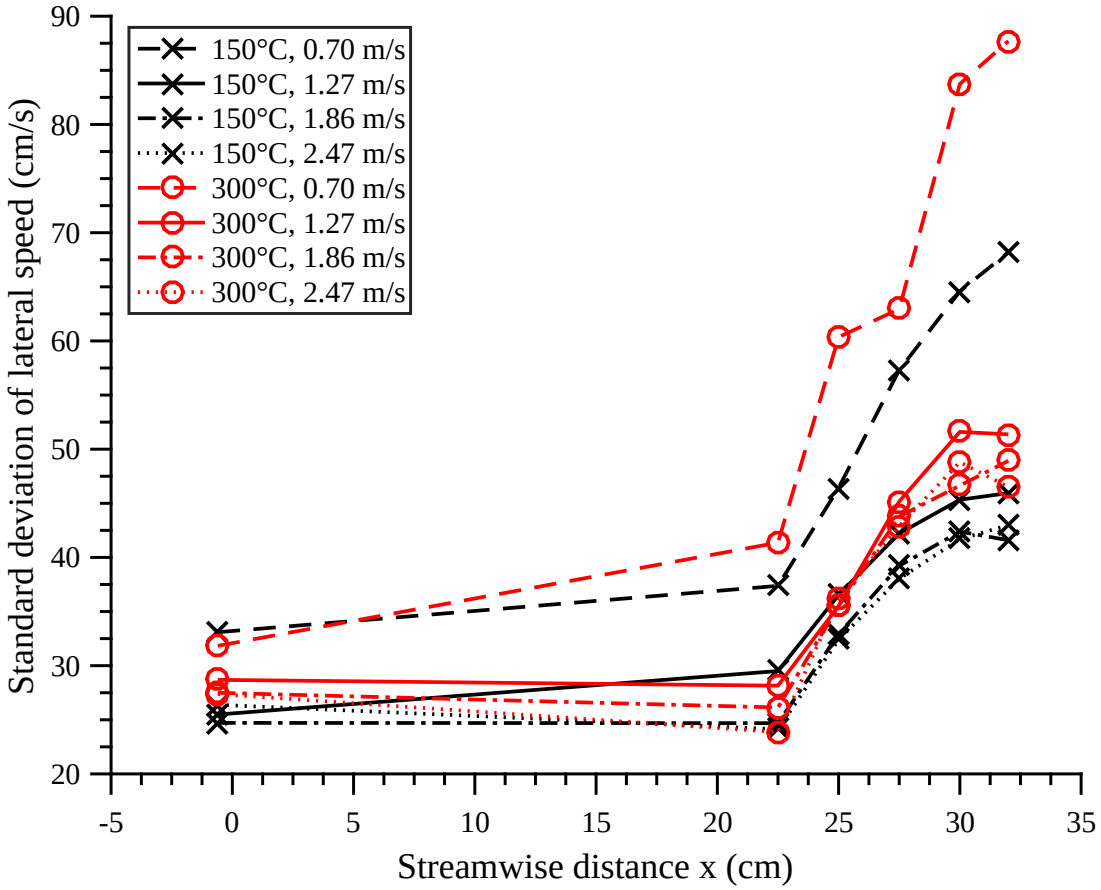

Figure A.9: Plot of the standard deviation of lateral (spanwise) streak speed vs. streamwise distance for all experimental conditions. The hot plate is located between $x = 0$ and 20.5 cm while the surrounding area is inert.

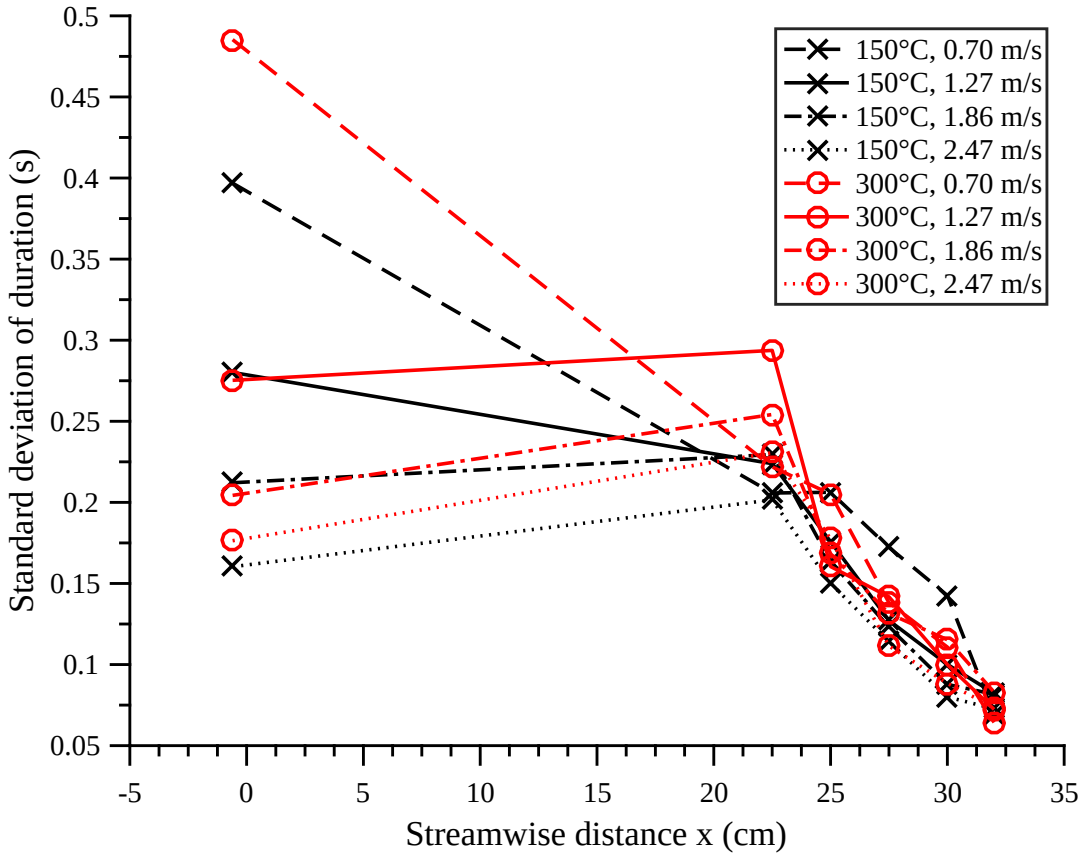

Figure A.10: Plot of the standard deviation of streak duration vs. streamwise distance for all experimental conditions. The hot plate is located between $x = 0$ and 20.5 cm while the surrounding area is inert.

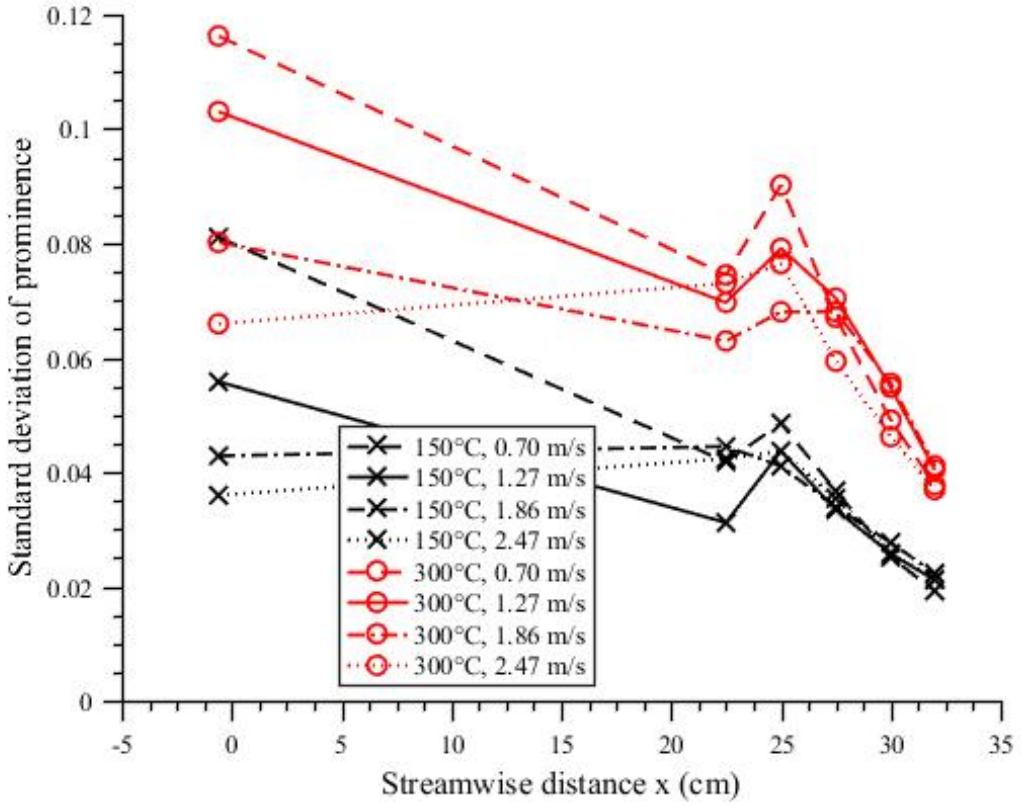

Figure A.11: Plot of the standard deviation of streak prominence (amplitude) vs. streamwise distance for all experimental conditions. The hot plate is located between $x = 0$ and 20.5 cm while the surrounding area is inert.

A.3 Lognormal distributions for flame streaks

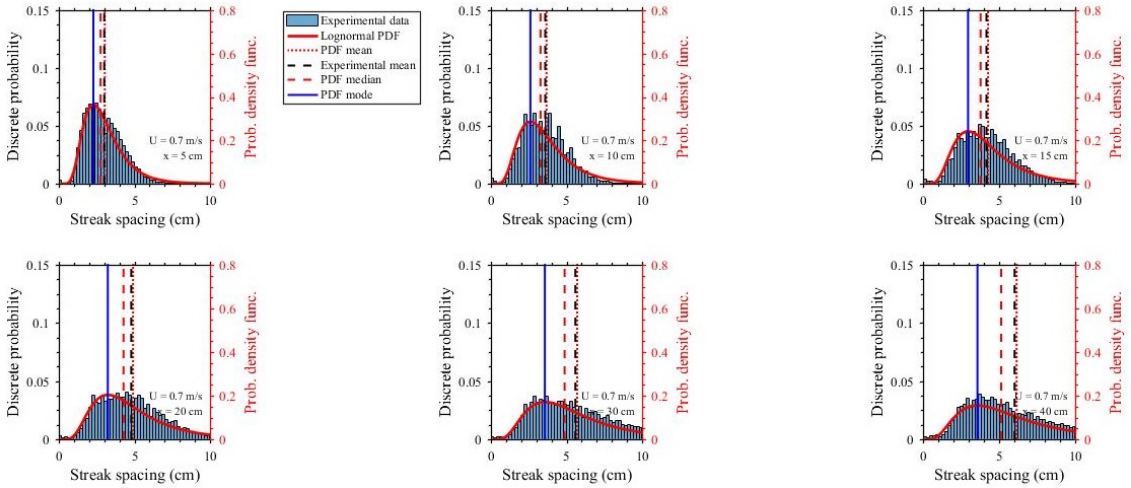

Figure A.12: Plots of experimental distributions of flame streak spacing along with a lognormal fit of the data. All data is taken from the isopropyl fuel wick with a wind speed of 0.7 m/s. The indicated experimental means are derived from experimental data while other values are derived from arithmetic properties of the lognormal PDF.

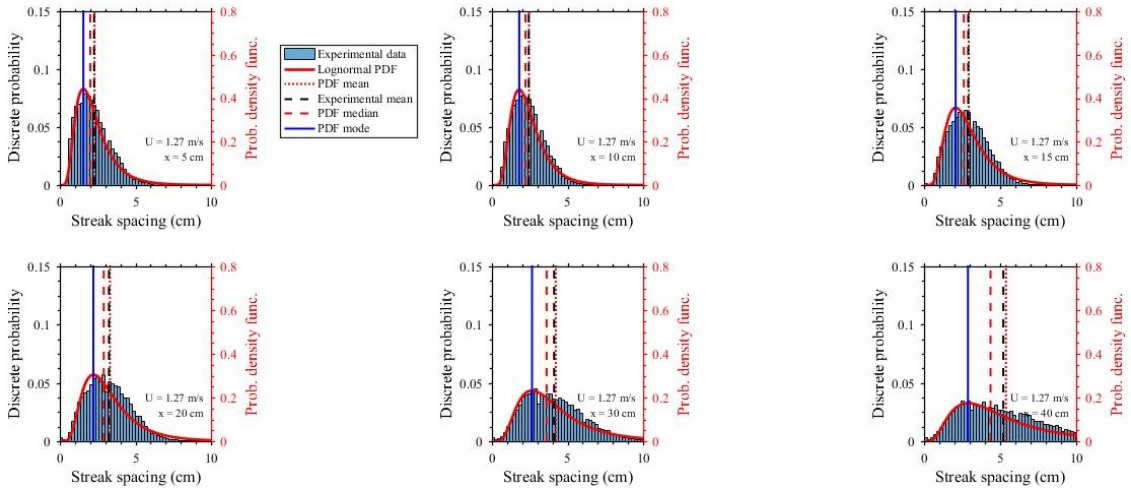

Figure A.13: Plots of experimental distributions of flame streak spacing along with a lognormal fit of the data. All data is taken from the isopropyl fuel wick with a wind speed of 1.27 m/s. The indicated experimental means are derived from experimental data while other values are derived from arithmetic properties of the lognormal PDF.

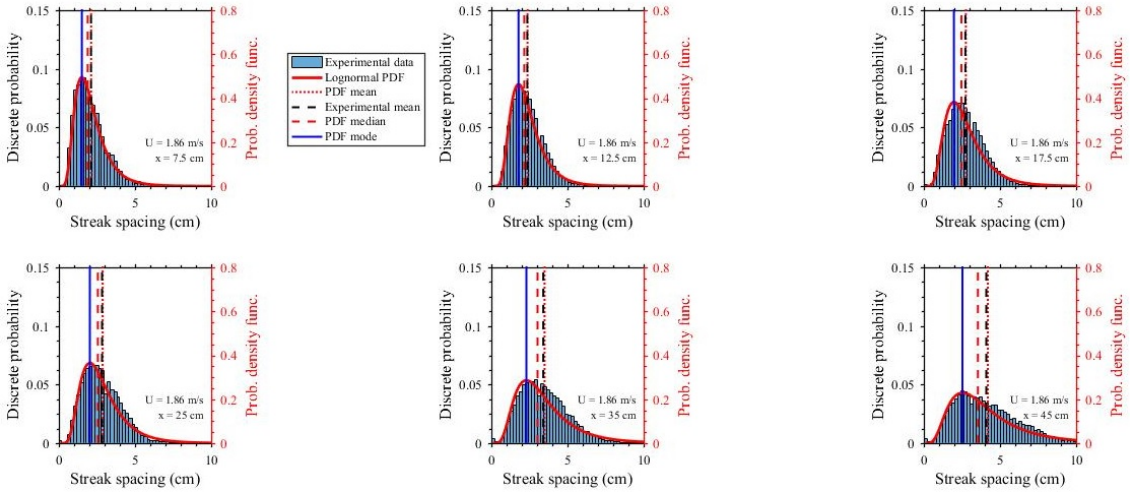

Figure A.14: Plots of experimental distributions of flame streak spacing along with a lognormal fit of the data. All data is taken from the isopropyl fuel wick with a wind speed of 1.86 m/s. The indicated experimental means are derived from experimental data while other values are derived from arithmetic properties of the lognormal PDF.

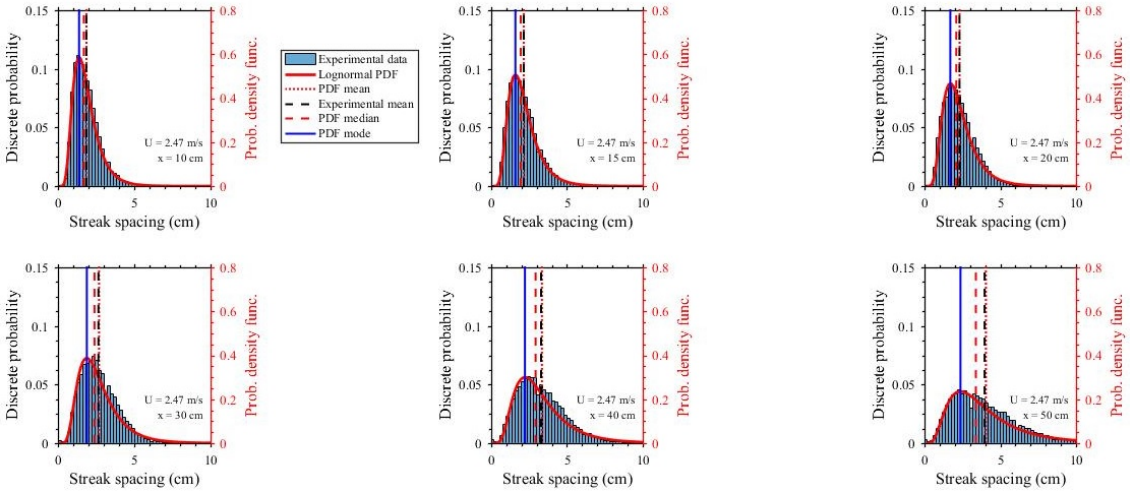

Figure A.15: Plots of experimental distributions of flame streak spacing along with a lognormal fit of the data. All data is taken from the isopropyl fuel wick with a wind speed of 2.47 m/s. The indicated experimental means are derived from experimental data while other values are derived from arithmetic properties of the lognormal PDF.

A.4 Standard deviation data for flame streaks

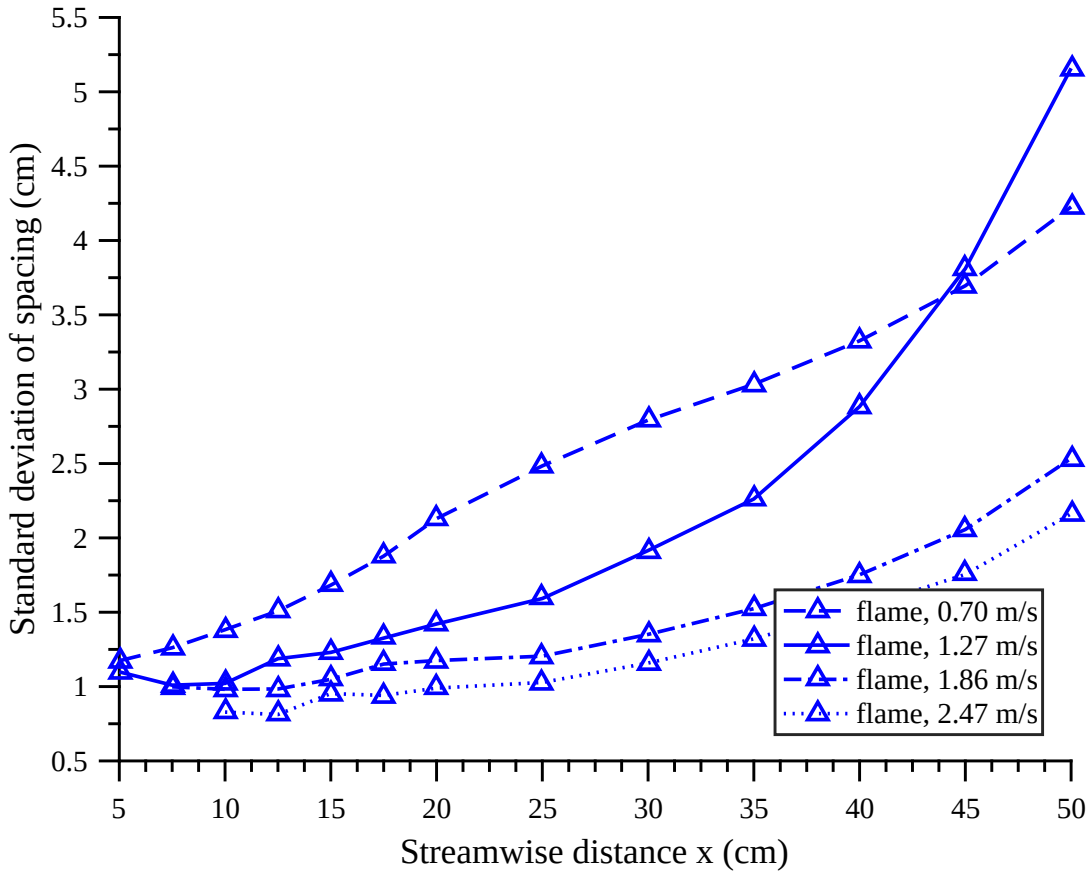

Figure A.16: Plot of the standard deviation of flame streak spacing vs. streamwise distance for all experimental conditions.

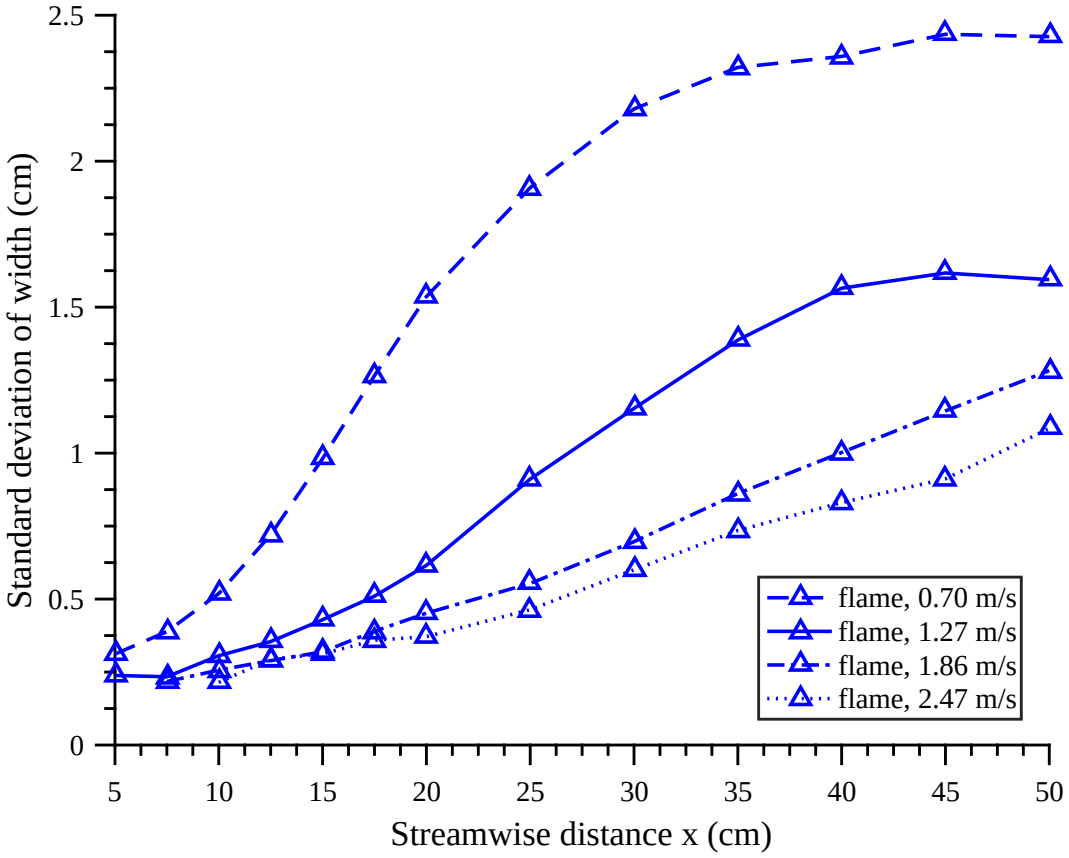

Figure A.17: Plot of the standard deviation of flame streak width vs. streamwise distance for all experimental conditions.

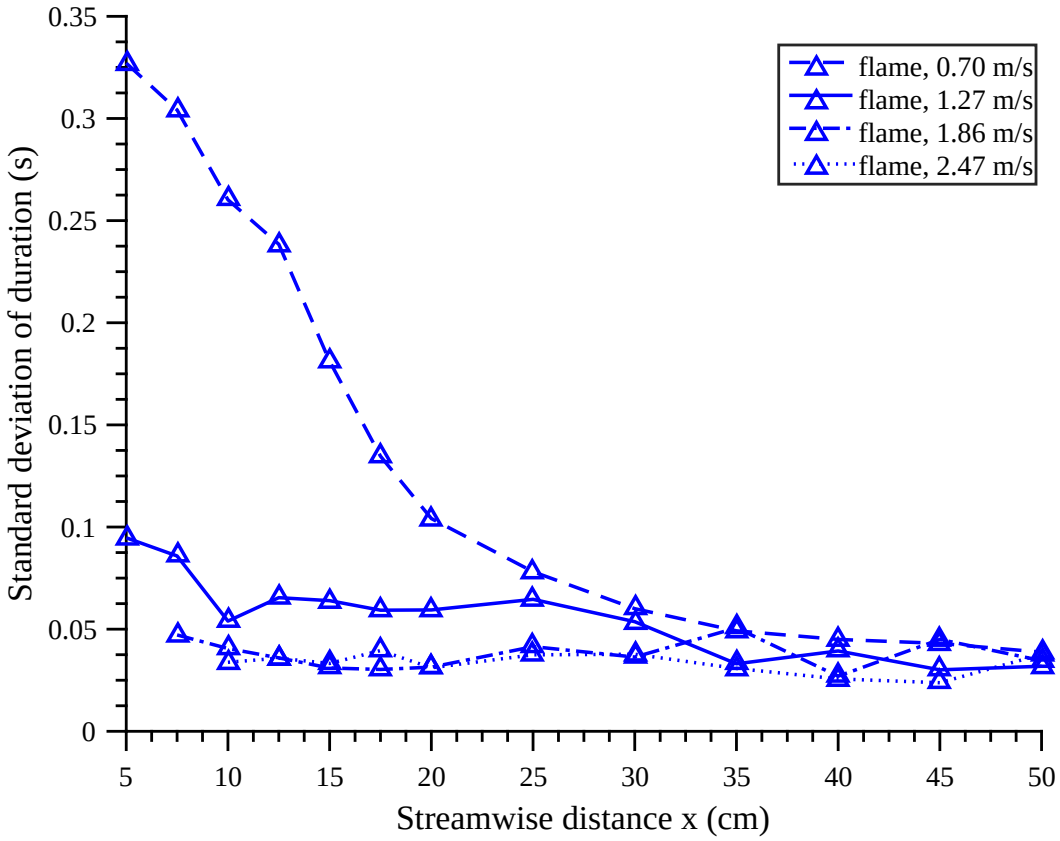

Figure A.18: Plot of the standard deviation of flame streak duration vs. streamwise distance for all experimental conditions.

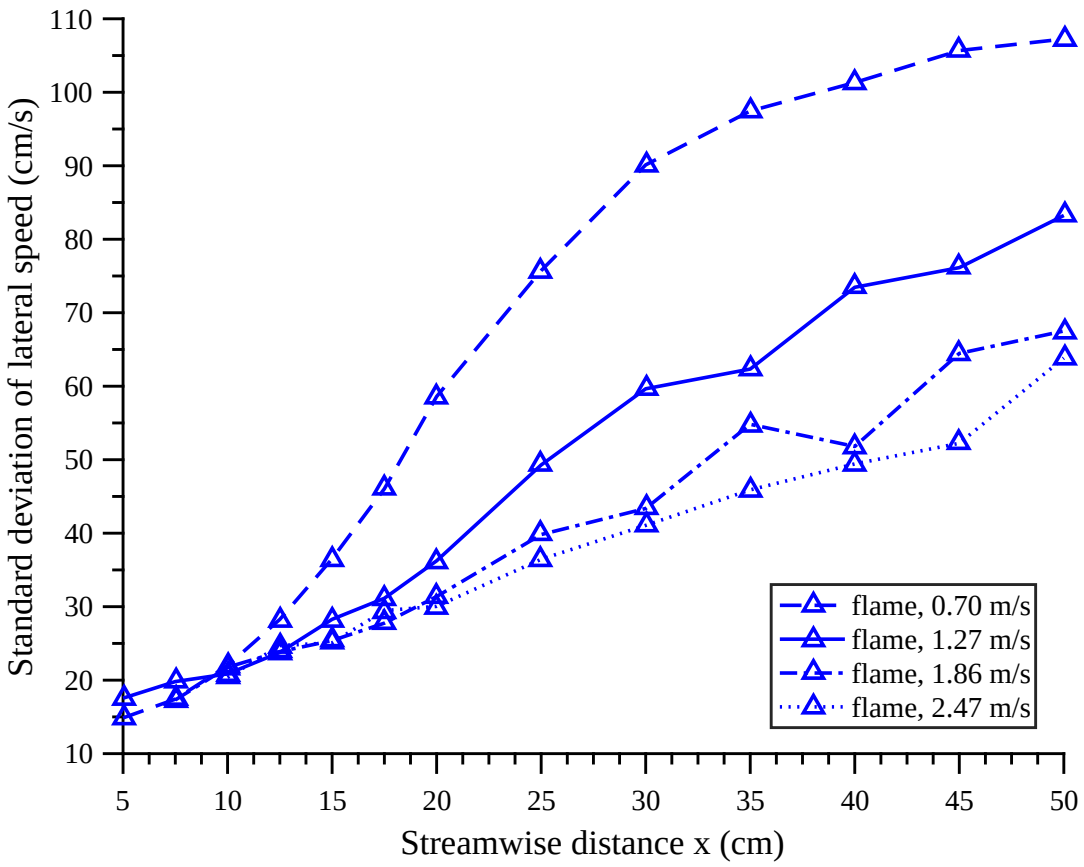

Figure A.19: Plot of the standard deviation of flame streak lateral (spanwise) speed vs. streamwise distance for all experimental conditions.

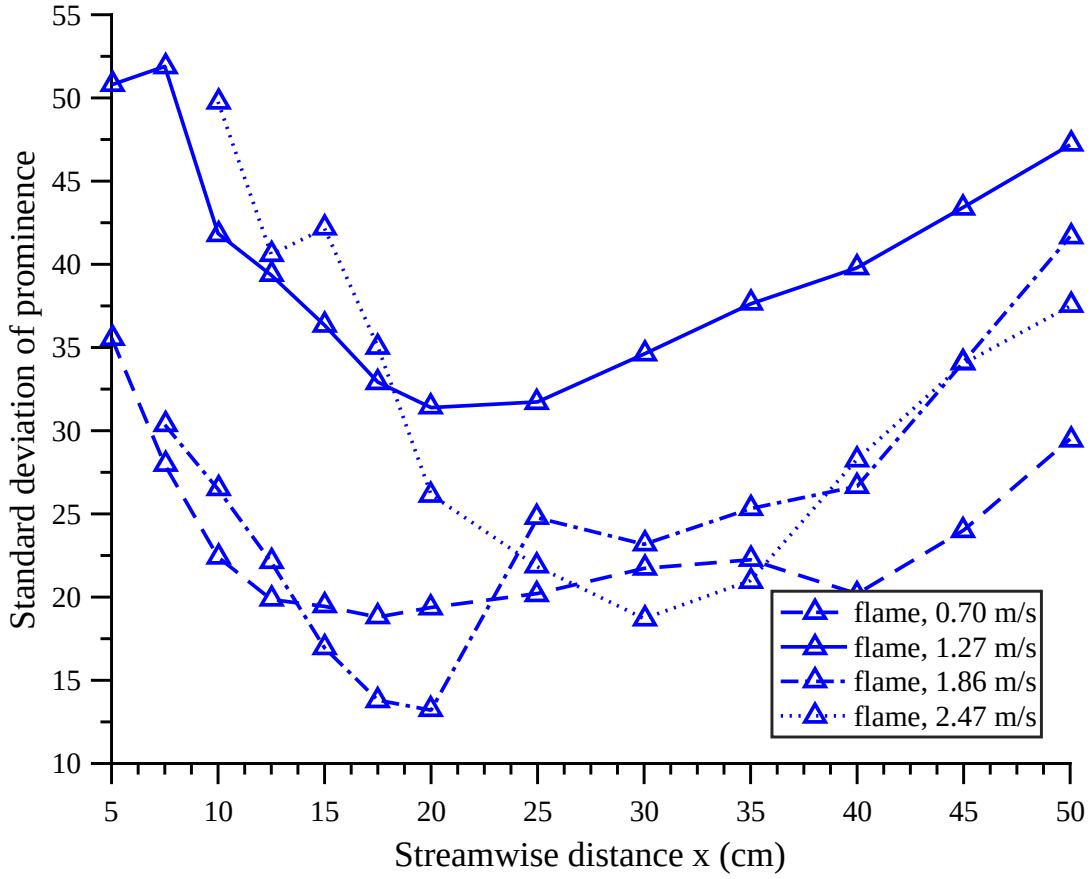

Figure A.20: Plot of the standard deviation of flame streak prominence (amplitude) vs. streamwise distance for all experimental conditions.

A.5 Miscellaneous hot plate figures

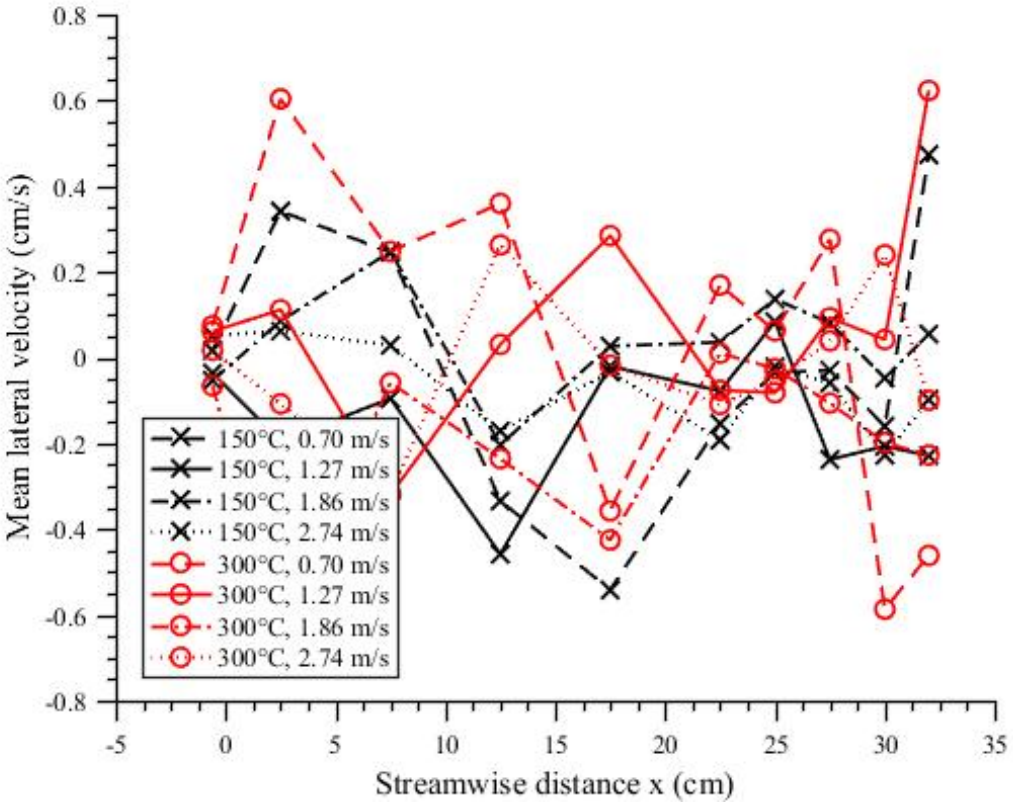

Figure A.21: Plot of the lateral (spanwise) streak velocity vs. streamwise distance for all experimental conditions. The hot plate is located between $x = 0$ and 20.5 cm while the surrounding area is inert.

A.6 Miscellaneous isopropyl flame figures

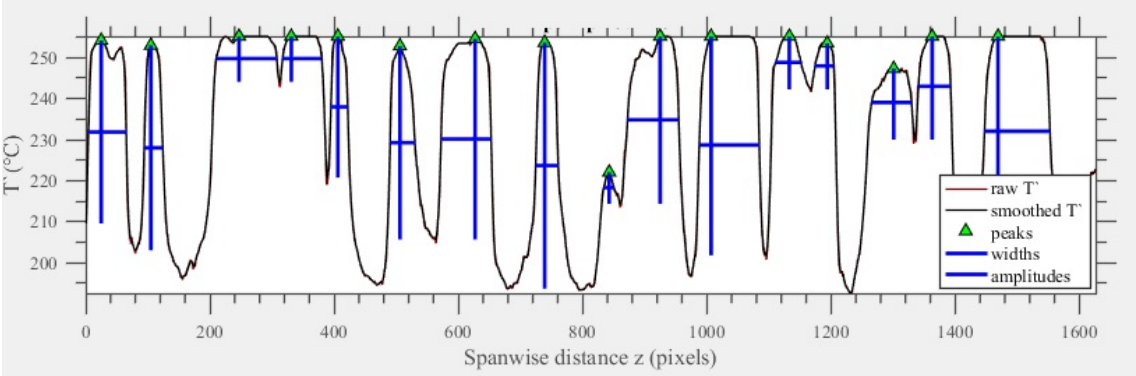

Figure A.22: Example of the streak detection algorithm with displayed results for one image. Here, the raw luminosity profile is shown as a thin red line while the smoothed profile is shown as the thicker black line. This image also shows derived streak locations or peaks (green triangles), streak widths (horizontal blue lines), and streak amplitudes (vertical blue lines).

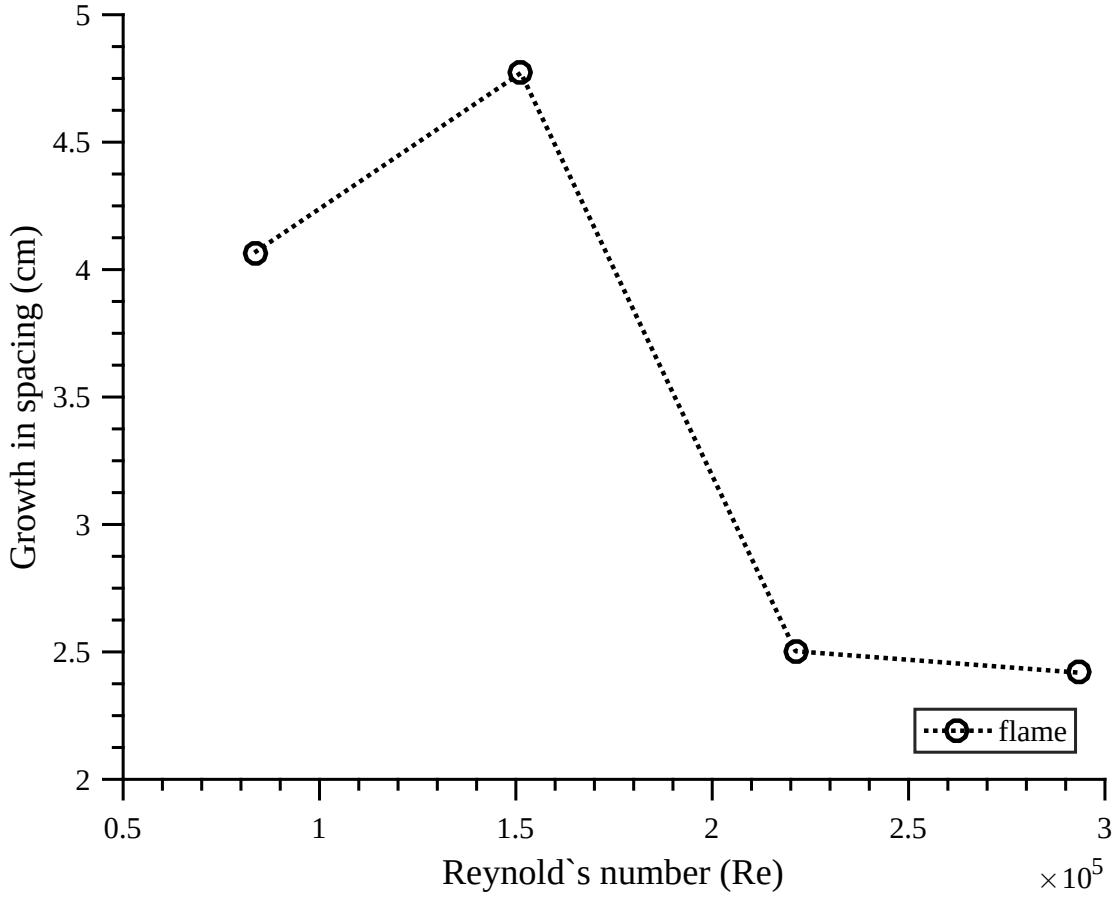

Figure A.23: Plot of the growth in flame streak spacing vs. the Reynold's number at the leading edge of the wick. The growth is calculated as the difference between the maximum value and the initial spacing.

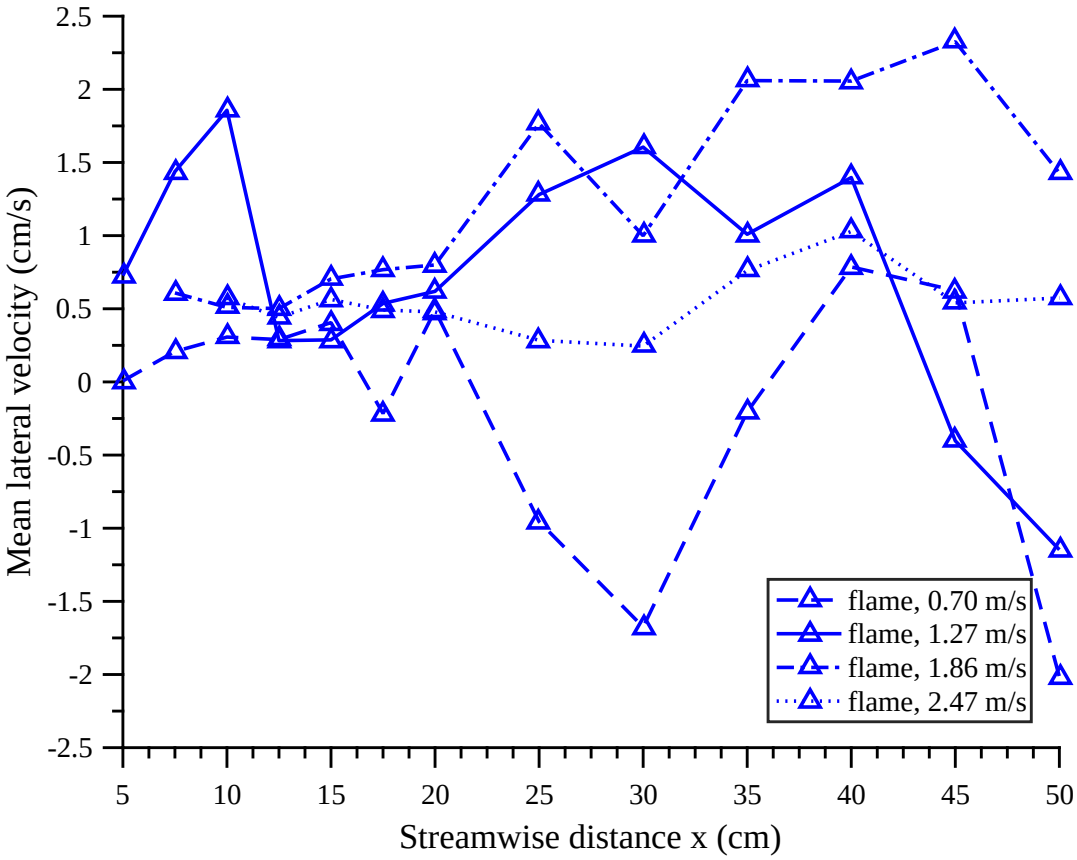

Figure A.24: A plot of the mean lateral (spanwise) speed of flame streaks vs. streamwise distance for all wind speeds.

Bibliography

[1] Mark A Finney, Jack D Cohen, Jason M Forthofer, Sara S McAllister, Michael J Gollner, Daniel J Gorham, Kozo Saito, Nelson K Akafuah, Brittany A Adam, and Justin D English. Role of buoyant flame dynamics in wildfire spread. *Proceedings of the National Academy of Sciences*, 112(32):9833–9838, 2015.

[2] EJ Weckman and AB Strong. Experimental investigation of the turbulence structure of medium-scale methanol pool fires. *Combustion and Flame*, 105(3):245–266, 1996.

[3] Paul E DesJardin, Timothy J OHern, and Sheldon R Tieszen. Large eddy simulation and experimental measurements of the near-field of a large turbulent helium plume. *Physics of fluids*, 16(6):1866–1883, 2004.

[4] Stephen K Robinson. Coherent motions in the turbulent boundary layer. *Annual Review of Fluid Mechanics*, 23(1):601–639, 1991.

[5] Klebanoff. PS. Effect of free-stream turbulence on a laminar boundary layer. In *Bulletin of the American Physical Society*, volume 16, page 1323, 1971.

[6] Amable Liñán, Marcos Vera, and Antonio L Sánchez. Ignition, liftoff, and extinction of gaseous diffusion flames. *Annual Review of Fluid Mechanics*, 47:293–314, 2015.

[7] William H Cabot and Andrew W Cook. Reynolds number effects on rayleigh–taylor instability with possible implications for type ia supernovae. *Nature Physics*, 2(8):562–568, 2006.

[8] Gregory C Burton. Study of ultrahigh atwood-number rayleigh–taylor mixing dynamics using the nonlinear large-eddy simulation method. *Physics of Fluids (1994-present)*, 23(4):045106, 2011.

[9] ÉP Volchkov, VV Terekhov, and VI Terekhov. Characteristics of the boundary layer with hydrogen combustion with variations of thermal conditions on a permeable wall. *Combustion, Explosion, and Shock Waves*, 45(3):237–244, 2009.

[10] Ronald L Panton. Overview of the self-sustaining mechanisms of wall turbulence. *Progress in Aerospace Sciences*, 37(4):341–383, 2001.

[11] Paul DesJardin, Thomas Smith, and Christopher Roy. Numerical simulations of a methanol pool fire. In *39th Aerospace Sciences Meeting and Exhibit*, page 636, 2001.

[12] JM Kendall. Experimental study of disturbances produced in a pre-transitional laminar boundary layer by weak freestream turbulence. In *AIAA, 18th Fluid Dynamics and Plasmadynamics and Lasers Conference*, volume 1, 1985.

[13] Si-Chao Deng, Chong Pan, and Jin-Jun Wang. Dynamics of low-speed streak evolution and interaction in laminar boundary layer. *Acta Mechanica Sinica*, 30(5):636–645, 2014.

[14] Y Kamotani, JK Lin, and S Ostrach. Effect of destabilizing heating on gortler vortices. *Journal of heat transfer*, 107(4):877–882, 1985.

[15] R Toe, A Ajakh, and H Peerhossaini. Heat transfer enhancement by görtler instability. *International journal of heat and fluid flow*, 23(2):194–204, 2002.

[16] JM Floryan. On the görtler instability of boundary layers. *Progress in Aerospace Sciences*, 28(3):235–271, 1991.

[17] H Imura, RR Gilpin, and KC Cheng. An experimental investigation of heat transfer and buoyancy induced transition from laminar forced convection to turbulent free convection over a horizontal isothermally heated plate. *Journal of Heat Transfer*, 100(3):429–434, 1978.

[18] RR Gilpin, H Imura, and KC Cheng. Experiments on the onset of longitudinal vortices in horizontal blasius flow heated from below. *Journal of Heat Transfer*, 100(1):71–77, 1978.

[19] XA Wang. An experimental study of mixed, forced, and free convection heat transfer from a horizontal flat plate to air. *Journal of Heat Transfer*, 104(1):139–144, 1982.

[20] Saeed S Moharreri, Bassem F Armaly, and TS Chen. Measurements in the transition vortex flow regime of mixed convection above a horizontal heated plate. *Journal of heat transfer*, 110(2):358–365, 1988.

[21] KC Cheng, T Obata, and RR Gilpin. Buoyancy effects on forced convection heat transfer in the transition regime of a horizontal boundary layer heated from below. *Journal of heat transfer*, 110(3):596–603, 1988.

[22] EM Sparrow and RB Husar. Longitudinal vortices in natural convection flow on inclined plates. *Journal of Fluid Mechanics*, 37(02):251–255, 1969.

[23] Giovanni Zocchi, Elisha Moses, and Albert Libchaber. Coherent structures in turbulent convection, an experimental study. *Physica A: Statistical Mechanics and its Applications*, 166(3):387–407, 1990.

[24] Lloyd Trefethen, Annee Trefethen, Satishc Reddy, Tobina Driscoll, et al. Hydrodynamic stability without eigenvalues. *Science*, 261(5121):578–584, 1993.

[25] Satish C Reddy and Dan S Henningson. Energy growth in viscous channel flows. *Journal of Fluid Mechanics*, 252:209–238, 1993.

[26] Kathryn M Butler and Brian F Farrell. Three-dimensional optimal perturbations in viscous shear flow. *Physics of Fluids A: Fluid Dynamics (1989-1993)*, 4(8):1637–1650, 1992.

[27] SP Burke and TEW Schumann. Diffusion flames. *Industrial & Engineering Chemistry*, 20(10):998–1004, 1928.

[28] V. A. Shvab. Relation between temperature and velocity fields of the gas plume. *Investigations of Natural Fuel Combustion (collected scientific papers) [in Russian]*, page 231248, 1948.

[29] Ya. B. Zeldovich. Theory of combustion of nonpremixed gases. *Zh. Tekh. Fiz.*, 19(10):11991210, 1949.

[30] DB Spalding. Combustion of liquid fuel in gas stream. *Fuel*, 29(1):2–7, 1950.

[31] HW Emmons. The film combustion of liquid fuel. *ZAMM-Journal of Applied Mathematics and Mechanics/Zeitschrift für Angewandte Mathematik und Mechanik*, 36(1-2):60–71, 1956.

[32] T. Hirano and Y. Kanno. Aerodynamic and thermal structures of the laminar boundary layer over a flat plate with a diffusion flame. *Proceedings of the Combustion Institute*, 14(1):391398, 1973.

[33] P Andreussi and L Petarca. Film combustion of ethyl alcohol in a parallel air stream. In *Symposium (International) on Combustion*, volume 18, pages 1861–1869, 1981.

[34] I . P. Volchkov B. F. Boyarshinov and V. I. Terekhov. Heat and mass transfer in a boundary layer with the evaporation and combustion of ethanol. *Combustion, Explosion, and Shock Waves*, 30(1), 1994.

[35] Ajay V. Singh and Michael J. Gollner. Estimation of local mass burning rates for steady laminar boundary layer diffusion flames. *Proceedings of the Combustion Institute*, 35(3):2527 – 2534, 2015.

[36] C.H. Miller, M.J. Gollner, M.J. Finney, and D.G. Gorham. An investigation of wildfire dynamics via fixed inclinable burners. In *9th U.S. National Combustion Meeting*, 2015.

[37] Daniel Jack Gorham. *Studying wildfire spread using stationary burners*. PhD thesis, 2014.

[38] Ajay Vikram Singh. A fundamental study of boundary layer diffusion flames. 2015.

[39] Louis Cattafesta, Chris Bahr, and Jose Mathew. Fundamentals of wind-tunnel design. *Encyclopedia of Aerospace Engineering*, 2010.

[40] Marvin E Goldstein and David W Wundrow. On the environmental realizability of algebraically growing disturbances and their relation to klebanoff modes. *Theoretical and computational fluid dynamics*, 10(1-4):171–186, 1998.

[41] Ronald E Hanson, Howard P Buckley, and Philippe Lavoie. Aerodynamic optimization of the flat-plate leading edge for experimental studies of laminar and transitional boundary layers. *Experiments in fluids*, 53(4):863–871, 2012.

[42] R Narasimha and SN Prasad. Leading edge shape for flat plate boundary layer studies. *Experiments in Fluids*, 17(5):358–360, 1994.

[43] John L de Ris. Mechanism of buoyant turbulent diffusion flames. *Procedia Engineering*, 62:13–27, 2013.

[44] Salman Verma. *Understanding flame structure in wildfires using Large Eddy Simulations*. PhD thesis, 2014.

[45] Andrew W Cook, William Cabot, and Paul L Miller. The mixing transition in rayleigh–taylor instability. *Journal of Fluid Mechanics*, 511:333–362, 2004.

[46] Paul Andersson, Martin Berggren, and Dan S Henningson. Optimal disturbances and bypass transition in boundary layers. *Physics of Fluids (1994-present)*, 11(1):134–150, 1999.

[47] Paolo Luchini. Reynolds-number-independent instability of the boundary layer over a flat surface: optimal perturbations. *Journal of Fluid Mechanics*, 404:289–309, 2000.

[48] S Berlin and DS Henningson. A nonlinear mechanism for receptivity of free-stream disturbances. *Physics of Fluids (1994-present)*, 11(12):3749–3760, 1999.

[49] Luca Brandt, Dan S Henningson, and Donatella Ponziani. Weakly nonlinear analysis of boundary layer receptivity to free-stream disturbances. *Physics of Fluids (1994-present)*, 14(4):1426–1441, 2002.

[50] SJ Leib, David W Wundrow, and ME Goldstein. Effect of free-stream turbulence and other vortical disturbances on a laminar boundary layer. *Journal of Fluid Mechanics*, 380:169–203, 1999.

[51] David W Wundrow and ME Goldstein. Effect on a laminar boundary layer of small-amplitude streamwise vorticity in the upstream flow. *Journal of Fluid Mechanics*, 426:229–262, 2001.

[52] Jonathan H Watmuff. Detrimental effects of almost immeasurably small freestream nonuniformities generated by wind-tunnel screens. *AIAA journal*, 36(3):379–386, 1998.

[53] Peter J Schmid and Dan S Henningson. *Stability and transition in shear flows*, volume 142. Springer Science & Business Media, 2012.

[54] ME Goldstein and Lennart S Hultgren. Boundary-layer receptivity to long-wave free-stream disturbances. *Annual Review of Fluid Mechanics*, 21(1):137–166, 1989.

[55] Tomi Haramina. *Coherent structures in turbulent Rayleigh-Bénard convection.* PhD, 2005.

[56] JC Klewicki, Meredith M Metzger, E Kelner, and EM Thurlow. Viscous sublayer flow visualizations at $r_\theta = 1500000$. *Physics of Fluids (1994-present)*, 7(4):857–863, 1995.

[57] Stanley Corrsin. Some current problems in turbulent shear flows. In *Symposium on Naval hydrodynamics*, volume 515. National Academy of Sciences, Publication, 1957.

[58] SJ Kline, WC Reynolds, FA Schraub, and PW Runstadler. The structure of turbulent boundary layers. *J. Fluid Mech*, 30(4):741–773, 1967.

[59] DC Collis and MJ Williams. Two-dimensional convection from heated wires at low reynolds numbers. *Journal of Fluid Mechanics*, 6(03):357–384, 1959.

[60] Late Max Jakob. *Heat Transfer: Vol. 1.* Wiley, 1967.

[61] N Chakrabarti and GS Lakhina. Collisional rayleigh-taylor instability and shear-flow in equatorial spread-f plasma. 2003.

[62] N Chakrabarti and KH Spatschek. Rayleigh–taylor modes in the presence of velocity shear and vortices. *Journal of plasma physics*, 59(04):737–750, 1998.

[63] D Thévenin, JC Rolon, PH Renard, DW Kendrick, D Veynante, and S Candel. Structure of a non-premixed flame interacting with counterrotating vortices. In *Symposium (International) on Combustion*, volume 26, pages 1079–1086. Elsevier, 1996.

[64] Miguel Hermanns, Marcos Vera, and Amable Liñán. On the dynamics of flame edges in diffusion-flame/vortex interactions. *Combustion and flame*, 149(1):32–48, 2007.

[65] Vito S Santoro, Dimitrios C Kyritsis, Amable Liñán, and Alessandro Gomez. Vortex-induced extinction behavior in methanol gaseous flames: a comparison with quasi-steady extinction. *Proceedings of the Combustion Institute*, 28(2):2109–2116, 2000.

[66] V Kottke. On the instability of laminar boundary layers along concave walls towards görtler vortices. In *Propagation in Systems Far from Equilibrium*, pages 390–398. Springer, 1988.

[67] JM Floryan. On the görtler instability of boundary layers. *Progress in Aerospace Sciences*, 28(3):235–271, 1991.

[68] NN Anuchina, Yu A Kucherenko, VE Neuvazhaev, VN Ogibina, LI Shibarshov, and VG Yakovlev. Turbulent mixing at an accelerating interface between liquids of different density. *Fluid Dynamics*, 13(6):916–920, 1978.

[69] David L Youngs. Numerical simulation of turbulent mixing by rayleigh-taylor instability. *Physica D: Nonlinear Phenomena*, 12(1):32–44, 1984.

[70] N Peters. Laminar flamelet concepts in turbulent combustion. In *Symposium (International) on Combustion*, volume 21, pages 1231–1250, 1988.

[71] Moshe Lavid and AL Berlad. Gravitational effects on chemically reacting laminar boundary layer flows over a horizontal flat plate. In *Symposium (International) on Combustion*, volume 16, pages 1557–1568. Elsevier, 1977.

[72] Moshe Lavid. *Buoyancy effects on chemically reacting laminar bondary layer flows*. State University of New York at Stony Brook, 1974.

[73] Terry L Clark, Mary Ann Jenkins, Janice Coen, and David Packham. A coupled atmosphere–fire model: convective feedback on fire-line dynamics. *Journal of Applied Meteorology*, 35(6):875–901, 1996.

[74] Terry L Clark, Mary Ann Jenkins, JL Coen, and David R Packham. A coupled atmosphere-fire model: Role of the convective froude number and dynamic fingering at the fireline. *International Journal of Wildland Fire*, 6(4):177–190, 1997.

[75] AL Sullivan. Convective froude number and byrams energy criterion of australian experimental grassland fires. *Proceedings of the Combustion Institute*, 31(2):2557–2564, 2007.

[76] Frederic Morandini and Xavier Silvani. Experimental investigation of the physical mechanisms governing the spread of wildfires. *International Journal of Wildland Fire*, 19(5):570–582, 2010.

[77] Ralph M Nelson. Re-analysis of wind and slope effects on flame characteristics of mediterranean shrub fires. *International Journal of Wildland Fire*, 24(7):1001–1007, 2015.

[78] Ray-Shing Wu and KC Cheng. Thermal instability of blasius flow along horizontal plates. *International Journal of Heat and Mass Transfer*, 19(8):907–913, 1976.

[79] Yasuo Mori. Buoyancy effects in forced laminar convection flow over a horizontal flat plate. *Journal of Heat Transfer*, 83(4):479–482, 1961.

[80] EM Sparrow and Wm J Minkowycz. Buoyancy effects on horizontal boundary-layer flow and heat transfer. *International Journal of Heat and Mass Transfer*, 5(6):505–511, 1962.

[81] Xiaobo Yao. *Characterization of Fire Induced Flow Transport Along Ceilings Using Salt-Water Modeling*. PhD thesis, 2006.

[82] DB Spalding. A single formula for the law of the wall. *Journal of Applied Mechanics*, 28(3):455–458, 1961.

[83] CR Smith and SP Metzler. The characteristics of low-speed streaks in the near-wall region of a turbulent boundary layer. *Journal of Fluid Mechanics*, 129:27–54, 1983.

[84] Qi Xiang Lian. A visual study of the coherent structure of the turbulent boundary layer in flow with adverse pressure gradient. *Journal of Fluid Mechanics*, 215:101–124, 1990.

[85] M Rashidi and S Banerjee. Streak characteristics and behavior near wall and interface in open channel flows. *J Fluids Eng*, 112(2):164–170, 1990.

[86] G Hetsroni and R Rozenblit. Heat transfer to a liquidsolid mixture in a flume. *International Journal of Multiphase Flow*, 20(4):671–689, 1994.

[87] D Kaftori, G Hetsroni, and S Banerjee. Funnel-shaped vortical structures in wall turbulence. *Physics of Fluids*, 6(9):3035–3050, 1994.

[88] BU Achia and DW Thompson. Structure of the turbulent boundary in drag-reducing pipe flow. *Journal of Fluid Mechanics*, 81(03):439–464, 1977.

[89] Daniel Sabatino. Instantaneous properties of a turbulent spot in a heated boundary layer. 1998.

[90] M Zacksenhouse, G Abramovich, and G Hetsroni. Automatic spatial characterization of low-speed streaks from thermal images. *Experiments in fluids*, 31(2):229–239, 2001.

[91] Gilead Fortuna and Thomas J Hanratty. The influence of drag-reducing polymers on turbulence in the viscous sublayer. *Journal of Fluid Mechanics*, 53(03):575–586, 1972.

[92] AK Gupta, J Laufer, and RE Kaplan. Spatial structure in the viscous sublayer. *Journal of Fluid Mechanics*, 50(03):493–512, 1971.

[93] Hiroji Nakagawa and Iehisa Nezu. Structure of space-time correlations of bursting phenomena in an open-channel flow. *Journal of Fluid Mechanics*, 104:1–43, 1981.

[94] Brian F Farrell and Petros J Ioannou. Dynamics of streamwise rolls and streaks in turbulent wall-bounded shear flow. *Journal of Fluid Mechanics*, 708:149, 2012.

[95] MT Landahl. A note on an algebraic instability of inviscid parallel shear flows. *Journal of Fluid Mechanics*, 98(02):243–251, 1980.

[96] MT Landahl. On sublayer streaks. *Journal of Fluid Mechanics*, 212:593–614, 1990.

[97] Peter W Carpenter, Karen L Kudar, Reza Ali, Pradeep K Sen, and Christopher Davies. A deterministic model for the sublayer streaks in turbulent boundary layers for application to flow control. *Philosophical Transactions of the Royal Society of London A: Mathematical, Physical and Engineering Sciences*, 365(1859):2419–2441, 2007.